FINAL REPORT NASA GRANT NGR 34-012-013 CREATION OF A CERAMICS HANDBOOK March 1, 1976

Principal Investigator
William J. Craft

Department of Mechanical Engineering

School of Engineering

North Carolina A & T State University

312 N. Dudley Street

Greensboro, N. C. 27411

REPRODUCED BY
NATIONAL TECHNICAL
INFORMATION SERVICE
U.S. DEPARTMENT OF COMMERCE
SPRINGFIELD, VA. 22161

(NASA-CR-146575) CREATION OF A CERAMICS N76-20274
HANDBOOK Final Report (North Carolina
Agricultural and Technical)
Unclas
G3/27 21485

Final Report NASA Grant NGR 34-012-013

Creation of a Ceramics Handbook

Principal Investigator

William J. Craft
Associate Professor of Mechanical Engineering
North Carolina A&T State University
312 N. Dudley Street
Greensboro, N. C. 27411
(919) - 379-7620

Graduate Assistants

Mr. Kwan Lok Lee M.S. Candidate in Engineering

Mr. Fred B. Goodnight
-M.B.A. Candidate (U.N.C.-G.)

Mr. Samuel A. Byers M.S. Candidate in Engineering

Abstract

The purpose of this research has been to characterize a group of common ceramic materials, alumina, magnesium oxide, silicon nitride, and silicon carbide through literature searches on physical properties of these materials. The files used were the NASA file, DDC/GRA File, Engineering Index File and standard library searches. The results of these searches, given by this report, are arranged by material properties including mechanical, electrical, electromagnetic, where applicable, and fracture; and the entries are arranged in chronological order by candidate. To bolster this approach and to make possible additional entries on similar topics, a list, by author, follows where tabular information including charts and figures of results is given along with a brief statement of the results and conclusions. In both cases, information on the independent variables along with their range is given. These variables are frequently temperature and material density.

Following this presentation are the results of an extensive industry survey asking for names of other candidates on which information is lacking and also what type of service, if any, is desired in keeping a current information file on general ceramic materials. Included in this survey is a list of research personnel and ceramics suppliers and users and governmental interest groups involved in general ceramics technology.

Acknowledgements

The principal investigator would like to acknowledge Dr. Juri G. Filatovs, of the Mechanical Department at A & T State University, for his helpful suggestions and comments as well as Mr. Philip I. Moynihan, project technical consultant. He would also like to acknowledge the several graduate and undergraduate students who spent many dedicated hours on library and computer search material which included viewing hundreds of sheets of microfiche in addition to printed copy material. They are: Mr. Samuel A. Byers, Mr. Fred B. Goodnight, and Mr. Kwan Lok Lee. Secretarial work was supplied by Ms. Mary M. Thomas and typing and reproduction work was contracted by Earle Secretarial Centers of Greensboro, N. C. Above all, the writer wishes to acknowledge and express appreciation to the National Aeronautics and Space Administration for it support of this survey and investigation.

Table of Contents

Ţ	PAGE
ABSTRACT	ii
ACKNOWLEDGEMENTS	iii
INTRODUCTION	1
CANDIDATE MATERIAL PROPERTY LISTING	6
MATERIAL PROPERTY REFERENCE CHART	7
ALUMINA	8
MAGNESIUM OXIDE	30
SILICON NITRIDE	43
SILICON CARBIDE	54
UNABRIDGED AUTHOR REFERENCE LIST	60
MATERIAL PROPERTY QUESTIONNAIRE SURVEY RESULTS	
INCLUDING SURVEY LISTING AND STATISTICS	261
CERAMICS INDUSTRY AND RESEARCHER LISTING	267

Introduction

Tabulated data for the selection of ceramics in advanced engineering is a necessity where an accurate appraisal of structureal applicability is required. Accurate data, in a primary sense, influences the continuum mechanics solutions for all materials, as well as providing a basis for selection through fracture and failure theory. Thus, in order that analytical techniques can be applied adroitly to ceramics to determine their environmental limitations, this study was undertaken. Primary properties required for analytically based elasticity solutions are:

Youngs Modulus

Bulk Modulus (Modulus of Compression)

Poissons Ratio

Modulus of Rigidity

Coefficient of Linear Expansion.

Primary properties required for a corresponding thermodynamic analysis are:

Specific heat

Thermal Conductivity

Emissivity.

Primary properties required for a corresponding electrical evaluation are:

dielectric constant

loss tangent.

Secondary properties required to determine the survival of the material are:

uniaxial tensile strength

uniaxial compressive strength

hardness

flexural strength and Modulus of Rupture

fracture energy and surface stresses fracture probability and Weibull Parameters.

There are some properties required less frequently which could be of use in certain conditions which were omitted. There are also instances where some duplication is present as with the Modulus of Rupture and flexural strength which may be regarded as equivalent for brittle ceramics at most temperatures, and with the modulus of rigidity which can be simply determined from Youngs Modulus and Poissons Ratio for isotropic materials. In certain instances some of the indicated properties either could not be referenced or do not apply, e.g., the dielectric constant for opaque ceramics.

The area of greatest controversy in these tabulated lists of papers is probably that of 'survival parameters' which includes the discrete and probabilistic failure models. Despite the great amount of information available, the large dispersion in the data and a lack of a meaningful mechanism to connect the results will necessarily generate a problem when a margin of safety or similar measure of satisfaction is assigned to the continuum mechanics results. If the probabilistic approach is ignored then the tension and compressive strengths may be viewed as special cases of biaxial fracture results which could form the basis of several failure strength theories.

The results as described above have been compiled for four ceramic materials, alumina, magnesium oxide, silicon nitride, and silicon carbide, which have found wide use in varied environments. Data in these tables was compiled beginning January 1974 with the final searches being made in April 1975. Manual searches were undertaken as well as computer abstract and keyword searches. In cases of computer searches, first keyword lists were used to generate abridged abstracts then the lists were reviewed and full abstracts were selected. From these, the full article was inspected and a decision was then reached to include or reject the entry. Three major files were searched

at least in part by computer; the first is the NASA file, comprised of general technical interest articles, aerospace applications being stressed, from Journals and Government sponsored reports. This file is made up in part of two former files, International Aerospace Abstracts (A prefixes) and Scientific and Technical Aerospace Reports ('N' prefixes). The A accession numbers generally refer to journal publications and are available from that source while the N accession numbers refer to report literature. This literature is generally available from the National Technical Information Service (NTIS)

P.O. Box 1553 Springfield, Va. 22151.

The second file is the DDC/GRA file, now called Government Reports Announcements, and articles from this source carry prefixes of 'AD'. These documents are also available from NTIS. As with 'N' numbers, the 'AD' numbers are generally the result of government sponsored research. Finally, the Engineering Index file was searched which is generally composed of bibliographical information of Journal publications. Reprints of this material as with the 'A' accession number articles must be obtained from that journal and are not generally available through NTIS. In all items of this report either the 'N' or 'AD' numbers are given or the Journal itself is referenced for convenience. In some cases, several combinations will appear, in any event, the article can be traced easily.

Arrangement of Material Property Data

The report is divided into three sections exclusive of the introduction and a brief material property vs. candidate table where page numbers are referenced. The sections are: 1) candidates material property listing,

2) unabridged reference list by authors, and 3) a material property questionnaire survey with results and a list of persons or companies with a significant interest in ceramics.

The candidate ceramic material listing contains material property data literature by specific property for each material. Under each property, arranged with the most recent reference first, are listed the publications along with the independent variables and their ranges used in the publication. Most primary property data is a function of both material sample density and temperature. Further information on the general article can be found by consulting the unabridged reference list by authors where the NTIS accession number or journal is given along with a list of tables, graphs, and a summary of the report. In many cases, the article is cited in more than one ceramic material or property. The unabridged reference list, section 2, also serves as a vehicle for listing information in research which does not precisely fall into the property categories as listed but which might otherwise be useful as in the case of certain alloyed ceramics or ceramic films or whiskers. As is seen, section 2 contains a larger set of information than is covered by the property lists of section 1.

Finally, to test the significance of the work in this report, and to find out what was already known about former research and how well this past work was known, and to view what directions future work should take, a simple questionnaire was designed and distributed to the ceramics industry, users, and researchers. The results of the responses to this questionnaire and a list of those people or companies polled is included. About 31% of those polled returned the completed questionnaires. A complete listing of companies, researchers, and institutions polled totaling about 380 is given as well as the response results in the last section. Only about 350 of those on the survey list were polled because the remaining were foreign universities. The 350 polled consisted of all domestic organizations or persons which were found to have a ceramics interest. At one time this list was significantly larger but was reduced by removing those companies and individuals for which the survey questionnaires were undeliverable. Undelivered mail ran about 18% of that which was originally posted.

At the end of each question of the questionnaire, a conclusion is given based on the responses along with the statistical breakdown.

One obvious fact throughout this compilation is that the data which was actually compiled is frequently incomplete and in some cases partially contradictory due to the scatter in the property data.

In advanced structural applications, the very wide scatter frequently encountered leads to a need for more batch testing of samples and sophisticated analysis of the results. In many cases fracture parameters, not directly measureable, are presented without mention of methods applied to their extraction. For instance, changes in the method of data reduction in the Weibull parameters, in particular can produce a 100% change in the parameters from the same experimental results as was evidenced in one report.

There is a need for more widespread use of the same test methods and data reduction methods in the determination of ceramics properties as well as a need to maintain data banks on the more common of the ceramics. These data banks should contain the common property data, how it was arrived at, the experimental raw data, and experimental testing details as well as an assey of the candidate and fabrication details. Further a standardized name should be assigned which fits the candidate when asseyed and processed within a specified tolerance.

Candidate Material Property Listing



Material Property Reference Chart

Candidate Material Page Numbers Property Alumina Magnesium Oxide Silicon Nitride Silicon Carbide 8 Poissons ratio 54 43 Youngs Modulus 9 30 43 54 Tensile/compressive 11 31 55 44 strength Flexural strength 46 14 33 Modulus of -56 48 18 34 Rupture Bulk Modulus 34 Shear Modulus . 35 Fracture Energy/ 20 35 49 Fracture Stress Modulus of 23 Rigidity Fracture Probability/ 24 36 57 Weibull Parameters Hardness 36 Thermal 25 50 37 57 Conductivity Linear Thermal 26 51 38 58 Expansion Specific Heat 52 26 39 59 Emittance 53 27 40 Thermal Diffusivity 41 Dielectric Constant 53 28 41 Loss Tangent 29 53 42

ALUMINA

POISSONS RATIO

Author	Title	Journal Vol. or Series	Description (Ind. Variables)	Date Published
Sines, G. Adams, M.	An Experimental Study on the Com- pressive Biaxial Strength of Ceramics	(N00019-72-C-0159) AD754-826	Young's Modulus	1/1972
Neuber, H. Wimmer, A.	Mechanics of Brittle Materials under Linear Temperature Increases	(AFML-TR-71-70) AD725761	Grainsize µm(17-24)	4/1971
Sedlacek, R.	Investigation of Elasticity and Strength of Ceramics Subjected to Tensile and Compressive Loads	(AF33(615)-5047)	Tensile Stress psi (3740-27040) E ₁ (69-498) E ₂ (15-111)	2/1967
	and compressive coads	AD850929	Compressive Strest (817000-34600) (1520-6600) (140-1720)	
Christian, W. J. et al	Evaluation of Thermal Protective Systems for Advanced Aerospace Vehicles, Vol. II: Appendices	(AF33(657)-9407) AD627140	emperature ^O R (500-3500)	4/1965
	<u>YOUNGS</u>	MODULUS E		
Sines, G. Adams, M.	An Experimental Study on the Com- pressive Biaxial Strength of Ceramics	(N00019-72-C-0159)	General properties	11/1972
Petch, N. J. et al	The Brittle Fracture of Alloyed Alumina	(DAJA37-71-C-2760) AD748110	Temp ^O C(0-800) wt. % Chromium .0005-1(%)	2/1972

YOUNGS MODULUS E

				D -:-
Author	Title	Journal Vol. or Series	Description (Ind. Variables)	Date Publish
Nagarojan, A.	Flasticity-Porosity	Journal of Applied Physics, Vol. 42, No. 10	Porosity (0-40%)	9/1971
Neuber, H. Wimmer, A.	Mechanics of Brittle Materials under Linear Temperature Increases	(AF60(052)-875) AD725-761	Surface conditions Porosity (%) 0-20	4/1971
Stiglich, J. J. et al	Characteristics of Hot-Pressed Alumina with A Mo-Dispersed Phase	(AMMRC-TR-70-35) AD722-239	Poisson's ratio 0.23-0.30	12/1970
Broutman, L. J. et al	Effect of Combined Stresses on Fracture of Alumina and Graphite	Journal of The Ameri- can Ceramic Society, Vol. 53, No. 12		12/1970
Mehan, R. L. Herzog, J. A.	Mechanical Properties of Whiskers	"Whisker Technology" A71-14946	Area $(\mu)^2 0-80$ $\frac{1}{e} (mm^{-1})0-55$	1970
Sedlacek, R.	Investigation of Elasticity and Strength of Ceramics Subjected to Tensile and Compressive Loads	(AF33(615)-5047) AD850-929	Stress (3500- 2800) psi Axial strain (66- 500) Lateral strain (13-110)	2/1969
Buessem, W. R. McKinstry, H. A.	Anisotropy and Strength of Ceramic Bodies	(Nr-656(27)) AD684-717	Density gm/cm ² 3.80-4.00	2/1969
Mackenzie, J. D.	Ceramics in Ocean Engineering	(Ocean Engineering, Vol. 1, pp. 55-571) AD696-825	General properties	1969
Rudnick, A. et al	The Evaluation and Interpretation of Mechanical Properties of Brittle Materials	(AF33(615)2335) AD670-190 s	Temp. ^O C (0-1200)	4/1968

REPRODUCIBILITY OF THE ORIGINAL PAGE IS POOR

YOUNGS MODULUS E

Author	Title	Journal Vol. or Series	Description (Ind. Variables)	Date Published
Poulos, N. E. et al	Ceramic Systems for Missile Structural Applications	(W-63-0143) AD811146	Al ₂ 0 ₃ Content(%) 0-100 Cristobalite Constant(v/c) 8.0 9.5. Grinding time(hr.) 24-96	10/1966
Neuber, H. Wimmer, A.	Experimental Investi- gation of the Behavior of Brittle Materials at Various Ranges of Temperature	(AF61(052)-875) N68-26125	Porosity(%)2-10 Grainsize(µ)5-50 Temp. C(-200-200) Diameter(mm) 2-8	9/1966
Naohiro Soga Anderson, O. L.	Simplified Method for Calculating Elastic Moduli of Ceramic Powder from Compressi- bility and Debye Temperature Data	(AF33(615)1700) AD638280	Porosity (%) 0-5	11/1965
Christian, W. J. et al	Evaluation of Thermal Protective Systems for Advanced Aerospace Vehicles Vol. II,	(AF33(657)-9407) AD627140	Temp. ^O F (0-2200) Grainsize	4/1965
Davies, L. G., et al	Appendices A Study of High Modulus, High Strength Filament Materials by Deposition Techniques	(W64-01766) AD611757	Density 3.1 gm/cm ³ Tensile strength 24x10 ³ psi	10/1964
Eliason, L. K. Zellner, G. C.	A Survey of High Tem- perature Ceramic Mate- rials for Radomes	(ML-TDR64-296) AD607619	Temp. ^O F (200-2800) % Main Constituent (84-99.9)	9/1964 :
Sedlacek, R.	Tensile Strength of Brittle Materials	(AF33(675)-10600) N64-25341	Loading rate psi/sec 50-4000	3/1964
(Editor) Hague, J. R. et al	Refractory Ceramics for Aerospace: A Materials Selection Handbook	The American Ceramic Society Columbus, Ohio	Temp. ^O F (0-2500)	1964

TENSILE and COMPRESSIVE STRENGTH				
Author	Title	Journal Vol. or Series	Description (Ind. Variables)	Date Published
Kirchner, H. P. Gruver, R. M.	Fracture Mirror in Alumina Ceramics	Ceramic Finishing Co., Box 498, State College, PA 16801	Distance from the rod axis	3/1973
Sines, G. Adams, M.	An Experimental Study on the Compres- sive Biaxial Strength of Ceramics	(N00019-72-C-0159) AD754-826	Density 3.85 gm/cc Grainsize (20-30) microns	11/1972
Lange, F. F.	Healing of Surface Cracks in Ceramics	The Science of Ceramic Machining and Surface Finishing p. 233-236, N72-29511	Heat treatment	5/1972
Starrett, H. S.	The Influence of Material Removal on the Strength and Surface of an Alumina	The Science of Ceramic Machining and Surface Fini- shing, p. 377-387 N72-29526	Surface conditions Tensile volume in ³ (10 ⁻⁴ -10)	5/1972
R.	The Effect of Grinding Variables on the Strength and Surface Finish of Alumina	(NOW-66-0383-d) (N72-29527	Gritsize 30-1200 Type of grinding, different surfaces	•
Simpson, L. A. Wasyly- shyn, A.	Measurement of Work of Fracture in High Strength Brittle Materials	(AECL-3677) (N73-12944)	Different ceramic materials	2/1972
Petch, N. J. et al	The Brittle Fracture of Alloyed Alumina	(DAJA-37-71-C-2760) AD748-110	Testing temp. OC (-265-1000)	2/1972
Buessem, W. R. Gruver, R. M.	Computation of Resi- dual Stress in Quenched Alumina	Journal of The Ameri- can Ceramic Society Vol. 55, No. 2	Distance from rod axis in. (-0.06~0.06)	1/1972
J. H.	Theoretical Approach to the Fracture of Two-phase Glass- Crystal Composites		Volume fraction of alumina (0.05-0.5)	1972
Gupta, T. K.	Strength Degradation and Crack Propagation in Thermally Shocked Alumina	Vol. 55, No. 5	Temp. difference of thermal shock ^O C(0-1000) Single crystal sapphire grainsize (microns 85, 40, 34, 10	12/1971)

TENSILE and COMPRESSIVE STRENGTH

Author	Title	Journal Vol. or Series (Description Ind. Variables)	Date Published
D. A. Hasselman,	Static and Cyclic Fatigue Behavior of a Polycrystal- line Alumina	(DA-ARO-D-31) Journal of The Ameri can Ceramic Society, Vol.55, No.4, April 1972 p. 208-211	Testing time -to failure log (.1-5) Sec	11/1971 .
Sedlacek, R. Jurgensen, P. J.	Processing of Cera- mics-Surface Finishing Studies	(NOOO019-70-C-0179) AD730-766	Grainsize (11.0 -420) micron Grinding technique test conditions	9/1971 e,
Kirchner, H. P. et al	Strenthening Alumina by Quenching in Various Media	Journal of Applied Physics, Vol. 42, No. 16	Refired tempera- ture to 1500 °C and quenched in silicone oil or still air	9/1971
Platts, D. R. Kirchner, H. P.	Comparing Tensile and Flexural Strength of a Brittle Material	Journal of Mate- rials, JMLSA, Vol. 6, No. 1	Different heat treatment relative area (1-100)	3/1971
Stiglich, J. J. et al	Characterization of Hot-Pressed Alumina with a Mo-Dispersed Phase	(AMMRC-TR-70-35) AD722239	Grainsize (1-50) microns	12/1970
Hasselman, D. P. H.	Strength Behavior of Polycrystalline Alumina Subjected to Thermal Shock	Journal of The Amer can Ceramic Society Vol. 53, No. 9		3/1970
Sedlacek, R.	Processing of Cera- mics-Surface Finishing Studies	(N00019-69-C-0229) AD870158	Stress rate psi/sec(30-3000)	3/1970
Mehan, R. L. Herzog, J. A.	Mechanical Properties of Whiskers	"Whisker Techno- logy" - A71-14946	Area $(\mu^2)0-80$ $\frac{1}{e}(mm^{-1})0-55$	1970
Wieder- horn, S. M.	Fracture of Sapphire	The American Cera- mic Society, Basic Science Division, No. 12, B-68	Flame polished	9/1969
Ainsworth, J. H. Moore, R. E.	Fracture Behavior of Thermally Shocked Aluminum Oxide	Journal of The Amer can Ceramic Society Vol. 52, No. 11	ri-Temperature dif- , ference C(100- 500)	8/1969

TENSILE and COMPRESSIVE STRENGTH

Author	Title	Journal Vol. or Series	Description (Ind. Variables)	Date Published
Reardon, E. F.	Exploratory Tests of Alumina Spheres under External Pressure	(NSRD C-3013) AD852947	Stress rate psi/sec (10 ⁻² -10 ⁵)	4/1969
Sedlacęk, R.	Processing of Cera- mics-Surface Finishing Studies	(N0009-69-C-0288) AD854140	Post grinding treatment (from 0-6) on different sample	3/1969
Sedlacek, R.	Investigation of Elasticity and Strength of Ceramics Subjected to Tensile and Compressive Loads	(AF33(615)5047) AD850929	Magnitude (psi) 0-336,000 No. of cycles 0-80 Ellipticity(%)0-5 Stress rate (psi/s 10,000 Stress rate (psi/s	sec)
Christian, W. J. et al	Evaluation of Thermal Protective Systems for Advanced Aerospace Vehicles, Vol. II: Appendices	(AF33(657)-9407) AD627140	Testing tempera- ture F (0-2200)	4/1965
Davis, L. G. et al	A Study of High Modu- lus, High Strength Filament Materials by Deposition Technique	(W-64-01766) AD611757	Density 3.1 gm/cc	11/1964
Eliason, L. K. Zellner, G. C.	A Survey of High Tem- perature Ceramic Mate- rials for Radomes	(MLTDR64296) AD607619	Testing tempera- ture OF (200- 2800) % Main Constitutent (94.0-99.9)	9/1964
Slonim, A. I.	Proceedings of the OSU-RTD Symposium on Electromagnetic Windows (7th) 2-4 June, 1964, Vol. III, Section B	(AF33(615)1081) AD605391	% of Alumina (97.5-99.5) Testing tempera- ture 1000 ⁰ F	6/1964
Salkind, M. J.	Candidate Materials for Whisker Composites	(WVTRR-6411) AD602132	Strength/density as a function of volume % fiber (0-100)	5/1964

TENSILE and COMPRESSIVE STRENGTH

Author	Title	Journal Vol. or Series	Description (Ind. Variables)	Date Published
Loser, J. B. et al	Thermophysical Proper- ties of Thermal Insulating Materials	(ML-TDR-64-5) AD601535	Temperature ^O R (400-2400)	4/1964
Sedlacek, R.	Tensile Strength of Brittle Materials	(AF33(657-10600)) N64-25341	Loading rate psi/sec (70-4000) Testing tempera- ture (0-1800) C	3/1964
(Editor) Hague, J. R. et al	Refractory Ceramics for Aerospace: A Materials Selection Handbook	The American Ceramic Society Columbus, Ohio	Testing tempera- ture (0-2500) F	1964
	FLEXURA	L STRENGTH		
Kirchner, J. P. Gruver, R. M.	Fracture Mirrors in Alumina Ceramics	Ceramic Finishing Co., Box 498, State College, PA 16801	Mirror radius MX10 ⁴ (1-30) Testing temp. (25-1400)°F	3/1973
Sines, G. Adams, Marc	An Experimental Study on the Compressive Biaxial Strength of Ceramics	(N00019-72-C-0159) AD754826	Density 3.85 gm/cc Grainsize (20-30) microns	1/1972
Kirchner, H. P. et al	Strength Effects Resulting from Simple Surface Treatments	The Science of Ceramic Machining and Surface Finishing p. 353-363 N72-29524	96% alumina, Testing time sec.(1-100,000), Refiring temp. F(600-1800) Axial scratch Average flexural strength psi (4500-60000), Kg/m ² x10 ⁶ (31-42); Scratch width (20 Load on diamond p gm(0-800); Flow d in inches(0-0.005 (96% alumina rods scored to various depths), Differen treatment conditi Temp. C 1500 and time is 1 hr.	oint epth) t on,

_
iΛ
<i>i</i> ,

Author	Title	Journal Vol. or Series	Description (Ind. Variables)	Date <u>Published</u>
Lange, F. F.	Healing of Surface Cracks in Ceramics	The Science of Ceramic Mach- ining and Surface Finish- ing p. 233-236 N72-29511	Strength as cut 35800 I 3% (2408)psi (thermal shocked specimens). Strength in % change through heat treatment 1100°C; different shapes (description)	5/1972
Starrett, H. S.	The Influences of Material Removal on the Strength and Surface of an Alumina	The Science of Ceramic Machining and Surface Finishing p. 377-387 N72-29526	Minimum fired thickness inches (0-2); Surface condition; Tensile Volume Vin ³ (6.1 x10 ⁻⁴ -6.1 x 10 ⁻¹)	5/1972
Petch, N. J. et. al.	The Brittle Fracture of Alloyed Alumina	(DAJA-37-71-C- 2760) AD748110	Testing Tempera- ture 70°C, 300°C, 600°C. Grainsize microns (0-1)	
Rhodes, W. H. Cannon, R. M.	Microstructure Studies of Refrac- tory Poly- crystalline Oxides	(NO0019-70-C- 0171) AD727-618	Testing Tempera- ture ^O C (0-1600)	2/1972
Rhodes, W. H. et. al.	Microstructure Studies of Refractory Poly- crystalline Oxides	(N00019-71-C-0325) AD740-828	Different specimens	1/1972
Buessem, W. R. Gruver, R. M.	Computation of Residual Stresses in Quenched Al ₂ 0 ₃	Journal of the American Ceramic Society Vol. 55, No. 2	Quenching in air 75.9(Ksi), in silicone oil (88-106)Ksi Temperature ^O C (1600-20)	1/1972
Miyata, N. Jinno, H.	Theoretical Approach to the Fracture of Two Phase Glass Crystal Composites	Journal of Material Science 7 (1972) 393-	Volume fraction of alumina (0-6.5)	1972

Author	Title	Journal Vol. or Series		Date ublishe
Gupta, T. K.	Strength Degrada- tion and Crack Pro- pagation in Thermally Shocked Alumina	(AF33(615)2669) The Journal of American Ceramic Society Vol. 55 No. 5, (1971)	Quenching 12 Temperature OC (25-800); Thermal shock obs. (6.2-24), Calc. (4.3-22.0)	2/1971
Kirchner, H. P.	Strengthening Alumina by Quenching in Various Media	Journal of Applied Physics Vol. 42, No. 10	Quenching temp- 9/ erature OC (1500- 1600), Liquid media silicone oil, motor oil, kerosene, etc.	'1971 '
Sedlacek, R. Jorgensen, P. J.	Processing of Ceramics-Surface Finishing Studies	(NOOO19-70-C- 0179) AD730-766	Grainsize microns 9 (10-50)	9/1971
Kirchner, H. P. Walker, R. E.	Delayed Fracture of Alumina Ceramics with Compressive Surface Layers	Ceramic Finishing Co., Box 498, State College PA 16801		5/1971
Katso- bashvili, Y. R. et. al.	Effect of the Chemical Composition of Alumina Oxide Catalysts on the Stability of the Structural Mechanical Pro- perties During Heat Treatment	Translated from Khimiyai Telchonologiya Toplivinlasel, No. 6 pp. 1-5, June, 1971*	Specific Vol. 6 m ² /g. (0-100); pore cm ³ /g. (0-0.4)	5/1971
Platts, D. R. Kirchner, H. P.	Comparing Tensile and Flexural Strength of a Brittle Material	Journal of Materials JMLSA Vol. 6 No. 1, 3/'71, p. 48-59	Different 3 treatment of 96% ·. alumina	3/1971
Degty- areua, E. V. et. al.	Selecting Alumina Grades for Making Densely Sintered Alumina Ceramics	Ukrainian Scientific- Research Institute of Refractories Translated from Ognenpory No. 7 pp. 39-45, 1970**	Open porosity 7% (23.0-33.0) Apparent density gm/cc 2.6-2.9	7/1970

Author	Title	Journal Vol. or Series	Description (Ind. Variable)	Date Publishe
Sedlacek, R.	Investigation of Elasticity and Strength of Ceramics Subjected to Tensile and Compressive Loads	(AF33(615)5047) AD850-929	Stress rate 3000 psi/sec (A1-995 alumina)	2/1969
Hassel man, . D.P.H.	Crack Growth and Creep in Brittle Ceramics	Journal of The Amer can Ceramic Society Vol. 55, No. 12	i-Quenching tempera- ture difference °C (0-800)	3/1970
Mehan, R. L.	Mechanical Proper- ties of Whiskers	"Whisker Technology"	Area (microns) ² 0.1-10,000; Test	1970
Herzog, J. A.	•	A71-14946	temp. $^{\circ}$ C (0-1800) Coating on strengt of α -Al ₂ O ₃ whisker (0.1-10,000) Cross section area (microns) ² (0-40)	'S
Cannon, R. M. Rhodes, W. H.	Deformation Processes in Forging Ceramics (progress report)	(NASW-1914) N70-24348	Grain growth in successive test cycles at 1450 °C, Cycle (0-6), Annealing temperatur 1500 °C	
Bakunov V. S. et. al	Creep in a Poly- crystalline Alumina Ceramic	ranslated rom Ogneupory o. 10 pp. 45-49. ct. 1969*	Grainsize microns (30-200) Relative density %(95-99.3), Mg0 additive wt.% 0.3	10/1969
Wieder- horn, S. M.	Fracture of Sapphire	ne American eramic ociety, Basic cience Div. No. 12B-68	Flame-polished rods	9/1969
Sarkar, B. K. Glinn, T.G.J.	Fatigue Behavior or High Alumina Ceramics	Trans British Society V69, N.5 Sep. 1970, P. 199-20	Cycle to fail (1-10 ⁸)	3/1969

-18-

Author	Title	Journal Vol. or Series	Description (Ind. Variables)	Date <u>Publish</u> e
Heuer, A. H. et al	Microstructure Studies of Poly- crystalline Refractory Oxides	(NOW-66-0506) AD653483	Temperature ^O C (23-1400) Grainsize microns (1-100)	4/1967
Christian, W. J. et al	Evaluation of Thermal Protective Systems for Advanced Aeropace Vehicles. Vol. II: Appendices	(AFML-TOR-64- 204-Vol. 2) AD627140	Temperature ^O R (500-3500) Grainsize microns (1-2)	4/1965
Eliason, L. K. Zellner, G. C.	A Survey of High Tem- perature Ceramic Materials for Radomes	(MLTDR-64-296) AD607619	Temperature ^O F (200-2800). % Main consti- tuent (94-99.9)	9/1964
Emrick, B. P.	Technology of New Devitrified Ceramics A Literature Review	(MLTDR-64-203) AD608217	Temperature ^O F (0-2600)	9/1964
Slonim, A. I.	Proceedings of OSU- RTD Symposium on Electromagnetic Windows (7th); 2-4 June, 1964. Vol.III, Session V.	(AF33-(615)1081) AD605391	Temperature ⁰ F (100-1600)	6/1964
Vasilos, T. et al	Microstructure Studies of Poly- crystalline Refractory Oxides	(NOW-62-0648c) N63-16176	Grainsize (microns) 1-1000	11/1962

^{*} Consultants Bureau, A Division of Plenum Publishing Corp., 227 West 17th St., New York, NY 10011.

MODULUS OF RUPTURE

Becher, P. F. Rice, R. W.	Flame Polishing of Flat Oxide Bars	The Science-of Ceramic Machining and Surface Fin- ishing P379-387 N72-29512	Surface finish	5/1972
Bakker, W. T.	Permeable Alumina Refractories	Journal of the American Ceramic Society Vol. 49, No. 7	Modulus of rupture of coarse-grained permeable refrac- tory at 1000° to 1500°C	2/1970

MODULUS OF RUPTURE

Author	Title	Journal Vol. or Series	Description (Ind. Variables)	Date <u>Publishe</u>
Palfreymans, M.	Hot Strength of High-Alumina Refractories	Journal of The American Ceramic Society, Vol. 49, No. 7	Testing temp. OC (0-1400) Firing time 1 hr. Firing temp. C (1600-1700) (99% pure alumina & 10µm grainsize)	1/1971
Gruszka, R. F. et al	Effect of Various Surface Treatments on the Band Strengtn of High Alumina Substrates	Journal of The American Ceramic Society, Vol. 49, No. 6	Treatment time in fused Borox, Anneal strength specimens	2/1970
Jones, J. T. Frasier, J. T.	Chemical Strength- ening of Alumina	(F33(615)68-C-1034) AD-708-707	Refining sample temp. C (1300-1750)	11/1969
Whitney, E. D. Yorihiro,	New and Improved Cutting Tool Materials	(AF33(615)3250) AD-853-733	Grain size (1-6) microns; Relative density % (99.5- 100); Bulk density g/cc (3.7-3.96) (99.2-99.5)	3/1969
Passmore, E. M. et al	Effect of Thermal Conditioning and Strain on The Microstructure and Mechanical Propertie of Alumina	AVSSD-0441-67 PR AD-663-835 s	Geometry 1.75 x .25 x 0.05 - 1.75 x .25 x . 2 inches	11/1967
Poulos, N. E. et al	Ceramic Systems for Missile Structural Applications	(W-63-0143) AD-811-146	Wt. ratio of alumina to fused silica (0:1-3:1-1:0) % (1-100) Cristobalite constant (v/c) 8.0-9.5 Grinding time (hr.) 24-96	10/1966
Rhodes, W. H. et al	Microstructure Studies of Poly- crystalline Refractory Oxides	(NOW-65-0316-f) N66-27434	Test temperature ^O C (200-20)	3/1966
Everhart, J. O. Muttart, L. E.	Strength of Struc- tural Ceramics under Impact Loading	(DA-ARO(D)-31- 124-G480) AD-646-879	Diameter (0.2-0.5)in % of alumina (85-100 Sp. gravity (2.3-3.8	0)

MODULUS OF RUPTURE

Author	Title	Journal Vol. or Series	Description (Ind. Variables)	Date <u>Published</u>
Davies, L. G. et al	A Study of High Modulus, High Strength Filament Materials by Depo- sition Techniques	(W-64-01766) AD611757	Density .143 lb/in ³	10/1964
Emich, B. R.	Technology of New Devitrified Ceramics- A Literature Review	(ML-TDR-64-203) AD608217	Grainsize (microns) 1-200 Temp. F (0-2400)	9/1964
	FRACTURE ENERG	Y AND FRACTURE STR	<u>ESS</u>	
Kirchner, H.R. Gruver, R. M.	Fracture Mirrors in Alumina Ceramics	Ceramic Finish- Co., Box 498, State College, PA 16801	(Mirror radius) $^{\frac{1}{2}}$ rm $^{\frac{1}{2}}$ (0-100) Distance from rod. axis (0-100)mm.	3/1973
Simpson, L. A.	Effect of Microstructure on Measurements of Fracture Energy of Al ₂ 0 ₃		Sintering temp. C (1400-2000) Notch ratio d/2 (0-1.0) % theoretical density (90-98) Grainsize microns (10-30)	1/1973
Turner, C. E.	Fracture Toughness and Specific Frac- ture Energy: A Re- analysis of Results	Material Science and Engineering, 11(1973)275-282. Imperial College, London, England.	Fracture area; Notch/width ratio, fracture resistance	7/1972
Starrett, H. S.	The Influences of Material Removal on the Strength and Surface of an Alu-mina	The Science of Ceramic Machining and Surface Fini- shing, May 1972. p377-387; N72-29526	Normalized stress (0-2.0)	5/1972
Rhodes, W. H. Berneburg, P. L.	Microstructure Studies of Refrac- tory Polycrystalline Oxides	(N00019-71-C- 0325) AD740-828	Different specimens at certain conditions (at room temp.)	1/1972

FRACTURE ENERGY AND FRACTURE STRESS

Author	Title	Journal Vol. or Series (1	Description Ind. Variables)	Date Publish
Kirchner, H. P. Walker, R. E.	Delayed Fracture of Alumina Ceramics with Compressive Surface Layers	Material Science Engineering, Vol. 8, No. 6, Dec. 1971, P.301-9	Flexural strength (0-100) X 10 ³ psi	6/1971
Neuber, H. Wimmer, A.	Mechanics of Brittle Materials under Linear Temperature Increases	(AFML-TR-71-70) AD725-761	Surface conditions	4/1971
Platts, D. R. Kirchner, H. P.	Comparing Tensile and Flexural Strength of Brittle Materials	Journal of Materials, JMLSA, Vol. 6, No. 1, 3/71, pp. 48-59	Strength psi (0-60) x 10 ³ psi	3/1971 .
Stiglich, J. J. et al	Characteristics of Hot-Pressed Alumina with a Mo-dispersed Phase	(AMMRC-TR-70-35) AD722-239	Density gm/cm ³ (3.9-4.4)	12/1970
Gruszka, R. F. et al	Effect on Various Surface Treatments on the Bend Strength of High Alumina Substrates	Journal of The American Ceramic Society, Vol. 49, No. 6.	Treatment time min. (1-30)	2/1970
Crouch, A. G. Jollife, K. H.	The Effect of Stress Rate on the Rupture Strength of Alumina and Mullite Refrac- tories	Proceedings of the British Ceramic Society, N 15, Jan. 1970;	Temperature ^O C (0-1400) Loading rate psi/min (10-10 ⁴)	1/1970
Gutshall, P. L. Gross, G. E.	Observations and Mechanisms of Frac- ture in Polycrystal- line Alumina	Engineering Fracture Mechanics 1969, Vol. 1, p. 463-471.	Average grain size microns (0-50) at temperature 25°C	1969
Wiederhorn, S. M.	Fracture of Sapphire	The American Ceramic Society, Basic Science Div. No. 12-B-68	Different conditions (room temperature)	1969

FRACTURE ENERGY AND FRACTURE STRESS

Author	Title	Journal Vol. or Series	Description (Ind. Variables)	Date Published
Hasselman, D. P. H.	Unified Theory of Thermal Shock Fracture Initiation and Crack Propagation in Brittle Ceramics	Journal of The American Cera- mic Society, Vol. 52, No. 11	Temperature ^O C (0-1000)	3/1969
Sarkar, B. K. Glinn, T. G. J.	Fatigue Behavior of High-Al ₂ O ₃ Ceramics	Trans. British Ceramic Society Vol. 69, No. 5, Sep. 1970, p.199- 203	Cycle to failure 10^0 - 10^7	3/1969
Wilshaw, T. R.	Measurement of Tensile Strength of Ceramics	(AFOSR-68-1497) AD672-428	Stress rate (psi/sec) 2 x 10 ³	2/1968
Passmore, E. M. et al	Effect of Thermal Conditioning and Strain on the Micro- structure and Mechanical Properties of Alumina	(AUSSD-0441-67- PR) AD663835	Grainsize microns (1.2-1.3) Fracture temperature C (0-1500) Plastic prestrain % (0-1.6)	11/1967
Heuer, A. H. et al	Microstructure Studies of Polycrys- talline Refractory Oxides	(NOW-66-0506) AD653483	Temperature ^O C (1400-1500)	4/1967
Neuber, H.	Experimental Investigations of the Behavior of Brittle Materials at Various Ranges of Temperatures	Scientific Annual Report, Apr. 1, 1965-Sep. 30, 1966 (West Germany) (AF61(052)-875)	Porosity (2-20) % Grainsize (5-50) microns, Temperature ^O C (-200-200) Length (22-360)mm	9/1966
Rhodes, W. H. et al	Microstructure Studies of Polycrys- talline Refractory Oxides	(NOW-65-0316-f) N66-27434	Room temperature annealed 16 hrs. at 1300°C, Heat treat- ment and abraded; surface treatment.	3/1966
Soltis, P. J.	Anistropic Mechanical Behavior in Sapphire (Al ₂ 0 ₃) Whiskers	(NAEC-ANL-1831) AD601447	Geometry of cross- section, Dimension and area of cross-section	4/1964

MODULUS OF RIGIDITY

Author	Title	Journal Vol. or Series	Description (Ind. 'Variables)	Date <u>Published</u>
Christian, W. J. et al	Evaluation of Thermal Protective Systems for Advanced Aerospace Vehicles. Vol.II: Appendices	(AFML-TOR-64-204) AD627140	Testing temperature R (500-3500)	4/1965
Davis, L. G. et al	A Study of High Modulus, High Strength Filament Materials by Deposi- tion Techniques	(W64-01766) AD611757	Density 1b/in ³ (.143)	10/1964
Eliason, L. K. Zellner, G. C.	A Survey of High Temperature Ceramic Materials for Radomes	(ML-TDR-64-296) AD60719	Testing temperature	4/1965
(Editor) Hague, J. R. et al	Refractory Ceramics for Aerospace: A Materials Selection Handbook	The American Ceramic Society, Columbus, Ohio	Testing temperature F (0-2500)	1964

FRACTURE PROBABILITY AND WEIBULL PARAMETERS

Author	Title'	Journal Vol. or Series	Description (Ind. Variables)	Date Published
Starrett, H. S.	The Influences of Material Removal on the Strength and Surface of an Alumina	The Science of Ceramic Machi- ning and Surface Finishing, May 1972, p.377-387 (N72-29256)	Probability of fracture (0-1) vs normalized stress for the macrotensile Al ₂ 0 ₃ specimens	5/1972
Kirchner, H. P. et al	Strength Effects Resulting from Simple Surface Treatments	The Science of Ceramic Machi- ning and Surface Finishing, May 1972, p.353- p.363 (N72-29524)	Probability of fracture (0-1) vs flexural strength Kg/m ² in millions(0-40)	5/1972
Harris, J. N. et al	Ceramic Systems for Missile Structural Applications	(NOO017-70-C- 4438) AD745-744	Fracture stress (10 ³ -10 ⁴) psi vs Log Ln(1/1-s)(Weibull plot of hydrostatic ring test data).	11/1971
Neuber, H. Wimmer, A.	Mechanics of Brittle Materials under Linear Temperature Increases	(AT-61-(052)- 815) AD725761	1/m (0-1045) vs porosity % (0-15) and grain sizes	4/1971
Carniglia, S. C.	Working Model for Porosity Effects on the Uniaxial Strength of Ceramics	Journal of The American Ceramic Society, Vol. 55, No. 12	$\sigma_{\rm p}/\sigma$ (0.9-0) vs poroSity volume fraction 0-0.4	4/1971 .
	Ceramic Processing (Chapter 5)	(DA-49-083-0SA- 3131) N69-28815	Tensile stress vs the probability of fracture	1968
Stofel, E. Conrad, H.	Brittle Fracture of Ceramics	(AF-04(695)-269) N64-17614	Fracture probabi- lity vs stress (10 ³ -10 ⁴) psi	5/1964

THERMAL CONDUCTIVITY

Author	Title	Journal Vol. or Series	Description (Ind. Variables)	Date Published
Weshsler, A. F.	Development of High Temperature Thermal Conductivity Standards	(AF33(615)2874) AD657024	Temperature ^O F (200-2800)	11/1966
Christian, W. J. et al	Evaluation of Thermal Protective Systems for Advanced Aerospace Vehicles, Vol. II: Appendices	(AFML-TDR-64-204 Vol. 2) AD627140	Temperature ^O R (400-4000)	4/1965
Christian, W. J. et al	Evaluation of Thermal Protective Systems for Advanced Aerospace Vehicles Vol. I	(AFML-TDR-64-204 Vol. 1) AD627139	Composition of Alumina-Nickel coating	4/1965
Brown, D. A.	Evaluation of Thermal Stress Resistance in Potential Radome Materials	(Nonr 421-300X) AD613009	Temperature ^O C (0-1200)	2/1965
Eliason, L. K. Zellner, G. C.	A Survey of High Temperature Ceramic Materials for Radomes	(ML-TDR-64-296) AD607619	Temperature ^O F (200-2800), % Main constituent (95-99.9); Temp. ^O F (200-2000)	9/1964
Loser, J. B. et al	Thermophysical Properties of Thermal Insulating Materials	(ML-TDR-64-5) AD601535	Temperature ^O C (0-1500)	4/1964
(Editor) Hague, J. R. et al	Refractory Ceramics for Aerospace: A Materials Selection Handbook	The American Ceramic Society, Columbus, Ohio	Mechanical properties	1964

LINEAR THERMAL EXPANSION

Author	Title	Journal Vol. or Series	Description (Ind. Variables)	Date Published			
Christian, W. J. et al	Evaluation of Thermal Protective Systems for Advanced Aerospace Vehicles, Vol. II: Appendices	(AFML-TOR-64-204 Vol. 2) AD627140	Temperature ^O R (500-3500)	4/1965			
Eliason, L. K. Zellner, G. C.	A Survey of High Temperature Ceramic Materials for Radomes	(ML-TDR-64-296) AD607619	Temperature ⁰ F (200-2800)	9/1964			
(Editor) Slonim, A. I.	Proceedings of the OSU-RTD Symposium on Electromagnetic Windows. 2-4 June, 1964, Vol. III. Section V-Fabrication and Testing of Air Borne Radomes. Section VI-Hypersonic Equipment		Temperature ^O F (100-1600)	6/1964			
Loser, J. B. et al	Thermophysical Properties of Thermal Insulating Materials	(ML-TDR-64-5) AD601535	Temperature ⁰ R (400-2400).	4/1964			
(Editor) Hague, J. R. et al	Refractory Ceramics for Aerospace: A Materials Selection	The American Ceramic Society, Columbus, Ohio	Temperature ^O F (0-4000)	1964			
	SPECIFIC HEAT						
Christian W. J. et al	Evaluation of Thermal Protective Systems for Advanced Aerospace Vehicles, Vol. II: Appendices	(AFML-TOR-64-204 Vol. 2) AD607140	Temperature ^O R (500-3500)	4/1965			
Eliason, L. K. Zellner, G. C.	A Survey of High Temperature Ceramic Materials for Radomes	(ML-TDR-64 - 296) AD607619	Temperature ^O F (200-2800)	9/1964			

SPECIFIC HEAT

Author	Title	Journal Vol. or Series	Description (Ind. Variables)	Date ublished
Loser, J. B. et al	Thermophysical Properties of Thermal Insulating Materials	(AF-33-657-10478) AD601535	Temperature ^O R (400-2400)	/1964
(Editor) Hague, J. R. et al	Refractory Ceramics for Aerospace: A Materials Selection Handbook	The American Ceramic Society, Columbus, Ohio	Temperature ^O F (0-4000)	964
	EMITTANCE	(TOTAL NORMAL & SPE	CTRAL)	
Richmond, J. C.	Thermal Radiation Properties of Ceramic Materials	(Mechanical and Thermal Properties of Ceramics, May 1969, p.125-138) N69-28431	Temperature ^O K (300-1000)	5/1969
Christian, W. J. et al	Evaluation of Thermal Protective Systems for Advanced Aerospace Vehicles, Vol. II: Appendices	(AFML-TDR-64-204 Vol. 2) AD627140	Temperature ^O R (100-400)	4/1965
Eliason, L. K. Zellner, G. C.	A Survey of High Temperature Cera- mic Materials for for Radomes	(ML-TDR-64-296) AD607619	Temp. ⁰ F(200-2800) % alumina (94-1-96),(94-100); Trade designation	9/1964
Folweiler, R. C. et al	Thermal Radiation Characteristics of Transparent Semi- transparent and Translucent Materials under Non-Isothermal Conditions	(AF33-657-11280) . AD607742	Wavelength (microns) 0-15 Temperature ^O C (500-1100)	6/1964
Loser, J. B. et al	Thermophysical Pro- perties of Thermal Insulating Materials	(AF33-657-10478) AD601535	Temperature ^O C (0-1500)	4/1964
Mitek, J. T.	Aluminum Oxide (Data Sheets)	N64-18384	Under different conditions (at room tempera-ture)	3/1964

DIELECTRIC CONSTANT

Author	Title	Journal Vol. or Series	Description (Ind. Variables)	Date <u>Published</u>
Degtyareva, E. V. et al	Selecting Alumina Grades for Making Densely Sintered Alumina Ceramics	Ukrainian Scientific-Research Institute of Refractories. Translated from Ogneupory, No. 7 pp.39-45, 1971	Apparent density gm/cm ³ (3.7-3.9)	7/1 <u>9</u> 70
Rice, D. H. Stowe, R. W.	Research on Aniso- tropy in Polycrys- talline Dielectric Materials	(W65-0440) AD638450	Testing temperature OF (200-2800) % alumina (94-99.9)	5/1966
Tallan, N. M. Graham, H. C.	Interfacial Polari- zation and Electri- cal Conductivity in Sapphire	(ASD-TDR-62-719- ft-3) AD630-345	Pretreatment, reducing oxidizing doped alumina single crystal	12/1964
Eliason, L. K. Zellner, G. C.	A Survey of High Temperature Ceramic Materials for Radomes	(MLTDR64296) AD60719	Temperature ^O F % alumina ~6 (85-99.9)	9/1964
Slonim, A. I. (Editor)	Proceedings of the OSU-RTD Symposium on Electromagnetic Windows. 2-4 June, 1964, Vol. III. Session V-Fabrication and Testing of Airborne Radomes	(AF33(615)1081) AD605391 n	Temperature ^O F (100-1600) a 9.375 G.C.	6/1964
Riley, R. M.	Measurement of the Dielectric Constant of Aluminum Oxide	(Nord-16498) AD651005	Total attenuation at cut off speci-mens.	8/1962

Consultants Bureau, a division of Plenum Publishing Corp., 227 West 17th Street, New York, NY 10011.

LOSS TANGENT

Author	Title	Journal Vol. or Series	Description (Ind. Variables)	Date Published
Degtyareva, E. V. et al	Selecting Alumina Grades for Making Densely Sintered Alumina Ceramics	Ogneupory n7 July 1970, p.39-45	Apparent density g/cm ³ (3.7-3.9)	7/1970
Sarkar, B. K. Glinn, T. G. J.	Fatigue Behavior of High Al ₂ O ₃ Ceramics	Trans-Brittain Ceramics Society Vol. 69, n5, Sept. 1970, p.199-203	Dwell time at T ₂ OC (170-250) Time min (4-9); Quenching bath at 18 C	3/1969
Iglesias, J. Westphal, W. B.	Supplementary Di- electric-Constant and Loss Measure- ments on High Temperature Materials	(NONR 1841(10), AF33(615)2199) AD650230	Temperature ^O C (0-700) Density gm/cc (3.23-3.84) % of alumina (99-99.999)	1/1967
Tallan, N. M. Graham, H. C.	Interfacial Polari- zation and Electri- cal Conductivity in Sapphire	(Rept. No. ARL-65- 262) AD630345	Pretreatment:- reducing or oxidizing	12/1964
Snow, G. S. Cutler, I. B.	Dielectic Loss in Magnesium Oxide and Sapphire	(Non 128806) AD609617	Room temperature of different specimens	11/1964
Eliason, L. K. Zellner, G. C.	A Survey of High Temperature Ceramic Materials for Radomes	(ML-TDR64-296) AD607619	Temperature ^O F (200-2800) % of alumina (99.85-99.9)	9/1964
Slonim, A. I.	Proceedings of the OSU-RTD Symposium on Electromagnetic Windows. (7th) 2-4 June, 1964. Vol.III Session V.	(AF33(615)1081) AD605391	Temperature ^O C (100-1600) at 9.375 Gc.	6/1964
Mitek, J. T.	Aluminum Oxide (Data Sheets)	(AF33(615)1235) N64-18384	Under different conditions (room temperature)	3/1964

MAGNESIUM OXIDE

YOUNGS MODULUS

Author_	Title	Journal Vol. or Series	Description (Ind. Variables)	Date <u>Published</u>
Rudick, Alfred et al	The Evaluation and Interpretation of Mechanical Properties of Brittle Materials	(AF33(615)-2335) AD-670-140	Temperature ^O C (0-1200)	1969
Lynch, J. F. et al	Engineering Properties of Ceramics, Databook to Guide Materials Selection for Structural Applications	(AF33(615)-2316) AD-803-765	Temperature ^O C (0-4000) Density % (0-100)	1966
Naohiro Soga Anderson, O. L.	Simplified Method for Calculating Elastic Moduli of Ceramic Powder from Compresi- bility and Debye Temperature Data	(AF33(615)-1700) AD-638-280	Porosity % (0-6)	1965
Christian, W. J. et al	Evaluation of Thermal Protective Systems for Advanced Aerospace Vehicles	(AF33(675)-9507) AD-627-140	Temperature ^O R (0-5000) Grain size	1965
Neuber, H. Wimmer, A.	Experimental Investi- gations of the Behavior of Brittle Materials at Various Ranges of Temperature	(AF61(052)-875) N68-26125	Temperature ^O C (-200-1400) Porosity	1965
(Editor) Hague, J. R. et al	Refractory Ceramics for Aerospace: A Materials Selection Handbook	The American Cera- mic Society, Inc. Columbus, Ohio	Temperature ^O F (0-3500)	1964
Stokes, F. J.	Microstructure and Mechanical Properties of Ceramics	(NONR-4076(00)) N64-17441	Porosity % (0-28)	1963

REPRODUCIBILITY OF THE ORIGINAL PAGE IS FOOR

TENSILE AND COMPRESSIVE STRENGTH

		•		
Author	Title	Journal Vol. or Series	Description (Ind. Variables)	Date Publis
Stokes, R. J.	Microstructure and Mechanical Properties of Ceramics	(NONR-4076(00)) N64-17441	Surface disloca- tions Heat treatment	1973
Rice, R. W.	Machining, Surface Work Hardening, and Strength of MgO	Journal of the American Ceramic Society, Vol. 56.	Porosity Máchining methods Grainsize µm (0-1000)	1973
Malyshkin, Y. K. Bas'yas I.P.	High Temperature Fatigue of Magnesia Refractories	Translated from Ogneupory, No.8, August	Temperature ^O C (100-1000)	1972
Rhodes, W. H. Cannon, R. M.	Microstructure Studies of Refrac- tory Polycrystalline Oxides	(NO0019-70-C0171) AD-727-618	Test environment	1971
Rice, R. W.	The Compressive Strength of Ceramics	A72-22388 Proceedings, Sixth Univ. Conf. on Ceramic Science, NCSU, Raleigh, N.C. Dec. 7-9, 1970, p.195-227.	Tables	1971
Langdon, T. G. Pask, J. A.	Effect of Microstruc- ture on Deformation of Polycrystalline MgO	Journal of the American Ceramic Society, Vol. 54, No.5, pp.240-246.	Temperature ^o C (-200-1600). Strain	1971
Pask, J. A.	Nature, Status, and Selection of Ceramic Materials	N-67-27041 Advisory Group for Aerospace Research and Development, Lecture Series No.5	Strain	1971
R. J.	Effects of Surface Finishing on Mechanical and Other Physical Properties of Ceramics	(N00014-69-C-0123 N71-21221	Grainsize	1970
Davidge, R. W. Evans, A. G.	The Strength of Ceramics	A71-11601 Materials Science and Engineering, Vol. 6, Nov. 1970, p.281-298.	Grainsize µm (10-500) Termperature ^O C (0-1800)	1970

TENSILE AND COMPRESSIVE STRENGTH

	Author	Title.	Journal, Vol. or Series	Description (Ind. Variables)	Date Publish
	Wiederhorn, S. M.	, Fracture of Ceramics	N69-28436 Mechanical and Thermal Properties of Ceramics, May. 1969, p.217-292.	Test environment Grainsize	1969
•	Neuber, H. Wimmer, A.	Experimental Investi- gations of the Behavior of Brittle Materials at Various Ranges of Temperature	(AF61(052)875) N68-26125	Temperature ^O C (-200-14000) Porosity	1968
•	Rudnick, A. et al	The Evaluation and Interpretation of Mechanical Properties of Brittle Materials	(AF33(615)2335) AD-670-190	Grain Diameter Strain	1968
	Leipold, M. H. et al	The Effect of Grain Boundaries on Mechanical Behavior in Polycrystalline Ceramics	(NAS7-100) N68-11944	Microstructure	1967
	Rice, R. W. Hunt, J. G.	Identifying Optimum Parameters of Hot Extrusions	(NAS7-276) N67-27371	Grainsize µ (2-400) Firing temp. OF (2000-2800) Temperature OF (2000-2900)	1967
	Lynch, J. F. et al	Engineering Properties of Ceramics, Databook to Guide Materials Selection for Structural Applications	(AF33(615)2316) AD-803-765	Temperature ^O F (0-4000) Grain size µ (0-200)	1966
	Lange, F. F.	Intrinsic Brittle Strength of Magnesia Bicrystals	(NONR-656(27)) AD-643-078	Tables	1966
	Rhodes, . W. H. et al	Microstructure Studies of Poly- crystalline Refractory Oxides	(NOW-65-0316)F) N66-27434	Tables	1966
	Christian, W. J. et al	Evaluation of Thermal Protective Systems for Advanced Aero- space Vehicles	(AF33(675)≈9407) AD-627-140	Temperature ^O R (0-5000)	1965

TENSILE AND COMPRESSIVE STRENGTH

Author	Title	Journal Vol. or Series	Description (Ind. Variables)	Publsihe
Burte, H. M. Jacobsen, L. A.	The Investigation of Microstructure in Structural Ceramics	N65-27965 The American Cera- mic Society, April, 1964	Temperature ^O C (0-1500) Grain size µ (0-200)	1965
Stokes, R. J. Li, C. H.	Dislocation of Configurations and the Initiation of Yielding in Magnesium Oxide	(NONR-4076-00) AD-601-863	Strain	1964
(Editor) Hague, et al	Refractory Ceramics for Aerospace: A Materials Selection Handbook	The American Cera- mic Society, Inc., Columbus, Ohio	Temperature ^O F (0-2500)	1964
Parker, E. R.	Mechanical Behavior of Solids	N63-19993 Proceedings, The American Ceramic Society, N.Y. April, 1962	%Elongation (0-6)	1963
Snyder, M. J. et al	Investigation of Sinterable MgO Powders and Ceramics Made from Them	(AF33(616)-7733) N63-12406	Mfg. process (Table)	1962
	FLEXURA	L STRENGTH	t.	
Koerneŕ, R. M.	A New Pressing Method: Triaxial Compaction	Ceramic Bulletin, Vol. 52, No.7, pp.566-569.	Theoretical density %(30-50)	1973
Rice, R. W.	Machining, Surface Work Hardening, and Strength of MgO	Journal of The American Ceramic Society, Vol. 56	Porosity Grain size µm (0-1000)	1973
Wiederhorn S. M.	, Fracture of Ceramics	N69-28436 Mechanical and Thermal Properties of Ceramics, May, 1969.	Grain size Test environment	1969
Lynch, J. F. et al	Engineering Properties of Ceramics, Databook to Guide Materials Selection for Structural Applications	(AF33(615)2316) AD-803-765	Temperature ^O F (0-4000) Grain size µ (0-200)	1966

FLEXURAL STRENGTH

Author	Title	Journal Vol. or Series	Description (Ind. Variables)	Date <u>Published</u>
Rhodes, W. H. et al	Microstructure Studies of Poly- crystalline Refractory Oxides	(NOW-65-0316-F) N66-27434	Tables	1966
Christian, W. J. et al	Evaluation of Thermal Protective Systems for Advanced Aero- space Vehicles	(AF33(675)-9407) AD-627-140	Temperature ⁰ k (0-5000) Grain size	1965
Vasilos, T. et al	Microstructure Studies of Poly- crystalline Refractory Oxides	(NOW-62-0648-C) N63-16176	Grain size µ (1-1000)	1962
	MODULUS_	OF RUPTURE		
Kessler, J. B. et al	Tne Effects of Microstructure on the Fracture Energy of Hot Pressed MgO	(N00014-68-A-0146) AD-768-840	Firing temp. ^O F (2000-3200)	1973
Rice, R. W. Hunt, J. G.	Identifying Optimum. Parameters of Hot Extrusions	(NAS7-276) N67-27371	Tables Grain size µ (2-400) Temperature	1967
Snyder, M. J. et al	Investigation of Sinterable MgO Powders and Ceramics Made from Them	(AF33-616-7733) N63-12406	Tensile strength (0-24 x 10 ³) psi	1962
	BULK	MODULUS		
Speteler, H. A. Anderson, D. L.	Discrepancies in Elastic Constant Data for MgO Poly- crystals and Single Crystals	Journal of The American Ceramic Society, Vol. 54, No. 10,pp.520-525, Oct., 1971.	Temperature ^O K (0-1200)	1971
Neuberger, M. Carter, D. B.	Magnesium Oxide	(F33615-68-C-1225) AD-698-343	Table	1969
Schreiber, E. Anderson, O. L.	Revised Data on Polycrystalline Magnesium Dxide	(AF49-638-1355) AD-671-472	Table	1968

SHEAR MODULUS

Author	Title	Journal Vol. or Series	Description (Ind. Variables)	Date Publishe
Koerner, R. M.	A New Pressing Method: Triaxial Compaction	Ceramic Bulletin, Vol. 52, No. 7, pp.566-569.	Density % (45-70)	1973
Stokes, R. J.	Microstructure and Mechanical Properties of Ceramics	(NONR-4076(00)) N64-17441	Porosity % (0-28)	1973
Neuberger, M. Carter, D. B.	Magnesium Oxide	(F33615-68-C-1225) AD-698-343	Table	1969
Lynch, J. F. et al	Engineering Properties of Ceramics, Databook to Guide Materials Selection for Structural Applications	(AF33(615)-2316) AD-863-765	Temperature ⁰ F (0-4000)	1966
Christian, W. J. et al	Evaluation of Thermal Protective Systems for Advanced Aerospace Vehicles	(AF33(675)-9607) AD-627-140	Temperature OR (0-5000)	1965
(Editor) Hague, J. R.,	Refractory Ceramics for Aerospace: A Materials Selection Handbook	The American Ceramic Society, Inc., Columbus, Ohio	Temperature ^O F (0-2500)	1964
Naohiro Soga Anderson, O. L.	Simplified Method for Calculating Elastic Moduli of Ceramic Powder from Compressibility and Debye Temperature Data	(AF33(615)-1700) AD-638-280	Porosity % (0-6)	1963
	FRACTU	RE ENERGY		
Kessler, J. B. et al	The Effects of Microstructure on the Fracture Energy of Hot Pressed Mg0	(N00014-68-A-0146) AD-768-840	Grain size µm (0 -20) Anneal temp. ⁰ C (100-1200) % Cross sectional area (0-50)	1973
	Effects of Surface Finishing on Mechani- cal and Other Physical Properties of Ceramics	(N00014-69-C0123) N71-21221	Grain size .	1970

FRACTURE ENERGY				6
Author	Title	Journal Vol. or Series	Description	Date Published
Davidge, R. W. Evans, A. G.	The Strength of Ceramics	A71-11601 Materials Science and Engineering, Vol.6, Nov.1970, p. 281-298	Grain size.µm (0-500) Temperature ^O C (0-1800)	1970
Rudnick, A. et al	The Evaluation and Interpretation of Mechanical Properties of Brittle Materials	(AF33(615)-2335) AD-670-190	Grain diameter	1968
Leipold, M. H. et al	The Effect of Grain Boundaries on Mechanical Behavior in Polycrystalline Ceramics	(NAS7-100) N68-11944	Grain size	1967
Christian, W. J. et al	Evaluation of Thermal Protective Systems for Advanced Aerospace Vehicles	(AF33(657)-9407) AD-627-140	Grain size	1965
	WEIBULL	PARAMETERS		
Schneider, S. J. Rice, R. W. (Editors)	The Science of Cera- mic Machining and Surface Finishing	National Bureau of Standards, Special Publication 348, Washington, D.C., May, 1972.	exponent a and velocity exponent	1972
	HARDNESS (KM	OOP & VICKERS)		
Rice, R. W.	The Compressive Strength of Ceramics	A72-22388 (From Proceedings of Sixth University Conference on Ceramic Science, Plenum Press, New York, pp. 195-227)	, -	1971
Neuberger, M. Carter, D. B.	Magnesium Oxide	(F33615-68-C-1225) AD-698-343	Table	1969
Groves, G. W. et al	The Mechanical Properties of Ceramic Alloys	(NONR-760-28) AD-628-396	Annealing time	1966

HARDNESS (KNOOP & VICKERS)

. Author	Title	Journal Vol. or Series	Description (Ind. Variables)	Date Published
de Lai, A. J. .et al	Synthesis of New Solid-state Materials by Ultrahigh Pressure Techniques	(AF19(628)-2943) N67-17660	Temperature ^O C (0-1100) Grain size _O (0-2000 Å)	1966
Kendall, E. G. McClelland	Non-metallic Mate- rials for High Temperature Structu- ral Applications	(AF04-695-264) AD-603-239	Table	1964
	THERMAL (CONDUCTIVITY		
Neuberger, M. Carter, D. B.	Magnesium Oxide	(F33(615)-68-C-122 AD-698-343	5)Temperature ^O K (5-500)	1969
Flynn, D. R.	Thermal Conductivity of Ceramics	N69-28430 Mechanical and Thermal Properties of Ceramics, May, 1969, 0.63-123.	Temperature ^O K (300-2100)	1969
Duderov, I. D. Poluboya- rinov, D. N.	Heat Conductivity of Pure Oxide Ceramics	AD-694-833 Edited Trans. of Heavy Duty Refrac- tory Materials, Moscow, 1966.	Temperature ^O C (300-900)	1969
Van Vlack, L. H.	Introduction: Ceramic Micro- structures	(NONR-1224(47)) AD-679-846	Fraction of MgO content (0-1.0)	1968
Lynch, J. F. et al	Engineering Properties of Ceramics, Databook to Guide Materials Selection for Structural Applications	(AF33(615)-2316) AD-803-765	Temeprature ^O F (0-4000)	1966
Pusto- valov, V. V.	Thermal Conducti- vity of Refractory Materials	(NSF-C-466) N71-15034	Pressure $(10^{-4}-10^{33})$ mm Hg	1966
Christian, W. J. et al	Evaluation of Thermal Protective Systems for Advanced Aerospace Vehicles	(AF33(675)-9407) AD-627-140	Temperature ^O R (0-5000)	1965

THERMAL CONDUCTIVITY

Author	Title	Journal Vol. or Series	Description (Ind. Variables)	Date Publish
Brown, D. A.	Evaluation or Thermal Stress Resistance in Potential Radome Materials	(AF33(675)-9407) AD-613-009	Temperature ^O C (0-1200)	1965
Evans, J. L.	A Feasibility Study on the use of Powders as Heat Transfer Media in Irradiation Capsules	International Research and Development Co., LTD., Newcastle, England.	Temperature ^O C (0-1200)	1965
Loser, J. B. et al	Thermophysical Properties of Thermal Insulating Materials	(AF33(657)-10478) AD-601-535	Temperature ⁰ R (0-4800)	1964
(Editor) Hague, JR. et al	Refractory Ceramics for Aerospace: A Materials Selection Handbook	The American Ceramic Society, Inc., Columbus, Ohio.	Temperature ^O F (0-4000)	1964
	COEFFICIENT OF	LINEAR EXPANSION		
Shakhtin, D. M. et al	Study of the Thermal Expansion of Refrac- tory Oxides at High Temperatures	AD-714-741 Edited Trans. of Ukranskii Nauch Issledovatelskii Institut Ogeneupor	3±5	1970
Schaake, H. F.	The Study of Thermal and Mechanical Pro- perties of Selected Solids from 4 Degrees to the Melting Point	(AF19(628)-5663) AD-699-579	Temperature K (0-300)	1969
Neuberger, M. Carter, D. B.	Magnesium Oxide	(F33(615)-68-C-122 AD-698-343	5)Temperature ^{:o} K (20-1200)	1969
Kirby, R. K.	Thermal Expansion of Ceramics	N69-28429 Mechanical and Thermal Properties Ceramics, National Bureau of Standard Washington, D. C.		1968
Sardi, Otto	Re-evaluation of the Crystal Structure of Selected Oxide Compounds	(AF-33(657)8941) AD-817-638	Temperature ^O C (0-1200)	1967

COEFFICIENT OF LINEAR EXPANSION

Author	Title	Journal Vol. or Series	Description (Ind. Variables)	Date Publishe
Lynch, J. F. et al	Engineering Properties of Ceramics, Databook to Guide Materials Selection for Structural Applications	(AF33(615)-2316 AD-803-765	Temperature ^O F (0-4000)	1966
Christian, W. J. et al	Evaluation of Thermal Protective Systems for Advanced Aerospace Vehicles	(AF33(675)-9407) AD-627-140	Temperature ^O R (0-5000)	1965
Loser, J. B. et al	Thermophysical Pro- perties of Thermal Insulating Materials	(AF33(657)-10478) AD-601-535	Temperature OR (0-4800)	1964
(Editor) Hague, . J. R. et al	Refractory Ceramics for Aerospace: A Materials Selection Handbook	The American Ceramic Society, Inc., Columbus, Ohio	Temperature ^O F (0-4000)	1964 -
Note:	Some data is in terms of	linear strain.		
	SPECI	FIC HEAT		
Duderov, I. G. Poluboya- rinov, D. N.	Heat Conductivity of Pure Oxide Ceramics	AD 694-833 Edited Trans. of Heavy Duty Refrac- tory Materials (1968)	Temperature ^O C (350-1000)	1969
Lynch, J. F. et al	Engineering Properties of Ceramics, Databook to Guide Materials Selection for Structural Applications	(AF33(615)-2316) AD-803-765	Temperature ^O F (0-4000)	1966
Christian, W. J. et al	Evaluation of Thermal Protective Systems for Advanced Aerospace Vehicles	(AF33(657)-9407) AD-627-140	Temperature ^O K - (0-5000)	1965
Kendall, E. G. McClelland, J. D.	Non-metallic Mate- rials for High Temperature Struc- tural Applications	(AF04-695-269) AD-603-239	Tables	1964

SPECIFIC HEAT

Author Title	Journal Vol. or Series	Description (Ind. Variables)	Date <u>Publishe</u>
(Editor) Refractory Ceramics for Aerospace: A Materials Selection Handbook	The American Cera- mic Society, Inc., Columbus, Ohio.	Temperature ^O F (0-5000)	1964
Loser, Thermophysical Pro- J. B., perties of Thermal et al Insulating Materials	(AF33(657)-10478) AD-601-535	Temperature ^O R (0-4800)	1964
EMITTANCE	(TOTAL & SPECTRAL)		
Neuberger, Magnesium Oxide M. Carter, D. B.	(F33615-68-C-1225) AD-698-343	Temperature ^O K (0-2400) Wave length µ (0-50)	1969
Richmond, Thermal Radiation J. C. Properties of Ceramic Materials	N69-28431 Mechanical and Thermal Properties of Ceramics, May 1969, pp. 125-138	Temperature ^O K (400-1000) Wave length µ (0-15)	1969
Flynn, Thermal Conducti- D. R. vity of Ceramics	N69-28430 Mechanical and Thermal Properties of Ceramics, May 1969, p. 125-138	Porosity (012)	1969
Christian, Evaluation of the W. J. Thermal Protective et al Systems for Advanced Aerospace Vehicles	(AF33(657)-9407) AD-627-140 d	Temperature ^O K (0-5000)	1965
Folweiler, Thermal Radiation R. C. Characteristics of Mallio, Transparent, Semi- transparent and Translucent Material under Non-isothermal Conditions		Wave length μ (0-14)	1964
oser, Thermophysical J. B., Properties of Therma et al Insulating Materials	1 AD-601-535	Temperature ^O R (0-4800)	1964

THERMAL DIFFUSIVITY

Author	<u>Title</u>	Journal Vol. or Series	Description (Ind. Variables)	Date <u>Publishe</u>
Litovskii, E. Ya. Landa, Ya. A.	Determination of the Thermal Diffusivity Coefficient of Mag- nesia and Magnesio- spinel Refractories	Translated from Ogneupory, No. 10, pp. 12-15, October, 1969	Temperature ^O C (200-8100)	1969
Loser, J. B., et al	Thermophysical Pro- perties of Thermal Insulating Materials	(AF33(657)~10478) AD-601~535	Temperature ^O R (0-4800)	1964
	DIELECTRI	C CONSTANT		
Osburn, C. M. Vest, R. W.	Electrical Properties of Single Crystals, Bicrystals and Polycrystals of MgO	Journal of The American Ceramic Society, Vol. 54 Sept. 1971.	Temperature ^O C (600-1600) Frequency (.1-100) KHZ	1971
Neuberger, M. Carter, D. B.	Magnesium Oxide	(F33615-68-C-1225) AD-698-343	Temperature (90 ^o K-700 ^o C) Frequency (0-4.0 x 10 ¹²)HZ	1969
Akawie, R. I. Milek, J. T.	Dielectric Constants of Rubbers, Plastics, and Ceramics	(F33615-68-C-1225) AD-735-628	Tables	1969
Guile, D. L.	Semiconducting Mate- rials. Part III: An Investigation of the Dielectric Properties of Single Crystal Versu Polycrystalline Materia		Temperature ^O C (0-500) Frequency (10-100,000)HZ	1965

LOSS TANGENT

Author	Title	Journal Vol. or Series	Description (Ind. Variables)	Date <u>Publish</u>
Neuberger, M. Carter, D. B.	Magnesium Oxide	(F33615-68-C-1225) AD-698-343	Temperature ^O C (0-700) Frequency (1-100)KHZ	1969
Guile, D. L.	Semiconducting Mate- rials. Part III: An Investigation of The Dielectric Properties of Single Crystal Versu Polycrystalline Materia	(N65-25980 •	Temperature ^O C (0-700) Frequency (10-100,000)HZ	1965
Snow, G. S. Cutler, I. B.	Dielectric Loss in MgO and Sapphire	(NONR-128806) AD-609-617	Frequency (.2-20)KHZ Temperature Time	1964

SILICON NITRIDE

POISSONS RATIO

Author	Title	Journal Vol. or Series (Description Ind. Variables)	Date Published
McLean, A. F. et al	Brittle Materials Design, High Tempera- ture Gas Turbine	AMMRC-CTR-72-19 **	Temperature ^O C (0-1400)	9/1972
Lange, F. F.	Dense Silicon Nitride and Silicon Carbide: Some Critical Proper- ties for Gas Turbine Application	ASME Paper 72-GT-56	Room Temperature, F (0-2600)	3/1972
Walton, J. D., Jr.	The State of Technology of Ceramic Radomes, Their Use and Possibilities for the Future	International Conference on Electromagnetic Windows; 2nd Paris, France Sep. 8-10, 1971 Proceedings. Vol. 2 A73-25286	At different temperature ^O F (0-2500)	1972
	<u>YOUNGS</u>	MODULUS		
McLean, A. F. et al	Brittle Materials Design, High Tempera- ture Gas Turbine	AMMRC-CTR-74-26	<pre>lemperature OF Elastic strain rate/min (0.01-0.0001)</pre>	4/1974
McLean, A. F. et al	Brittle Materials Design, High Tempera- ture Gas Turbine	AMMRC-CTR-73-32 **	Temperature ^O F (0-4000)	9/1973
Caw, R. B. et al	Silicon Nitride Materials for Gas Turbine Components	ASME Paper 73-G7-47 (A73-33508)	General Proper- ties (Table form)	4/1973
McLean, A. F. et al	Brittle Materials Design, High Tempera- ture Gas Turbine	AMMRC-CTR-73-!	Temperature ^O F (80-800) Si ₃ N ₄ %(0-100)	3/1973

^{**} Army Materials and Mechanical Research Center, Watertown, Mass. 02172

YOUNGS MODULUS

Author	Title	Journal Vol. or Series (Description Ind. Variables)	Date Published		
McLean, A. F. et al	Brittle Materials Design, High Tempera- ture Gas Turbine	AMMRC-CTR-72-19	Temperature ⁰ F (200-2800)	9/1972		
Lange, F. F.	Dense Si ₃ N ₄ and SiC: Some Critical Proper- ties for Gas Turbine Application	ASME Paper 72-GT-56	Room temperature	3/1972		
Walton, J. D., Jr.	The State of Technology of Ceramic Radomes, Their Use and Possibilities for the Future	International Conference on Electromagnetic Windows; 2nd Paris, France Sep. 8-10, 1971*** A73-25286	Temperature (0-2500) °F	1972		
Slonim, A. I.	Proceedings of the OSU-RTD Symposium on Electromagnetic Windows. 2-4 Jun 64. Vol. I. Session I-Objectives and New Techniques. Session II Materials for High Temperature Applications.	(AF33(615)1081) AD605390	(Table form) General proper- ties	·6/1964		
(Editor) Hague, J. R. et al	Refractory Ceramics for Aerospace: A Materials Selection Handbook	The American Ceramic Society Columbus, Ohio	Mechanical properties	1964		
TENSILE and COMPRESSIVE STRENGTH						
McLean, A. F. et al	Brittle Materials Design, High Tempera- ture Gas Turbine	AMMRC-CTR-74-26	$m(4.07-10.99)$ Strain 10^{-3} $(0-4)$ Burst speed R.P.M. $(96000-91700)$ Effective volume under stress KV $in^3(10^{-4}-10^0)$	4/1974		

^{**} Army Materials and Mechanical Research Center, Watertown, Mass. 02172
*** Proceedings V.2.

TENSILE and COMPRESSIVE STRENGTH

Author	Title	Journal Vol. or Series	Description (Ind. Variables)	Date Published
McLean, A. F. · et al	Brittle Materials Design, High Tem- perature Gas Turbine	AMMRC-CTR-73-32' **	Log Kv (in ³) (10 ⁻⁵ -10 ⁰), Strain rate in/in (0.0001-0.01), Temp. OF (500-4000)	9/1973
Lange, F. F. Terwil- liger, G. R.	Fabrication and Properties of Silicon Compounds	(N0019-72-C-0278) AD764639	Time of Loading min (0-24)	4/1973
McLean, A. F. et al	Brittle Materials Design, High Tem- perature Gas Turbine	AMMRC-CTR-73-9 **	Strain rate in/in /min (.0001-0.01)	-
McLean, A. F. et al	Brittle Materials Design, High Tem- perature Gas Turbine	AMMRC-CTR-72-19 . **	Testing tempera- ture OF (200- 2400) Strain rate in/in/ min (10 ⁻⁴ -10 ⁻¹)	9/1972
Lange, F. F.	Dense Silicon Nitride and Silicon Carbide: Some Critical Proper- ties for Gas Turbine Application	ASME Paper 72-GT-56	Testing tempera- ture (0-2600) ⁰ F	3/1972 ·
Walton, J. D., Jr.	The State of Technology of Ceramic Radomes, Their Use and Possibilities for the Future	International Conference on Electromagnetic Windows. 2nd; Paris, France. Sep. 8-10, 1971*** A73-25286	Testing of the strength at different condi- tions (0-2500) F	1972
Lange, F. F.; Terwil- liger, G. R.	Fabrication and Properties of Silicon Compounds	(N00019-71-C-0107) AD738-865	Density gm/cc (3.01-3.25)	12/1971

^{**} Army Materials and Mechanical Research Center, Watertown, Mass. 02172 *** Proceedings V.2.

TENSILE and COMPRESSIVE STRENGTH

		_ 80 _		ь.
Author	Title	Journal Vol. or Series	Description (Ind. Variables)	Date Published
Lindley, M. W. Godfrey, D. J.	Silicon Nitride Ceramic Composites with High Toughness	Ministry of Defense/Navy/ Admiralty Mate- rials Labs, Poole, Dorset, England. Vol. 229	Mid-span deflection mm (0-0.5)	1/1971
Mehan, R. L. Herzog, J. A.	Mechanical Proper- ties of Whiskers	"Whisker Techno- logy" A71-14946	Area µ ² (0.1-10.0)	1970
(Editor) Hague, J. R. et al	Refractory Ceramics for Aerospace: A Materials Selection Handbook	The American Ceramic Society Columbus, Ohio	Room and dif- ferent testing temperature (0-2500) F	1964
	FLEXURAL	STRENGTH		
McLean, A. F. et al	Brittle Materials Design, High Tem- perature Gas Turbine	AMMRC-CTR-74-26 **	Density gm/cc (3.20-3.25) Average strength (psi)(14200-16200% of hydrogen (0-0xygen content wt Volume solid % (6 Material standard microns (-20-40)	85) ; %. 50-62)
McLean, A. F. et al	Brittle Materials Design, High Tem- perature Gas Turbine	AMMRC-CTR-73-32	Log Kv $(in^3)10^{-5}$ - 10^0 Density gm/co 3.3-3.4 Temp $F(0-2800)$ Stress rate psi/min $(10^0-2.3 \times 10^5)$ Corrosion Time at $2000 \times F$ hr. $(90-250)$	9/1973 :
Lange, F. F.; Terwil- liger, G. R.	Fabrication and Properties of Silicon Compounds	(N00019-72-C-0278) AD764639	Load Kgm. (0-350) Normalized in- dentor load 0-50 Kgm.	4/1973

^{**} Army Materials and Mechanical Research Center, Watertown, Mass. 02172

REPRODUCIBILITY OF THE ORIGINAL PAGE IS POOR

FLEXURAL STRENGTH

Author	Tit]e	Journal Vol. or Series	Description (Ind. Variables)	Date Published
Koerner, R. M.	A New Pressing Method: Triaxial Compaction	Materials and Equipment Division No. 22-M-72	At temperature 1200°C, Time in hours (0:1-100	3/1973)
McLean, A. F. et al	Brittle Materials Design, High Tem- perature Gas Turbine	AMMRC-CTR-73-9 **	Temperature OF (0-3200) (Ca+Na+K) wt % (0.01-1.0)	3/1973
McLean, A. F. et al	Brittle Materials Design, High Tem- perature Gas Turbine	AMMRC-CTR-72-19	Density gm/cc 2.6-3.2;% of T.D. (84-99.5) Grainsize (micron (1.1-1.6) Temp. F (200-2800) Loadin ratio in terms of cross head speed (in/min)(0.0002-0.002)	
Lange, F. F.	Dense Si ₃ N ₄ and SiC: Some Critical Proper- ties for Gas Turbine Application.	ASME Paper 72-GT-56	Temperature ^O F (0-2600)	3/1972
Walton, J. D., Jr.	The State of Technology of Ceramic Radomes, Their Use and Possibilities for the Future	International Conference on Electromagnetic Windows. 2nd; Paris, France. Sep. 8-10, 1971***	Temperature ^O F (0-2500)	1972
Lange, F. F. Terwil- liger, G. R.	Fabrication and Properties of Silicon Compounds	(N00019-71-C-0107) AD738-865	Milling time hr.(0-72)	12/1971
Lindley, M. W. Godfrey, D. J.	Silicon Nitride Ceramic Compsites with High Toughness	Ministry of Defense/Navy/ Admiralty Mate- rials Labs, Poole, Dorset, England, Vol. 229	Mid-span deflection (mm)(0-0.5)	1/1971

^{**} Army Materials and Mechanical Research Center, Watertown, Mass. 02172 *** Proceedings, Vol. 2, p.279-308.

FLEXURAL STRENGTH ·

Auth	or <u>Title</u>	Journal Vol. or Series	Description (Ind. Variables)	Date Publishe			
(Edito Hague, J. R. et al		The American Ceramic Society Columbus, Ohio	Mechanical properties	1964			
	MODULUS of RUPTURE						
McLean A. F. et al	Brittle Materials Design, High Tem- perature Gas Turbine	AMMRC-CTR-74-26 **	Life hr. $(10^{-4}$ - $10^{-1})$ Stress 1000 psi Time hrs. (4-20)	4/1974			
Caws, R. B. et al	Silicon Nitride Materials for Gas Turbine Components	ASME Paper 73-GT-47 (A73-33508)	Testing tempera- ture C (0-2000)	4/1973			
McLear A. F. et al	, Brittle Materials Design, High Tem- perature Gas Turbine	AMMRC-CTR-73-9	Testing density gm/cc (3.16-3.20)	3/1973			
McLear A. F. et al	Design, High Tem- perature Gas Turbine	AMMRC-CTR-72-19 **	Testing tempera- ture F (2300- 2500) Stress 1000 psi Time hrs.(0.8- 600)	1/1972			
Lange, F. F. Terwil liger, G. R.	Properties of -	(N00019-71-C-0107) AD764639	Density gm/cc (3.01-3.25)	12/1971			
Coe, R. R. et al	Special Ceramics 5 (Some Properties and Applications of Silicon Nitride)	British Ceramic Research Asso- ciation. Penkhull, Stoke-on-Tye.	Total pressing time sec (50-150), Time above 90% full density sec.(20-120), Hardness at 500 g load (VPN) (2200-2900)	7/1970			

^{**} Army Materials and Mechanical Research Center, Watertown, Mass. 02172

MODULUS of RUPTURE

_ Author	Title	Journal Vol. or Series	Description (Ind. Variables)	Date <u>Publishe</u> c
(Compiler) Slonim, A. I.	Proceedings of the OSURTD Symposium on Electromagnetic Windows. 2-4 June, '64, Vol I.	(AF33(615)1081) AD605390	At different testing conditions	6/1964
	FRACTURE ENERGY	and FRACTURE STRESS		
McLean, A. F. et al	Brittle Materials Design, High Tem- perature Gas Turbine	AMMRC-CTR-74-26	% Blade Ht 0-100 Time (sec)(0-50) Burst speed RPM 90000-96000	4/1974
Caws, R. B. et al	Silicon Nitride Materials for Gas Turbine Components	ASME Paper 73-GT-47 (A73-33508)	Temperature ^O C (0-2000)	4/1973
McLean, A. F. et al	Brittle Materials Design, High Tem- perature Gas Turbine	AMMRC-CTR-73-9 **	Temperature ^O C (0-1400)	3/1973
McLean, A. F. et al	Brittle Materials Design, High Tem- perature Gas Turbine	AMMRC-CTR-72-19 **	Temperature ^O F (2300-2500) Stress 100 psi (10-15)	9/1972
Ceipold, M. H. et al	Mechanical Behavior of Polycrystalline Ceramics: Brittle Fracture of SiC-Si ₃ N ₄ Materials	(NASA-CR-129671) N73-14585	Typical properties of silicon nitride (room temperature)	9/1972
Coppola, J. A. et al	Fracture Energy of . Silicon Nitrides	The American Ceramic Society (Basic science division No. 20B71)	Density (gm/cc) 2.17-3.24 Grainsize (microns 0.5-1.5 Temperature (-200-1400)°C	5/1972 s)
Lange, F. F. Terwil- liger, G. R.	Fabrication and Properties of Silicon Compounds	(N00019-71-C-0107) AD738865	Density gm/cc (3.01-3.25)	12/1971

^{**} Army Materials and Mechanical Research Center, Watertown, Mass. 02172

FRACTURE ENERGY and FRACTURE STRESS

Author	Title	Journal Vol. or Series	Description (Ind. Variables)	Date Publishe
Mehan, R. L. Herzog, J. A.	Mechanical Proper- ties of Whiskers	"Whisker Techno- logy" A71-14946	Area (micron) ² (0.1-100)	1970
	THERMAL (CONDUCTIVITY		
McLean, A. F. et al	Brittle Materials Design, High Tem- perature Gas Turbine	AMMRC-ÇTR-73-32 **	Temperature ^O C (0-1800)	9/1973
Caws, R. B. et al	Silicon Nitride Materials for Gas Turbine Components	ASME Paper 73-GT-47 (A-73-33508)	At different temperatures (and room temp.)	4/1973
McLean, A. F. et al	Brittle Materials Design, High Tem- perature Gas Turbine	AMMRC-CTR-73-9	Temperature ^O C (0-1800)	3/1973
McLean, A. F. et al	Brittle Materials Design, High Tem- perature Gas Turbine	AAMRC-CTR-72-19 **	Temperature ^O C (0-1400)	9/1972
Ceipold, M. H. et al	Mechanical Behavior of Polycrystalline Ceramics: Brittle Fracture of Silicon Nitride and Silicon Carbide Materials	(NASA-CR-129671) N73-14585	Maximum use in temperature (°C)	9/1972
Lange, F. F.	Dense Silicon Nitride and Silicon Carbide: Some Critical Proper- ties for Gas Turbine Application	ASME Paper 72-GT-56	Temperature ^O F (0-2600)	3/1972
Walton, J. D., Jr.	The State of Techno- logy of Ceramic Radomes, Their Use and Possibilities for the Future	International Conference on Electromagnetic Windows; 2nd Paris, France Sep. 8-10, 1971*** A73-25286	At different conditions, temp. F (0-2500)	1972
Loser, J. B. et al	Thermophysical `Properties of Thermal Insulating Materials	(AF33-657-10478) AD601535	Temperature ^O C (0-1500)	4/1965

 $^{^{**}}$. Army Materials and Mechanical Research Center, Watertown, Mass. 02172 *** . Proceedings, Vol. 2.

THERMAL CONDUCTIVITY

Author	Title	Journal Vol. or Series	Description (Ind. Variables)	Date <u>Published</u>
(Com- piler) Slonim, A. I.	Proceedings of the OSU-RTD Symposium on Electromagnetic Windows. 2-4 June, 1964, Vol. I.	(AF33(615)108 AD605390	Temperature ^O F (0-2400)	6/1964
(Editor) Hague, J. R. et al	Refractory Ceramics for Aerospace: A Materials Selection Handbook	The American Ceramic Society Columbus, Ohio	Temperature ^O F (0-2400)	1964
	LINEAR THER	MAL EXPANSION		
McLean, A. F. et al	Brittle Material Design, High Tem- perature Gas Turbine	AMMRC-CTR-73-9 **	Temperature ^O F (80-2500)	3/1973
Ceipold, M. H. et al	Mechanical Behavior of Polycrystalline Ceramics: Brittle Fracture of Silicon Nitride and Silicon Carbide Materials	(NASA-CR-129671) N73-14585	Maximum use in temperature (⁸ C)	9/1972
Lange, F. F.	Dense Silicon Nitride and Silicon Carbide: Some Critical Proper- ties for Gas Turbine Application	ASME Paper 72-GT-56	Temperature ^O F (75-2200)	3/1972
Walton, J. D. Jr.	The State of Technology of Ceramic Radomes, Their Use and Possibilities for the Future	International Conference on Electromagnetic Windows; 2nd, Paris, France Sep. 8-10, 1971*** A72-25286	At different conditions temp. F (0-2500)	1972
(Com- piler) Slonim, A. I.	Proceedings of the OSU-RTD Symposium on Electromagnetic Windows. 2-4 June 1964, Vol. II.	(AF33(615)1081) AD605390	Temperature ^O F (0-2400)	6/1964

^{***} Army Materials and Mechanical Research Center, Watertown, Mass. 02172
*** Proceedings, Vol. 2.

LINEAR THERMAL EXPANSION

					
	Author	Title	Journal Vol. or Series	Description (Ind. Variables)	Date Published
	Loser, J. B. et al	Thermophysical Properties of Thermal Insulating Materials	(AT-33-657-10478) AD601535	Temperature ^O C (0-1500)	4/1964
	(Editor) Hague, J. R. et al	Refractory Ceramics for Aerospace: A Materials Selection Handbook	The American Ceramic Society Columbus, Ohio	Temperature ^O F (75-3270)	1964
		. <u>SPECI</u>	FIC HEAT		
	McLean, A. F. et al	Brittle Materials Design, High Tem- perature Gas Turbine	AMMRC-CTR-73-32	Temperature ^O C (0-2800)	9/1973
•	Caws, R. B. et al	Silicon Nitride Materials for Gas Turbine Components	ASME Paper 73-GT-47 (A73-33508)	Temperature ^O C (0-1000)	4/1973
	McLean, A. F. et al	Brittle Materials Design, High Tem- perature Gas Turbine	AMMRC-CTR-73-9 **	Temperature ^O F (80-2500)	3/1973
	Lange, F. F.	Dense Silicon Nitride and Silicon Carbide: Some Critical Proper- ties for Gas Turbine Application	ASME Paper 72-GT-56	Temperature ^O F (0-2600)	3/1972
	Walton, J. D. Jr.	The State of Technology of Ceramic Radomes, Their Use and Possibilities for the Future	International Conference on Electromagnetic Windows; 2nd, Paris, France Sep. 8-10, 1971*** A73-25285	At different conditions Temperature F (0-2500)	1972
	Loser, J. B. et al	Thermophysical Properties of Thermal Insulating Materials	(AF33-657-10478) AD601-535	Temperature ^O C (0-1500)	4/1964

^{**} Army Materials and Mechanical Research Center, Watertown, Mass. 02172 *** Proceedings, Vol. 2.

SPECIFIC HEAT

Author	Title	Journal Vol. or Series	Description (Ind. Variables)	Date <u>Published</u>		
(Editor) Hague, J. R. et al	Refractory Ceramics for Aerospace: A Materials Selection Handbook	The American Ceramic Society Columbus, Ohio	Temperature ^O F (75-3270)	1964		
	TOTAL NORM	MAL EMITTANCE				
Loser, J. B. et al	Thermophysical Properties of Thermal Insulating Materials	(AF33(657)10478) AD601535	Temperature ^O C (0-1500)	4/1964		
	DIELECTE	RIC CONSTANT		-		
Walton, J. D. Jr.	The State of Techno- logy of Ceramic Radomes, Their Use and Possibilities for the Future	International Conference on Electromagetic Windows; 2nd, Paris, France Sep. 8-10, 1971***	Typical proper- ties Temperature ^O F (0-2500)	1972		
	LOSS TANGENT					
Walton, J. D. Jr.	The State of Techno- logy of Ceramic Radomes, Their Use and Possibilities	International Conference on Electromagetic Windows; 2nd, Paris, France Sep 8-10, 1971***	Typical proper- ties (at room temperature)	1972		

REPRODUCIBILITY OF THE ORIGINAL PAGE IS POOR

SILICON CARBIDE

	<u> </u>	CON CARREDE		
Author	Title	Journal Vol. or Series	Description (Ind. Variables)	Date <u>Published</u>
	. <u>P0</u>	ISSONS RATIO		
McLean, A. F. et al	Brittle Materials Design, High Tem- perature Gas Turbine	(AMMRC-CTR-72-19) **	Temperature ^O C (0-1400) Density gm/cc (3.08-3.15) Sonic velocity cm/s	6/1972 sec
	<u> </u>	JNGS MODULUS		
McLean, A. F. et al	Brittle Materials Designs, High Tem- perature Gas Turbine	(AMMRC-CTR-74-26) **	Temperature ^O F (1000-2500)	12/1973
McLean, A. F. et al	Brittle Materials Design, High Tem- perature Gas Turbine	(AMMRC-CTR-73-9)	Temperature ^O C (500-1000)	12/1972
Crane, R. L.	An Investigation of the Mechanical Pro- perties of Silicon Carbide and Sapphire Filaments	(AFML-TR-72-180) AD753-711	Temperature ^O C (0-800)	∂/1972 <u>́</u>
McLean, A. F. et al	Brittle Material Design, High Tem- perature Gas Turbine	(AMMRC-CTR-72-19) **	Temperature ^O F (0-1400)	6/1972
Larige, F. F.	Dense Si ₃ N ₄ and SiC: Some Critical Proper- ties for Gas Turbine Application	ASME Paper 72-GT-56	Room temperature, Poisson ratio (0.168-0.17)	5/1972
Coppola, J. A. Bradt, R. C.	Measurement of Fracture Surface Energy of SiC	Presented 73rd Annual Meeting- The American Ceramic Society	Room temperature	3/1972
Clougherty, E. V. et al	Research and Deve- lopment of Refractory Oxidation-Resistant Diborides	(AF33(615)-3671) AD866-558	Density gms/cc (4.6-6.2)	1/1970
** Army Ma	aterials and Mechanics	Research Center, Wat	ertown, Mass. 02172	

YOUNGS MODULUS

Author	Title	Journal Vol. or Series (Description Ind. Variables)	Date Published
Mehan, R. L. Herzog, J. A.	Mechanical Properties of Whiskers	"Whisker Technology" A71-14946	· Area μ ² (0-40)	1970
Gulden, T. D.	Mechanical Properties of Polycrystalline B-SiC	Journal of The American Ceramic Society, Vol.52, No. 1	Temperature ^O C (25-1400) Grain diameter (05)um	11/1969
Clougherty, E. V. Anthony, F. M.	Research and Develop- ment of Refractory Oxidation Resistant Diborides	(AFML-TR-68-190) AD873-010	Mechanical properties	11/1969
Rudnick, A. et al	The Evaluation and Interpretation of Mechanical Properties of Brittle Materials	(AFML-TR-67-31-6) AD670-190	Temperature ^O C (0-1200)	1/1968
Salkind, M. J.	Candidate Materials for Whiskers Composi- ties	(WVT-RR-6411) AD602-132	Density, melting point, etc.	5/1964
(Editor) Hague, J. R. et al	Refractory Ceramics for Aerospace: A Materials Selection Handbook	The American Cera- mic Society, Columbus, Ohio	- Temp <u>era</u> ture ^O F (0-2500)	1964
	TENSILE AND	COMPRESSIVE STRENGTH	<u> </u>	
McLean, A. F. et al	Brittle Material Design, High Tem- perature Gas Turbine	(AMMRC-CTR-74-26) **	Specimen sizes, effective volume under stress KV in 3 (10 ⁻⁴ -10 ⁰)	12/1973
Crane, R. L.	An Investigation of the Mechanical Pro- perties of Silicon Carbide and Sapphire Filaments	(AFML-TR-72-180) AD753-711	Temperature ^O C (0-1400)	9/1972

TENSILE AND COMPRESSIVE STRENGTH

Author	Title	Journal Vol. or Series (Description Ind. Variables)	Date Publishe	
Demin, A. V. et al	Influence of Silicon on the Structure and Properties of Carbonic Material During Heat a Thermomechanical Treat	nd	Change in the strength of samples during heat and thermochemical treatment	5/1972	
Mehan, R. L. Herzog, J. A.	Mechanical properties of Whiskers	"Whisker Technology" A71-14946	Cross sectional area μ^2 (10-100) Cleavage or eutectic solification	1970	
Clougherty, E. V. Anthony, F. M.	Research and Develop- ment of Refractory Oxidation-Resistant Diborides. Part II. Vol. VII	(AF33(615)367) AD873-010	At different therma stress for 11,100 and 7000 second trajectory	1 11/1969	
Davies, G. et al	A Study of High Modu- lus, High Strength Filaments Materials by Deposition Techniques	(NOW-640-17-6-C) AD611-757	Density of coating gm/cc (1.5-3.5)	1/1965	
MODULUS OF RUPTURE					
McLean, A. F. et al	Brittle Materials Design, High Tem- perature Gas Turbine	(AMMRC-CTR-73-9). **	Density gm/cc (3.31-3.28)	12/1972	
McLean, A. F. et al	Brittle Materials Design, High Tem- perature Gas Turbine	(AMMRC-CTR-72-19)	Specimen width in. (.2127) Specimen thickness in. (1.1-1.8) Breaking loads lbs. (50-200)	6/1972	
Coppola, J. A. Bradt, R. C.	Measurement of Fracture Surface Energy of Silicon Carbide	American Ceramic Society. Basic Science Division No. 19-B-71	Room temperature and density	3/1972	
Gulden, T. D.	Mechanical Properties of Polycrystalline B-SiC	Journal of The American Ceramic Society, Vol. 52, No.1	Grain diameter µm (1-15) Density gm/cc (2.9-3.3) Testing temp. °C (25-1400)	11/1969	

^{**} Army Materials and Mechanical Research Center, Watertown, Mass. 02172

COACTION	DDODADTI TTV	Ω	UCTOILL	DADAMETED
FRACTURE	PROBABILITY	Ōέ	METROFF	PARAMETER

			 			
	Author	Title	Journal Vol. or Series	Description (Ind. Variables)	Date Publishe	
	McLean, A. F. et al	Brittle Materials Design, High Tem- perature Gas Turbine	(AMMRC-CTR-74-26) **	Probability of failure vs. flexural stress (0-120) x 10 ³ psi for Norton hot-pressed SiC	4/1974	
	Lange, F. F. Terwilli- ger, G. R.	Fabrication and Pro- perties of Silicon Compounds	(73-9D4-SERAM-R1) AD764-639	Normalized strength $(0.5-1.5) \sigma/\sigma_0 \text{Vs.}$ Normalized indentor $(0-0.5) \text{p/p}_0$	3/1973	
	Harris, J. N. et al	Ceramic Systems for Missile Structural Applications	(N00017-70-C-4438) AD745-744	Flaw density con- stant; Weibull para- meter of SiC; Factor of safety, rq for 99% probability of survival		
THERMAL CONDUCTIVITY						
	Ceipold, M. H. et al	Mechanical Behavior of Polycrystalline Ceramics: Brittle Fracture of Silicon Nitride Silicon Carbide Materials	(NASA-CR-129671) N73-14585	Temperature ^O C (2000)	9/1972	
	Demin, A. V. et al	Influence of Silicon on the Structure and Properties of Carbonic Material Duri	(FTD-MT-24-1594-71) AD747-601 ng Heat	Silicon content % (0-5)	5/1972	
	Lange, F. F.	and Thermomechanical Tr Dense Silicon Nitride and Silicon Carbide: Some Critical Proper- ties for Gas Turbine Application	(ASME Paper 72-GT-56)	Temperature ^O F (0-2600)	5/1972	
	Christian, W. J. et al	Evaluation of Thermal Protective Systems for Advanced Aerospace Vehicles. Vol. II: Appendices	(AFML-TDR-64-204) AD627-140	Temperature ^O R (500-4000)	4/1965	
	Loser, J. B. et al	Thermophysical Properties of Thermal . Insulating Materials	(ML-TDR-64-5) AD601-535	Temperature ^O R (400-2400)	1964	

^{**} Army Materials and Mechanical Research Center, Watertown, Mass. 02172

THERMAL CONDUCTIVITY

_Author	Title	Journal Vol. or Series	Description (Ind. Variables)	Date Published
(Editor) Hague, J. R. et al	Refractory Ceramics for Aerospace: A Materials Selection Handbook	The American Ceramic Society, Columbus, Ohio .	Temperature ^O F (0-4000)	1964
	LINEAR THE	RMAL EXPANSION		·
McLean, A. F. et al	Brittle Materials Design, High Tem- perature Gas Turbine	(AMMRC-CTR-73-32) **	Temperature ^O C · (25-1400)	9/1973
McLean, A. F. et al	Brittle Materials Design, High Tem- perature Gas Turbine	(AMMRC-CTR-73-9)	Temperature ^O F (0-2400)	12/1972
Ceipold, M. H. et al	Mechanical Behavior of Polycrystalline Ceramics: Brittle Fracture of Silicon Nitride-Silicon Carbide Materials	(NASA-CR129671) N73-14585	Temperature ^O C (2000)	9/1972
Lange, F. F.	Dense Silicon Nitride and Silicon Carbide- Some Critical Proper- ties for Gas Turbine Application	(ASME Paper 72-GT-56)	Temperature ^O F · (0-2400) ·	5/1972
Christian, N. J. et al	Evaluation of Thermal Protective Systems for Advanced Aerospace Vehicles, Vol. II: Appendices	(AFML-TDR-64-204) AD627-140	Temperature ^O R (500-4000)	4/1965
Gardner, W. J.	Thermal Expansion of BeO-SiC Composite	(AF-04-695-469) AD608-653	Time hrs ₀ (1-100) at 1000 °C	10/1964
Loser, J. B. et al	Thermophysical Pro- perties of Thermal Insulating Materials	(ML-TDR-64-5) AD601-535	Temperature ^O R (400-2000)	1964
(Editor) Hague, J. R. et al	Refractory Ceramics for Aerospace: A Materials Selection Handbook	The American Ceramic Society, Columbus, Ohio	Temperature ^O F (0-4000)	1964

^{**} Army Materials and Mechanical Research Center, Watertown, Mass. 02172

SPECIFIC HEAT

Author	Title	Journal Vol. or Series (1	Description Ind. Variables)	Date <u>Published</u>
McLean, A. F. et al	Brittle Materials Design, High Tem- perature Gas Turbine	(AMMRC-CTR-73-32) **	Temperature ^O C (0-1600)	9/1973
Lange, F. F.	Dense Silicon Nitride and Silicon Carbide: . Some Critical Proper- ties for Gas Turbine . Application	(ASME Paper 72-GT-56)	Temperature ^O F (0-2600)	5/1972
Christian, W. J. et al	Evaluation of Thermal Protective Systems for Advanced Aerospace Vehicles, Vol. II: Appendices	(AFML-TDR-64-204) AD627-140	⁻ emperature ^O R (500-4000)	4/1965
Loser, J. B. et al	Thermophysical Pro- perties of Thermal Insulating Materials	ML-TDR-64-5) AD601-535	Temperature ^O R (400-2400)	1964
(Editor) Hague, J. R. et al		The American . Ceramic Society, Columbus, Ohio	Temperature ^O C (0-1600)	1964

^{**} Army Materials and Mechanical Research Center, Watertown, Nass. 02172

Unabridged Author Reference List



STATIC & CYCLIC FATIGUE OF CERAMIC MATERIALS by S. Acquaviva & R. Chait

This report concerns the static and cyclic fatigue response of two ceramic materials ${\rm Al}_2{\rm O}_3$ and hot-pressed ${\rm B}_4{\rm C}$.

Static fatigue tests were conducted in 3-point bending with a deadweight load suspended from the center of the specimen. Cyclic fatigue tests consisted of applying a load at the end of a cantilevered specimen at the rate of 15 cps.

Table I, page 1, gives the flexual strength, modulus, density and grain sizes of the two specimens.

Figure 2 is a graph of life in hours versus stress (in psi) for static fatigue.

It was found that a stress level of 60% of the reference stress would produce a life of 72 hours for Al_2O_3 . (At this stress level, life was considered infinite). For B_4C , at 75% of the reference strength, static fatigue life exceeded the arbitrary limit of 72 hours.

The results of the cyclic tests are shown in Figure 3, page 3. It was found that the threshold level for both ${\rm Al}_2{\rm O}_3$ and ${\rm B}_4{\rm C}$ was approximately 57% of the reference strength.

Scanning of the fracture surfaces by electron microscopy revealed that the fracture is both a transgranular and intergranular nature. Fracture mechanics concepts, based on the Griffith theory, were used to determine strain energy release rates and critical flaw size for the two materials.

<u>Material</u>	Strain Energy Release Rate	Critical Flaw Size
A12 ⁰ 3	.270 in-1b/sq.in.	75 µm
B _A C	.192 in-lb/sq.in.	40 µm

TENSILE TESTING OF INORGANIC WHISKERS by Iqbal Ahmad

The technique for the measurement of elastic modulus and tensile strength of the fine filaments and whiskers, using the Marsh machine, has been evaluated. Influence of heat cycle of diphenyl carbazide, gauge length of the specimen, and stiffness of the machine on the strain measurement has been determined and discussed. Tensile strength and elastic modulus data of whisker phase including NiO, $W_{18}O_{49}$, $W_{20}O_{58}$, WO_3 , CaB_6 , gamma-TaB2, beta-rhombohedral boron, and alpha Al_2O_3 , obtained by this experiment, has been presented. Problem areas in the characterization of whiskers have been indicated.

Table I, page 22: Machine stiffness using various torsion bars. Table II, page 23: Effect of remelting diphenyl carbazide on the elastic modulus values of nickel wire.

Table III, page 24: Elastic modulus of Ni wire using diphenyl carbazide and Eastman 910 with a 10mm gauge length.

Table IV: Elastic modulus of tungsten wire measured on the Marsh machine using different gauge length and correction factors from Table 4.

Table V, page 26: Gauge length effect on the elastic modulus of Ni and tungsten wire measured on the Instron machine.

Table VI, pages 27, 28: Stress-strain data on NiO whiskers.

Table VII, page 29: Stress-strain data on $\rm W_{18}^{0}_{49},\,W_{20}^{0}_{58}$ and $\rm W_{03}^{0}$ whiskers.

Table VIII, page 30: Tensile strength and elastic modulus of selected CaB_6 whiskers.

Table IX, page 31: Tensile strength and elastic modulus of boron whiskers.

Table X, page 32: Tensile strength and elastic modulus of selected gamma TaB whiskers.

Table XI, page 33: Stress-strain data on SnO₂ whisker.

Table XII, page 34: Stress-strain data on MoO₃ whisker.

Table XIII, page 35: Stress-strain data on alpha Al_2O_3 whiskers.

Figure 8, page 45: .Stress-strain curves of $\mathrm{W}_{18}\mathrm{O}_{49},\,\mathrm{W}_{22}\mathrm{O}_{88}$ and WO_3 whiskers.

Figure 10, page 47: Stress-strain curves for CaB₆.

Figure 12a and 12b, page 49: Stress-strain curves of boron whiskers.

Figure 14: Stress-strain curves of gamma TaB.

Figure 17, page 54: Stress-strain curve of SnO₂.

Figure 18, page 55: Stress-strain curve of MoO₃.

*Figure 19, page 56: Stress-strain curves of alpha ${\rm Al}_2{\rm O}_3$ whiskers.

*Figure 22, page 59: Tensile strength of alpha Al_20_3 whiskers as a function of the cross-section area (Mehan).

FRACTURE BEHAVIOR OF THERMALLY SHOCKED A1203

by John H. Ainsworth & Robert E. Moore

Strength data is observed after heating high purity $\frac{\text{Al}}{2}0_3$ specimens at temperatures varying from 150 to 500 ^{0}C and quenching in ice water.

Figure 1: Bend Strength & Tensile Strength vs. Thermal Shock Temperature Difference.

Figure 2: Strength Dispersions as a Function of Thermal Shock Temperature Difference.

(Journal of The American Ceramic Society, Vol. 52, No. 11, pp. 628-629.)

DIELECTRIC CONSTANTS OF RUBBERS, PLASTICS AND CERAMICS, A DESIGN GUIDE by R. E. Akawié & J. T. Milek

Report contains tables and charts (prepared from tabular data) of dielectric constants for various plastics, rubber, and ceramics.

Materials are arranged on the bar graphs by ascending value of the high end of their dielectric constant range. The tables are arranged in alphabetical order for materials. A table is presented for each class of material.

AD-697-686

HEAT-RESISTANT INORGANIC COATINGS (Selected Portion) by A. A. Appen

This book examines formulas, methods of application and properties of different heat resistant inorganic coatings which are able to protect structural materials from corrosion and erosion at elevated and high temperatures. The physicochemical and technological principles of the formation of inorganic coatings on solid surface from melts are also presented.

The book is intended for scientific and engineering-technical workers studying the protection of metal from corrosion and erosion in aggressive media, and also can serve as an aid for students of corresponding specialties. It can be useful for specialists in glass and ceramics.

Figure 5, page 18: Temperature-viscosity dependence of melted sodium disilicate ($Na_20.2Sio_2$).

Table 1, page 9: Change of activation energy of viscous flow with temperature.

Table 2, page 20: Viscosity of alkali-silicate melts at 1400 $^{\rm O}$ C. Table 4, page 34: Viscosity of certain metals at the melting point. Figure 11, page 40: Effect of additions of oxides of the first group on surface tension of a sodium-silicate melt 16.7 Na $_2$ 0 83.3 SiO $_2$ at 1300 $^{\rm O}$ C.

Figure 12, page 41: Influence of additions of oxides of the second group on the surface tension of sodium silicate melt 16.7 $\rm Na_20~83.3~Sio_2$. Table 6, page 44: Surface tension of free melted.

Table 7, page 44: Surface tension of a sodium-lime-silicon melts at 700° in a medium of different gases.

Figure 16, page 60: Typical curves of viscous hysteresis of melting. Table 13, page 65: Wetting of steel by fused sodium silicate (30 $Na_20.70 Sio_2$) at 910^{0} .

Table 57, page 142: Averaged partial numerical factors for calculation of coefficient of expansion and elastic modulus of nitreous silicates.

(Ceramic Bulletin, Vol. 49, No. 7, (1970), pp. 664-669.)

PERMEABLE ALUMINA REFRACTORIES by W. T. Bakker & G. E. D. Snyder

The development of permeable high alumina refractories for blowing gases through molten iron or steel contained in a ladle is discussed. Also some data given on MOR vs. temperature.

Figure 3: Airflow & Permeability vs. Inlet Pressure

Figure 4: Effect of forming pressure on density, porosity, and strength.

Figure 5: Effect of forming pressure on permeability.

Figure 7: MOR vs. Temperature

A NEW AXIAL TENSION TESTER FOR BRITTLE MATERIALS by Francis I. Baratta & George W. Driscoll

A unique and accurate device aimed specifically at tension testing of brittle materials has been devised. This device effectively minimizes in a simple manner parasitic bending stresses that usually arise in conventional tension testing. A comparison of the results obtained from this proposed method of testing to those already in practice is included in this report.

Sixteen specimens of high grade POCO graphite type AXF-5Q machined from 16 individual billets of 1 3/4 inches in diameter by six inches long were used for the investigation.

Table I: Tensile strength and density of each specimen. Pressure at failure 370-500 psi, density (gm/cc) 1.83-1.89, eccentricity, e (inch) 0.0001-0.001, tensile strength (psi) 8000-9900 psi.

Table II: Fracture toughness of POCO graphite, grade AXF-5Q.

Table III: Comparison of uniaxial tension test results (material: POCO graphite AXF-5Q).

Figure E-1: σ (stress, psi) 0-500 vs. 200-3000 e(X10⁻⁶/in). Stress-strain curve of POCO graphite type AXF-5Q.

Figure F-1: Stress concentration factor as a function of axial distance $\pm X$. k(0.5-1.1) vs. x(0-1.0)

AD-660-587

GROWTH, PROCESSING AND CHARACTERIZATION OF BETA-SILICON CARBIDE SINGLE CRYSTALS by R. W. Bartlett & R. A. Mueller

A literature survey and design and construction of a versatile vapor deposition apparatus were completed. Continuously orientated (111)/(111) β -silicon carbide deposits were obtained by pyrolysis of methlitrichlorosilicone and, independently, silane/propane mixtures. Oxidation experiments were conducted on solution grown beta-silicon carbide platelets in dry oxygen and steam and so on.

Table I: Review of silicon carbide epitaxial vapor growth studies

Table II: Process conditions for vapor deposition of silicon carbide.

Figure 10: Parabolic rate constants for oxidation of alpha-silicon carbide, silicon and transport of oxygen through silica.

Figures 11 & 12: Oxide growth for silicon of (111) orientation in oxygen and steam, respectively. Oxide thickness (1000-100,000)Å vs. time $\sec(10^3-10^5)$.

Table III: Summary of beta-silicon carbide oxidation experiments.

Figure 15: $C/C_0(0.95-1.00)$ vs. V_g -volts (40-60). Capacitance-voltage characteristics of beta-silicon carbide structure $X_0 = 3100\text{\AA}$.

Figure 16: $C/C_0(0.95-1.00)$ vs. V_g -volts (40-50). Capacitance-voltage characteristic of beta -silicon carbide structure, $X_0 = 3400 \text{Å}$.

Figure 17: Similar to Figure 16, MOS beta-silicon carbide structure $\chi_0 = 1400 \text{\AA}$.

Figure 18: Width of the depletion region as a function of the total charge induced with silicon at 300° K.

Figure 19: Donor concentration-capacitance curves MOS beta-silicon carbide structures.

PROPERTIES OF MOLTEN CERAMICS by J. L. Bates, et al

This report describes some of the techniques successfully used to study various properties of molten ceramics. Some charts and tables are included, also schematics of test apparatus.

- Figure 1: Facility for radiographic measurement of liquid density.
- Figure 2: (Chart) Radiograph of ${\rm Al}_2{\rm O}_3$ showing partial melting and volume change and density of ${\rm UO}_2$.
- Table I: Surface tension and density of molten ceramics (by various methods) Al_2O_3 , $MgAl_2O_4$, Sm_2O_3 , and UO_2 .
- Figure 3: Viscosity apparatus and viscosity data for ${\rm Al}_2{\rm O}_3$, ${\rm UO}_2$, and ${\rm MgAl}_2{\rm O}_4$.
- Figure 4: Ultrasonic velocity measuring apparatus for high temperature liquid ceramics.
 - Figure 5: Adiabatic compressibility and ultrasonic velocity for molten Al_2O_3 .
 - Figure 6: Thermal diffusivity apparatus and chart of temperature vs. thermal diffusivity for Dresser basalt.
 - Figure 7: Differential thermal analysis (DTA) apparatus in block diagram form.
 - Figure 9: DTA results for $Pn_20_3 Sn_20_3$ binary system.

N72-29512

FLAME POLISHING OF FLAT OXIDE BARS by P. F. Becher & R. W. Rice

In this report some of the problems and limitations of flame polishing flat bars are discussed. Results are presented for single crystal ${\rm Al}_2{\rm O}_3$ as well as ${\rm MgAl}_2{\rm O}_3$, ${\rm TiO}_2$, and soda lime glass. The wide variability of strength is partially related to variations in surface, but twinning also appears to be important in sapphire and ${\rm TiO}_2$.

Table I: Room temperature strengths of α -Al $_2$ 0 $_3$ single crystal bars (mechanically finished and flame polished).

Table II: Strengths of various (MgAl $_2$ 0 $_3$, TiO $_2$, soda lime glass) ceramic oxides; page 241.

It was noted that flame polishing treatment of flat bars is not as effective as on round bars. Also, there is a "dome" effect on the flat bars as a result of flame polishing.

AD-658-695 or ... N67-39952

ANALYSIS OF MECHANICAL TESTING PROCEDURES FOR BRITTLE MATERIALS by S. A. Bortz & T. B. Wade

The purpose of this research is to provide a guide for investigators in the performance of mechanical tests and the interpretation of test results. A review of several philosophies of failure is included.

The research effort consists of investigating mechanical test procedures and analyzing property data with regard to these test procedures so that the best practice can be determined. Evaluated information is organized in three sections:

- (1) Test philosphy, techniques, and analytical methods.
- (2) Correlation of laboratory tests and recommended procedures.
- (3) Tabular presentation of data.

AD-658-695 (cont.)

Materials tested include: (1) graphite, (2) lava, (3) alumina. Table 3, Page 56: Flexural data on alumina. Figure 34, Page 59: Load vs. deflection for alumina beam (4 point flex.).

AD-693-501

ACTIVATION OF SINTERING PROCESSES IN MAGNESIUM OXIDE
AND CERTAIN TECHNICAL PRODUCTS ON ITS BASE
by V. A. Bron, et al

This report investigates the effects of varying the manufacturing process of sintered MgO. The figures listed below were of particular interest. Note: This is a translation of the original article.

Table I, Page 2: Porosity and particle size of sintered MgO specimens obtained from the carbonates and hydrates.

Table II, Page 3: Effect of heating rate during thermal activatio of MgO on subsequent sintering at 1600° C (material, heating rate, porosity, density).

Table III, Page 6: Effect of the temperature of heating of magnesium carbonate on the crystalline lattice parameters and the specific gravity of MgO.

Journal of The American Ceramic Society, Vol. 53, No. 12, pp. 649-654.

OF ALUMINA AND GRAPHITE' by L. J. Broutman, et al

A new, unique method for testing brittle materials is developed by internal and external pressurization of tubular specimens. Biaxial tensile strengths of alumina and graphite are lower than uniaxial strengths.

. Table I: Mechanical properties at 77°F.

Figure 4: Probability of failure vs. fracture stress for ${\rm Al}_2{\rm O}_3$ and graphite.

Figure 6: Experimental tension-compression stress quadrant for ${\rm Al}_2{\rm O}_3$.

Figure 7: Comparison of experimental and failure criterion for ${\rm Al}_2{\rm O}_3$.

AD-613-009

Evaluation of Thermal Stress Resistance in Potential Radome Materials by D. A. Brown

his paper gives many physical and thermomechanical properties (especially thermal shock) for five different ceramics. They are:

- (1) Pyroceram 9608
- (2) Pyrex 7740
- (3) MgO (99+% density)
- (4) Alumina (AD-99)
- (5) Alundum (RA-3360)

A list of charts and graphs of particular interest is as follows:

Figure 3: Thermal conductivity vs. temperature

Figure 5: Time to cracking vs heat flux-alumina RA-3360

Figure 6: Time to cracking vs heat flux-Mgo

Figure 7: Time to cracking vs heat flux-AD-99 alumina

Figure 8: Time to cracking vs heat flux-pyrex 7740

Figure 9(a): Time to cracking vs heat flux-pyroceram 9608

Figure 9(b): Time to cracking vs heat flux-pyroceram 9608

Figure 10: Comparison of cracking characteristics vs heat flux

for untouched 3/8 inch wall specimens of each material.

Figure 11: Comparison of cracking characteristics vs heat flux

for untouched 1/4 inch wall specimens of each material.

Figure 12: Comparison of cracking characteristics vs heat flux

for untouched 3/8 inch wall specimens of each material.

Table I: Material thermal stress resistance parameters (p-parameters

Table II: Material constants used in calculated p-parameters.

AD-613-350

Anistropy and Strength of Ceramic Bodies by W. R. Buessem, et al

This paper examines the effect of elastic and thermal expansion anisotropy on the strength of fused silica and aluminum titanate. Also on pages 41-52 tables of elastic constant data for a variety of ceramics are given. Charts and tables given in the report are shown below:

Figure 2: Relative velocity of longitudinal waves vs temperature (fused silica)

Figure 3: Relative velocity of shear waves vs temperature (fused silica)

Figure 1 & 2-page 28 & 33: Thermal expansion vs temperature for cold-pressed aluminum titanate.

Page 41-52: Compilation of elastic constant data for cubic materials (using five different methods to obtain constants)

Journal of The American Ceramic Society, Vol. 55, No. 2, Feb. 1972.

Computation of Residual Stresses in Quenched $A1_20_3$ by Buessem, W. R. & Gruver, R. M.

A method of computing the residual stress profile in quenched alumina rods was developed. For these calculation certain material parameters must be determined. The strain rate has measured as a function of stress for 96% ${\rm Al}_2{\rm O}_3$ at $1300^{\rm O}$ to $1500^{\rm O}$ C, and the heat transfer rates for cylindrical samples quenched in several media were determined. Using calculated temperature distributions and measured strain rate, plastic strains were computed for the entire quenching period, and these strains were used to determine a profile of residual room temperature stresses. The substantial increases in flexural strength observed in ${\rm Al}_2{\rm O}_3$ after quenching is thought to originate in the residual compressive surface layers.

AD-684-717

ANISOTROPY AND STRENGTH OF CERAMIC BODIES by W. R. Buessem and H. A. McKinstry

Whereas much of the present and past research on the strength of crystalline solids has concentrated on dislocations and their movements, this report concentrates on some of the other factors which determine the strength of polycrystalline bodies, i.e. the anisotropies. The experimental and theoretical studies presented include thermal expansion anisotropy, bulk strength anisotropy, and grain boundary strength anisotropy.

Table I: Pressure deviation of crystalline Al, Cu, and MgO at different thermodynamic boundary conditions ($\sim 300^{\circ}$ K).

Table II: Comparison of predicted and experimental isotropic pressure deviation of polycrystalline elastic modulus of Al, Cu, α -Fe and MqO ($\sim 300^{\circ}$ K).

Table V: Elastic and thermoelastic data for crystalline Al, Cu, α -Fe and MgO.

Table VI: Acoustic and thermal data for crystalline Al, Cu, α -Fe, and MqO ($\sim 300^{\circ}$ K).

Figure 3: Young's modulus $(x10^{11} \text{ dyne/cm}^2)24-30 \text{ vs. density } (gm/cm^3)$

395-425. Young's modulus of polycrystalline TiO_2 (rutile). Figure 4: Shear modulus (x10¹¹ dyne/cm²)900-1200 vs. density (gm/cm³) 395-425. Shear modulus of polycrystalline TiO2 (rutile).

Table I, Page 2780: Literature value of single crystal elastic

constant of ZnO, TiO $_2$ (rutile), and α -Al $_2$ O $_3$. Figure 5: Young's modulus (x10 11 dyne/cm 2)32-42 vs. density (gm/cm 3)

380-400 of polycrystalline α -Al $_2$ 0 $_3$. Figure 6: Shear modulus (x10 11 dyne/cm 2)13-17 vs. density (gm/cm 3) 370-400 of polycrystalline α -Al₂0₃.

Table III: Comparison of measured polycrystalline elastic moduli with VRH modulii calculated from the single crystal elastic constants.

Appendix I: Elastic stiffness constants, technical elastic modulii, and parent elastic anisotropy of cubic crystal. .

Table I: Second and third order elastic constants of cubic crystals at room temperature (in 106 dyne/cm²).

N65-27965 or AD-614-076

THE INVESTIGATION OF MICROSTRUCTURE IN STRUCTURAL CERAMICS

by H. M. Burte L. A. Jacobson

This paper discusses the importance of and the need for better synthesis methods (for specimens) so that microstructure-property research can be carried on and meaningful results achieved. It was noted that much of the information available is not readily identifiable with a well-characterized material and, therefore, its usefulness is limited.

Figure 6: Oxidation products of Hastelloy X as a function of time and temperature.

Figure 12, Page 21: Strength-temperature-grain size surface for dense hot-pressed MgO..

Philosophical Magazine, Vol. 24, No. 190 (Oct. 1971), pp. 829-834.

OBSERVATIONS OF DISLOCATION IN B-SILICON NITRIDE by E. Butler

Foils of beta-Si $_3$ N4 containing dislocations generated as result of fracture at room temperature have been examined by transmission electron microscopy. The dislocations have been shown to lie on(1010)and to be near edge orientation with a Burgers vector C(0001) . The application of visibility criteria to bilocation in beta-Si $_3$ N4 is considered.

N70-24348

DEFORMATION PROCESSES IN FORGING CERAMICS by R. M. Cannon and W. H. Rhodes

This report (a semi-annual progress report) describes the work done on an investigation of the deformation processes involved in the forging of refractory ceramic oxides. The results given in this report are preliminary, and are for alumina only. The mechanical results show strong strain hardening effects and an apparent Bauschinger effect.

Microstructural examination of the specimens revealed extensive evidence of grain boundary sliding. The compressive surfaces revealed more deformation features than the tensile surfaces; some of the surfaces are suggestive of dislocation motion. Evidence of strain enhanced grain growth was presented; this may be responsible for some of the apparent strain hardening.

Stress-strain curves were constructed from results of 4-point bend tests, a complete analysis was not completed, so results in this report are derived from the equation: $\sigma = 6M$

bh²

Figures 1 and 2-pages 3 and 4-Apparent stress vs total strain at $14500\mathrm{C}$

Table I-page 15-Grain growth in successive test cycles at 1450°C

Journal of the American Ceramic Society, Vol. 55, No. 12, pp. 610-618

WORKING MODEL FOR POROSITY EFFECTS ON THE UNIAXIAL STRENGTH OF CERAMICS

by S. C. Carniglia

The intent of this paper is to inspect the available data and theories relating porosity to the low-temperature uniaxial strength of ceramics and to construct a model which is physically supported and empirically correct.

N73-14585

MECHANICAL BEHAVIOR OF POLYCRYSTALLINE CERAMICS BRITTLE FRACTURE OF SiC--Si₃N₄ MATERIALS by M. H. Ceipold, et al

This is concentrated on investigating the behavior of materials of considerable technological importance—silicon carbide and silicon nitride. The report is divided into two parts. Part 1 is about oxide research and Part 2 is on nitride—carbide research.

The oxide research has emphasized the role of anion impurities on the fabrication and the behavior of magnesium oxide.

Section I. Fabrication - The effort here was designed to determine the effect of anion impurities on the hot pressing behavior of MgO.

Section II. Grain boundary microhardness--no extra-experiment had been performed.

Section III. Grain growth. Grain growth studies in MgO has been furthered by annealing it at 1300°C and 1500°C and the annealing time ranged from 1 hour to 200 hours. Consequently, some further studies of grain growth in doped MgO specimens with higher as-pressed densities. (96% theoretical) were being conducted. The specimens studied previously were hot pressed to intermediate stage densities and hence contain open porosity. This led to a possibility of further loss of the volatile dopant during the grain growth anneals carried out in open atmosphere giving a graduate variation in their concentration for a given specimen at different annealing period. Also, if concentrations reach neglible levels after a fairly long anneal time, then the influence of these anions on grain growth kinetics cannot be established.

In specimens with a higher as-pressed densities (final stage), the possibility of further loss of these volatile species during grain growth anneals is considerably lessened and hence the studies of any effect of anions on kinetics would be more apparent. A summary of these runs is given in Table I. Previously OH $^-$ doped MgO was studied only at 1500° C. Data is now obtained for temperature of 1300° C as well.

Part 2 . Nitride-Carbide Research

Silicon carbide and silicon nitride are very useful structural material for high temperature application such as in gas-turbine engines because of their properties such as very high fracture energy, low thermal expansion and good thermal conductivity. (See Table 6). Also, they are good in inherent erosion and abrasion resistance to the gaseous environment and have high temperature stability. To improve the fracture toughness of these materials in order to make them more reliable as structural materials, their fracture mechanism should be clearly understood.

Table 2, page 24, Table 3, page 24, Table 4, page 25, Table 5, Table 6, page 261, Table 7,8, page 27.

EVALUATION OF THERMAL PROTECTIVE SYSTEMS FOR ADVANCED AEROSPACE VEHICLES (VOL. I) by W. J. Christian, et al

This report contains summaries of (a) a survey of literature on structural and design aspects of thermal protection systems, on compatibility of refractory meterials, on thermal and mechanical properties of refractory materials, and on methods for measuring emittance of materials at high temperatures;

- (b) experimental determination of the thermal conductance of plasma sprayed coatings of alumina-nickel and zirconia-nichromes;
- (c) measuring of total emittance of materials in an oxidizing atmosphere at temperatures of 1000° F to 4000° F;
- (d) experimental investigation of the effects of composition on the thermal expansion and total normal emittance of magnesia;
- (e) analytical and experimental studies of the general characteristics and weight requirements of transpiration cooled nose caps using porous materials.
 - Table 11: Spray powders used in producing thermal conductance samples.
 - ·Table 12: Spray parameters used in producing thermal conductance samples.
 - Table 13: Thickness of single layer coatings.
 - Figure 35: Thermal conductivity of plasma sprayed zirconia-nichrome coatings.
 - Figure 36: Effect of composition on thermal conductivity of aluminanickel coatings.
 - Figure 37: Effect of composition on thermal conductivity of zirconianichrome coatings.
 - Figure 38: Comparison of measured and calculated values of apparent thermal conductivity of alumina-nickel graded coatings.
 - Table 14: Nominal thickness of individual layers of alumina-nickel and zirconia-nichrome graded coatings.
 - Figure 46: Total normal emittance 0-1.00 vs temperature 0-3000.F.
 - Polycrystalline SiO self bonded, working standard.
 - Figure 45: Total emmittance 0-1.00 vs temperature $0-3000^{0}$ F. Theoretical total emittance of fresnel cavity.

80

Table 17: Total normal emittance of magnesia and zirconia compositions.

Table 18: Total normal emittance of zirconia specimens of differing

grain size and stabilizers.

AD627140

Christian, W. J. et al

Evaluation of Thermal Protective Systems for Advanced Aerospace Vehicles (Vol. II - Appendices)

(Continuation of Vol. I)

Evaluation of thermal protective systems for advanced aerospace vehicles $(500^{\circ} - 4000^{\circ})$ oR.

Thermal conductivity. BTU/hr. OF vs temperature OR.

Figure 1: Thermal conductivity - aluminum oxide.

Table 4: Densities and melting points of selected refractory materials.

Figure 2: Thermal conductivity - aluminum oxide and zirconium oxide.

Table 5: Thermal conductivity - aluminum oxide.

Figure 3: Specific heat - aluminum oxide ($^{0}0-3500^{0}R$).

Figure 4: Linear Thermal expansion – aluminum oxide $(500^{\circ}-3500^{\circ}R)$

Figure 5: Linear thermal expansion-aluminum oxide and chromium

oxide. (1-2 micron grain size):

Figure 6: Emittance-aluminum oxide vs temperature (250-3000^oR).

Figure 7: Flexural strength-aluminum oxide vs temperature.

Figure 8: Flexural strength as functions of grain size-aluminum oxide.

Figure 9: Failure stress vs strain rate-Lucalox aluminum oxide.

Figure 10: Failure stress vs strain rate-Wesgo Al-995 alumina.

Figure 11: Shear strength-aluminum oxide.

Figure 12: Compressive strength-aluminum oxide (vs temperature).

Figure 13: Tensile strength-aluminum oxide (vs temperature).

Figure 14: Deflection with load on transverse bending-aluminum oxide.

Figure 15: Strain vs time at 17500F-aluminum oxide.

- Figure 16: Tensile creep-aluminum oxide.
- Figure 17: Grain size effect on creep behavior of aluminum oxide.
- Figure 18: Modulus of elasticity-aluminum oxide.
- Figure 19: Modulus of elasticity as a function of grain size-
- aluminum oxide.
- Figure 20: Elasticity vs density-aluminum oxide.
- Figure 21: Modulus of rigidity-aluminum oxide.
- Figure 22: Poisson Ratio-(800-3800⁰R)
- Figure 23: Grain size vs time of grain growth-aluminum oxide.
- Figure 24: Thermal conductivity-beryllium oxide.
- Figure 25: Thermal conductivity-beryllium oxide and magnesium oxi
- Figure 26: Specific heat-beryllium oxide.
- Figure 27: Linear thermal expansion-beryllium oxide.
- Figure 28: Emittance-beryllium oxide.
- Figure 29: Flexural strength-beryllium oxide.
- Figure 30: Failure stress vs strain rate-beryllium oxide.
- Figure 31: Compressive strength-beryllium oxide.
- Figure 32: Tensile strength-beryllium oxide.
- Figure 33: Tensile creep at $3092^{\circ}F$ vs time-beryllium.
- Figure 34: Modulus of elasticity-beryllium oxide.
- Figure 35: Modulus of rigidity-beryllium oxide.
- Figure 36: Thermal conductivity-hafnium oxide.
- Figure 37 39: Data on test of hafnium oxide.
- Figure 40: Total normal emittance-hafnium dioxide.
- Figure 41: Thermal conductivity-thorium oxide.
 - Figure 42: Specific heat-thorium oxide.
 - Figure 43: Linear thermal expansion-thorium oxide.
 - Figure 44: Emittance-thorium oxide.
 - Figure 45: Compressive strength of thorium oxide.
 - Figure 46: Modulus of elasticity-thorium oxide.
 - Figure 47: Modulus of rigidity-thorium oxide.
 - Figure 48: Thermal conductivity-magnesium oxide.
 - Figure 49: Specific heat-magnesium oxide.
 - Figure 50: Linear thermal expansion-magnesium oxide.
- Figure 51: Emittance-magnesium oxide.
- Figure 52: Flexural strength-magnesium oxide.
- Figure 53: Failure stress vs strain rate-magnesium oxide.

Figure 54: Flexural strength as a function of grain size-magnesium oxide.

Figure 55: Flexural strength-magnesium oxide.

Figure 56: Torsional sheer strength-magnesium oxide.

Figure 57: Fracture strength as a function of grain size-MgO.

Figure 58: Deflection with load on transverse bending-MgO.

Figure 59: Creep torsion-MgO.

Figure 60: Modulus of elasticity-MgO.

Figure 61: Modulus of elasticity as a function of grain size-MgO.

Figure 62: Modulus of rigidity-MgO.

Figure 63: Grain sizes vs time of grain growth-MgO.

Figure 64: Thermal conductivity-spinel (Mg-aluminate).

Figure 65: Specific heat-spinel.

Figure 66: Linear thermal expansion-spinel.

Figure 67: Torsional shear strength-spinel.

Figure 68: Compressive strength-spinel.

Figure 69: Tensile strength-spinel.

Figure 70: Modulus of elasticity-spinel.

Figure 71: Modulus of rigidity-spinel.

Figure 72: Thermal conductivity-zirconium oxide and c...

Figure 73: Specific heat-zirconium oxide.

Figure 74: Linear thermal expansion-zirconium oxide and calcium oxide

Figure 75: Linear thermal expansion-zirconium oxide and magnesium oxi

Figure 76: Linear thermal expansion-zirconium oxide and thorium oxide

Figure 77: Emittance-zirconium oxide.

Figure 78: Compressive strength-stabilized zirconium oxide.

Figure 79: Tensile strength-stabilized zirconium oxide.

Figure 80: Modulus of elasticity-stabilized zirconium oxide.

Figure 81: Grain growth vs time-stabilized zirconium oxide.

Figure 82: Thermal conductivity-boron nitride (BN).

Figure 83: Thermal conductivity-BN and C.

Figure 84: Specific heat-BN.

Figure 85: Linear thermal expansion-Bil.

Figure 86: Thermal conductivity-SiC.

Figure 87: Thermal conductivity-SiC + Si + C.

Figure 88: Thermal conductivity-23 SiC - 77C.

Figure 89: Specific heat-SiC.

- Figure 90: Linear thermal expansion-SiC.
- Figure 91: Linear thermal expansion-zirconium carbide and graphite.
- Figure 92: Emittance-SiC.
- Figure 93: Flexural strength-zirconium carbide + graphite.
- Figure 94: Creep elongation-titanium carbide.
- Figure 95: Tensile creep elongation-zirconium carbide.
- Figure 96: Flexural strength-zirconium boride + molybdenum disilicide.
- Figure 97: Creep deflection-zirconium diboride + molybdenum disilicide.
- Figure 98: Thermal conductivity-extruded acheson graphite; multi-
- crystalline.
- Figure 99: Thermal conductivity-pyrolytic graphite "a" direction.
- Figure 100: Thermal conductivity-pyrolytic graphite "c" direction.
- Figure 101: Thermal conductivity-boron pyralloy "a" direction.
- Figure 102: Thermal conductivity-boron pyralloy "c" direction.
- Figure 104: Specific heat of graphite.
- Figure 105: Linear thermal expansion-multicrystalline acheson graphite.
- Figure 106: Linear thermal expansion-pyrolytic graphite "a" direction.
- Figure 107: Linear thermal expansion-pyrolytic graphite "c" direction.
- Figure 108: Linear thermal expansion-boron pyralloy "c" direction.
- Figure 109: Emittance-graphite.
- Figure 110: Flexural strength-pyrolytic, parallel to basal plane.
- Figure 111: Flexural strength-pyrolytic graphite, normal to basal plane.
- Figure 112: Flexural strength-pyrolytic graphite, zirconia carbide alloy.
- Figure 113: Room temp. Mechanical properties-boron pyrolytic alloy.
- Figure 114: Ultimate tensile strength-ATJ graphite.
- Figure 115: Ultimate tensile strength-ZTA graphite.
- Figure 116: Ultimate tensile strength-pyrolytic graphite "a" direction.
- Figure 117: Ultimate tensile strength-pyrolytic graphite "c" direction.
- Figure 118: Total strain to rupture-ZTA graphite.
- Figure 119: Modulus of elasticity-ATJ graphite.
- Figure 120: Modulus of elasticity-ZTA graphite.
- Figure 121: Modulus of elasticity-pyrolytic graphite "a" direction.
- Figure 122: Thermal conductivity-columbium.
- Figure 123: Thermal conductivity of Cb-5Mo-5V-1Zr.
- Figure 124: Thermal conductivity of Cb-10W-5Zr.
- Figure 125: Thermal conductivity of Cb-10Ti-1Zr.
- Figure 126: Thermal conductivity of Cb-10Ti-5Zr.

REPRODUCIBILITY OF THE ORIGINAL PAGE IS POOR

- Figure 127: Thermal conductivity-Cb-15W-5Mo-1Zr.
- Figure 128: Thermal conductivity-Cb-27Ta-12W-0.5Zr.
- Figure 129: Specific heat-columbium.
- Figure 130: Specific heat of Cb-5Mo-5V-1Zr.
- Figure 131: Specific heat of Cb-10W-5Zr.
- Figure 132: Specific heat of Cb-10Ti-5Zr.
- Figure 133: Specific heat of Cb-10W-5Zr.
- Figure 134: Specific heat of Cb-15W-5Mo-1Zr.
- Figure 135: Specific heat of Cb-27Ta-12W-0.5Zr.
- Figure 136: Linear thermal expansion of columbium.
- Figure 137-Figure 153: All graphs are about the properties of columbium and its alloyed materials.
- Figure 154: Thermal conductivity of molybdenum.
- Figure 155: Thermal conductivity of 70% molybdenum + 30% tungsten.
- Figure 156: Specific heat of molybdenum.
- Figure 157: Specific heat of molybdenum + 30% tungsten.
- Figure 158: Linear expansion of molybdenum.
- Figure 159: Linear expansion of molybdenum + 30% tungsten.
- Figure 160: Normal emittance-molybdenum.
- Figure 161: Hemispherical total emittance-molybdenum.
- Figure 162: Flexural strength-molybdenum.
- Figure 163: Compressive strength-molybdenum + titanum.
- Figure 164: Ultimate tensile strength-molybdenum + titanum.
- Figure 165: Tensile strength-molybdenum + titanium.
- Figure 166: Yield strength-molybdenum + titanium + zirconium.
- Figure 167: Elongation-molybdenum + titanium + zirconium.
- Figure 168: Elongation-molybdenum + titanium.
- Figure 169: Creep properties-molybdenum.
- Figure 170: Creep and rupture properties-molybdenum.
- Figure 171: Modulus of elasticity-molybdenum + titanium.
- Figure 172: Thermal conductivity-molybdenum + titanium.
- Figure 173: Thermal conductivity-90% molybdenum +10% tungsten alloy.
- Figure 174: Thermal conductivity of Ta-8W-2HF alloy.
- Figure 175: Thermal conductivity of Ta-30Cb-7.5V.
- Figure 176: Specific heat-tantalum.
- Figure 177: Specific heat-Ta-10W.

```
Figure 178: Specific heat-Ta-8W-2Hf.
```

Figure 179: Specific heat-Ta-30Cb-7.5V.

Figure 180: Linear thermal expansion-tantalum.

Figure 181: Linear thermal expansion of Ta-10W alloy.

Figure 182: Linear thermal expansion of Ta-8WO2Hf.

Figure 183: Linear thermal expansion of Ta-30Cb-7.5V.

Figure 184: Emittance-tantalum.

Figure 185: Ultimate tensile strength-tantalum.

Figure 186: Tensile and yield strength-tantalum + tungsten.

Figure 187: Tensile and yield strength-tantalum + tungsten + hafnium.

Figure 188: Tensile properties-tantalum + columbium + vanadium.

Figure 189: Tensile properties-tantalum + tungsten + molybdenum.

Figure 190: Tensile properties vs strain rate-tantalum.

Figure 191: Yield strength-tantalum.

Figure 192: Yield strength-Tantalum, tungsten + hafnium.

Figure 193: Elongation - tantalum.

Figure 194: Elongation-tantalum + tungsten.

Figure 195: Elongation-tantalum + columbium + vanadium.

Figure 196: Elongation-tantalum + columbium + vanadium.

Figure 197: Elongation-tantalum + tungsten + molybdenum.

Figure 198: Creep and rupture properties of tantalum alloys

Figure 199: Stress rupture properties of tantalum alloys.

Figure 200: Modulus of elasticity-tantalum alloys.

Figure 201: Modulus of elasticity-tantalum, tungsten.

Figure 202: Thermal conductivity of tungsten.

Figure 204: Linear thermal expansion-tungsten.

Figure 205: Linear thermal expansion-tungsten

Figure 206: Linear thermal expansion-tungsten + copper(mixture).

Figure 207: Emittance-tungsten.

Figure 208: Ultimate tensile strength-tungsten.

Figure 209: Ultimate tensile strength-tungsten.

Figure 210: Ultimate tensile strength-tungsten.

Figure 211: Tensile strength vs strain rate-tungsten.

Figure 212: Yield strength-tungsten.

Figure 213: Yield strength-tungsten.

Figure 214: Yield strength-tungsten + molybdenum.

Figure 215: Yield strength vs strain rate-tungsten.

Figure 216: Elongation-tungsten.

Figure 217: - Elongation-tantalum.

Figure 218: Elongation-tungsten alloy.

Figure 219: Elongation vs strain rate-tungsten.

Figure 220: Reduction of area vs strain-tungsten.

Figure 221: Creep and rupture properties-tungsten.

Figure 222: Creep and rupture properties-tungsten alloys.

Figure 223: Modulus of elasticity-tungsten.

Table 228: Minimum detectable power and long wave cutoffs

for detectors.

Table 230: Hot-filament vacuum method for determining emittance.

AD-731-853

HIGH TEMPERATURE CREEP OF CERAMIC OXIDES by A. H. Clauer & B. A. Wilcox

The high temperature creep behavior of crystalline materials is usually quite sensitive to microstructure. Not only can creep behavior be altered by changing the initial microstructure, but during the creep test the decreasing creep rate during primary creep reflects a changing dislocation substructure. The mechanistic creep models are all based on microstructural features in the form of grain boundaries, second phase particles, or dislocation configuration substructure. The mechanistic creep models are all based on microstructural features in the form of grain boundaries, second phase particles, or dislocation configurations developed during creep. Determining the dependence of the creep rate on stress and temperature is not sufficient to differentiate between the mechanisms, since many of them predict similar behavior. Hence, the dislocation substructure formed during creep must be investigated to assist in identifying the appropriate creep mechanism(s).

This report deals with creep of MgO single crystals with the emphasis on correlating the creep behavior with the dislocation substructure evolved creep. MgO is ideal for such a study, since it etch pits readily and transmission electron microscopy specimens are easily prepared.

RESULTS:

<u>Creep Behavior</u>

Representative creep curves are shown in Figure 2. A long steady state region was observed in only a few specimens. These specimens were used for the temperature and stress change experiments and extended up to 0.30 to 0.40 creep strain before the experiment was discontinued. Usually after loading, the creep rate decreased with increasing creep strain up to a strain range of 0.03 to 0.10, after which the creep rate slowly accelerated, as shown in Figure 2. The acceleration creep rate appeared to be due either to the beginning of a necked region within the gage length, or to slowly opening cracks at the contact between the shoulder of the specimen and the grips, thus where this behavior was observed, the minimum creep rate is reported.

AD-731-853

CONCLUSION:

Tensile creep in (110) oriented MgO single crystals at 1400°C has an activation energy of $Q_{\rm c}$ =94 Kcal/mol. and the stress dependence of the creep rate can be described by ${\rm e}{\rm c}{\rm c}^{\rm n}$ where n=4. At low stresses a uniform distribution of dislocations formed during creep, but above about 6,500 psi, bends of high etch pit density were observed which appeared to be slip bands. Few subboundaries formed during creep. The dislocation arrangement consisted of relatively long segments having screw or edge characteristics and numerous dislocation loops. An empirical comparison with creep behavior in metals indicates that the creep behavior was probably dislocation climb controlled rather than dislocation glide controlled, but it is not yet clear whether creep is diffusion controlled or whether alternative mechanisms should be sought.

Table 1, Page 19: Summary of creep results for single crystal MgO. Figure 2, Page 20: Representative creep curve of (011) oriented MgO single crystals tested at different stresses at 1400° C.

Figure 3, Page 21: Temperature dependence of the creep rate of (011) oriented MgO single crystals determined at 6850 psi.

Figure 4, Page 22: Stress dependence of the creep rate of (011) oriented MgO single crystals.

Figure 7, Page 25: Stress dependence of the creep substructure after creep to 0.10 creep strain at 1400°C. The views are the (100) surfaces of the specimens.

Figure 9, Page 27: Stress dependence of the dislocation density determined at 1400° C.

Figure 10, Page 28: Strain dependence of the dislocation density at 1400°C and 6800 psi.

AD-865-321

RESEARCH & DEVELOPMENT OF REFRACTORY

OXIDATION-RESISTANT DIBORIDES - PART II, VOL. V

by E. V. Clougherty, et al

This report is a continuation of AD-865-809, but in this paper the thermal, physical, electrical, and optical properties are examined.

AD-865-321

Thermal conductivity was measured from 100°C to 1000°C and was calculated from specific heat and density data from 1000°C to 2000°C for varying compositions and microstructures of ZrB_2 and HfB_2 with SiC and C. additives.

Linear expansion data from room temperature to 1000°C was obtained by direct view and thermal dilatometry.

Electrical resistivity data is included from room temperature to 1000°C.

Total normal emittance data were measured from $1600^{\rm o}{\rm C}$ to $2300^{\rm o}{\rm C}$ for unoxidized diboride compositions.

Approximately 37 pages of graphs are included, some are:

Temperature vs. specific heat

Temperature vs. thermal diffusivity

Temperature vs. thermal conductivity

Temperature vs. linear thermal expansion

Temperature vs. total normal emittance

Table 1, page 67 lists the compositions of the various test materials.

Tabular presentation of data is also included for some tests; also, Tables 5, 6, 7 and 8 give specific heat, enthalpy and entropy data for various materials.

AD-839-956

OXIDATION-RESISTANT DIBORIDES by E. V. Clougherty, et al

The oxidation, mechanical and physical properties of zirconium diboride and hafnium diboride and composites prepared from these diborides with appropriate additives have been determined as a function of composition, microstructure and test temperature. The composites were designed to enhance oxidation resistance, strength and thermal stress resistance without sacrificing high temperature stability.

AD-839-956

The principal additives were silicon carbide or graphite. Several hundred diborides, in sizes from two-inch diameter to six inches square, were fabricated by conventional hot pressing. All lot pressed billets were subjected to extensive nondestructive testing correlation and flaw identification criterial. A unique role of ceramic additives has evolved in enhancing the fabricability of diboride materials and producing fine grained crack-free billets. All powder materials and hot pressed microstructure subjected to properties evaluations have undergone extensive characterization through qualitiative and quantitative chemical analyses, phases and grain size and density measurements.

An exploratory fabrication effort was initiated to develop alternate means to hot pressing for producing dense diboride materials; hot forging, plasma spraying and sintering are being studied. In addition, the hot pressing of diboride compositions containing additives such as SiC whiskers, carbon filaments or tungsten filaments is being studied.

Oxidation screening evaluations were performed in hot sample cold gas furnace tests in which low velocity air at a linear flow rate of 0.9 ft/sec is passed over specimens at temperatures from 1700°C to 2200°C. The beneficial effect of SiC in reducing the rate of diboride oxidation and increasing the adherence characteristics of protective oxide coatings was confirmed and extended in temperature range and composition. The introduction of graphite, for improved thermal stress resistance, detracts from the oxidation resistance. Hafnium diboride compositions display superior oxidation resistance to analogous zirconium diboride compositions.

Mechanical properties screening evaluations comprising bend strength measurements up to 1800°C and static elastic modulus measurement up to 1400°C were performed for selected diboride compositions with variations in porosity and grain size. The fine grained fully dense diboride composite composition possess the highest elevated temperature strength; bend strengths of 40,000 psi to 60,000 psi at 1800°C are found in several compositions. Porosity and graphite substantially reduce the Young's modulus of HfB2 and ZrB_2 from 70 to 80 X 10^6 psi level, whereas SiC does not significantly alter the composite modulus. The temperature and strain rate dependence for the onset of plasticity is being established, all compositions have shown limited plasticity in bending at 1800°C .

AD-839-956

Preliminary steady state thermal stress resistance measurements were performed in which hollow cylindrical specimens were heated by a concentrically positioned carbon rod in order to induce thermal stress sufficient to cause brittle failure. Transient thermal stress data of materials from this program are being obtained in a variety of hot gas/cold sample arc plasma evaluations under a separate study.

The results of the current program provide an increased confidence in the choice of a diboride material as a monolithic ceramic body for applications in environment which will produce thermal stresses and surface oxidation

The diboride of zirconium and hafnium have been identified as excellent candidate materials for application involving exposure to oxidizing environments at elevated temperatures.

Figure 2, Page 61: Comparison of hot pressing characteristics of materials 102A and VO2A.

Figure 3, Page 62: Comparison of hot pressing characteristics of materials 103A and V03A.

Figure 36, Page 90: Bend strength of material I as a function of test temperature.

Figure 37: Bend strength of material V as a function of test temperature.

Figure 38: Bend strength of material II as a function of test temperature.

Figure 39: Bend strength of material IIIO5 as a function of test temperature.

Figure 40: Bend strength of material IVO5 as a function of test temperature.

Figure 41: Bend strength at 1800°C of $\text{ZrB}_2\text{-SiC}$ and $\text{HfB}_2\text{-SiC}$ composites as functions of SiC content.

Figure 47: Effect of porosity on room temperature elastic modulus for various diborides.

Figure 188, Page 169: Shape factors of cylindrical thermal stress specimens.

Table 6, Page 182: Characterization of zirconium diboride powder, IO3.

.Table 7, Page 183: Characterization of zirconium diboride powder, IO7.

Table 8, Page 184: Characterization of zirconium diboride powder, IO5A

Table 9, Page 185: Characterization of zirconium diboride powder, IIO5 and IIO5A.

Table 17, Page 193: Material 1 hot pressing conditions and results.

Table 18, Page 197: Material 1 with intentional impurity phase additions, fabrication conditions and results.

Table 20, Page 198: Material V fabrication conditions and results.

Table 22, Page 201: Microstructure study of special materials used for material V analysis.

Table 23, Page 202: Material VIII fabrication conditions and results.

Table 24, Page 203: Material X fabrication conditions and results.

Table 25, Page 204: Material XII fabrication conditions and results.

Table 26, Page 205: Material II hot pressing conditions and results.

Table 28, Page 207: Material III hot pressing conditions and results.

Table 29, Page 208: Material IV fabrication conditions and results.

Table 30, Page 209: Material VI fabrication conditions and results.

Table 33, Page 212: Press forging of Material I.

Table 35, Page 214: Sintering conditions and results.

Table 36, Page 215: Reinforced composites fabrication conditions and results.

Table 40, Page 220: Bend strength as a function of temperature.

Table 41, Page 223: Phase II bend strength as a function of temperature.

Table 42, Page 224: Bend strength versus test temperature for two

commercial lots of hot pressed zirconium diboride.

Table 43, Page 225: Bend strengths of preoxidized commercial hot pressed zirconium diboride.

Table 45, Page 227: Dynamic elastic modulus measurements.

Table 46, Page 228: Elastic modulus as a function of temperature.

Table 47, Page 230: Static and dynamic modulus values for hot pressed zirconium diboride.

Table 48, Page 231: Comparison of post- 1800° C-test fracture grain size with as-hot pressed grain size.

Table 49, Page 232: Density measurements on bend specimens tested at 23°C.

Table 66, Page 251: Summary of preliminary results of thermal stress evaluation.

· N

AD-688-201 or N69-37125

BASIC RESEARCH IN NONOXIDE CERAMICS by R. L. Coble

This is a final report covering several materials, including titanium nitride (vapor deposited), calcium flouride, and SiC. Topics covered under silicon carbide include creep, diffusion, and deformation.

Table I and Figure 1, Page 116: Creep results for SiC.

Figures 1a, 1b, 2, 3, Page 625: Charts of diffusion coefficients in SiC as a function of temperature, etc.

Figure 4 and Table II, Page 266: Stress-strain rates for SiC. Figure 5, Page 267: Stress-strain rates for SiC.

from: <u>Proceedings of the 5th Symposium on Special Ceramics</u>.

(Pinkhull, Stoke-on-Trent: British Ceramic Research Association), 1970.

SOME PROPERTIES AND APPLICATIONS OF HOT-PRESSED SILICON NITRIDE by R. F. Coe, et al

Changes occurring during hot-pressing of $\mathrm{Si_3N_4}$ powder containing a large percentage of alpha- $\mathrm{Si_3N_4}$ with 1% MgO added are discussed and related to variations in properties. Some data on Weibull parameters is included.

Figure 2, Density vs pressing time.

Figure 3, MOR vs pressing time and time above 90% full density.

Table 2, Bend strength test data and Weibull analysis.

Figure 4, Hardness vs load.

Figure 5, Hardness vs strength (MOR).

Figure 8, Percentage beta vs time above 90% full density

AD-748-110

THE BRITTLE FRACTURE OF ALLOYED ALUMINA by J. Congleton, et al

Polycrystalline discs of pure alumina and of alumina containing 0.5 Cr or 0.5 Ti was prepared by vacuum hot pressing and the bend strength was determined. The Cr alloys did not show any very definite evidence of an increase in strength compared to pure alumina. The Ti alloys showed weakening, but this could be due to the presence of a few large grains.

Air-annealing of polycrystalline allumines (pure or alloyed) at 1250°C after vacuum hot-pressing in graphite die reduced the strength by 25%. Similarly, air-annealed single crystals were weaker than those that had been vacuum annealed while enclosed in a graphite crucible.

Table 1, Page 3: Vacuum hot pressing fabrication details.

Table 2, Page 4: Grain sizes for vacuum hot pressed aluminas in a range of heat-treat conditions. Grain sizes quoted in microns.

Table III, Table IV: Strength data

Table V, Figure 1, Figure 4:

Table VII, Page 12: Strengths of notched single crystals of alloyed alumina Table VIII, Page 13: Strengths of notched single crystals of alloyed alumin Table VIII, Table IX, Page 14:

Table X, Page 17, Strength of polycrystalline, as-pressed pure alumina (tests in various environments at 600°C).

This effect of annealing atmosphere may reflect an influence of non-stoichiometry on the flaw stress or it may reflect a microscopic internal stress set up, due to differences between the surface and the interior or it may reflect a thermal etching effect on the geometry of the defect that originates the fractures.

Figure 6, Page 21: Young's modulus vs temperature for alloyed alumina. Figure 7, Page 22: Effect of alloying with chromium on the room temperature Young's modulus of alumina.

· AD-715-988

THE BRITTLE FRACTURE OF ALLOYED ALUMINA

by J. Congleton

L. M. Linnett

N. J. Petch

A hot-pressing facility has been commissioned and fabrication procedures established for the manufacture of high density, fine grained pure and alloyed alumina. Mechanical testing of the products, by four point bend tests, has commenced. A suitable chemical analysis procedure for determining Cr in alumina has been developed that is accurate to within $\frac{1}{2}$ 0.5 μg Cr. Additionally, a theoretical consideration of the notch strength of alumina has been developed. This is based on a simple model for fracture and suggests that the mechanistic details of fracture nucleation close to the notch tip are of significant importance in determining the relationship between notch-strength and stress concentration factor at a blunt notch.

During recent years, it has been suggested that the fracture of alumina below 1000°C is not a completely brittle process even though the macroscopic fracture appearance is quite brittle. Both direct and indirect evidence has been obtained that indicates the involvement of plastic deformation in the fracture.

Table I.1, Page 4: Hot-pressing details.

Table IV.1, Page 10: Notch-tensile data for Lucalox alumina.

Figure 1: $A1_20_3-Cr_20_3$ phase diagram.

Figure 2: Al₂O₃-TiO₂ phase diagram.

Figure IV.2, Page 19: Notch-strength data for. Lucalox alumina. Full circles indicate experiments performed at 20°C in a silicone oil environment.

Journal of The American Ceramic Society, Vol. 55, No. 9, Sept. 1972. pp. 455-460.

MEASUREMENT OF FRACTURE SURFACE ENERGY OF Sir by J. A. Coppola & R. C. Bradt

This paper measures the fracture surface energies of polycrystalline SiC by the use of three different methods: (1) double-cantilever beam, (2) notched beam,

(3) work of fracture. All three methods gave similar results.
Table I: Room temperature properties of silicon carbides.

Ceramics Bulletin, Vol. 51, No 11 (1972), pp. 847-851.

FRACTURE ENERGY OF SILICON NITRIDES by J. A. Coppola, et al

The fracture energy of four hot-pressed and two reaction sintered Si_3N_4 specimens were measured from -196 0 to 1400 0 C by the work fracture method. Table I: Room temperature properties of specimens.

Table II: Temperature dependence of the work of fracture of specimens. Figure 4: Graphical presentation of temperature variation of work of fracture of specimens.

AD-753-711

AN INVESTIGATION OF THE MECHANICAL PROPERTIES OF SILICON CARBIDE AND SAPPHIRE FILAMENTS by R. L. Crane

The tensile strength and Young's modulus of both SiC and ${\rm Al}_2{\rm O}_3$ filaments have been documented as a function of temperature.

Figure 4, Page 12: Strength of Si rich AVCO SiC filament as a function of temperature.

Figure 5, Page 12: Tensile strength as a function of temperature for both virgin and abraded, stoichmetric AVCO SiC filaments.

Table I: Comparison of room temperature tensile strength of virgin and abraded French SiC filaments.

Figure 7, Page 16: Young's modulus as a function of temperature (AVCO stoichiometric SiC filaments).

Figure 8, Page 16: Tensile strength as a function of temperature for both virgin and abraded TYCO C-axis sapphire.

Figure 9, Page 18: Tensile strength vs temperature for virgin and abraded TYCO a-axis sapphire.

Figure 10, Page 18: Tensile strength vs temperature for ${\rm Cr_20_3}$ coated TYCO c-axis sapphire.

Figure 11, Page 20: Tensile strength vs temperature for virgin and abraded ADL (Arthur D. Little, Cambridge, Mass.) Cr^{+3} doped c-axis sapphire.

Figure 12, Page 20: Tensile strength vs temperature for virgin and abraded ADL (Arthur D. Little, Cambridge, Mass.) Cr +3 doped a-axis sapphire.

Figure 13, Page 23: Young's modulus of TYCO c-axis sapphire vs temperature.

Table II, Page 21: Spark source spectrometric chemical analysis of an exceptionally strong and average strength ADL Cr⁺³ doped c-axis filament.

Proceedings of the British Ceramic Society, Jan. 1970, p. 37-46.

THE EFFECT OF STRESS RATE ON THE RUPTURE STRENGTH OF
ALUMINA AND MULLITE REFRACTORIES
by A. G. Crouch & K. H. Jolliffe

Modulus of rupture tests are carried out at temperatures up to 1400°C on an 85% alumina and a fused-grain mullite refractory.

Figure 1: Fracture stress vs temperature for 85% alumina.

Figure 7: Fracture stress vs loading rate for 85% alumina.

Computers and Structures, Vol. 3, pp. 849-863. Pergamon Press 1973.

FINITE ELEMENT ELASTIC-PLASTIC-CREEP ANALYSIS OF TWO-DIMENSIONAL CONTINUUM WITH TEMPERATURE DEPENDENT MATERIAL PROPERTIES by N. A. Cyr & R. D. Teter

A technique is presented for this test. The plastic analysis utilized the Prandtl-Reuss flow equations assuring isotropic material properties and linear strain-nardening. A power creep flow law formulated by Odquist is used to determine the steady state creep strain rate. The plastic and creep flow laws are employed to derive a 'softened' plastic-creep stress-strain matrix. These modified stress-strain relations are then used to formulate the element stiffness matrix in the usual manner.

Materials Science and Engineering, Vol. 6, Nov. 1970, pp. 281-298.

THE STRENGTH OF CERAMICS by R. W. Davidge & A. G. Evans

This report gives tensile strengths of alumina, magnesia, silicon nitride, and uranium dioxide.

Figure 6: Variation of inherent crack size with grain size in fully dense polycrystalline MgO.

Figure 12: Fracture stress vs temperature of Si_3N_4 (two different densities).

Figure 13: Temperature dependence of strength of Al_20_3 (polycrystalline-99% and 99.5% dense).

Figure 15: Strength vs grain size of MgO at 20°C.

Figure 16: Temperature dependence of the strength of fully dense and 97% dense MgO.

AD-611-757

A STUDY OF HIGH MODULUS, HIGH STRENGTH FILAMENT MATERIALS BY DEPOSITION TECHNIQUES by L. G. Davies, et al

The objective of this program was to establish the feasibility for depositing the desired materials by state-of-the- art vapor deposition techniques upon a substrate in filament form. The following materials were selected for study on the basis of their high modulus to density ratio: boron carbide, silicon carbide, and aluminum oxide. The filament were characterized by their physical appearance and by the measurements of their tensile strength.

A study of high modulus, high strength filament materials by deposition techniques.

Table 1: Potential filament reinforcement materials, density ($1b/in^3$) 0.06--0.16., modulus $10^61b/in^2$ 30--70, modulus to density ratio 1-7. Material tested: boron, beryllium, beryllium carbide, silicon carbide, boron carbide, beryllium oxide, aluminium oxide, zirconium oxide, vanadium carbide, tungsten carbide E-glass.

Table II: Summary of physical test results. Density of coating g/cm³ 1.5--3.5, modulus of elasticity X10⁶ psi 2--80. Tensile strength 3--246. Material used: boron carbide, silicon carbide, boron titanium carbide, titanium boride, aluminium oxide, beryllium.

AD-600-614

EQUATION OF STATE FOR SOLID BODIES by B. I. Davydov

Prodeeding from the general concepts of the Quantum Theory of solid bodies approximation expressions are obtained for the free energy of basic types of crystalline solid bodies (ions, volents and molecular crystals, metals). These expressions make it possible to obtain the equation of state, as well as, the compressibility and coefficient of thermal expansion as a function of pressure and temperature by the usual method. Constants entering into the formulas may be determined on the basis of experiments carried out at low pressure. The equation obtained are valid up to the pressure at which some phase changes take place. Date given for NaCl, MgO, Fe_2O_A , Si, Ge, and Fe.

Figure 1: Pressure vs atomic volume at 00K.

Figure 2: Pressure vs atomic volume at 0° & 1000° K.

- AD-609-351

GRAIN BOUNDARIES AND THE MECHANICAL BEHAVIOR OF MAGNESIUM OXIDE by R. B. Day & R. J. Stokes - (1964)

This paper compares the mechanical behavior of single crystal and poly ystalline MgO at various temperatures. Relevant charts are listed below. ny photomicrographs are also shown.

Table 1, Page 4: Type of MgO polycrystals (gives density, grain size, and microstructure).

Figure 1, Page 8: Resolved shear stress vs resolved shear strain (single crystal MgO at 1800° C).

Table II, Page 13: Summary of relevant tindings on mechanical behavior of single crystals at high temperatures.

AD-609-479

SOME RECENT.ADVANCES IN MICROWAVE PHONON GENERATION AND DETECTION WITH APPLICATIONS TO THE STUDY OF PHONON-LATTICE INTERACTIONS IN DIELECTRIC MATERIALS by J. de Klerk

This paper gives many charts for attenuation measurements in quartz, Mg0, $Ti0_2$, and Al_20_3 . A theory for the behavior of attenuation as a function of temperature is also given. The following charts and graphs were noted:

Figure 51: Attenuation vs temperature at 1Gc/sec in MgO (Norton #1) for compressional waves in (100) direction.

Figure 52: Attenuation vs temperature at 1 and 3 Gc/sec in MgO.

for compressional waves in (100) direction before and after UV irradiation

Figure 53: Attenuation vs temperature at 1Gc/sec in MgO.

Figure 54: Intrinsic attenuation vs temperature in MgO for shear waves.

Figure 55: Attenuation vs temperature at 1Gc/sec of compressional waves in MgO after anneal.

Figure 56: Attenuation vs temperature at 1Gc/sec of compressional waves along "C"-axis in TiO₂.

Figure 57: Intrinsic attenuation vs temperature for compressional waves in TiO_2 . (#1).

Figure 58: Attenuation vs temperature for compressional waves in Al_2O_3 (Linde #5) along C-axis at 1 Gc/sec.

Figure 59: Attenuation vs temperature for compressional waves in Al_2O_2 along the c-axis at 1Gc/sec using ZrS transducer.

N67-17660 or AD-643-861

SYNTHESIS OF NEW SOLID-STATE MATERIALS BY ULTRAHIGH PRESSURE TECHNIQUES by A. J. DeLai, et al

This paper studies the microstructure and physical properties of dense oxides prepared at ultrahigh pressures and low temperature. Completely dense, transparent MgO has been prepared in submicron grain sizes with hardness values twice that of single crystal material and 30% or 50% greater than that for hot-pressed material.

Figure 11, page 28: Grain size vs. temperature - MgO.

Figure 12, Page 29: Knoop hardness vs. temperature - MgO.

Figure 13, Page 30: Knoop hardness vs. grain size.

Journal of Research, Vol. 77A, No. 4, July-August 1973, pp. 391-394.

AN ALUMINA STANDARD REFERENCE MATERIAL FOR RESONANCE FREQUENCY AND DYNAMIC ELASTIC MODULI MEASUREMENT II. Characteristic Values for Use from 25°C to 1000°C by Robert W. Dickson & Edward Schreiber

The temperature dependence of Young's modulus and the shear modulus of polycrystalline alumina is given over the range of 25°C to 1000°C . Results are expressed in terms of the dimensionless ration modulus value at temperature divided by modulus value at 25°C . These results are intended for use with Standard Reference Material No. 718 which is intended for calibration of apparatus used to determine elastic modulus of solids by resonance techniques.

Heat Conductivity of Pure Oxide Ceramics by I. G. Duderov and D. N. Poluboyarinov

This article is translated from Russian by D. Koolbeck. It is a study that determines the heat conductivity of pure ${\rm Al}_2{\rm O}_3$, MgO, BeO, and ZrO samples experimentally in the temperature range of $100\text{-}1000^{\rm O}{\rm C}$. It was noted that results differed according to diameter of the sample, grain structure, and the thermal heat treatments given the samples prior to testing.

Table 2; page 3: Mean heat capacity C of the specimen (K cal/Kg. deg. Figure 1, page 5: Dependence of the magnitude of heat conductivity coefficient of ${\rm Al}_2{\rm O}_3$ ceramics.

Figure 2; page 2: Coefficent of heat conductivity for Al₂U₃ ceramics

Figure 3: Coefficient of heat conductivity for MgO ceramics.

Figure 4: Coefficient of heat conductivity of BeO ceramics.

Table 3, page 7: Coefficients of heat conductivity.

Figure 5, page 8: Coefficients of heat conductivity for ZrO2.

Table 4, page 9: Heat conductivity of pure oxide ceramics.

Figure 6: Coefficient of heat conductivity of Al₂0₃ ceramics.

Table 5; page 12: Coefficient of heat conductivity of corundum ceramic manufactured by various methods.

Conclusion:

- 1. The values of heat conductivity for dense specimens of ceramics made from ${\rm Al}_2{\rm O}_3$, MgO, and BeO, measured by the methods of stationary and regular heat regimes, differ wishes the limits of experimental error.
- 2. The λ of specimens with similar density depends on the character of their structure, which in turn is caused both by the method of their manufacture and by the heat treatment during annealing and their service.
- 3. The values of λ obtained in our investigation for dense ceramics of pure oxides at low temperature (400-600°C) turned out to be significantly smaller than the values given in many foreign sources.

A SURVEY OF HIGH TEMPERATURE CERAMIC MATERIALS FOR RADOMES by L. K. Eliason & G. C. Zellner

A comprehensive survey was conducted of available information concerning the use of nonmetallic inorganic refractory materials in the fabrication of radomes for elevated temperature use. In conducting this survey, both open literature and contract reports were studied. These were augmented with facility visits and personal communications with bomissile contractors and materials suppliers.

The available data were analyzed to determine their validity, and that information considered to be reliable and accurate was compiled in both tabular and graphical form.

Figure 1: Temperature variation of K at 4 x 10^9 c/s for Al $_2$ 0 $_3$ -SrTi0 $_3$ compositions. Dielectric constant K 12.0-11.0 vs. temperature 0 C(0-900)

Table II: Materials index and property indicator.

Figure 2: Maximum available temperature data. Electrical properties locator chart p. 92-109.

Figure 16: Dielectric constant 8.5-13.0 vs. temperature $200-2800^{\circ}$ F of 99.9% alumina.

Figure 17: Loss tangent 0.00001-0.001 vs. temperature $^{0}F(200-2800)$ of 99.85% alumina.

Figure 18: Dielectric constant 8.5-13.0 vs. temperature $200-2800^{\circ}$ F of 99.5% alumina.

Figure 19-Figure 92: Dielectric constant and loss tangent vs. temperature of different ceramics.

Figure 93-Figure 103: Resistivity ohm cm vs. temperature ${}^{\rm O}{\rm F}$ of different ceramics.

Figure 104-110: Specific heat o-.5 vs. temperature $^{\rm O}$ F(200-2800). Figure 111-Figure 117: Thermal conductivity cal cm/cm $^{\rm 2}$ sec $^{\rm O}$ C x 10^{-2} vs. temperature $100-1800^{\rm O}$ C ($200-2800^{\rm O}$ F).

Figure 118-Figure 129: Total normal emissivity 0-100 vs. temperature ${}^{0}F(0-2800)$.

Figure 130-133: Linear thermal expansion percent 0-2.0 vs. temperature 0 F 0-2800.

Figure 134-135: Thermal expansion in/in \times 10⁻⁴ vs. temperature 0 F 200-2800.

Figure 136-137: Thermal diffusivity $cm^2/sec \times 10^{-2}$.1-1.0 vs.200-2800 0 F.

Figure 138-143: Tensile strength 0-50 \times $10^3 \mathrm{psi}$ temperature $^{0}\mathrm{F}$ 200-2800.

- Figure 139-148: Flexural strength 0-50 X 10³psi temperature ^oF 200-2800.

Figure 149: Young's modulus \times 10 6 psi 10-60 vs. temperature 0 F 200-2800.

Figure 155-160: Shear modulus $\times 10^6$ 0-50 vs. temperature 200-2800 $^{\rm o}$ F.

Page 254-265: Dielectric constant and loss tangent of alumina.

Page 266-268: Dielectric constant and loss tangent of beryllia.

Page 269-274: Dielectric constant and loss tangent of boron nitride.

Page 275: Dielectric constant and loss tangent of magnesia.

Page 276: Dielectric constant and loss tangent of spinel.

Pages 277-280: Volume resistivity of alumina.

Page 281: Volume resistivity of silicas.

- Pages 282-283: Volume resistivity of spinel

Page 284: Dielectric strength of alumina.

Page 285: Dielectric strength of beryllia.

Pages 286-188: Specific heat of alumina.

Page 289: Specific heat of pyroceram.

Pages 290-292: Thermal conductivity of alumina.

Pages 293-294: Thermal conductivity of silica.

Page 295: Thermal conductivity of beryllium

Pages 296-299: Thermal expansion of alumina

Pages 300-301: Thermal expansion of beryllium.

Page 302: Thermal expansion of pyroceram.

Pages 303-304: Emissivity of alumina.

Pages 305-306: Emissivity of beryllium.

Pages 307-308: Emissivity of silica.

Page 309: Emissivity of pyroceram.

Page 310: Thermal diffusivity of silica.

Page 311: Thermal diffusivity of pyroceram.

Page 312: Compressive strength of alumina.

Pages 313-316: Tensile strength of alumina.

Pages 317-318: Young's modulus - shear modulus - Poisson's ratio of alumina

Page 319: Tensile strength, compressive strength, flexural strength, Young's modulus of beryllia.

Page 320: Tensile strength, compressive strength, flexural strength, Young's modulus of pyroceram.

Page 321: Tensile strength, compressive strength, flexural strength, Young's modulus of magnesia.

Page 322: Tensile strength, compressive strength, flexural strength, Young's modulus of fused silica.

AD-765-478

COMBINED STRESS STRENGTH RESULTS FOR A HIGH-PURITY, SLIP-CAST FUSED SILICA by R. E. Ely

The behavior of a high-purity SCFS was determined under ten biaxial stress states at room temperature. Modulus of rupture data was also determined.

Four point loading was employed in the flexural tests, and the "pressure vessel" test method (previously described in Mr. Ely's papers) was used to obtain the ten biaxial stress states. Loading was accomplished by various combinations of internal, external, and axial pressures.

Equations used for calcuation of stresses are given on page 4.

Table I - page 7 - Modulus of rupture of high-purity, SCFS.

Table II - page 8-10 - combined stress results for 57 tests (hoop stress, axial stress, and fracture time).

Table III - Modulus of rupture for round specimens (density, surface finish, specimen diameter, modulus of rupture).

Figure 5 - Plot of strength results of Table II.

Figure 6 - Theoretical curve (from Leon Theory) and results of lot. 6A plotted.

AD-608-217

TECHNOLOGY OF NEW DEVITRIFIED CERAMICS - A LITERATURE REVIEW by Barry R. Emrich

A comprehensive review of the worldwide open literature was made to assist the research and development engineer in future work and inform the applications engineer of the present uses and capabilities of devitrified ceramics. The devitrified ceramics of primary concern are those materials which are predominantly crystalline bodies produced by induced and controlled nucleation and crystallization of preformed glass articles. The study includes information on compositional and processing factors, fundamental phenomena, properties, the effects of crystal sizes, heat treatment, composition on properties, and applications. It also includes selected abstracts.

Table II: Crystal size, modulus of rupture and Young's modulus as a function of heat treatment after nucleation for 4-6 hours at 760° C.

Figure 5: Modulus of rupture as a function of crystal size and surface condition of a fine-grained devitrified ceramic.

Figure 6: Schematic graph of postulated relationship between strength, crystal size and surface flaws in ceramics. (Ref. 1).

Figure 7: Effect of grain size on strength of polycrystalline aluminum oxide (Ref. 133).

Figure 13: Modulus of rupture comparison data between pyroceram 9606 and BeO, ${\rm Al}_2{\rm O}_3$ and fused silica.

Figure 14: Maximum temperature from which Al_20_3 , pyroceram and slip-coat fused silica may be quenched as a function of ab. Walton and Bowen (Ref. 172).

a=half the thickness

b-heat transfer coefficient

Figure 15: Effect of temperature on transverse strength of ${\rm Al}_2{\rm O}_3$, pyroceram, and slip-cast fused silica. Walton and Bowen (Ref. 172). Figure 16: Frontside-backside temperature of ${\rm Al}_2{\rm O}_3$, pyroceram and slip-cast fused silica as a function of time in oxygen-hydrogen rocket

motor exhaust. Samples 1/4 inch thick. Walton and Bowen (Ref. 172). Figure 17: T Between frontside and backside of Al₂O₃, pyroceram, and slip-cast fused silica as a function of average wall temperature in oxygen-hydrogen rocket motor exhaust. Walton and Bowen (Ref. 172). Table IV: Expansion in mils per inch vs temperature in degreed centigrade.

Table VIII: Relative physical and thermal merit ratios Noble et al (Ref. 182).

Figure 29: Comparison of coefficient of expansion for low expansion materials.

N66-14174

A FEASIBILITY STUDY ON THE USE OF POWDERS AS HEATRANSFER MEDIA IN IRRADIATION CAPSULES by J. L. Evans

This paper studies the possible use of ceramic powders as a heat transfer media in irradiation capsules. The desirable properties of such powders are high thermal conductivity, compatability with capsule material, and sufficient flexibility to allow unimpeded distortion of the irradiation specimen. The factors affecting these properties are discussed and a high degree of flexibility has been found to be incompatible with a high conductivity. Therefore, the use of powders for high heat rating applications is not feasible.

Figure 1: Thermal conductivity of MgO/He mixture at $1000^{\frac{\pi}{n}}/\text{in}^2$ abs.

Figure 2: Thermal conductivity of MgO/He mixture at $500 \frac{\#}{100} / in^2$ abs.

Figure 3: Thermal conductivity of MgO/He mixture at 50 $^{\#}/\text{in}^2$ abs.

Figure 4: Thermal conductivity of MgO/He mixture and solid MgO,

BeO, SiC, Al_2O_3 , and graphite at $15\#/in^2$ abs.

Figure 5: Thermal conductivity of MgO/He and BeO/He mixtures and He at $15\#/\text{in}^2$ abs.

Figure 6: Thermal conductivity of MgO and BeO/He mixtures at various packing fractions (calculated from Euben's and Laubitz's equations).

THERMAL CONDUCTIVITY OF CERAMICS by D. R. Flynn

In this paper, thermal conductivity is defined and a brief phenomenological description of the energy transport mechanisms involved are presented. The influence of environmental effects on thermal conductivity is discussed (temperature, stress, pressure, etc.) There is also discussion on the effects of composition and structure on thermal conductivity.

Some remarks are made on the reliability of some thermal conductivity data. Techniques for measuring thermal conductivity are described and there are comments on the availability and use of thermal conductivity reference standards.

Equations for different methods of computing thermal conductivity are presented:

Figure 8-Page 69: Idealized temperature dependence of thermal conductivity for a single-crystal - (Al_2O_3) .

Figure 18-Page 79: Thermal conductivity of some non-metallic crystals compared with very pure copper (Al₂0₃, LiF, quartz, diamond NaF).

Figure 21: High temperature thermal conductivity of TiC

Figure 19: High temperature thermal conductivity of several ceramic materials (SiC, MgO, Al₂O₃, Spinel, Graphite, ZrO₂, fused SiO₂, etc.)

Figure 23: Volume-temperature diagram for SiO2.

Figure 30-Page 56: Effect of stress on the expansivity of alumina.

AD-607-742

THERMAL RADIATION CHARACTERISTICS OF TRANSPARENT, SEMI-TRANSPARENT AND TRANSLUCENT MATERIALS UNDER NON - ISOTHERMAL CONDITIONS by R. C. Folweiler & W. J. Mallio

This report compares calculated and experimentally measured values of emissivity for smaples of ${\rm Al}_2{\rm O}_3$, ${\rm MgO}$, ${\rm SiO}_2$, and ${\rm SrTiO}_3$. Experimenal values were measured from room temperature to $1200^{\rm O}{\rm C}$ and at wavelengths from one to fifteen microns. Numerous graphs are presented for comparison of calculated vs experimentally measured values.

Figure 6.1: Absorption coefficient of single crystal Al₂0₃.

Figure 6.2: Absorption coefficient of single crystal MgO.

Figure 6.3: Absorption coefficient of single crystal SrTiO₃.

Figure 6.5: Absorption coefficient of single crystal SiO_2 glass.

Figure 7.1 - 7.15: Measured vs calculated emissivity of ${\rm Al}_2{\rm O}_3$ (at different temperatures and different samples of ${\rm Al}_2{\rm O}_3$).

Figure 7.16 - 19: Measured vs calculated emissivity of SiO2 glass.

Figure 7.20 - 25: Measured vs calculated emissivity of MgO (Mg-) at different temperatures.

Figure 7.26, 7.27, 7.28, 7.29: Measured vs calculated emissivity of SrTiO₂ (at different temperatures).

Figure 7.30 - 7.36: Measured vs calculated emissivity of commercial ${\rm Al}_2{\rm O}_3$ at different temperatures.

Figure 9.2: Comparison of isothermal and non-isothermal emissivity of an Al_2O_3 body (Western Gold and Platinum Company) Al-3-96%, $SiO_2-4\%$). Non-isothermal radiating surface at 898° C - Thermal gradient 60° C/cm. Isothermal radiating surface at 895° C.

AD-740-255

THERMOPHYSICAL PROPERTIES OF SOLID MATERIALS by E. Fitzer

The thermal expansion behavior of pure platinum, sintered ${\rm Al}_2{\rm O}_3$, sintered and arc cast tungsten, and three types of polycrystalline graphite was determined

experimentally at temperatures from 1000°C to 2600°C .

Table 5: Experimental results of thermal expansion on alumina compared with literature data.

Table 11: Experimental results on thermal expansion of R.V.D. graphite (across grain).

Figure 15 & 16: Thermal expansion and deviation of alumina vs temperature.

AD-753-85

CERAMIC MATERIALS FOR HIGH TEMPERATURE GAS BEARINGS by P. J. Gielisse, et al

The attempt of this study is to determine the order of magnitude of the temperature between the sliding surfaces, both at a macroscopic and microscopic level. The macroscopic approach provides little other than the prediction of the bulk temperature distribution in the material and at the surface of it. It also provides some guidance as to the magnitude of the thermal stresses that might occur immediately below the surface. The macroscopic analysis also provides a mean temperature and an estimate of the magnitude of the thermal energy generated at a particular portion of the disc. This information can then be used as a starting point for the analysis to estimate the microscopic surface temperature which is a function of the light and spectrum distribution of the aspecities. Knowing the microscopic temperature distribution, one can write various chemical note equations and postulate and interpret the reactions that are or might be occurring at the surface at the microscopic level.

Table II: Surface analysis data for the nominally 30 micro inch surfaces of hot pressed silicon nitride.

Figure 1-18: Coefficient of friction vs time (continuous run, and stop-start cycles for various materials).

Table VIII, Page 48: Abrasive size and concentration used in polishing experiments on hot-pressed ${\rm Si_3N_4}$.

Table IX, Page 67, Table X, Page 68: Data obtained inneutron activation analysis of $\mathrm{Si_3N_4}$ sample.

Figure 36, Page 88: Temperature developed by two rotating discs as a function of radius (R) and depth (Z) in inches.

Page 112-115: Appendix 1 - Chemical properties of silicon nitride.

Page 116-118: Electrical properties.

Page 119-130: Mechanical and physical properties.

Page 131-135: Thermal properties.

Journal of The American Ceramic Society, Vol. 53, No. 7, pp. 399-406.

EFFECT OF SMALL AMOUNTS OF POROSITY ON GRAIN GROWTH IN HOT-PRESSED MAGNESIUM OXIDE AND MAGNESIOWUSTITE by R. S. Gordon, et al

Grain growth was studied at 1300° , 1400° and 1500° C in nearly theoretically dense (0.1 to 0.8% porosity) hot pressed magnesium oxide (99.99 + %) and magnesiowustite (0.10 and 0.48 wt% Fe_2O_3). Small amounts of porosity had large effects on the kinetics of grain growth. Grain growth is probably porosity-controlled in MgO at all temperature and in magnesiowustite at 1400° and 1500° C if pores remain on grain boundaries or at grain intersections. The tendency for the entrapment of porosity is enhanced as the temperature is increased and as the dopant (Fe_2O_3) concentration is decreased. Small amounts of porosity (<1%) can cause limiting growth situations at grain sizes well below $100~\mu\text{m}$. The Fe_2O_3 dopant stabilizes squared grain growth kinetics at 1300° C and decreases the rate of grain growth at all three temperature.

N73-13576 or AD-748-389

DEVELOPMENT OF A HIGH STRENGTH BERYLLIA MATERIAL by J. Greenspan

Beryllia powders mixed with minute (but sufficient) amounts of alumina were pressure sintered from low temperature to high integrity. The minute amount of alumina greatly improved the densification process, and provided a combination of fine grain size and low porosity. The alumina power particles

are much finer than that of beryllia. The hot pressure temperature is approximately 1360° C to 1500° C.

Densification of the powder mass was composed of the two distinct processes: (1) "chemical combination" of alumina (Al_20_3) with beryllia (BeO) to form chrysoberyl (BeAl $_20_4$). (2) the "sintering" of the particles to an integral mass by interatomic diffusion.

This kind of combination sintering has to follow two principal requirements: (1) sufficient temperature (2) sufficient alumnina.

The microsturctures were examined by both optical and electron miscroscopy and it comes out that the wave frequency was of the order of 5 to 10 megahertz. Flexural strength was determined by simple beam, single point flexture for which the span was two inches. The content of alumina varies from 5% to 20% by weight and the pressing temperature was of the order of 1390° C to 1400° C.

The product of unusual combination of fine grain size and low porosity is characterized also by higher strength. The flexural strength valves obtained here which were of the order of 46 to 51 thousand psi were significantly greater than those typical of sintered monophase beryllia and the moduli is 56 to 57 million psi, the same as monophase beryllia. Experiments proved when the alumina content was decreased to 3% (from 5%). "Combination sintering" did not occur at the 1390° to 1400° C, but it did take place when temperature is 1500° C.

Another analysis found that under the present circumstances of processing the minimum temperature for "combination sintering" must be greater than 1390° C (2479°F). But the strength peak is defiend by pressing temperature near 1400° C (2550°F). This would yield the typical dense, fine grained high strength microstructure.

Finally, the article summarizes that the combination sintering of beryllia with minute (but sufficient amounts) of alumnina can produce a fine grain size with low porosity, high strength beryllia material. The practical aspects are that the important temperature and time parameters for pressure sintering are significantly less than those normally required for beryllia.

N63-21233

A STUDY OF THE PHYSICAL BASIS OF THE MECHANICAL PROPERTIES OF CERAMICS by G. E. Gross

A literature survey of the properties of ceramics, both classical nd solid state theory, is presented. A better understanding of the eramic properties as related to their electron - lattice structure was ained by correlating the mechanical properties of brittleness and uctility with the electronic and crystalline (lattice) properties of aterials.

Experimental methods and results are given for surface energy and all coefficients measurements.

Figure 3 - Page 13: Critical force curve for a MgO specimen.

-N66-23566 or AD-628-396

THE MECHANICAL PROPERTIES OF CERAMIC ALLOYS by G. W. Groves, et. al.

This paper deals with MgO and Al_2O_3 crystals that were deliberately impurified with Ti (.2%). An increase in the resistance to dislocation motion was observed as a result of heat treatment. The micro-structure of an MgO crystal is also described.

Figure 4: Surface hardness of MgO - .2% Ti vs annealing time at 1000°C .

N67-15019 (AD-641-657)

THE FRACTURE TOUGHNESS OF IMPURE MgO Crystals by G. W. Groves & D. A. Shockey

Fracture surface energies of MgO and MgO with Ti impurities were measured using the technique of driving cracks thru the crystals in a series of small jumps.

The values obtained by testing agreed fairly well with calculated values. A histogram of surface energies obtained is also included.

Figure 3: Surface energy vs length of crack.

Figure 56: Instron chart.

Ceramic Bulletin, Vol. 49, No. 6 (1970). pp. 575-579

EFFECT OF VARIOUS SURFACE TREATMENTS ON THE BEND STRENGTH OF HIGH ALUMINA SUBSTRATES by R. F. Gruszka, et a

This paper studies the variation of the strength of a fine-grained 99.5% alumina substrate as a function of the surface condition. Various machining methods are used on the substrates and they are then tested.

Table I: Modulus of rupture (MOR) tests.

Table II: MOR results vs. treatment time in fused borax.

Table III: MOR results for diffusion annealed specimens.

N65-25980 · · or AD-614-472

SEMICONDUCTING MATERIALS, PART III - AN INVESTIGATION OF THE DIELECTRIC PROPERTIES OF SINGLE CRYSTAL VERSUS POLYCRYSTALLINE MATERIALS

by D. L. Guile

This paper concerns studies to determine the effects of grain boundaries upon polycrystalline ceramic dielectrics. Dielectric measurements of polycrystalline samples are compared with measurements from single crystals.

It was determined that the Koops approach of analyzing the results was invalid.

The dielectric properties of single crystal and polycrystalline MgO, polycrystalline MgF $_2$, and ZnS samples are presented in graphic form over a wide range of temperatures and frequencies. Activation energies are also given for the loss mechanisms present.

Journal of The American Ceramic Society, Vol. 52, No. 11, pp. 585-590.

MECHANICAL PROPERITES OF POLYCRYSTALLINE BETA-SiC by T. D. Gulden

This paper gives various mechanical properties of chemically vapor-deposited beta-SiC over a range of temperatures (room temperature to 1400° C).

Table I: Density, grain diameter, mean fracture stress, and Young's modulus for samples of SiC tested at room temperature.

Table II: Same as above as functions of temperature and grain diameter.

Figure 3: Bend strength vs. temperature.

Figure 4: Young's modulus vs. temperature.

Figure 5: Typical stress-strain curves at various temperatures.

Journal of The American Ceramic Society, Vol. 55, No. 5, pp. 249-253.

.STRENGTH DEGRADATION AND CRACK PROPAGATION IN THERMALLY SHOCKED AL_2O_3 by T. K. Gupta

This report shows that strength degradation and crack propagation are a function of grain size and initial strength. Aluminum oxide specimens were heated to a temperature of 1200° C and then quenched at various temperatures and the room temperature strengths measured. All data is for alumina.

Table II: Room temperature strengths of thermally shocked aluminas as functions of quenching temperatures.

Figure II: Modulus of rupture vs. quenching temperature (MOR at room temperature).

Journal of Materials Science, 8, (1973), pp. 1283-1286.

RESISTANCE TO CRACK PROPAGATION IN CERAMICS SUBJECTED TO THERMAL SHOCK by Tapan K. Gupta

In this article, the author shows that the resistance to crack propaga in ${\rm Al}_2{\rm O}_3$, zirconia, and porcelain when subjected to thermal shock is related

the materials initial strength.

Figure 1: Resistance vs initial strength for Lucalox alumina, commercial alumina, and porcelain.

N71-15878

DYNAMIC YIELD STRENGTHS OF LIGHT ARMOR MATERIALS by W. H. Gust E. B. Boyce

The dynamic compressive yield strength, or Hugoniot elastic limits were determined for a number of light ceramics. (B_4 C, BeO, Al $_2$ O $_3$, SiC, TiB $_2$, AlB $_{12}$, TiBe $_{12}$, Be $_2$ B, Si, and ZrBe $_{13}$) Hugoniot parameters to about 1Mbar were measured for B $_4$ C, BeO, and four aluminas, and to about .5 Mbar for Si. Equations are given for various stresses, velocities, etc.

Table II, Page 8: Hugoniot parameters (for materials studied).

Table III, Page 9: Hugoniot elastic limits.

Table IV, Page 10: Axial yield strengths and phase-transition pressures Figure 4 and 5: Experimental Hugoniot for SiC, ${\rm TiB}_2$, Vascomax 350, and crystalline silicon.

Figure 13, Page 17: Longitudinal, bulk and shear moduli vs density for alumina ceramics for ultrasonic measurements.

Table 5: Ultrasonic bulk moduli for materials at theoretical density

Figure 13: Distention ratio versus stress for alumina ceramics.

Table 6: Distention ratios and stress offsets in BeO and Al O

Engineering Fracture Mechanics, 1969, Vo⁷. 1, pp. 463-471.

OBSERVATION AND MECHANISMS OF FRACTURE IN POLYCRYSTALLINE ALUMINA by Paul L. Gutshall & Gordon E. Gross

The fracture mechanisms of polycrystalline alumina have been investigated using the double cantilever beam cleavage method. The fracture resistance of alumina was measured at temperatures up to 1500° C. The fracture resistance of alumina increased with increasing grain size for temperature studied.

The lower softening point of SiO₂ causes alumina with this material as a binder to lose its strength at lower temperatures than does MgO bonded material. The mechanism of fracture in these polycrystalline ceramics leads to a suggested method for improved mechanical strength.

AD-745-744

CERAMIC SYSTEMS FOR MISSILE STRUCTURAL APPLICATIONS by J. N. Harris, et al

This report has numerous graphs and tables of mechanical properties of fused silica. There is also a small amount of data on Weibull parameters.

Table I: Mean values of results for sample composition.

Table II, Page 11: Equal weight comparison of area.

Table IV: Thermally and mechanically biased test of performance improvement.

Table V: Hot surface heat impact test conditions.

AD-745-744

Figure IX, page 32 - Effect of time at temperature on impact damage to slip-cast fused silica

Table VI, page 35 - Effect of multiple impacts on damage to slip-cast fused silica.

Table VII, page 47- Properties of slip-cast fused silica specimens prior to creep testing.

Figure 22, page 49 - Definition of creep rates in the determination of viscosity values

Figure 23, page 51 - Variation of viscosity with time for commercial C silica.

Figure 24, page 52 - Variation of viscosity with time for high purity HPA silica

Figure 27, page 56 - Schematic of Ring Tensile Test

Table X, page 63 - Physical property data for 3/4 inch test bars sintered six hours at 2210° and 2250° F

Table XI - Test results on 5 3/4 inch inside diameter rings

Table XII, page 65 - Test results on 16 - 1/2 inch diameter rings

Table XII, page 66 - Test results on 29 - 1/2 inch diameter rings

Table XIII, page 67 - Test results on 29 - 1/2 inch inside diameter rings

Table XIII, (cont.) page 68 - Test results on 29 - 1/2 inch inside diameter rings

A summary of test results is shown in Table XIV. It is seen that there does exist a consistent variation of strength with volume and it is believed that the strength characteristic of slip-cast fused silica can be described by the Weibull statistic. It also appears that there is a variation of the modulus of elasticity with volume but it is not believed that a general conclusion should be drawn with respect to this property.

Table XIV, page 69 - Summary of test results

Figure 31, page 70 - Weibull plot of hydrostatic ring test data

Figure 33, page 78 - Illustration of the chronological development of ceramic radomes in terms of mach number and flight altitude.

Table XV, page 79 - Individual mechanical test specimen data

Table XVI, page 83 - Individual ablation test specimen data

Table XVII - Flow density constants for various materials

Figure 34 - Required factor of safety as function of material flow density constant

FUSED SILICA DESIGN MANUAL by J. N. Harris & E. A. Welsh

This volume provides a summary of the current status of the knowledge of designing slip-cast fused silica hardware. It is intended to provide the user with a basic knowledge of material and processing techniques as well as basic design information. Pages, figures and tables have been numbered by chapters. Subjects covered in this volume are: fused silica raw material preparations, size reduction and slip preparation, slip casting, drying and firing and room temperature and elevated temperature properties.

Page 1 - 3, Figure 1-1 - Viscosity of fused silica

Page 1 - 6, Figure 1-2 - Dielectric constant versus temperature for candidate radome materials

Page 1 - 7, Figure 1-3 - Loss tangent versus temperature for candidate radome materials

Page 1 - 8, Table 1-1 - Weight parameter for radome materials Table 2 - 3, Page 2-13 - Properties of technical and high purity silica slips

Figure 2 - 5 - Particle size distributions for fused silica slips Figure 3 - 1, Page 3-8 - Cast wall thickness versus time of casting for fused silica

Figure 3 - 3, Page 3-17 - Hypothetical strengthening processing in slip-casting fused silica

Figure 3 - 6, Page 3-21 - Percent porosity versus sintering time for high purity and technical grade fused silica slips sintered at 2100° F, 2250° F, and 2400° F.

Figure 3 - 7, Page 3-22 - Modulus of rupture versus sintering time for high purity and technical grade fused silica slips sintered at 2100° F, 2250° F, and 2240° F.

Figure 3 - 10, Page 3-27 - Bulk density of technical grade slip-cast fused silica fired in different atmospheres at $2200^{\circ}F$

Figure 3 - 11, Page 3-28 - Modulus of rupture of technical grade slip-cast fused silica in different atmosphere at 2200°F

AD-766-494

Figure 3 - 12, Page 3-29 - Dynamic Young's modulus versus sintering time for high purity slip-cast fused silica, with mean particle diameter of 4.7 and 17 micrometers

Page 3 - 31, Figure 3-13 - Bulk density versus sintering time for high purity fused silica slips with mean particle diameter of 4 and 7 micrometer sintered at 2100^{0} F, and 2400^{0} F

Page 3 - 32, Figure 3-14 - Percent porosity versus sintering time for high purity fused silica slips with mean particle diameters of 4 and 7 micrometers sintered at 2100° F, 2250° F, and 2400° F.

Page 3 - 33, Gifure 3-15 - Modulus of rupture versus sintering time for high purity fused silica slips with mean particle diameters of 4 and 7 micrometers sintered at 2100°F, 2250°F and 2400°F.

Figure 3 - 16, Page 3-34 - Dynamic Young's modulus versus sintering time for high purity slip-cast fused silica prepared from slips with mean particle diameter of 4 and 7 micrometers sintered at 2100° F, 2250° F, and 2400° F.

Page 3 - 35, Figure 3-17 - Bulk density of technical grade slip-cast fused silica in air at one atmosphere

Page 3 - 36, Figure 3-18 - Porosity of technical grade slip-cast fused silica fired in air at one atmosphere

Page 3 - 37, Figure 3-19 - Modulus of rupture of technical grade slip-cast fused silica fired in air at one atmosphere

Figure 3 - 20, Figure 3-40 - Transisent heat conduction in a radome initially at temperature Ti, as external sufrace is held at temperatur Ts while internal surface is insulated

Figure 3 - 21, Figure 3-41 - Transisent heat conduction in a cylindric test bar, initially at temperature T, as the surface is held at temperature Ts

Figure 3 - 22 - Transisent heat conduction in a radome or cylindrical test bar initially at temperature Ti, as the surface is raised to a temperature Tx at a constant rate

Figure 4 - 1 - Elastic modulus versus density for high purity and technical grade slip-cast fused silica

Figure 4 - 2 - Elastic modulus with respect to density for slip-cast fused silica from 30 to 139 lb/ft^3

Figure 4 - 3 - Modulus of rupture versus density for high purity slip-cast fused silica

Figure 4 - 4 - Modulus of rupture versus density for a technical grade slip-cast fused silica

Table 4 - 1 - Surface and volume effect on modulus of rupture of slip-cast fused silica

Table 4 - 2 - Volume effects on tensile strength of large diameter rings Figure 4 - 5 - Compressive strength of slip-cast fused silica with respect to bulk density \cdot

Figure 4 - 6 - Flexural modulus of elasticity versus temperature for slip-cast fused silica

Figure 4 - 7 - Modulus of rupture versus temperature for slip-cast fused silica

Figure 4 - 8 - Tensile strength versus temperature for slip-cast fused silica

Figure 4 - 9 - Compressive strength versus temperature for high purity and technical grade slip-fused silica

Figure 4 - 10 - Poisson's ratio of slip-cast fused silica

Figure 4 - 11 - Expansion coefficient of fused silica

Figure 4 - 12 - Thermal expansion of slip-cast fused silica determined in a graphite dilatometer

Figure 4 - 13 - Variation of viscosity with time for technical grade slip-cast fused silica

Figure 4 - 14 - Variation of viscosity with time for high purity slipcast fused silica

Figure 4 - 15, Page 4-27 - Cristobalite levels in high purity and technical grade slip-cast fused silica after viscosity tests

Figure 4 - 16, Page 4-29 - Thermal conductivity of slip-cast fused silica at various porosity levels

Table 4-3 - Constants for the density function for high purity SCFS Figure 4-17, Page 4-35 - Density of slip-cast fused silica versus time at temperature

Figure 4 - 18, Page 4-37 - Thermal conductivity of slip-cast fused silica

Figure 4 - 19, Page 4-40 - Heat capacity of fused silica

Figure 4 - 20, Page A-41 - Enthalpy of fused silica

AD-766-494

Figure 4 - 21, Page 4-43 - Thermal diffusivity of slip-cast fused silica and foamed fused silica

Figure 4 - 22, Page 4-44 - Electrical resistivity of fused silica Figure 4 - 23, Page 4-45 - Dielectric constant of slip-cast fused silica versus density measured at X-band

Figure 4 - 24, Page 4-48 - Dielectric constant of slip-cast fused silica as a function of density

Figure 4 - 25, Page 4-49 - Dielectric constant versus temperature for slip-cast fused at 6 GHZ

N71-25315

OF CERAMIC MATERIALS by T. M. Heslin

This report is the text of a very brief talk given by the author at a symposium. The author briefly describes the work going on to investigate the relationship between surface conditions and strength and the distribution of strength values and to try to develop methods for improving ceramics in these areas.

Apparently, most of the work has been done on ${\rm Al}_2{\rm O}_3$ and the best results from the application of a compressive glaze. One table is given on page 255.

Table: Effects of flow elimination and compensation on the strength of Al_2O_3 . (Gives the mean strength and "spread" of values for various finished samples under a 4-point loading test).

AD635-621

THERMAL RADIATION CHARACTERISTICS OF TRANSPARENT,

SEMI-TRANSPARENT AND TRANSLUCENT MATERIAL

UNDER NON-ISOTHERMAL CONDITIONS

by Henry A. Hobbs & Robert C. Folweiler

Over a range of wavelengths from one to six microns where oxide ceramics are partially transparent, radiant energy emission must be treated as a volume rather than a surface phenomena. As a result the absorption coefficient (mainly determined by composition) and the scattering of coefficient mainly determined by microstructure are important variables. In addition, temperature gradient affects radiant energy emission so that effective "emissivity" under non-isothermal conditions is neither a material constant nor a sample constant.

AD635-621

- Figure 3.3: Temperature of sample versus distance from axis during non-isothermal furnace operation. (sample A1-4). Sample temperature $500-1300^{\circ}\text{C}$ vs distance from axis 0.5-1.3 inches.
- Figure 3.5: Ratio $(\epsilon_{\eta}/\epsilon_{\infty})$ 0.75-1.25 vs $\lambda(\mu)$ 0-1.4; emissivity ratio vs wavelength for AD-995 at approximately 600°C.
- Figure 3.6: Similar to Figure 3.5 at 900°C.
- Figure 3.7: Similar to 3.6 at 1100°C.
- Figure 3.8: Ratio $(\epsilon_n/\dot{\epsilon}_\infty)$ 0.75-1.25 vs $\lambda(\mu)$ 0-1.4; emissivity ratio vs wavelength for AD-85 at approximately 600°C.
- Figure 3.9: Emissivity ratio at approximately 900°C.
- Figure 3.10: Emissivity ratio at approximately 1100°C.
- Figure 3.11: Emissivity ratio for Al-1 at approximately 600°C.
- Figure 3.12: Emissivity ratio at 900°C.
- Figure 3.13: Emissivity ratio at 1100°C.
- Figure 3.14: Emissivity ratio for Al-4 at approximately 600°C.
- Figure 3.15: Emissivity ratio at approximately 900°C.
- Figure 3.16: Emissivity ratio at approximately 1100°C.
- Figure 3.17: Emissivity ratio for SrTiO3A at approximately 600°C.
- Figure 3.18: Emissivity ratio for $SrTi0_3A$ at approximately $900^{\circ}C$.
- Figure 3.19: Emissivity ratio at approximately 1100°C.
- Figure 3.20: Emissivity ratio for SrTiO3B at approximately 600°C.
- Figure 3.21: Emissivity ratio for SrTiO3B at approximately 900°C.
- Figure 3.22: Emissivity ratio for pyroceram 9606 at approximately 900°C.
- Figure 3.23: Emissivity ratio for pyroceram 9608 at approximately 600°C .
- Figure 3.24: Emissivity ratio for pyroceram 9608 at approximately 900°C.
- Figure 5.2: Extinction coefficient vs wavelength for AD-995
- Figure 5.3: Extinction coefficient vs wavelength for AD-85.
- Figure 5.4: Extinction coefficient vs wavelength for Al-1.
- Figure 5.5: Extinction coefficient vs wavelength for Al-4.
- Figure 5.6: Extinction coefficient vs wavelength for SrTiO3A.
- Figure 5.7: Extinction coefficient vs wavelength for pyroceram 960
- Figure 5.8: Extinction coefficient vs wavelength for pyroceram 9608.

EPRODUCIBILITY OF THE PAGE IS POOR

AD-635-621

Figure 5.10: Transmissivity 0 - 0.16 vs wavelength 0 - 5; measured and calculated transmissivity vs wavelength for AD-995

Figure 5.11: Transmissivity for AD-85

Figure 5.12: Transmissivity for Al-1

Figure 5.15: Transmissivity for A1-4

Figure 5.14: Transmissivity for SrTiO3A

Figure 5.15: Transmissivity for pyroceram 9606

Figure 5.16: Transmissivity for pyroceram 9608

Table 5-I: Calculated and measured extinction coefficients. (all samples 6 mils thick except where noted).

Journal of The American Ceramic Society, Vol. 53, No. 9, pp. 490-495.

STRENGTH BEHAVIOR OF POLYCRYSTALLINE ALUMINA SUBJECTED TO THERMAL SHOCK by D. P. H. Hasselman

Theoretical predictions of crack propogation behavior in brittle solids under conditions of thermal shock were verified by water quenching of cylindrical polycrystalline alumina rods followed by strength testing. The caluclated quenching temperature difference (Tc) required to initiat thermal stress fracture agreed fairly well with experimental data. When fracture was initiated, strength decreased catastrophically in agreement with theory. An expression for the strength remaining after thermal stre fracture was derived in terms of the pertinent physical parameters.

AD-653-483

MICROSTRUCTURE STUDIES OF POLYCRYSTALLINE REFRACTORY OXIDES by A. H. Heuer, et. al.

This report describes the synthesis of high purity ceramics (MgO and Al_2O_3) from powders and also discusses the microstructures of the final product. Mechanical properties are given as a function of microstructure, temperature, and fabrication method.

Table 2.2: Particles size of alumina and magnesia powders

Table 2.3: X-ray diffraction identification of high purity powders

Table 2.6: Fabrication conditions for high purity Al₂0₃

- Figure 2.7: Pressure-sintering densification kinetics for high and low purity alumina powders.
- Figure 2.9: Impurity profile for hot-pressed alumina specimen fabricated from United Mineral ${\rm Al}_2{\rm O}_3$.
- Table 2.7: Comparison of impurity concentration for alumina hot pressed sample 1188 and base powder.
- Figure 3.1: Variation of recrystallized grained size with deformation.
- Table 3.1a: Conditions for forgings from Al_2O_3 powder.
- Table 3.1b: Conditions for forgings from Al_2O_3 powder.
- Table 3.2a: Conditions for forging dense Al_20_3 billets.
- Table 3.2b: Conditions for forging dense $Al_2O_3 + 1/4\%$ MgO billets.
- Table 3.3: Process conditions for fabrication of $A1_20_3 + 1/4\% \text{ MgO}$ billets.
- Table 3.4: Forging strain rate data.
- Table 3.7: Modes of plastic deformation in alumina.
- Table 3.8: Preliminary bend strength results for press forged ${\rm Al}_2{\rm O}_3$ and ${\rm Al}_2{\rm O}_3$ + 1/4% MgO.
- Table 3.9: Transverse bend strength (Kpsi) at -196° and 1200° C and reference comparison values.
- Figure 3.38: Plot of -196° C strength data as a function of grain sizes
- Figure 3.39: Plot of 1200°C strength (Table 9.3) data as a function of grain sizes.
- Table 3.10: Strength properties at 1400-1500°C.
- Figure 3.40: Strength vs temperature plots for a number of pressed forged samples.
- Table 4.1: Strength of flame-polished Lucalox.
- Figure 5.1: Isothermal grain growth curves for ultra-high pressure sintered MgO.

AD-649-274

THERMAL CONDUCTIVITY OF ALUMINUM OXIDE by M. Hoch

The list of charts are from experiments with a method of measuring thermal conductivity at elevated temperatures at the Air Force Materials Laboratory. All data is for Al_2O_3 discs of various size and grain size.

Table 2: Total emittance of aluminum oxide (1350°K).

Table 3: Thermal conductivity of Al₂O₃.

Figure 5: Temperature-distance relationship on the surface of Al_2O_3 samples (To=1275 $^{\rm O}$ K).

Figure 6: Temperature-distance relationship on the surface of Al_2O_3 samples (To=1340°K).

Figure 7: Temperature-distance relationship on the surface of Al_2O_3 samples (To=1340°K).

Figure 8: Temperature-distance relationship on the surface of AI_2O_3 sample (To=1450°K).

N69-28435

PLASTIC DEFORMATION OF CARBIDES by G. E. Hollox

This paper reviews the current understanding of the mechanical behavior of carbides. It concentrates on evaluating the properties of single crystals rather than sintered polycrystalline materials.

Titanium carbide is the main material studied.

Figure 2, Page 202: TiC equilibrium diagram.

Figure 7, Page 204: Temperature dependence of yield stress in TiC.

Figure 12: The yield strength of some TiC - VC alloys.

Figure 18, Page 211: Microhardness of carbides as a function of temperature.

Figure 20, Page 213: Strength-to-density ratio for several carbides.

AD-650-230

SUPPLEMENTARY DIELECTRIC-CONSTANT AND LOSS MEASUREMENTS ON HIGH TEMPERATURE MATERIALS by J. Iglesias & W. B. Westphal

This is a summary report on dielectric constant and loss measurements conducted at the Laboratory for Insulation Research at the Massachusetts Institute of Technology after 1958, excepting high-dielectric constant materials. The emphasis is on high-temperature materials (those melting point above 1200° C). The sample of solids includes oxides of Al, Be, Mg, various silicates, rocks and minerals, and others. Pure samples of Al₂O₃, MgO, BeO, and SiO₂ all show loss temperatures less than 0.01 at 1500° C in the microwave region.

Table 1: Melting points of oxides.

Table 2: Melting points of binary tri-element compounds.

Page 15: Loss tangent 0.5001 - 4.0 vs temperature Oc - 700

Page 16: High purity alumina (99.99%) density $3.32g/E^{1}/E$.

(7-11) vs $T^{O}C$ 0-600.

Page 17: Loss tangent 0.00002 - 0.1 vs temperature °C - 700 (alumina density 3.32 gm/cc.)

Page 18: Alumina (99.999%) density 3.23 g/cm 3 . K 1 7-12 vs temperature OC 0-600.

Page 19: Loss tangent 0.00002 - 0.1 vs temperature °C 0 - 700.

AD-697-358

DIELECTRIC PROPERTIES OF GLASS by J. O. Isard

Amorphous inorganic materials are becoming more important in solid state electronics as substrates, encapsulating materials, and dielectric layers.

The high dielectric strength and impermeability of amorphous layers result from the absences of pores and grain boundaries; however, the range of properties is somewhat limited. A good dielectric is usually required to have a high permittivity, a low loss tangent, and low temperature coefficient of permittivity. Glasses have been found to be somewhat limited in all of these respects, especially by temperature coefficient.

CALCIUM BORALUMINATE GLASSES

The d.c. conductivity was found to be very low and the audio-frequency losses were low up to 250-300°C; above this temperature range the loss was rapid, with temperature and showed a frequency dispersion characteristic of the high frequency tail of a Debye relaxation phenomenon as for the migration losses in ordinary glass.

The dielectric constant ranged from about 5 to 9, depending chiefly on CaO content.

FUSED SILICA - (4 commercially prepared samples were investigated)

D.C. conductivity showed a correlation with alkali impurity.

Activation energies ranged from 17 to 34 k cal/mole a dielectric constant of 4 independent of frequency up to about 300°C.

BARIUM GLASSES

Permittivities ranged from 6 to 9.5 depending mostly on BaO content; temperature coefficients in the range 80-200 ppm/ $^{\circ}$ C, the loss tangent low (.0005) over a wide range of frequency and temperature. PbO-Al $_{2}$ O $_{3}$ -B $_{2}$ O $_{3}$.

Conductivities were markedly higher at corresponding compositions due to lower activation energies (28.5-35 kcal/moles) Permittivities were 8.5 to 17 depending on Pb content and showed temperature coefficients of 80 to 350 ppm/°C. Loss tangent was low, approximately 0.001.

LEAD SILICATE GLASSES - comparisons made, but no data given.

OF SELECTED DIELECTRICS by J. R. Jasperse, et al

The infrared spectra was measured for LiF and MgO at temperatures ranging from 7.5° K to near the melting point of each crystal. Data was curve-fitted to a two-pole, damped, harmonic oscillator model and a temperature dependent expression for the dielectric constant was determined.

Figure 6, Page 25: Reflectivity vs. normalized frequency for LiF.

Figure 7, Page 26: Reflectivity vs. normalized frequency for MgO.

Table II & III, Pages 27 & 33: Damping constants for main band and side band (for LiF).

Figure 9, Page 29: $\frac{1}{R_{\text{max}}}$ vs. $\frac{\gamma}{w_0}$ for MgO.

Figure 8, Page 30: $\frac{1}{R_{\text{max}}}$ vs. $\frac{\gamma}{w_0}$ for LiF.

Figures 10 & 11, Pages 31 & 32: Percent reflectivity vs. wavenumber for LiF at various temperatures.

Figure 12: Extinction coefficient vs. wavenumber for LiF at various temperatures.

Figures 13 & 14, Pages 35-36: Percent reflectivity vs. wavenumber for MgO at various temperatures.

Figure 16, Page 37: Percent reflectivity vs. wavenumber for amorphous quartz at various temperatures.

Figure 15, Page 38: Extinction coefficient vs. wavenumber for MgO (temperature and frequency as parameters).

Figures 17 & 18, Pages 39 & 40: Percent reflectivity vs. wavenumber for quartz.

Figure 19, Page 41: Damping constant vs. temperature for MgO and LiF.

Figure 21, Page 46: Centrofrequency vs. temperature for LiF & MgO.

AD-643-464

EFFECT OF WATER VAPOR ON DIELECTRIC LOSS IN MgO by H. B. Johnson, et al

This paper is about a study conducted at the University of Utah on the effects of water vapor on dissipation factors of pure MgO (99.99+%) samples. Graphs of dielectric constants, dissipation factor, and arc conductivity are included.

Figure 1: Dissipation factor vs. frequency at various PH20.

Figure 3: Dissipation factor vs. contact parameters.

Figure 6: Dielectric constant vs. frequency at various PHO.

Figure 7: Arc conductivity vs. P_{H2}0 at various temperaturés.

Figure 9: Dissipation factor vs. frequency at various temperature $(P_{H_2O} = 3 \times 10^{-2} \text{ atm constant})$

AD-708-707

CHEMICAL STRENGTHENING OF $A1_20_3$ by J. T. Jones & J. T. Fraiser

This report deals with the strengthening of alumina by chemically orming a surface layer of various oxides by annealing the samples while enclosed in the various oxide powders.

The authors list various causes of fracture in brittle ceramics and then explain that fracture is a two-step process: first, the creation of a crack or flaw, and then the propagation of a crack through the material. The strength could be increased by making either of these steps more difficult. "It appears the most promising method...would be to impede the movement of the flaws through the structure rather than removing the flaws." The author explains this might be accomplished in various ways—one is by addition of an "internal" compressive stress by adding a compressive laver to the alumina.

AD-708-707 (cont.)

A three-point loading test was used to evaluate samples (loading rate 30 lb/min). Formulas used include:

MOR = $3/2 \frac{PL}{bd^2}$ for rectangular specimen

 $MOR = \frac{8PL}{bd^3}$ for round rods

Table 5, Page 13: Flexural strength data for polycrystalline samples.

Table 6: Statistical data for polycrystalline data.

Tables 7 & 8, Page 14: Flexural strength data for sapphire rods.

A paragraph for each sample type is included. Discussion of test results included.

N67-29106 or AD-650-883

FABRICATION OF DENSE FINE GRAINED CERAMIC MATERIALS by D. Kalish, E. V. Clougherty, & J. Ryan

High pressure hot pressing was used to prepare dense, crack free billets of boron carbide, silicon carbide, titanium carbide and titanium nitride. These materials were fabricated from high purity powders without additions of densification promoters. Fabrications were generally performed in the vicinity of 1800° C at 120,000 psi for 10 minutes.

Reactive high pressure hot pressing was investigated with varying atomic ratios of boron and carbon. Microstructures and mechanical properties were obtained for selected materials prepared by this technique. The results for high pressure hot pressed boron carbide and SiC materials were compared with conventionally fabricated materials.

Tables 1 thru 6: Characterization of test materials.

Figure 2, Page 12: Time-temperature-pressure cycle for high pressure hot pressing.

N67-29106 (cont.) or AD-650-883

Table 8, Page 26: Transverse bend strength of HPHP $\mathrm{B_4C}$.

Table 9, Page 28: Microhardness of HPHP B_AC .

Table 10, Page 29: Transverse bend strength of conventionally hot pressed B_AC (temperature, bend strength, modulus of elasticity).

Figure 11, Page 31: Microhardness as a function of B/C ratios in HPHC boron carbide.

Table 11, Page 34: Microhardness for conventionally hot pressed B_4C .

Table 13, Page 45: Bend strength of conventionally hot pressed SiC.

Figure 23, page 48: Knoop hardness vs. load for HPHC TiC.

Figure 24, Page 49: Grain size variation along HPHP TiC billet.

Table 14: Bend strength of TiC prepared by EDM.

Table 15: Bend strength of TiC at 25°C prepared by diamond machining.

Table 16: Bend strength of TiC heated in vacuum at 1500°C (1 hr.).

Table 17, Page 54: Modulus of elasticity at 25°C (HPHP TiC).

Figure 30, Page 60: Knoop hardness vs. load for HPHP titanium nitride

Figure 31: Grain size variation along the length of HPHP TiN compact.

N64-30928

APPLICATION AND EVALUATION OF REINFORCED REFRACTORY CERAMIC COATINGS by Charles Kallup, Jr., et al

Subjects reported on in this paper include: (1) Welding or retractory metal reinforcement media to a substrate and subsequent attempts to provide sufficient oxidation protection to the refractory metal, (2) the optimization of coating compositions, (3) selection and optimization of application techniq of vibratory casting, (4) fabrication and coating of nose cone and leading edge models, (5) compilation of thermophysical data, and (6) a bibliography of the state of the art of ceramic coating systems for use above 3000°F.

N64-30928 (cont.)

Tables VIII & IX, Page 17: Results of thermal drop testing for modified TherMarq ZPF-100 bodies.

Table X, Page 18: Emittance values of samples ZSF 115 thru 123 as compared to ZSF-101.

(Note: Appendix III gives composition of ZSF & ZPF samples).

Tables XI-XIV: Thermal evaluation of samples (includes test time, front face temperature, emittance, etc. Some include thermal drop $({}^{\circ}F/mil)$.

Table XV, Page 23: Comparative thermal drop Gata (for different samples in two different modes of test).

Tables XVI & XVII, Page 24: Qualitative comparison of impact strength of samples (weight of ball, diameter of ball, number of times dropped, remarks, and distance dropped).

Table XVIII, Page 26: Ultimate impact strengths of samples ZSF 124 through 130.

Table XIV: Modulus of rupture comparisons of ZSF 101, 124, and 131. Figure 10, Page 44: Graph of thermal expansion of TherMarq ZSF 124 (as dried in air, cured at 450°F, and cured at 2700°F) temperature vs. linear thermal length change (%).

Translated from Khimiya i Tekhnologiya Topliv i Masel, No. 6, pp. 1-5, June 1971.

EFFECT OF THE CHEMICAL COMPOSITION OF ALUMINUM OXIDE CATALYSTS ON THE STABILITY OF THEIR STRUCTUROMECHANICAL PROPERTIES DURING HEAT TREATMENT by Ya. R. Katsobashvili, et al

Increasing the heating temperature for γ -alumina results in a gradual decrease in its porosity, specific surface, and catalytic activity. This is related to recrystallization and the polymorphic transitions of γ -Al $_2$ O $_3$ which results in the formation of the inactive α form or corundum (2-4). If the aluminum oxide does not contain impurities, then its conversion into

Katsobashvili (cont.)

corundum is completed at $1200-1300^{\circ}$ C. The presence of impurities can lower this temperature markedly (5-8).

The change in the structuromechanical properties of the catalyst was studied which is associated with the change in the phase composition of the carrier during heat treatment. The results are given in Tables 1-3 and Figures 1 and 2.

AD-603-239

NON-METALLIC MATERIALS FOR HIGH TEMPERATURE STRUCTURAL APPLICATIONS by E. G. Kendall, et al

This paper is a study of the use of carbides, borides, beryllides, oxides, and fraphite in high temperature structural applications. Electrical, mechanical, and physical properties are presented.

. Table 1: Physical and mechanical properties of the refractory carbides.

Table 2: Physical properties of selected graphites.

Table 3: Conversion factors for high temperature properties of graphite.

Figure 4, Page 17: Percent transmission vs. wave length for alumina, beryllia, and magnesia.

Table 4: Physical and mechanical properties of refractory oxides.

Table 5: Physical and mechanical properties of refractory oxides.

Table 6: Physical and mechanical properties of refractory beryllides.

AD-768-840

THE EFFECTS OF MICROSTRUCTURE ON THE FRACTURE ENERGY OF HOT PRESSED MgO by J. B. Kessler, et al

The work-of-fracture technique was used to investigage the effect of various microstructural parameters on the fracture energy of relatively dense and hot MgO. Grain size, amount and location of porosity, and grain boundary precipitates were the parameters of major interest. The fracture energy measurements were found to be dependent on the microstructure and ranged from 0.47 and 0.27 X 10^4 ergs/cm². Grain boundary precipitates, found in as hot-pressed samples with LiF additives, weakened intergranular bonding and caused the lowest fracture energies. Limited porosity (up to 1.0%) had only a small effect on the fracture energy when found at grain boundaries, although this porosity did facilitate intergranular fracture. Porosity found within the grains appeared to promote a tearing between cleavage planes which in turn increased the fracture energy. The effect of grain size on fracture energy was not conclusive, although the percentage of transgranular fracture increased with grain size. These fracture energy values are compared to strength measurements and the limitations of the Griffith equation in explaining the results are discussed.

Conclusion:

- 1. Grain boundary precipitates in the as hot-pressed MgO with LiF causes intergranular fracture and low fracture energies.
- 2. For dense MgO with essentially no porosity present, fracture energy did not appear to depend on grain size up to $200\mu m$.
- 3. For "porous" MgO with up to 1.0% porosity, fracture energy increases with grain size up to $100 \, \mu \text{m}$. This behavior is thought to be caused by a shift in the location of porosity from intergranular at small grain sizes to within the grains at large grain sizes.
- 4. Intergranular porosity encourages intergranular fracture; however, it has little, if any, effect on fracture energy.

- 5. Within grain porosity produces a very rough appearing fracture surface with numerous cleavage steps and increases fracture energy.
- 6. When microstructure relates to crack propagation and initiation in different ways, fracture energy (as measured by the work-of-fracture technique) and strength cannot be compared on the basis of a Griffith-type relationship.

Table 1, Page 14: Effect of the initial anneal on the fracture energy of as hot-pressed MgO. Initial anneal was for about one hour at $1100-1200^{\circ}$ C in air.

Figure 1, Page 18: MgO strength and grain size versus firing temperatures.

Figure 3, Page 20: Typical plot of fracture energy versus percentage of remaining cross-sectional area to find minimum fracture energy.

Figure 4, Page 21: Dependence of fracture energy in grain size for "porosity" MgO.

Figure 6, Page 23: Dependence of fracture energy on grain size for dense MgO.

THERMAL EXPANSION OF CERAMICS by R. K. Kirby

This paper describes and defines several types of coefficients of thermal expansion and gives their applications. The theory of thermal expansion is reviewed and several applications to ceramics are given. Also, in this paper four general types of test methods are described.

The effect of several characterization parameters on the expansion of ceramics is discussed (phases, quantity of phases, grain size, orientation of anisotropic grains, microcracks, and stress).

Table 1, Page 42: Coefficients of linear thermal expansion for some ceramic materials at 300° K (MgO, Al₂O₃, SiC, and others).

Figure 2: Coefficients of thermal expansion for rutile (single crystal) in various directions from c-axis.

Figure 3: Expansivity of MgO as a function of temperature.

Figure 4: Expansivity of single-crystal rutile as a function of temperature.

Figure 5: Expansivity of indium antimony as a function of temperature.

Figure 10: Comparison between observed and calculated values of the expansivity of alumina in the crystallographic directions.

N71-23282 or AD-717-983

CHEMICAL STRENGTHENING OF CERAMIC MATERIALS by J. P. Kirchner, et al

This report investigates the use of compressive surface layers to improve the strength of ceramics. Various treatments such as glazing, glazing and quenching, reaction with powders at high temperatures, and chemical vapor deposition of low expansion surface layers are investigated. The materials studied include alumina, zirconium diboride, SiC, and zircon porcelain bodies.

The report also contains many tables and figures (26 tables and 41 figures, plus two appendices). Tables and figures concern flex strength, impact strength, creep rates, heat transfer coefficients, strains, stress profiles, density, porosity, additions of various chemicals to enhance strength, etc.

AD-724-315

STRENGTHENING OXIDES BY REDUCTION
OF CRYSTAL ANISOTROPY
by J. P. Kirchner & R. M. Gruver

In single phase polycrystalline ceramic bodies composed of anisotropic crystals, the stress resulting from applied loads, large scale residual stresses, and localized stresses combine to cause fracture. The localized stresses caused by crystal anisotropy are substantial in magnitude and in large grain size bodies cause local crack formation even in the absence of an applied load. In earlier investigations, compositions with reduced thermal anisotropy were made by solid solution additions. In the present investigation the flexural strength of alumina

ceramics, and of a composition in the system ${\rm Al}_2{\rm O}_3$ - ${\rm Cr}_2{\rm O}_3$ having reduced thermal anisotropy, were compared over a range of grain sizes in the as machined and quenched conditions. The fracture surfaces were studied. Very high strengths were observed.

Figure 1, Page 5: Schematic diagram of strength vs. grain size for oxide ceramics.

Table II, Page 11: Flexural strength vs. grain size for pressure sintered alumina in as polished and quenched conditions.

Figure 2: Flexural strength vs. grain size of pressure sintered alumina.

Table IV, Page 18: Flexural strength of CFC (Linde A) alumina with various additions of MgO after polishing and quenching.

Figure 5, Page 19: Flexural strength of alumina containing varying additions of magnesia.

Figure 8, Page 23: Flexural strength vs. grain size of pressure sintered alumina.

Table V, Page 24: Flexural strength vs. grain size for pressure sintered alumina + 0.25% magnesia in as polished and quenched conditions.

Figure 10: Flexural strength vs. grain size of quenched alumina.

Figure 11: Flexural strength vs. $(grain size)^{-\frac{1}{2}}$ for alumina with MgO added.

Table VI: Flexural strength of CFC (Linde A \pm 0.25% MgO) alumina quenched from 1700 0 C into silicone oil.

Figure 13, Page 37: Residual stress and combined stress profiles for cylindrical alumina rods quenched from 1700°C into silicone oil.

Figure 14, Page 40: Flexural strength vs. grain size for 72% ${\rm Al}_2{\rm O}_3$ + 28% ${\rm Cr}_2{\rm O}_3$ solid solution.

Figure 15, Page 62: Flexural strength of 72% $A1_20_3 + 28\%$ Cr_20 containing varying additions of magnesia.

Table VII, Page 43: Flexural strength of 72% ${\rm Al}_2{\rm O}_3$ -28% ${\rm Cr}_2{\rm O}_3$ bodies with various additions of MgO after polishing and quenching.

Table VIII, Page 44: Flexural strength vs. grain size for 72% Al $_2$ 0 $_3$ -28% Cr $_2$ 0 $_3$ in as machined and quenched conditions.

STRENGTHENING OXIDES BY REDUCTION OF CRYSTAL ANISOTROPY by H. P. Kirchner, et al

Literature information was used to demonstrate that the grain size dependence of strength increases with increasing crystal anisotropy in well-made pure oxide ceramics. Based upon this information a large grain size dependence of strength was predicted for rutile (TiO₂) bodies. The lack of strength at large grain sizes was attributed to the presence of localized cracks formed by relief of stress caused by thermal expansion anisotropy. The lengths of these cracks were measured and were used to calculate the strength of the bodies using the Griffith theory.

Solid solution compositions with reduced thermal expansion anisotropy were available from previous investigations. Ceramic bodies of these compositions were prepared by hot pressing. Specimens of various average grain sizes were prepared and the strength versus grain size was determined. The weight of the evidence available at present indicates that the grain size dependence of strength of the solid solutions with reduced thermal expansion anisotropy is less than of the comparable pure oxide.

Figure 1, Page 4: Schematic diagram of strength vs. grain size for oxide ceramics.

Table 1, Page 6: Degrees of anisotropy and grain size exponents for some oxides.

As the grain size of TiQ_2 bodies increases, the tendency for localized cracks to form during cooling after sintering also increases. The formation of these cracks is attributed to the thermal expansion anisotropy. The predicated strong dependence of the strength on the grain size was observed. The strength versus grain size values plotted in Figure 3 do not accurately determine a grain size exponent. However, by using various possible lines determined by the data it is evident that the slope is greater than $-\frac{1}{2}$ and less than -1.

Table II, Page 11: Grain size, density and strength of titania samples. Figure 3: Strength vs. average grain size for TiO.

Figure 4, Page 14: Variation of maximum crack length with average grain size.

Figure 5, Page 19: Linear thermal expansion of 90% ${\rm Ti0}_2$ -10% ${\rm U0}_2$ solid solution.

Figure 7, Page 22: Flexural strength vs. grain size for ${\rm Ti0}_2$ and 90% ${\rm Ti0}_2$ -10% ${\rm U0}_2$.

Figure 8, Page 23: Linear thermal expansion of ${\rm Al}_2{\rm O}_3$ - ${\rm Cr}_2{\rm O}_3$ solid solutions.

Table III: Flexural strength of 72% ${\rm Al}_2{\rm O}_3$ -28% ${\rm Cr}_2{\rm O}_3$ using Meller alumina and pressed in the resistance furnace.

Table IV: Flexural strength of 72% ${\rm Al}_2{\rm O}_3$ -28% ${\rm Cr}_2{\rm O}_3$ using Meller alumina and pressed in the induction furnace.

Table V: Flexural strength of other Al_2O_3 - Cr_2O_3 compositions using Meller alumina.

Table VII: Flexural strength of 72% Al $_2$ 0 $_3$ -28% Cr $_2$ 0 $_3$ using A-16 aluminating Figure 13, Page 38: Flexural strength vs. grain size for 72% Al $_2$ 0 $_3$ -28% Cr $_2$ 0 $_3$ solid solutions.

Figure 14, Page 39: Flexural strength vs. grain size for 72% Al $_2$ 0 $_3$ -28% Cr $_2$ 0 $_3$ solid solution (strongest billet only).

Figure 15, Page 41: Flexural strength vs. grain size for other ${\rm Al}_2{\rm O}_3{\rm -Cr}_2{\rm O}_3$ compositions.

Journal of Applied Physics, Volume 42, Number 10

STRENGTHENING ALUMINA BY QUENCHING IN VARIOUS MEDIA by H. P. Kirchner, et al

Improvements in flexural strength, tensile strength, thermal shock resistance and impact resistance are observed when compressive layers were formed on specimens by quenching.

.Table I: Flexural strength of 96% alumina quenched into various media. Figure 2: Flexural strength vs. rod diameter for 96% alumina quenched in silicone oil.

Table II: Tensile strength of alumina as machines, refined to 1500° C and quenched in air, and quenched in oil.

Table III: Flexural strength of glazed alumina quenched in various media.

Figure IV: Flexural strength and change in diameter vs. quenching temperature (quenched in oil).

Ceramic Finishing Company, Box 498, State College, Pennsylvania 16801, U.S.A.

FRACTURE MIRRORS IN ALUMINUM OXIDE. by H. P. Kirchner & R. M. Gruver

Fracture mirror radii (r_m) of strong, fined-grained alumina ceramics were measured and correlated with fracture stress (σ_f) to show that the relation $\sigma_f r_m^{\frac{1}{2}}$ = Constant; previously established for glass, applies for alumina ceramics at room temperature and at elevated temperature. The mirror measurements were used to estimated the residual stresses in quenched alumina rods and to construct a residual stress profile. Using this stress profile and local stress due to the applied load, the stresses acting to causes fracture at internal flaws in the quenched rods were estimated. These results show that the local stresses causing fracture decrease with increasing relative distance from the rod axis.

Ceramic Finishing Company, Box 948, State College, Pennsylvania 16801, U.S.A.

DELAYED FRACTURE OF ALUMINA CERAMICS
WITH COMPRESSIVE SURFACE LAYERS
by H. P. Kirchner & R. E. Walker

The use of compressive surface layers prevent surface flaws from acting to cause failure. Therefore, greater loads can be carried and for increasing amounts of time. The compressive layers in this study were formed by quenching and by glazing and quenching 96% alumina specimens.

- Figure 1: Delayed fracture of specimen "as received" and quenched.
- Figure 2: Probability of failure vs. flexural strength at various humidities as determined by 4-point loading.
- Figure 3: Flexural stress vs. time to failure for glazed and quenched and untreated specimen.
- Table III: Comparison of the flexural strength of abraded 96% alumina rods with and without delayed fracture treatment.
- Table 4: Short-time flexural strength of 96% alumina rods surviving the delayed fracture test.
- Figure 5: Distribution curves for 96% alumina before and after 290 day period.

N72-29324

STRENGTH EFFECTS RESULTING FROM SIMPLE SURFACE TREATMENTS by H. P. Kirchner, et al

In this report, artificial flaws are introduced into test samples (96% alumina) by various means (single point tools, abrading, thermal show and abrasive machining). The flaws were then treated by refiring, chemical and flame polishing, chemical etching and prolonged storage in various environments. The changes in the flaws were analyzed by microscopy and

profilometry. Both flexural and tensile strengths were measured. Also, static fatigue was measured (involving water). There are numerous tables and graphs regarding changes in the average strength of the specimens and variations in the distributions of the individual strengths.

Figure 2, Page 354: Delayed fracture of 96% alumina.

Figure 3, Page 354: Flexural strength of 96% alumina rods refired to various temperatures.

Table I: Flexural strengths of abraded (by various methods) alumina rods treated by refiring and glazing.

Figure 9: Flexural strength of 96% alumina rods scored to various depths.

Figure 11, Page 359: Surface profiles for thermally shocked 96% alumina. Tables 4 & 5, Page 360: Flexural strength of alumina rods with flaws introduced by thermal shock.

Summary and Conclusions:

- 1. Humidity variations in test environment can cause variations of at least 14% in flexural strength of alumina.
- Abrasion by coated abrasives and scoring with single point tools decrease average flexural strength, but these losses can be recovered by refiring or glazing.
- 3. Thermal shock has the most severe effect on the strength. Again, the loss of strength is more than recovered by refiring.

N71-16395 or AD-714-419

AN ASSESSMENT OF SURFACE AND SUB-SURFACE DAMAGE INTRODUCED IN CERAMICS BY SEMI-FINISH OPERATIONS by B. G. Koepke

In this paper, the nature and extent of grinding damage introduced by surface grinding is studied. The ceramic materials studied are alumina MgO, silicon, and B_4 C, and ferrite. The type of grinding used was that typical of semi-finishing operations. The report discusses with surface conditions (surface damage) and sub-surface damage encountered in terms of the properties of the ceramic workpiece, the characteristics of the grinding system, and the tool-workpiece interaction.

The results indicate that damage is mainly composed of three types:

- When material is removed efficiently from low impact resistance ceramics (MgO and ferrite) the surfaces are generated by brittle fracture and are composed of regions of transgranular and intergranular fracture.
- 2) When grinding is inefficient (when the wheel loads up) material is removed by plastic flow. The resultant surfaces are smooth and burnished but may contain thermal cracks due to heat generated. In this instance, subsurface damage consists of a discrete, highly deformed layer containing cracks in most cases.
- 3) When material is removed efficiently from high impact, nondeformable samples (alumina and B_4C) material is removed by plastic flow and by transgranular fracture.

There are many photo micrographs:

Table III, Page 34: Summary of observations for MgO.

Table IV, Page 35: Summary of observations for silicon.

Table V, Page 36: Summary of observations for polycrystalline ceramiics $(Al_2O_3, MgO, B_4C, ferrite)$.

Ceramic Bulletin, Vol. 52, No. 7 (1973), pp. 566-569.

A New Pressing Method: Triaxial Compaction by R. M. Koerner

A new method for pressing ceramic powders is presented. It is shithat greater densities are obtained when tests are conducted on three different ceramics (MgO and two different Al $_2$ O $_3$ samples).

Figure 4: Triaxial compaction density response to shear stress at various confining pressures for MgO powder.

Figure 3: Green density a strength result, by various compaction methods.

Figure 5: Triaxial compaction density response to shear stress a various confining pressures for γ -Al₂0₃ powder.

Figure 6: Transverse rupture strength data for various density green compacts.

Figure 7: Triaxial compaction density response to shear stress at various confinary pressures for α -Al $_2$ 0 $_3$ powder.

Figure 8: Flexural stress rupture of $HS-130 \text{ Si}_30_4 \text{ @ } 1200^{\circ}\text{C}$.

AD-611-840

DEVELOPMENT OF METHODS AND INVESTIGATION OF MECHANICAL PROPERTIES OF GRAPHITES AND CARBIDES AT TEMPERATURES OF UP TO 3200°C

by G. G. Konradi M. A. Fedotov

This report described the state of the problem of investigating mechanical properties of graphites and carbides in accordance with domestic and foreign literature data and analysis of same is given. A method is briefly discussed and its accuracy is evaluated.

Listed results of investigating mechanical properties of a series of types of graphites in temperature range from normal to $3200^{\circ}\mathrm{C}$, and also certain

data on mechanical properties of carbide at high temperatures were given. Development of methods and investigation of mechanic properties of graphite and carbide at temperature up to 3200° C.

Figure 5: Diagrams of niobium carbide compression at high temperatures

AD-763-569

DEPENDENCE OF CREEP RATE ON POROSITY by T. G. Langdon

This is a brief journal article written in 1972 that concerns the dependence of creep rate on porosity of ${\rm Al}_2{}^0{}_3$. Equations for steady-state creep rate given along with two graphs.

Figure 1: Creep rate vs porosity for values of N from 1 through 5.

Figure 2: Experimental data for $A1_20_3$ (creep rate vs porosity).

Journal of The American Ceramic Society, Vol. 54, No. 5, pp. 240-246.

EFFECT OF MICROSTRUCTURE ON DEFORMATION OF POLYCRYSTALLINE MgO

by T. G. Langdon

J. A. Pask

Six types of polycrystalline MgO are tested in compression up to 1400°C . It was noted that above 1200°C all materials deformed plastically.

Table III: Density, grain size, and average pore size of specimens.

Figure 2: Stress-strain curves at various temperatures for all six

specimens at constant loading rate of 20 psi/sec.

Figure 7: Yield stress vs temperature.

AD-643-078

INTRINSIC BRITTLE STRENGTH OF MAGNESIA BICRYSTALS by F. F. Lange

This paper describes a standard method which has been developed that determines five parameters necessary for defining a bicrystal. Twist and tilt parameters are calculated from these five parameters. The following is a list

of the mechanical property data given in the article:

Table 1, page 42: Strength values for MgO single crystals (tensile load 100 direction).

Table 2, pages 54-55: The five parameters and the twist and tilt parameters for bicrystals 1-52.

Table 4, pages 62-63: Strength value for MgO bicrystals.

Figure 14, Page 73: Strength vs total rotation angle.

Figure 26, Page 101: Plot of maximum observed bicrystal strengths divided by the highest value observed (370,000 psi) vs the twist tilt angles.

Note: Computer programs for determining 5 parameters given in appendix - page 123.

AD-764-639

FABRICATION AND PROPERTIES OF SILICON COMPOUNDS

by F. F. Lange

G. R. Terwilliger

This is a final report on three different topics:

- I) Hot-pressing behavior of silicon carbide powder with additions of ${\rm Al}_2{\rm O}_3$.
- II) Pressureless sintering of Si_3N_4 .
- (II) Relative resistance of dense Si_3N_4 and SiC to surface damage introduced by Hertzian contact stresses.

Each topic is considered as a complete report.

I. Hot-pressing behavior SiC powders with additions of $A1_20_3$

The objectives were to determine the conditions required to fabricate high-strength, dense silicon carbide bodies and to determine the effect of the fabrication parameters on the materials' mechanical properties:

The conclusions reached by Task I are:

1) SiC powders with an average particle size of <3 μ m milled with additions of Al $_2$ O $_3$ can be hot-pressed to densities $\geq 99\%$ of theoretical at temperature $\geq 1950^{\circ}\text{C}$ with an applied pressure of 4000 psi. Between $1950^{\circ}\text{C}-2025^{\circ}\text{C}$ the equiaxed grain structure of the resulting material has an average grain size <5 μm .

- 2) The $A1_20_3$ additive forms a liquid phase which dissolves the silicon carbide particles to promote densification by a solution-reprecipitation mechanism.
- 3) Large, second phase streaks, found in some of the dense bodies, were identified as ${\rm Al}_2{\rm O}_3$. These can be eliminated by minimizing the laminar void space in the pre-pressed powder compacts.

Table III, Page 26: Density of three powders containing .02 VF of Al $_2$ 0 $_3$ hot-pressed at 1950 0 C and 4000 psi.

Table VI, Page 30: Grain size of hot-pressed SiC (at varying densification temperatures).

Figure 3, Page 33: Temperature vs fractional density (at 4000 psi Figures 4, 5, 6, Pages 34-36: Relative density vs time $(1975^{\circ}C)$ and 4000 psi).

II. Pressureless sintering of silicon nitride

Silicon nitride with 5w/o MgO can be densified to at least 90% of theoretical without the application of pressure if the proper time/temperature schedule is followed. Shrinkage is consistent with liquid phase sintering and the initial stage can be described as a relaxation process. Above 1650° C, decomposition reduces densification by causing weight losses and pore enlargement which reduces the driving force for shrinkage.

Table I: Time, temperature and density resulting from heat treatment in graphite mold.

Table II and III: Densities and weight losses during isothermal experiments.

Figures 2 and 3, pages 58-59: Non-isothermal shrinkage of silicon nitride -5w/o MgO, time vs fractional length change and temperature $^{\text{O}}\text{C}$.

Figure 4: Temperature vs density (for a 5 min. isothermal anneal).

Figure 5: Isothermal relative shrinkage at four different temperatures.

Figure 8: Arrhenius plot of the relaxation time for the rearrangement step of liquid phase sintering.

Task III: Relative resistance of dense silicon nitride and silicon carbide to surface damage introduced by Hertzian contact stresses.

Spherical indenters (1/8" dia. steel) were used to introduce surface damage into dense $\rm Si_3N_4$ and SiC specimens, which were then fractured in 4-point loading to access the degree of surface damage due to the contact stresses.

REPRODUCIBILITY OF THE ORIGINAL PAGE IS POOR

Approximately four times the indentor load was required to damage the ${\rm Si}_3{\rm N}_4$ relative to the SiC. It was also observed that size of the contact area between the ball and the materials surface was governed by the plastic deformation of the steel ball, <u>not</u> by the materials elastic properties.

After surface damage has been introduced, fracture due to subsequent external loading initiates from a portion of the sub-surface cone crack. The fracture surface is characterized by a protruding portion of the cone crack which can be used to identify the cause of failure.

Figure 3, Page 79: Diagram of observed flats on steel spheres vs normal indentor load.

Figure 5, Page 81: Flexural strength vs indentor load for hot-pressed $\mathrm{Si}_3\mathrm{N}_4$.

Figure 6, Page 82: Flexural strength vs indentor load for hot-pressed SiC.

Figure 7, Page 83: Normalized strength (σ/σ_0) vs normalized applied load (p/p $_0$) for SiC and Si $_3$ N $_4$.

AD-738-865

FABRICATION AND PROPERTIES OF SILICON COMPOUNDS

by F. F. Lange

G. R. Terwilliger

inis is a final report that covers four different subjects or "tasks", each of which is written as a complete report. They are:

- I) Relation Between Strength, Fracture Energy and Microstructure Pages 7-21).
- II) Hot-Pressing Behavior of Si_3N_4 (pages 21-43).
- III) The Powder-Vehicle Hot-Processing Technique (pages 69-75).
- IV) Dielectric Constant and Loss Measurements (pages 81-83).
- I. The fracture energy and strength were dependent primarily on the starting powder used to fabricate silicon nitride. "Alpha-phase" powder resulted in high flexural strength (95,000 psi) and an elongated grain morphology, whereas, "Beta-phase" powder resutled in a low-fracture energy (16,000 ergs/cm 2), a low flexural strength (55,000 psi), and a more equiaxed grain morphology. The high-strength material had directional properties due, presumably, to its elongated grain structure.

Table I, Page 23: Strength and fracture energy data for various samples.

Task II. Hot-Pressing Behavior of Si₃N_A

A study concerning the kinetics of hot-pressing revealed that no single hot-pressing model adequately describes the not-pressing behavior of $\mathrm{Si_3N_4}$. A rather high activation energy of approximately 175 Kcal/mole was formed. Other experiments showed that the alpha to beta phase change is not necessary to hot-press silicon nitride as previously suggested. The role of MgO in hot-pressing was not clearly defined, but evidence for a second phase at grain boundaries was obtained and it was also shown that magnesium silicates wet silicon nitride powders.

Figures 3 and 4, Pages 48 and 49: Plot of hot-pressing data for two powders at 4000 psi according to classical hot-pressing equation.

Figures 5 and 6, Pages 50 and 51: Arrhenius plot for powders.

Figure 7: Applied stress vs hot pressing rate (at 1525°C).

Figure 8: Applied stress vs hot pressing rate (at 1600°C).

Figure 9: Effect of additive content on the densification of AME powder at 1650° C and 4000 psi.

Figures 10 and 11, Pages 55-56: Effect of milling time on the hot-pressing behavior of AME powder (1% and 5% without MgO).

Figure 12, Page 57: Fit of data to the empirical densification equation $P/P_0 = Kt^{1/3}$.

Figure 13-16: Time vs $\Delta L/L_0$ (log-log plot).

Figure 20, Page 65: Ratio after hot-pressing for four hours.

Figure 22, Page 67: The effect of increased ${\rm SiO}_2$ content on the densification of AME powder at $1650^{0}{\rm C}$ and 4000 psi.

Task III. The Powder-Vehicle Hot-Pressing Technique

This is a study of a technique for hot-pressing an object that is already in the desired engineering shape. The body is embedded in a powder, termed the powder-vehicle, which is contained in a hot-pressing die. At the temperature required to densify the preformed body, a pressure is applied to the powder-vehicle through the end plungers. The powder vehicle conveys the pressure to the object which then densifies.

Limitations: (1) The powder should <u>not</u> react with the body.

- (2) The powder should be easily removed.
- (3) The magnitude of the tri-axial stresses exerted on the formed object depends on the distance between the objects surface and the die wall.
- (4) Flat surfaces tend to become concave after densification.

Task VI: Dielectric Constant and Loss Measurements

The dielectric properties of 100% and 70% dense silicon nitride between 1 - 10 GHz are:

- a) 70% dense (reaction sintered)
 dielectric constant -- 6.5 6.71
 loss tangent -- 0.08 0.10
- b) 99% dense (hot-pressed)
 dielectric constant -- 6.93 6.94
 loss tangent -- 0.055 0.067

ASME Paper 72-GT-56

DENSE Si₃N₄ AND SiC: SOME CRITICAL PROPERTIES FOR GAS TURBINE APPLICATION by F. F. Lange

This paper presents useful mechanical and thermal properties for the subject materials.

Figure 1: Flexural strength vs. temperature for Si_3N_4 .

Figure 2: Flexural strength vs. temperature for SiC.

Table I: Youngs modulus and Poissons ratio for SiC and Si_3N_4 .

Table II: Thermal expansion coefficients.

Figure 3: Thermal expansion vs. temperature for hot-pressed SiC and $\mathrm{Si}_3\mathrm{N}_4$.

Figure 4: Thermal conductivity vs. temperature for hot-pressed SiC and $\mathrm{Si}_3\mathrm{N}_4$.

Figure 5: Specific heat vs. temperature for SiC and Si_3N_4 (hot-pressed).

N72-29511

HEALING OF SURFACE CRACKS IN CERAMICS by F. F. Lange

This report shows that cracks introduced into ceramic by mechanical machining processes can be eliminated or "healed" by either resintering (as is the case for oxides) or oxidizing (for the case of materials such as SiC).

Results of crack healing experiments on Al_2O_3 , ZnO, and SiC are reviewed.

Table I: Flexural strengths of "as-cut" and thermal shocked specimens (ZnO, ${\rm Al}_2{\rm O}_3$, SiC).

Figure 1: Fractional recovery of initial flexural strength of both thermal shocked ZnO heated to 1100° C and Al_2o_3 heated to 1700° C.

Figure 2: Static oxidation behavior and strength recovery of 80% dense SiC (thermal shocked) heated to 1400° C.

Table II. Coming size of heated encomment

Table II: Grain size of heated specimens.

Table III: Strength change for diamond cut specimens after heat treatment.

N73-20814

THE CHEMICAL AND PHYSICAL NATURE OF SURFACES by R. M. Latanision

The surface of a solid is often considered to be a sharp discontinuity in an otherwise infinite continuum. It is not surprising to find that the presence and condition of the surface has been found to exert a considerable influence on both the flaw and fracture behavior of various inorganic solids. The mechanical behavior of a crystalline material is determined by the generation, motion and interaction of dislocation.

N73-20814 (cont.)

One of the most surprising and exciting observations to come from studies of the surface structure of metals is the large effect that small amounts of adsorbed gas atoms can have on the structure of an otherwise clean surface. Besides the adsorbing of gases, it is recognized that segregation of bulk impurities may occur as well as at the free surface as at internal surfaces (gain boundaries, twin boundaries) at dislocation. The driving force for solute segregation at free surfaces may be the same as that leading to solute accumulation about internal interfaces.

In addition to equilibrium and segregation of impurities near surfaces, Westbrook and associates also point out that non-equilibrium solute segregation may arise because of the development of a gradient in vacancy concentration near free surfaces as well as at grain boundaries, both being effective sinks for vacancies.

The surface has been structurally and chemically distinguished from the bulk of a crystalline solid. To this, we should add that at the surface there is in general an electrostatic potential difference associated with some kind of charge double layer.

The Double Layer and the Mechanical Behavior of Non-Metals

Because of the low concentration and mobility of change carriers in MgO and Al_2O_3 , the change transfer which occurs during chemisorption on such semiconductor or insulator surfaces may have a profound effect on the change distribution in the space change layer far beneath the surface of the solid. Therefore, we find that the adsorption-induced changes in the change distribution may well affect the plastic deformation as well as the fracture behavior of such solids. They often exhibit adsorption induced increases or decreases in microhardness (i.e., near-surface dislocation mobility).

N67-36691

FABRICATION AND CHARACTERIZATION OF HOT ISOSTATICALLY PRESSED MgO . by M. H. Leipold & T. H. Nielson

This report outlines the procedure used to hot-press some specimens of MgO. Charts are included showing particle size, and density of the samples before and after pressing.

N68-11944

THE EFFECT OF GRAIN BOUNDARIES ON MECHANICAL BEHAVIOR IN POLYCRYSTALLINE CERAMICS by M. H. Leipold, et al

Discussion of grain size and grain boundary on various mechanical properties and mechanical behaviors of ceramics is included in this paper. Chart (Figure 1): Fracture stress vs. grain size for various crack-tip radii. Plastic work equals zero (the number of atomic spacings used as a parameter) MgO.

Chart (Figure 2): Fracture stress vs. grain size for various

amounts of plastic work (plastic work expressed as ratio to the

surface energy). Crack tip radius equals one interatomic distance.

PROCEEDINGS OF THE OSV-RTD SYMPOSIUM ON ELECTROMAGNETIC WINDOWS by P. C. Li, et. al.

The chemical vapor deposition (CVD) of boron nitride results in a unique material which could find application as a superior microwave and infrared window.

Process techniques are discussed for hot-pressed and CVD boron nitride. Shortcomings and advantages of both methods are outlined.

Figure 8: Oxidation of graphite and BN.

Figure 10: Strength vs temperature of CVD BN (Flexural strength 10,000-30,000 vs temperature 0 C 0-2000).

Figure 11: Dielectric properties of BN (loss tangent (0.001-0.009) vs temperature 0 C (0-1400)).

Table: Composition and properties of high temperature enamels (SiO $_2$, Al $_2$ O $_3$, MgO, ZrO $_2$).

Figure 1: Flexural strength for glass reinforced AIPO₄ (psi x 10^3 , 4-24 vs temperature 0 F 200-1200).

Figure 2: Flexural modulus for glass reinforced AIPO $_4$ (0.8-48 psi x 10^6 vs temperature 200-1200 F).

Figure 3: Tensile strength for glass reinforced AlPO $_4$ (6-30 psi x 10^3 vs temperature 200-1200 F).

Figure 4: Compression strength for glass reinforced AlPO₄ (2-12 psi \times 10³ vs temperature ^oF 200-1200 ^oF).

Figure 5: Dielectric constant and loss tangent vs temperature for aluminum phosphate ratio 1A with $S\sim994$ reinforcement at 10.0 K C. (table form. temperature ^{0}F ambient-1200; dielectric constant 3.3-3.6; loss tangent, 0.006-0.02.)

Figure 6: (table form) Percent power reflection coefficients (angle of reflection $\sqrt{60}^{\circ}$ - -60° , perpendicular normal % 0.02-0.2 polarization $\lambda/4\%$ 0.02-0.2 parallel polarization normal % 0.02-0.2., /4%, 0.02-0.2).

Figure 7: Coefficient of thermal expansion for ${\rm AlPO}_4$ matrix.

AD-605-390 cont.

Figure 8: Percent thermal expansion (10% silica modified matrix).

Figure 9: Summary of target goals and achievements.

Figure 10: Flexural strength vs aging for AIPO, laminates.

Figure 1, C-3: Thermal expansion of silicon nitride. (Expansion % 0-0.50 vs temperature 0 F 0-2800):

Table 1: Modulus of rupture results for silicon nitride.

Table 2: Modulus of elasticity for two silicon nitride specimens.

Figure 4: Thermal conductivity of silicon nitride ($BTU-in/ft^2-hr-{}^0F$ mean temperature 0F 1600-2400).

Figures 5 - 7: Thermal conductivity of silicon nitride ($BTU-in/ft^2-hr-o^2F$ vs mean temperature o^2F 1600-2400).

Figure 8: Compressive creep data for silicon nitride (creep % 0-0.2 vs time hour 0-10).

N64-13860

. A STUDY OF FUNDAMENTAL MECHANICAL PROPERTIES OF CERAMIC SINGLE CRYSTALS BY R. S. Liebling

Load capacity of bar shaped silicon carbide single crystals varies inversely with the length-width ratio and boron concentration. As thickness increases, load capacity increases.

Figure 1: Load capacity of SiC crystal containing .005% boron (thickness inches) vs load (lbs) for varying length-width ratios).

Figure 2: Load capacity of SiC crystals having a length-width ratio of 1.36 (thickness vs load with varying amounts of boron concentration as parameters).

Translated from Agneupory, No. 10, Oct. 1969. English translation in Refractories, No. 9, pp. 611-613.

DETERMINATION OF THE THERMAL DIFFUSIVITY
COEFFICIENT OF MAGNESIA AND MAGNESIOSPINEL REFRACTORIES

. by E. Ya. Litovskii

Ya. A. Landa

A translated article from Ogneupory that gives data from experimental determination of thermal diffusivity coefficients of magnesia bricks at high temperatures.

Figure 1: Thermal diffusivity coefficient vs temperature in air, argon, and nitrogen.

Figure 2: Thermal diffusivity coefficient vs temperature measured parallel and perpendicular to sample pressing.

Note: Temperature range 200-1800°C.

AD-657-024

DEVELOPMENT OF HIGH TEMPERATURE THERMAL CONDUCTIVITY STANDARDS by ARTHUR D. LITTLE, Inc.

This project encompasses an analytical and experimental study to establish high temperature thermal conductivity and diffusivity standards and to test these standards at thermal property measurement laboratories. This report described the work carried out in Phase I of this program, the identification, selection, characterization and preliminary experimental examination of candidate standard materials for use in the subsequent measurement program. Based on criteria such as phase change, melting point, reproductivity, isotropy, fabricating, homogeneity, and availability, the following materials were selected for experimental evaluation-ceramics-alumina, beryllia, . . ., silicon carbide, etc.

Table 1: Candidate ceramic materials. Phase change, melting point $({}^{0}\text{C}/{}^{0}\text{F})$. Radiative heat transfer, reproducibility availability,

AD-657-024 cont.

Anisotropy, hemogenenity, microstructure all stability vapor pressure at 3500°F., mechanical strength and ductility, thermal shock, cost, fabricability, shelf life.

Table II: Candidate internationalic materials similar as Table 1.

Table V: Candidate materials-tantalum, tantalum alloys, rhenium and platinium, similar to Table II.

Figure 2: Thermal conductivity of candidate standards, (thermal conductivity 0-1.6 watt/cm $^{\rm O}$ K) vs temperature 200-2600 $^{\rm O}$ K.

Figure 7: Temperature (100's C) vs test duration hours 0-30.

Temperature history for typical heating tests.

Table X: Typical temperature difference for samples tested in cut bar apparatus; material, thermal conductivity, sample thickness, and temperature difference across sample.

Table XI: Summary of Alumina heating test.

Page 72: Results of preliminary thermal conductivity measurements with alumina.

Table XIII: Summary of zirconia heating tests.

Page 84: Results of preliminary thermal conductivity measurements with zirconia.

Table XIV: Summary of silicon carbide heating tests.

AD-601-535

THERMOPHYSICAL PROPERTIES OF THERMAL INSULATING MATERIALS by J. B. Loser, et al

This handbook is a compilation of thermophysical properties data of insulating materials, which can be used both in cryogenic and high temperature applications. Thermal conductivity, linear thermal expansion, specific heat, total normal emittance, thermal diffusivity and compressive strength are plotted with respect to temperature, density, and melting point. Continuous service temperature, typical available form and modulus of elasticity are given in tabular form in a general properties table.

- Pages 11-14: General properties.
- Page 16: Aluminium-chromium oxide system thermal conductivity.
- Page 17: Aluminium-chromium oxide system, linear thermal expansion.
- Pages 18-21: Aluminum oxide, thermal conductivity
- Pages 22-23: Aluminum oxide, linear thermal expansion.
- .Page 24: Aluminum oxide, specific heat.
- Page 25: Aluminum oxide, total normal emittance.
- Page 26: Aluminum oxide, thermal diffusivity.
- Page 27: Aluminum oxide, compressive strength.
- Page 28: Aluminum oxide granules apparent thermal conductivity.
- Page 29: Aluminum oxide-Lithium Carbonate system, thermal conductivity.
- Page 30: Linear thermal expansion.
- Page 31: Aluminum phosphate coatings thermal conductivity.
- Page 32: Linear thermal expansion.
- Page 33: Total normal emittance.
- Pages 34-37: Aluminum silicate, thermal conductivity.
- Page 38: Linear thermal expansion.
- Page 39: Specific heat.
- Page 40: Total normal emittance.
- Page 42: Barium Fluoride, thermal conductivity.
- Page 43: Beryllium carbide, thermal conductivity
- Page 44: Beryllium carbide, specific heat.
- Page 45: Beryllium oxide, thermal conductivity.
- Pages 46-47: Beryllium oxide, linear thermal expansion.
- Page 48: Beryllium oxide, specific heat.
- Page 49: Beryllium oxide, total normal emittance.
- Page 50: Beryllium oxide, compressive strength.
- Page 51: Boron carbide, thermal conductivity.
- Page 51: Boron carbide, linear thermal expansion.
- Page 52: Boron nitride, specific heat.
- Page 53: Boron nitride, thermal conductivity.
- Page 54: Boron nitride, linear thermal expansion.

- Page 55: Boron nitride, specific heat.
- Page 56: Boron nitride, total normal emittance.
- Page 57: Calcium fluoride, thermal conductivity.
- Page 58: Calcium fluoride, linear thermal expansion.
- Page 59: Calcium oxide, thermal conductivity.
- Page 61: Calcium oxide, linear thermal expansion.
- Page 62: Calcium silicate, thermal conductivity.
- Page 63: Calcium silicate, thermal conductivity.
- Page 64: Calcium silicate, apparent thermal conductivity.
- Page 65: Calcium silicate, specific heat.
- Page 66: Calcium silicate, thermal diffusivity.
- Page 67: Calcium silicate, compressive strength.
- Pages 68-69: Carbon special forms, thermal conductivity.
- Page 70: Carbon special forms, apparent thermal conductivity.
- Pages 71-72: Carbon special forms, linear thermal expansion.
- Page 73: Carbon special forms, specific heat.
- Page 74: Carbon special forms, normal total emittance.
- Page 75: Carbon special forms, thermal diffusivity.
- Page 76: Carbon special forms, compressive strength.
- Page 78: Cerrium dioxide, thermal conductivity.
- Page 79: Cerium dioxide, linear thermal expansion.
- Page 80: Cerium dioxide, specific heat.
- Page 81: Cerium dioxide, total normal emittance.
- Page 82: Cerium branide, thermal conductivity.
- Page 83: Cerium lodide, thermal conductivity.
- Pages 98-102: Glass fiber, apparent thermal conductivity.
- Page 103: Glass fiber board, apparent thermal conductivity.
- Page 105: Hafnium carbide, thermal conductivity.
- Page 106: Hafnium carbide, linear thermal expansion.
- Page 107: Hafnium carbide, specific heat.
- Page 108: Hafnium dioxide, thermal conductivity.
- Page 109: Hafnium dioxide, linear thermal expansion.
- Page 110: Hafnium dioxide, specific heat.

- Page 111: Hafnium nitride, thermal conductivity.
- Page 112: Hafnium nitride, linear thermal expansion.
- Page 113: Hafnium nitride, specific heat.
- Page 114: Hair felt, apparent thermal conductivity.
- Page 118: Lithium hydride, thermal conductivity.
- Page 119: Lithium hydride, linear thermal expansion.
- Page 120: Lithium hydride, specific heat.
- Page 121: Lucite, thermal conductivity.
- Page 122: Magnesium-aluminum oxide system, thermal conductivity.
- Page 123: Magnesium-aluminum oxide, linear thermal expansion.
- Page 124: Magnesium-aluminum oxide, compressive strength.
- Page 125: Magnesium-beryllium oxide, thermal conductivity.
- Page 126: Magnesium-fluoride, thermal conductivity.
- Page 127: Magnesium-fluoride, linear thermal expansion.
- Page 128: Magnesium fluoride, specific heat.
- Page 129: Magnesium-nickle oxide system, thermal conductivity.
- Pages 130-131: Magnesium oxide, thermal conductivity.
- Page 132: Magnesium oxide, linear thermal expansion.
- Page 133: Magnesium oxide, specific heat.
- Page 134: Magnesium oxide, total normal emittance.
- Page 135: Magnesium oxide, thermal diffusivity.
- Page 136: Magnesium oxide and others, thermal conductivity.
- Page 137: Magnesium oxide-spinel system, thermal conductivity
- Page 138: Magnesium silicate, thermal conductivity.
- Page 139: Magnesium silicate, apparent thermal conductivity.
- Page 140: Magnesium silicate, linear thermal expansion.
- Page 141: Magnesium silicate, specific heat.
- Page 145: Molybdenum disilicide, thermal conductivity.
- Page 146: Molybdenum disilicide, linear thermal expansion.
- Page 147: Molybdenum disilicide, specific heat.
- Page 154: Mylar, thermal conductivity.

- Page 155: Nickel monoxide, thermal conductivity.
- Page 156: Nickel monoxide, linear thermal expansion.
- Page 157: Nickel monoxide, specific heat.
- Page 158: Niobium beryllium, thermal conductivity.
- Page 159: Niobium beryllium, specific heat.
- Page 180: Potassium chloride, thermal conductivity.
- Page 181: Potassium titanate, thermal conductivity.
- Page 182: Potassium titanate, specific heat.
- Page 189-191: Silica-aerogel, apparent thermal conductivity.
- Page 192-194: Silica-aerogel and metal, apparent thermal conductivi
- Page 195-197: Silicon carbide, thermal conductivity.
- Page 197: Silicon carbide, linear thermal expansion.
- Page 198: Silicon carbide, specific heat.
- Page 199: Silicon carbide, total normal emittance.
- Pages 200-202: Silicon dioxide, thermal conductivity.
- Pages 203-204: Silicon dioxide, linear thermal expansion.
- Page 205: Silicon dioxide, specific heat.
- Page 206: Silicon dioxide, total normal emittance.
- Page 207: Silicon dioxide, thermal diffusivity.
- Page 208: Silicon dioxide and carbon, thermal conductivity.
- Page 213: Silicon nitride, thermal conductivity.
- Page 214: Silicon nitride, linear thermal expansion.
- Page 215: Silicon nitride, specific heat.
- Page 216: Silicon nitride, total normal emittance.
- Page 217: Sillimanite, thermal conductivity.
- Page 218: Sillimanite, total normal emittance.
- Page 219: Sodium chloride, thermal conductivity.
- Page 220: Sodium silicate laminate, apparent thermal conductivity.
- Page 221: Teflon, thermal conductivity.
- Page 222: Teflon, linear thermal expansion.
- Page 223: Teflon, specific heat.
- Page 224: Thorium dioxide, thermal conductivity.
- Page 225: Thorium dioxide, linear thermal expansion.
- Page 226: Thorium dioxide, specific heat.
- Page 327: Thorium dioxide, total normal emittance.
- Page 228: Thorium dioxide, compressive strength.

- Page 229: Titanium carbide, thermal conductivity.
- Page 230: Titanium carbide, linear thermal expansion.
- Page 231: Titanium carbide, specific heat.
- Page 232: Titanium carbide, total normal emmittance.
- Page 233: Titanium dioxide, thermal conductivity.
- Page 234: Titanium dioxide, linear thermal expansion.
- Page 235: Titanium dioxide, specific heat.
- Page 236: Titanium dioxide powder, apparent thermal conductivity.
- Page 237: Titanium nitride, thermal conductivity.
- Page 238: Titanium nitride, linear thermal expansion.
- Page 239: Titanium nitride, specific heat.
- Page 240: Titanium nitride, total normal emittance.
- Pages 241-242: Uranium dioxide, thermal conductivity.
- Page 243: Uranium dioxide, linear thermal expansion.
- Page 244: Uranium dioxide, specific heat.
- Page 256: Zinc oxide, thermal conductivity.
- Pages 257-258: Zirconium dioxide, thermal conductivity.
- Pages 259-260: Zirconium dioxide, linear thermal expansion.
- Page 261: Zirconium dioxide, specific heat.
- Page 262: Zirconium dioxide, total normal emittance.
- Page 262: Zirconium dioxide, thermal diffusivity.
- Page 263: Zirconium dioxide, compressive strength.
- Page 264: Zirconium hydride, thermal conductivity.
- Page 265: Zirconium hydride, linear thermal expansion.
- Page 267: Zirconium nitride, thermal conductivity.
- Page 268: Zirconium nitride, linear thermal expansion.
- Page 269: Zirconium nitride, specific heat.
- Page 270: Zirconium silicate, thermal conductivity.
- Page 271: Zirconium silicate, linear thermal expansion.
- Page 272: Zirconium silicate, specific heat.

AD-803-765

ENGINEERING PROPERTIES OF CERAMICS DATA BOOK TO GUIDE MATERIALS SELECTION FOR STRUCTURAL APPLICATIONS by J. F. Lynch, et. al.

This data book provides a selective compilation of the best available property data on refractory ceramics and ceramic-like materials. It is intended to supersede a "Materials Selection Handbook" issued in 1963. This book (AD-803-765) also contains some updating material (1967 and 1970 vintage) on some sections.

The materials selection index alone covers 19 pages, so it is easy to see that hundreds of ceramics and ceramic compounds are included. Such data as crystal system, density, melting point, specific heat, thermal conductivity and expansion, bend strength, tensile and compressive strength, impact strength Youngs modulus, shear and bulk modulus, Poissons ratio, creep, hardness, therm stress, and oxidation and corrosion are included. The data is presented graphically and in tables.

This report is 13 sheets on microfiche. Technical discussions are included as appended sections. Included are sections on factors that affect and influence physical properties as well as those factors that are important in using brittle materials for structural applications.

AD-696-047

HIGH TEMPERATURE MATERIALS by E. N. Marmer, et. al.

In this book properties of high-temperature materials are described which are applied or can be applied in new technological processes, especially occurring in avacuum in inert media. In the book are generalized, literary materials and the experience of the authors on refractory metals, high-refractory oxides, graphite, and refractory carbide. There are discussions on certain peculiarities of the measurement of temperature with the aid of thermocouples and optical pyrometers.

AD-696-047 cont.

Table 1, Page 1: Basic physical chemistry properties of refractory metals. Page 67: Aluminum ôxide.

Aluminum oxide ${\rm Al}_2{\rm O}_3$ is the most widespread high refractory oxide. Articles from aluminum oxide are produced under various names: alundum, corundum, sinter-corundum, corundise, microlite and others. From aluminum oxide there are manufactured crucibles for melting of metal, containers, tubes, various-shaped articles, cases for thermocouples and others.

Manufactured articles of granular structure have more than 97% ${\rm Al}_2{\rm O}_3$, up to 25% porosity and temperature of application 1,850°C, and articles with densened shells at the same ${\rm Al}_2{\rm O}_3$ content have up to 7% porosity and temperature of application up to 1900°C (122).

Articles made from high-alumina chamottes, constituting Al_2O_3 - SiO_2 are very widespread. From these materials there are manufactured both mass production in the form of bricks, pipes, plates, etc. and also special shapes of articles. (Up to page 81, gives a very good detailed, informative description of Al_2O_3 in every aspect.)

Page 159, Chapter IV: Properties of Carbide (refractory)

As was indicated above, with high temperature technologies there are refractory metals; tungsten, molybdenum, tantalium, niobium, and rehenium and also graphite.

The creation of vacuum installations with an operating temperature 3000°C and above excludes the application of niobium, molybdenum, and tantalums, having melting points below 3000°C . An essential disadvantage of the application of graphite for these purpose is the high rate of its evaporation in a vacuum at temperature about 2100°C which leads to severe reduction of the service life of articles.

Powder Metallurgy, 1969, Vol. 12, No. 23

CREEP OF SILICON CARBIDE by P. Marshall and R. B. Jones

The creep behavior of high-density silicon carbide is examined by the use of four-point bending test in air at temperatures from 1000° C to 1300° C.

Figures 2-4: Variation of creep strain with time at 1000, 1100 and $1200^{\circ}\mathrm{C}$ respectively.

Figures 5-6: Effect of stress and temperature on value of A respectively (from eq. $E_{\rm p}={\rm At}^{\rm k}$).

Figure 8: Calculated creep rates as a function of temperature.

AD-697-923

THE EFFECT OF SURFACE FINISHING ON STRUCTURAL CERAMIC FAILURE .

BY K. R. McKinney and C. M. Herbert

A relationship between fracture strength and surface finish of brittle nonmettalic materials was examined and related to surface crack theory. An experimental illustration used AlSiMg614, a 94% pure alumina with a near zero porosity. Specimen disks 3.625 inches in diameter by 0.085 inches thick were prepared, each having a specific surface finish. Testing was done with a biaxial ball and ring test. Observations were made regarding other materials and other abrasive powders.

Because of ceramics' high compressive strength, chemical inertness and mechanical integrity over a wide range of temperatures, there is a great interest in their use as structural materials. Any such use makes it necessary at times to change the shape of the piece of ceramic through machining. This is a rather brutal treatment and may impair the strength of brittle materials such as ceramics. Even if components could always be used "as fired", this would not guarantee the absence of flaws that could be equally dangerous. So, it is profitable to investigate how the surface crack fracture theory reported by Tiffany and Lorenz (2) could be applied to scratches induced by grinding procedures.

Table 1, Page 2: Breaking stress for various surface finishing of AlSiMag614 as compared to those computed using surface-crack fracture theory.

Figure 6, Page 5: Figure from Tiffany and Lorenz used to simplify the use of surface-crack fracture equations derived by Irwin (3).

Conclusion:

- (1) A relationship between fracture stress and surface finish exists for low porosity ceramics.
- (2) By use of the relationship between experimental fracture stress and surface crack theory a prediction of fracture strength of ceramic materials with particular surface finishes can be made.

Chapter from: Whisker Technology, A. P. Levitt, ed., New York, Wiley-Interscience, 1970.

MECHANICAL PROPERTIES OF WHISKERS by Mehan and J. A. Herzog

Strength and elastic modulus data is provided on a number of ceramic compounds. Various shapes and sizes of whiskers are employed in the tests conducted.

Figure 6-2: Tensile strength vs area (μ^2) of ${\rm Al}_2 {\rm O}_3$ whiskers. Figure 6-4: Elastic modulus vs area of ${\rm Al}_2 {\rm O}_3$ whiskers.

Figure 6-5: Apparent elastic modulus of alpha- ${\rm Al}_2{\rm O}_3$ as a function of reciprocal gauge length.

Figure 6-10: Applied stress vs delay time of fracture for alpha -A1₂0₃ whiskers.

Figure 6-11: Tensile strength of SiC whiskers.

Figure 6-12: Load vs extension of SiC whiskers.

Figure 6-13: Room temperature bend strength of SiC whiskers

(strength vs temperature).

Figure 6-15: Elastic modulus of SiC whiskers (elastic modulus vs are

Figure 6-16: Strength of $\mathrm{B}_4\mathrm{C}$ whiskers.

Figure 6-18: Tensile strength of Si_3N_4 whiskers (strength vs area).

Figure 6-20: Ultimate tensile strength of MgO whiskers vs diagonal of the square cross section.

Note: Data also given on whiskers of tungsten, iron, copper, cobalt, chromium, and others.

N72-31581

KINETICS OF FABRICATION OF SILICON NITRIDE BY REACTION SINTERING by D.R. Messier & P. Wong

The reaction sintering process for the fabrication of silicon nitride i.e. the reaction of silicon powder compacts with nitrogen, was investigated in the temperature range from 1150 to 1450° C and the resulting silicon nitride was characterized by various analytical techniques. Oxygen impurities in the nitrogen atmosphere at high levels caused the formation of SiO_2 and at low level caused weight losses due to the formation of SiO_3 gas. Fine particle size and iron impurities enhanced the reaction rate. The kinetics of the reaction of pure (99.98%) silicon powder compacts along with nitrogen follows the Jander relationship $(1 - \sqrt[3]{1 - \chi})^2 = Kt$.

Table II, Page 4: Fabrication of silicon nitride pellets by reaction sintering.

N64-18384 or . AD-434-173

ALUMINUM OXIDE DATA SHEETS by John T. Milek

The paper is a compilation of the electrical properties of a wide range (80-100%) Al $_2$ O $_3$. Included are sapphire, sintered single crystal, and polycrystalline material. Detailed electrical properties for each material include dielectric constant, dielectric strength, dissipation factor, electrical conductivity and resistivity, loss factor and Te value. Each property is compiled over the widest possible range of temperatures and frequencies. Also, the crystal structure, applications and phase diagrams are briefly reviewed.

DETERMINING THE THERMAL CONTACT RESISTANCE BETWEEN METAL CERAMIC SURFACES by V. S. Miller

The construction materials that are utilized for high temperatures should have a high strength and resistance to strain, and be stable against oxidation and heat fatigue.

The present-day cast metal alloys, on a base of nickel, cobalt iron and chromium with various' additives, cannot be used past temperatures of 850°C. Such temperature can be withstood by materials with a high melting point and hardness, and they are metal-ceramic alloys such as carbides, nitrides, silicides and bromides.

The problems which are encountered during the manufacture of components specially stipulated are: some residual porosity, low heat conductivity and poor deformation.

- Page 2 (Table): Composition and heat conductivity of three metalceramic specimens of silicon carbide.
- Figure 3: Dependency of the thermal resistance of contact on the pressure, composition of the metal ceramic alloy, and quality of the surface finish.
- Figure 4: Dependency of the thermal contact resistance of the unfinished surfaces on the pressure and composition of the metal ceramic alloy.
- Figure 5: Dependency of the thermal resistance of contact of a mixed pair metal-ceramic alloy (1st series--metal steel 45) on the quality of surface finish and pressure.

AD-680-005

RESEARCH ON ELECTRICAL CONDUCTIVITY AND CONDUCTION MECHANISMS IN ALUMINA by J. J. Mills - (1968)

This paper describes a research study undertaken to better understand conduction mechanisms in Al_2o_3 . The following list of figures give specific electrical properties of interest:

Figure 1: Typical graph of decaying current vs. time.

Table IV: Heat treatment schedules for several samples.

Figure 7: Graph of log electronic resistivity vs. reciprocal temperature (oxygen heat treatment).

Figure 8: Graph of log electronic resistivity vs. reciprocal temperature (vacuum heat treatment).

Figure 9: Enlargement of the low activation energy section of electronic resistivity of specimen No. 3 as a function of reciprocal temperature.

Figure 10: Graph of log ionic resistivity vs. reciprocal temperature for specimen No. 9.

Figure 12: Graph showing permanent change in resistivity with order measurement for specimen No. 9.

Translated from Ogneupory, No. 7, pp. 39-45, July, 1971.

ON THE PROPERTIES OF ALUMINA AND CERTAIN ADDITIVES ON THE PROPERTIES OF ALUMINA SLIPS AND PRODUCTS by D. B. Min'kov, et al

This article deals with the effect of the particle size of calcined alumina, ground in a vibration mill for 14 hours and 4 hours.

Table 1: Characteristics of alumina and slips from various factories

Table 2: Properties of casting after drying and firing at 750°C.

Table 3: Effect of additives of GKZR-94 on the grain size alumina fired at 1500° C after grinding.

Table 4: Effect of GKZR additives on the properties of slip and casting made from it.

Table 5: Effect of GKZR additives on the shrinkage and deformation of specimens during heating.

Table 6: Properties of sintered ceramics.

AD-707-340

THE EFFECTS OF SIZE AND ENVIRONMENT ON THE UNIAXIAL COMPRESSIVE BREAKING STRENGTH OF GLASS, ALUMINA, AND PYROCERAM by D. H. Moreno & M. L. Salive

The effects of size and environment on the uniaxial compressive breaking strength of glass, alumina, and pyroceram were investigated to establish realistic design criteria for deep-depth hulls and/or systems of non-metallic materials. The influence of specimen size (diamet of $\frac{1}{2}$ ", 1", and $\frac{1}{2}$ "), test environment (air, sea water at atmosphere, and sea water at 10 ksi) and strengthening level (50 and 100 ksi) are discusse and tentative conclusions drawn.

Some tables are included, but the author explains that such a small number of samples were tested that these figures may not be reliable.

Some tables give a range of the values of the test results.

Figures 3-8, incl.: Effects of size and environment on the uniaxial compressive breaking strength of alumina, glass, and pyroceram. Conclusions:

- 1. Compressive breaking strength of alumina is greater than pyroceram, pyroceram greater than glass.
- 2. Compressive strength of large alumina specimens is unaffected by sea water.
- 3. Compressive breaking strength of glass and pyroceram are markedly improved by strengthening treatment provided the material was not subsequently exposed to sea water.
- 4. Strengthening treatments improved strength of large specimens more than smaller specimens for glass and pyroceram.
- 5. For unstrengthened glass and as-fired alumina, smaller specimens tended to indicate higher breaking strengths.
- 6. Soaking in sea water tended to minimize or eliminate the beneficial effects of strengthening.
- 7. The effect of exposure to sea water was negligible for annealed and as-fired materials, but was pronounced for strengthened materials.
- 8. Soaking glass, alumina, and pyroceram was just as detrimental at atmospheric pressure as at 10 ksi pressure.
- 9. Failure of a material is possible during unloading from a high compressive stress level.
- 10. It appears that unloading at the same rate as loading will prevent failure during unloading from a high compressive stress level.

N73-24604 or AD-757-748

RESEARCH ON DENSIFICATION, CHARACTER AND PROPERTIES OF DENSE SILICON NITRIDE

by P. E. Morgan

The intense attention was put to investigate the covalent compounds carbides and nitrides ceramics. They have special program for sintering and hot pressing because the grain boundary free energy may be higher than the surface free energy. As has been demonstrated in silicon carbide, even in regular hot pressing, additives have been necessary to densify silicon carbide and nitride by lowering the G. B. energy, usually general G. B. phases. Unfortunately, this must lead to an impairment of high temperature strength and creep performance.

The main purpose of it is to disclose a possible method of preparing superior β -Si $_3$ N $_4$ using either the reactive hot pressing technique, or by hot pressing with minimum additives, silicon carbide powder produced by the decomposition of pure silicon nitrides.

For more than a decade silicon nitride has been used for high temperature turbines and bearings. The true form of silicon nitride is the $\beta\text{-Si}_3N_4$, density 3.19 g/cc. The coefficient of thermal expansion 2.5 X 10-6/°C is extremely low and confers exceptional thermal shock resistance. The substance has a hardness of about 1800 Kg/mm² at room temperature but with silicon carbide alone has exceptional hot hardness. The material is resistant to oxidation up to about 1600° C. Low coefficient of sliding friction has been reported at low and high temperature. But, unfortunately, as has been well recognized for many years, ceramics do not even approach their intrinsic attainable physical properties unless both porosity and grain size are closely controlled, usually, so that porosity is zero and grain size is in a range of 1-5 μ . The density of reaction sintered silicon nitride does not exceed 85% theoretical and the microstructure is homogeneous. Since the properties of hot pressed ceramic materials are

N73-24604 (cont.)

generally far superior to those achieved by sintering techniques, yet unfortunately, it was discovered that silicon powder could not be densified by hot pressing up to temperature (1800°C) where problems were encountered with sublimation. Magnesium oxide was found to be the most beneficial to densification suring hot pressing. A 5% addition, the usual amount formerly used, gives good hot pressing but causes deterioration in the high temperature performance. It has found out that this may be due to the formation of an amorphous phase approximating the Forsterite composition ${\rm Mg}_2{
m SiO}_4$ along the grain boundaries. The high temperature mechanical properties then are largely governed by this amorphous phase.

Recently clarified also was the troublesome controversy of the relative roles of the α and β phases. The α phase contain oxygen and has the probable formula $Si_{11.5}N_{15}O_{0.5}$. It is surprising that this was not detected earlier; the literature gives examples where contamination by oxygen to produce the phase was clearly indicated. The effect of the magnesium oxide addition during hot pressing is to abstract silicon and oxygen from a typical "silicon nitride" which contain both α and β phases; the only detectable crystalline phase afterwards is the β -Si₃N₄.

Conclusion:

The 85% theoretical density already achieved by reactive hot pressing of silicon imides $Si(NH)_2$ is the highest that has been attained in pure material without additives at reasonable temperature and pressures. The presence of some \$-form indicates that oxygen activity is low. Hitherto; β -form has not been made by the decomposition of silicon imides.

Proceedings of the British Ceramic Society, August, 1970

THE ELECTRIC STRENGTH OF ALUMINA: THE EFFECT OF POROSITY by C. T. Morse & G. J. Hill

The electric strength of hot-pressed and single crystal alumina are investigated. Samples range in density from 85% to 100% of the theoretical. Tests show that electric strength varies significantly with thickness.

Figure 5: Electric strength vs. thickness.

Table 2: Variation of electric strength with pressing parameters.

Figure 6: Electric strength vs. density of hot-pressed alumina.

AD-672-921

CHARACTERIZATION OF FUSED SILICA SLIPS by C. A. Murphy

The purpose of this report is to perform research and development directed towards the development of techniques to fully explore the potential of readily available ceramic system for use as structural components in hypersonic missile applications.

Table I: Parameters used to characterize fused silica slips.

Table II: Characterization data on fused silica slips.

Figure 1: Percent less than diameter 0-100. Diameter (microns). 2-40. Particle size distributions of fused silica slips on mass basis as determined using a counter with a 100 micron aperture.

Figure 2: As above.

Figure 3: Cristobalite content (v/o) 0-35 vs. time 0-6. time (hours). Cristobalite content vs. sintering time at 2200° F.

Figure 4: Dynamic Young's modulus (10^6 lb/in^2) vs. time (hr.) 0-6. Young's modulus vs. sintering time at 2200° F.

Figure 5: Sediment thickness (millimeter) 0-10 vs. time (minutes) 0-300. Sediment thickness vs. time for three fused silica slips.

STRENGTH OF STRUCTURAL CERAMICS UNDER IMPACT LOADING by L. E. Muttart & J. C. Everhart

In this report static stress values are calculated for a point on the linear portion of the loading curve. These values then are corrected for time to failure, and for inertial correction at the time of failure.

Table I: Specimens and their physical properties. Static MOR (psi) times 10^3 12-62, E (psi X 10^6)9-57, resonant frequency (cps)588-5000, diameter in. 0.2-0.5. Al $_2$ 0 $_3$ 85-100%, specific gravity 2.3-3.8. Table II: Kimble glass rods strengths at failure. Table IV: Average of results of impact test. Stress at failure, psi X 10^3 (10-70), resonant period μ sec (200-1100), failure time

AD-698-343

MAGNESIUM OXIDE by M. Neuberger & D. B. Carter

(80-200+), load time 18-100, specimen.

A wide range of electrical and optical properties are covered in these data sheets on magnesium oxide. Particular emphasis has been placed on the dielectric properties and the energy band structure. A data table which includes the best available information on the crystallographic, thermal, mechanical, physical, electronic and photoemissive properties is included.

The refractory and insulating properties and uses of magnesium oxide have been thoroughly studied for material in the form of polycrystalline and pressed grain or powder forms as well as for ceramic binary and ternary compounds of MgO with other metallic oxides. With the development of solid state technology, the unique properties of single crystals united with the refractory and insulating character of MgO as well as its useful optical

AD-698-343 (cont.)

properties make this compound a very promising material; e.g., as a host lattice in laser research. This presentation, therefore, is concerned primarily with the fundamental solid state electronic properties of magnesium oxide as determined during the past few years.

* All the graphs and figures and tables in this report are important and very informative.

AD-725-761

MECHANICS OF BRITTLE MATERIALS UNDER LINEAR TEMPERATURE INCREASES by H. Neuber & A. Wimmer

The results of work done to show the effects of surface roughness, residual stresses, strain rate, microstructure, alternating bending fatigue loading and a non-uniform stress field on the strength of small (2-8mm diameter) alumina rods are given. The rods used in the work were characterized by determinations of grain size, porosity, hardness, surface roughness and damping factor. Static bend tests at room temperature are used to determine the Young's modulus, the fracture stress, and the strain at fracture and to show the influence of specimen volume on the fracture stress. The effect of grain size and of porosity on these characteristics are shown. A new tensile test specimen is designed which achieves an almost uniform stress field in the test area. Some test results are given to show the validity of this procedure for brittle specimens.

Table 2, Page 36: Distribution of the grain size and the porosity over the length of alumina rods.

Table 3, Page 39: Dependency of the "Rauhtiefe" $\rm R_t$, "Glattungstiefe" $\rm R_p$, and center-line-average (CLA) from the grain size and the porosity of $\rm Al_2O_3$ round bar specimens.

Table 4, Page 40: Dependency of Vickers-micro-hardness from the grain size and the porosity of ${\rm Al}_2{}^0{}_3.$

AD-725-761 (cont.)

Table 5, Page 41: Vickers-micro-hardness on single grains of varying size of ${\rm Al}_2{\rm O}_3$.

Table 6, Page 42: Variation of damping factor with porosity and grain size.

Table 7, Page 43: Dependency of fracture stress, Young's modulus and fracture strain from surface condition of ${\rm Al}_2{\rm O}_3$.

Tables 8, 9, 10 (Figure 21): Residual stresses in Al995 (for varying grain sizes).

Table 11, Page 47: Dependency of fracture stress, Young's modulus, and strain at fracture from strain rate.

Tables 12 thru 15: Dependency of fracture stress from number of cycles to fracture for alternate bend fatigue tests at room temperature.

Table 16, Page 53: Dependency of fracture stress, Young's modulus and fracture strain from porosity and grain size (room temperature).

Table 17, Page 63: Dependency of fracture stress from specimen volume, porosity, and grain size (from bend test at room temperature).

Table 18 and Figure 41: Dependency of Weibull exponent 1/m from the porosity for various grain size.

Ceramic Bulletin, Vol. 51, No. 9 (1972), pp. 677-680

STRENGTH CHARACTERIZATION OF POWDER AGGREGATES by D. E. Niesz, R. B. Bennett, & M. J. Snyder

Pressure-density data were obtained for two commercial reactive ${\rm Al}_2{\rm O}_3$ powders, for aluminum and copper powders and for a series of ${\rm Al}_2{\rm O}_3$ powders prepared by calcining a dry-milled reactive ${\rm Al}_2{\rm O}_3$ powder at selected temperatures. The data yielded several linear regions when plotted as logarithm of pressure versus relative density. The mechanism believed to control compaction in each linear region is identified, and a technique for determining the strength of aggregates in powders from pressure-density data is proposed.

Journal of The American Ceramic Society, Vol. 54, No. 9, Sept. 1971, pp. 428-435

ELECTRICAL PROPERTIES OF SINGLE CRYSTALS, BICRYSTALS, AND POLYCRYSTALS OF MgO by C. M. Osburn

Conductivity and dielectric constants as functions of temperature and oxygen partial pressure are given in graphical form.

Figure 2: Conductivity isotherm for high-purity single-crystal MgO.

Figure 3: Conductivity isobars at high and loss pressures for single-crystal MgO.

Figure 5: Dielectric constant versus temperature--single-crystal MgO.

Figure 6: Conductivity isotherms for low-purity MgO single crystal.

Figure 7: Conductivity isotherms for polycrystalline MgO.

Figure 8: Voltage dependence of dc conductivity in polycrystalline MgO.

Ceramics Bulletin, Vol. 49, No. 7 (1970), pp. 638-642

HOT STRENGTH OF HIGH-ALUMINA REFRACTORIES by M. Palfreyman

Modulus of rupture tests (MOR) are made from room temperature to 1400° C. Figures 1 thru 3, Page 640: MOR vs. temperature (alumina 99%-10 μ m).

AD-607-778

GROWTH AND DEFORMATION MECHANISMS IN SINGLE CRYSTAL SPINEL by H. Palmour, III, et al

This report includes a description of an R. F. plasma growth facility and its operation. The main conclusion from the growth experiments is that the instabilities of spinel at its melting point precludes the growth of large stoichiometric single crystals by direct fusion. Alternative techniques are discussed.

Table, Page 23: Changes in the spinel lattice constant resulting from plasma treatment.

Figure 9: Intensity vs. diffraction angle, 2 compressive strength psi X 10^4 15-50 (microhardness difference -100-500) vs. $50-100 \frac{1}{T}$ X 10^4 (temperature 1727-727).

Figure 11: Load vs. deflection for alumina-rich spinel single crystal with a (110) load axis tested at 1500° C load in pounds 0-1000 vs. deflection in inches 0-0.14

N63-19993

MECHANICAL BEHAVIOR OF CRYSTALLINE SOLIDS by Earl R. Parker, et al

This paper is the proceedings from a symposium (1962) which was held to review the science and advancements of defect properties of solids (dislocation behavior, etc.) and how they are related to the mechanical behavior of ceramics. There are actually six papers presented, they are:

- 1. Plastic Flow & Fracture of Crystalline Solids E. R. Parker
- 2. Theory of Dislocations: An Elementary Introduction R. DeWit
- 3. Observations of Dislocations H. G. F. Wilsdorf
- 4. Fracture Mechanisms in Crystalline Ceramics T. L. Johnston
- 5. Strength of Ceramic Crystals J. J. Gilman .
- 6. A Review of the Effect of Microstructure on Mechanical Behavior of Polycrystalline Ceramics W. D. Kingery & R. L. Coble

N63-19993 (cont.)

Figure 14, Page 77: Typical stress-elongation curve for chemically polished MgO at room temperature.

Table 4, Page 93: Possible strengths of various crystals, crystal, density, maximum strength, strength-density ratio.

Figure 2, Page 112: Effect of grain size on strength of polycrystalline ${\rm Al}_2{\rm O}_3$.

Figure 4, Page 113: Effect of porosity on creep of polycrystalline ${\rm Al}_2{\rm O}_3$.

N71-27041

NATURE, STATUS, AND SELECTION OF CERAMIC MATERIALS by J. H. Pask

Ceramic materials are identified as having ionic-covalent bonding, being composed of compounds and being either crystalline or glassy. The oxides are of particular interest due to their chemical stability up to high temperatures. Brittle behavior makes them sensitive to flaws, either intrinsic or extrinsic, thus requiring a uniform distribution of uniform flaws to achieve reliability. Intrinsic flaws can be correlated with character features. Extrinsic flaws are in themselves character features. Both are correlated with mechanical properties. A number of applications of ceramics based on their unique properties are reviewed.

Figure 4: Stress-strain curves for six different MgO samples at 1000° Figure 6: Volume fraction of pores vs. transverse strength for polycrystalline alumina (at 25° C and 750° C).

EFFECT OF THERMAL CONDITIONING AND STRAIN ON THE MICROSTRUCTURE AND MECHANICAL PROPERTIES OF ALUMINA

by E. M. Passmore, et al

Stress-strain curves obtained from four-point bend tests are used to study yielding and fracture in dense, fine grained ${\rm Al}_2{\rm O}_3$. Numerous mechanical properties are presented in graphical form as a function of temperature and microstructure. The following list gives specific figures of interest:

Table I: Summary of fabrication and related data for hot pressed Al_20_3 .

Table II: Yield and strain hardening parameters for polycrystalline Al_2O_3 .

Table III: Correlation of estimated brittle-ductile transition temperatures with material variables for several alumina tiles.

Table VI: Summary of constant temperatures yield and fracture data for fine grain alumina.

Table VII: Summary of prestrain experiments for fine grain alumina.

Table IV: Order of decreasing fracture strength at 1150°-1200°C.

Table V: Effect of thermal and mechanical (prestrain) treatments on the brittle fracture stress (rupture modulus) of polycrystalline alumina at 1300° C.

Table VIII: Effect of prestrain direction on room temperature fracture stress of vacuum pressed alumina.

Table IX: Summary of mechanical test result on vacuum hot pressed $Al_2O_3 + \frac{1}{4}\%$ MgO.

Table X: Summary of mechanical test (in bending) of sapphire crystal:

Table A1: Modulus of rupture.

Figure 1: Typical load vs. deflection curves determined in bending ambient-pressed aluminum oxide.

Figure 3: Room temperature stress-strain curve for rolled brass plat

Figure 6: Elevated temperature stress-strain curves for ambientpressed alumina oxide.

AD-663-835 (cont.)

Figure 7: Temperature dependence of yielding for ambient-pressed alumina oxide.

Figure 8: Effect of test temperature on plastic strain at fracture in bending for several series of alumina specimens.

Figure 9: Effect of test temperature on fracture stress for alumina.

Figure 10: Effect of test temperature on strength and ductility of ambient-pressed aluminum oxide (D96B) in bending, 2% porosity.

Figure 11: Stress-strain curves for representative curve specimens showing relationship of plastic flow at 135° C with brittle fracture stress at 1200° C.

Figure 12: Effect of plastic strain on the brittle fracture stress in bending of fine grained ambient-pressed alumina at 1200° C.

Figure 13: Effect of plastic strain on the brittle fracture stress in bending of fine grained ambient-pressed alumina 1200° C.

Figure 14: Effect of plastic strain on the brittle fracture stress on bending of fine grain ambient-pressed alumina at room temperature.

AD-867-785

A QUANTITATIVE EVALUATION OF TEST METHODS FOR BRITTLE MATERIALS by C. D. Pears, et al

Many brittle materials exhibit a somewhat different response to tensile, flexural and compressive loads as well as when loaded as a disc. The tensile and compressive fracture strengths often differ by a factor of 2 and can differ by a factor of 10 or more. Modulus of Rupture values of 1½ to 3 times the measured tensile strengths are frequently reported in the literature. It is possible to conceive physical models to explain the difference in response of a material to tensile and compressive loads. However, it is more difficult to conceive a model that will explain why gross departure of MOR values from ultimate tensile strength. Generally, brittle materials

are characterized as being governed by a weakest link fracture mechanism such that cracks initiate and/or propagate to fracture as soon as the stress in any localized region of stressed material reaches the ultimate value. Evidence thus far obtained indicates that brittle materials are weakest in tension. Consequently, one would expect flexural specimens to fracture when the extreme outer fibers reached the ultimate in tension.

<u>Surface Finish</u>. There were strength increases when progressing from highly irregular as-fired surfaces to shop-machined surfaces, but no differences were detected between the shop-machined, the shop-polished, and laboratory lopped ones.

Griffith Cracks. The relation $\sigma = \sqrt{2ET/\pi C}$ gives a theoretical crack size of about 0.0015 inch using T = 20,000 ergs/cm². Microscopic examination revealed no cracks of this type in the material. However, the larger void sizes are about 0.002 inch (or bigger) so that, given a crack tip, they could serve as initiators or propagators. The interference is that any crack significantly smaller than this may provide for subsequent crack nucleation but not crack propagation without growth.

Grain Size. The average grain size varied from 2.8 to 3.4 microns, and the maximum size was about 5 to 25 microns. There was no indication of nonuniformity or nonreproducibility with respect to grain size or shape. Several blanks were fired purposely to a high temperature and the grain size for these specimens averaged 6.9 microns with a maximum size of 30-35 microns; however, with only one exception these high-fired pieces had nominal strength in spite of the larger grain size.

Figures of the configuration of the specimen blank:

Figure 77, Page 127: Average ultimate tensile strength vs. volume. Figure 89, Page 139: Pore size distribution for specific flexural, macro specimen of Table 10.

Figure 129, Page 179: Average density vs. average flexural strength for macro specimen.

Figure 131, Page 181: Average flexural strength vs. grain size for macro flexural specimen.

AD-867-785 (cont.)

Figure 132, Page 182: Average flexural strength vs. porosity for macro flexural specimen.

Table 1, Page 183; Table 2, Page 184; Table 3, Page 185: Firing analysis data.

Table 1 continued, Page 186; Table 2 Page 187; Table 2, Page 188; Table 2 continued, Page 189; Table 2, Page 190.

Table 3, Page 191: Table of mean stress, standard deviation, and coefficient of variation for phase 1 flexural data on macro specimens. Table 4, Page 192, Pages 183-184.

Table 5, Page 195: Table of mean stresses, standard deviations, and coefficient of variation for phase 1 tensile data on macro specimens.

Table 6, Page 196: Table 7, Page 197: Results of tensile evaluations of polished macro specimens removed from SRI Part 1831-A-10.

Table 8, Page 198: Results of surface finish study on macro specimens. Table 9, Pages 199-200.

Journal of the American Ceramic Society, Vol. 52, No. 6, pp. 348.

DIELECTRIC PROPERTIES OF TITANATE-ALUMINA CERAMICS by G. S. Perry & J. R. Alderton

The idea that the addition of alkali earth metal titanates to alumina might lead to the stabilization of its permittivity with respect to temperature was proposed by Atlas et al in 1962.

Recently alumina ceramics containing calcium titanate were investigated and examined at room temperature, their dielectric properties in the 9300 MHz range. Table 1 shows the results for some of the compositions together with values calculated using the logarithmic mixing rule.

JOURNAL OF THE ALL-UNION CHEMICAL SOCIETY (SELECTED ARTICLES) by D. N. Poluboyarinov, et al

These articles include two sections: Section 1 is The Hot Extrusion of Pure Oxide Ceramics by D. N. Pluboyarinov and Ye. I. Shal'nov; and Section 2 is Modern Ideas about Thermal Stability of Refractory-Ceramic Materials and Ways of Increasing Same by G. V. Kukolev and I. I. Nemets.

Figure 3: Shrinkage during sintering and hot pressing of beryllium oxide; (a) fired BeO; (b) hot pressed BeO.

Figure 4: Change in density of beryllium oxide at hot pressing; (a) volumetric weight; (b) temperature.

Figure 5: Dependence of volumetric weight on dimension of crystals; crosses: kilned beryllium oxide; circle: hot pressed BeO.

Figure 6: Dimension of BeO crystals in dependence upon temperature at hot pressing and purity of basic material.

Figure 7: Resistance against thermal shock:circles--hot pressed BeO (porosity 2%); crosses--sintered BeO (porosity 13%) (1) resistance against thermal shock; (2) temperature.

Figure 8: Packing of MgO at hot pressing: (a) raw magnesium oxide, (b) fired at 1600, (c) fired at 600^{0} and exposed to air for a period of 1 year, (d) secondarily fired after storing in air at 1600^{0} , (e) hot pressed MgCO₃.

Table 2: Pressure necessary for the obtainment of given density of MgO.

Table 4: Density and weight loss of aluminum oxide when calcining in vacuo.

Table 5: Characterisite of initial material of $A1_20_3$.

Table 6: Density of aluminum oxide at hot pressing.

N66-18596



MECHANICAL STRENGTH OF HIGHLY ALUMINOUS CERAMIC by N. L. Plyakova & T. P. Mikhaylova

This paper is a translation of a Russian paper on determining the mechanical strength of ultra-porcelain in dependence on the content of aluminum oxide. The samples were:

Composition %

Sample	SiO ₂	A1203	Other Oxides
UR-3	20-21	63-64	15-17
UF-46	14-15	74-75	10-12
UF-50	6-7	83-84	3-11

The strength was determined by evaluating the maximum strength of static bending.

It is shown in Table 2 that strength depends on temperature of annealing, nature of sample fracture, and value of water absorption.

Figure 1 gives curves for samples UF-46 and UF-50 showing dependence of strength on the annealing temperatures.

It is shown that an increase in aluminum oxide has a positive effect on strength.

Grain size dependence on annealing temperature is also noted.

AD-811-146

CERAMIC SYSTEMS FOR MISSILE STRUCTURAL APPLICATIONS by N. E. Poulos, et al

Five slip-cast fused silica radomes were fabricated and evaluated in a mach 2.2, 4000°F, 140 psi Typhon ramjet exhaust at the General Dynamic/Pomona Ordnance Aerophysics Laboratory July 6-18, 1966. Studies for

applying metal films on slip-cast fused silica, boron nitride, zirconia, magnesia, and silicon carbide coated graphite fibers and impregnation of a phenolic embedded ablator in these felts and comparison of thermal evaluation results of these embedded felts with standard ablators under a heat flux of 450 and 1500 BUT/ft²-sec. are described.

Table II: Predicted temperatures and thermal stresses in SCFS radomes during 1966 OAL Test $2/\ .$

Figure 1: Inside surface tensile stress (psi) 0-300 vs. time (seconds) 0-100 for X and C band SCFS radomes.

Figure 2: Temperature $0-3500^{0}$ F vs. time (seconds) 0-100 for X and C band SCFS radomes.

Table IV: Time - $\frac{1}{4}$ hr. - 18 hrs., room temperature - 2200°F. Time-temperature schedule used to sinter slip-cast fused silica radome structures.

Table VI: Modulus of rupture data on specimens cut from VK-5T and VK-6T radomes. Modulus of rupture at position I. II. 3060-3329 psi. Radomes VK-5T, VK-6T.

.Table VII: Modulus of rupture and cristobalite content of specimen from SCFS radomes and 3/4 inch diameter SCFS bars. Modulus of ruptur $1b/in^2$ 3078-3905. Cristobalite content v/o 4.6-9.0.

Table VIII: Similar to Table VII but with 3.3 inch section.

Table X: Modulus of rupture for unnotched and notched, water saturated, dry and resin coated SCFS test specimens. Modulus of rupture $1b/in^2$ 2400-2900. Specimen condition dry, dry-notched, wet, etc.

Table XI: Modulus of rupture, elastic modulus, critical strain and cristobalite content of specimens from the excess skirt sections of the OAL test radomes. Modulus of rupture 2600-2900 psi, elastic modulus 3.6-4.0 (10^6 psi), critical strain (10^3 in/in) 0.74-0.66 cristobalite content 3.5-4.5.

Figure 11, Page 31: Percent (0-100%) less than stated size vs diameter (microns) (0.1-100) count & mass basis distributions of particles sizes in fused silica slip batch OAL-1.

Figure 12, Page 32, Figure 13, Page 33: Similar to Figure 11 but just with fused silica slip batch OAL-2 & 3 respectively.

Table XII: Apparent viscosities of alumina slips with various solids concentration. Alumina content (w/o) 70-85 ph 3.0-4.7; apparent viscosity (centipoise) 20-2000.

Figure 15, Page 38: Weight percent less than stated size 0-100 vs diameter microns 0.1-200; distribution of particle sizes for alumina slips after 18 hours of milling.

Table XIII: Apparent viscosities of alumina skips subjected to various grinding time. Apparent viscosity (centipoise) 340-1000 ph 4.0; grinding time (hr.) 24-96. Alumina content (w/o) 82.

Figure 16: ph(0-10) vs milliequivalent of HCl per gm. of Al_20_3 (0-0.38) ph as a function of acid concentration for slips containing 82 w/o alumina.

Figure 17: Apparent viscosity (centipoise) 10^2-10^4 vs milliequivalents of HCl per gm. of Al₂0₃ 0.01-1.0; apparent viscosity as a function of acid content for a slip containing 82 w/o alumina.

Figure 18: Weight % less than stated size 0-100 vs diameter (microns) 0.1-100; distribution of particle sizes for the alumina slip.

Table XII: Apparent viscosity (centipoise) 110-830, ph 3.9-5.0, solid content of slip (w/o) 82, wt. ratio of alumina to fused silica 1.0-3.1.; properties of alumina fused silica slips.

Figure 19: Apparent viscosity (centipoise) 400-1000 vs aging time (days) 0-24; change in viscosity and ph with time for 82 w/o alumina slip.

Figure 20: Amount of fused silica devitrified (v/o) 0.1-100 vs total sintering time (minute) 0-600; percent of total fused silica devitrified as a function of total time at 2200° F.

Figure 21, Page 48: Dynamic elastic modulus (psi x 10^{-6}) 0-7 vs amount of fused silica devitrified (v/o) 0-40; dynamic elastic modulus of slip-cast fused silica as a function of density and amount of devitrification.

Figure 22, Page 49: Similar to Figure 21, but of 1:3 alumina-fused silica composite.

Figure 23, Page 50: As above, but of 1:1 alumina fused silica composite.

Figure 24, Page 51: As above but of 3:1 alumina fused silica composite.

Table XIV: Percent of fused silica devitrified (v/o) 8-40, porosity (v/o) 12-32, elastic modulus (10 $b/b/in^2$) 2-11 Modulus of Rupture 1300-9000 (psi), wt. ratio of alumina to fused silica. 0:1-3:1-1:0; Properties of slip-cast alumina-fused silica composites.

Figure 25: Variation of Modulus of Rupture & Dynamic Elastic Modulus with alumina content for slup-cast alumina-fused silica composites. Elastic modulus (psi $\times 10^{-6}$) 0-10, Modulus of Rupture (psi $\times 10^{-6}$) 0-10. vs. Al₂0₃ content (w/o) 0-100.

Figure 26: Variation of porosity with alumina content for slip-cast alumina-fused silica composites; porosity v/o (10-30) vs Al_20_3 content (w/o) 0-100.

Figure 29: Viscosity (centipoise) 0-1400 vs grinding time (hr.) 0-168; fused silica slip viscosity as a function of grinding time. Table XVI: Modulus of Rupture ($1b/in^2$) 1200-5300; porosity (v/o) 10-13. Dynamic Elastic Modulus ($1b/in^2$) 4 x 10^6 - 7 X 10; cristobalite content (v/c) 8.0-9.5; grinding time (hr.) 24-96.

Table XVII: Theoretical density (gm/cm^3) 2.2-2.4, porosity (v/o) 17.6-2; grinding time (hr) 24-96. Porosity & theoretical density of dried test bars fabricated from ground fused silica slip.

Table XVIII: Porosity, theoretical density, and cristobalite content of sintered test bars fabricated from ground fused silica slip; cristobalite content (v/o) 5.5-6.8 theoretical density (gm/cm^3) 2.22-2.23; porosity (v/o) 0.9-13; grinding time (hour) 24-96.

AD-811-146 (cont.)

Table XIX: Similar as XVIII but critical strain instead of cristobalite content was introduced - critical strain 0.30-0.65.

Table XX: As above with fused silica specimens from new, used (one time) and graphite plastic molds were used in the experiments.

AD-668-866

CERAMIC SYSTEMS FOR MISSILE STRUCTURAL APPLICATIONS by N. E. Poulos, C. A. Murphy & P. Boland

The research program conducted during the contract year is described. eport is abbreviated to provide broad interpretation of program. Specific details of completed investigations offering improvements in state of the art are to be presented in Special Technical Reports.

Areas of study included embedded ablator concept for thermal protection systems, characterization of commercially available fused silica slips, time temperature thickness relationships for sintering of S.C.F.S. hardware; determination of the influence of grinding on the particle distribution, time-temperature-cristobalite behavior and physical properties of pure fused silica, and fabrication of S.C.F.S. radome structures and attachments for thermal evaluation in the General Dynamics/Pomona Ordnance Aerophysics Laboratory Typhon Combustor.

Table I: Measurements used to characterize fused silica slip.

Table II: Anticipated participant contribution to the thermal tests of slip-cast fused silica radome structure.

Figure 3: Dielectric constant 3.20-4.30 vs. temperature ^OF ambient-3000; dielectric constant vs. temperature for slip-cast silica and density, high purity fused silica.

Figure 4: Loss tangent 10^{-5} - 10^{-1} vs. temp. (0 F) ambient- 3000; loss tangent vs. temperature for slip-cast fused silica and high density, high purity fused silica.

N73-24602

INVESTIGATION OF CERAMICS FOR HIGH-TEMPERATURE TURBINE VANES by Svante Procházka

The objective of this work was to investigate the parameters which limit the mechanical properties of SiC at high temperatures. The results show that carbon reduction of amorphous silica containing 0.5% boron at 1650°C to 1800°C temperatures in agron which yields submicron B-SiC powders well sinterable under nominal hot-pressing conditions. Three different microstructures are obtained, depending on whether the powders are oxidized in air at 700°C , oxidized and leached with HF, or blended with hyperstoichiometric carbon conditions. Measurements of three point bending strength up to 1600°C , creep rate, delayed failure, and oxidation rate at 1600°C show improvements are obtained by these small carbon conditions. At this temperature, strengths in excess of 60 psi have been developed.

It is believed that SiC has the largest potential of any known compound and that a dense, single phase, fine grained, high purity form will yield the desired ceramics. Its strength will be controlled by various factors that determine the local stress level at fracture, such as microscopic inhomogenieties, surface flaws, grain size or microplastic yielding.

Table 1, Page 4: Characteristics of typical SiC powders.

Table III, Page 11: Effect of some fabrication variables on hotpressed density.

The important conclusion is that the addition of small amounts of carbon can suppress exaggerated grain growth in SiC and generate fine grained bodies. This fact will be of unusual significance for the generation of SiC with desired high temperature mechanical properties.

Table VI: Density-composition characteristic of hot-pressed specimens.

Exaggerated grain growth was a critical problem in the study because large grain size limits strength. Although the technique of carbon addition was found to suppress it, a future understanding of this phenomenon is

N73-24602 (cont.)

highly desirable to prevent unexpected failures due to poor microstructure development. Exaggerated grain growth (EGG) has frequently been observed in ceramics, such as ferrites and alumina and has been attached to the presence of a small amount of a substance having an appreciable solubility for the main constituent. The investigator concluded that a liquid growth mechanism promotes EGG in ferrites as he observed right-angle intersections of the matrix grain boundaries with the boundaries of larger grains. Besides the presence of the liquid, a small nucleation frequency is obviously a necessary condition for the phenomenon to occur. The observations made about EGG in SiC are summarized in the following:

- 1. EGG was observed above 1800°C in all stages of densification; i.e. in fully dense body as well as in a loose powder.
- 2. Small amounts of silicon are frequently found in the vicinity of the large grains. However, 1% silicon addition to SiC does not induce EGG.
- 3. Small amounts of oxygen, a few tenths of a percent, were typical for powders exhibiting EGG. Bodies with suppressed EGG had lower oxygen contents.
- 4. EGG was also observed on pressureless annealing of the pressings having A-type microstructure at temperature equal to or above the sintering temperature.
- 5. There were two distinct morphologies of the tabular grains:
 - (a) Thin, very large plate, up to several millimeters long, with an aspect ratio up to 100, growing in dense bodies.
 - (b) Smaller and thicker paltes with an expect ratio of about 10, which grow at early stages of densification in porous compacts and in loose powders.
- 6. The large crystals are invariably $\alpha\text{-SiC}$ and grow from a $\beta\text{-SiC}$ matrix or $\beta\text{-SiC}$ powder; they are mostly transparent and colorless.
- 7. A brown phase, apparently a soldified melt, is frequently found trapped in pores.

N73-24602 cont.

The experimental observations led us to conclude two transport mechanisms. In the early stages of densification (porous compacts) a liquid transport mechanism is unlikely and hence vapor transport is likely. In dense specimens, a vapor transport is impossible and a dissolution reprecipitation process is likely to be responsible.

Table VIII, Page 20: Flexural strength of hot-pressed SiC, psi 5.3. Flexural Strength Material R-63. The R-63 SiC was dense (99.5%) but contained isolated randomly distributed large grains, up to several hundred microns. It was to be determined whether or not large grains in the fine grained matrix would act as inherent flaws and would consistently initiate fracture.

Table IX, Page 22: Size of grains initiating fracture.

<u>Creep Measurement.</u> Data available on creep and diffusion in SiC predict strain rates of the order of 10^{-6} to 10^{-9} per second at 1600° C.

Table X, Page 26: Summary of creep experiment.

Table XI, Page 27: Summary of data on delayed fracture.

Creep tests in bending of SiC conducted at temperatures of 1600° C and stresses of 30,000 psi and higher also yielded delayed fracture data. Ten measurements for material R-30 (SiO₂ containing) and four for R-90 (carbon containing) have been made. The results suggest that there is a slow crack growth in SiC at 1600° C under stresses above 60% of the fracture stresses measured in normal quick loading flexural tests.

Table XII, Page 28: Strength and flaws, size of SiC R-30.

THERMAL CONDUCTIVITY OF REFRACTORY MATERIALS by V. V. Pustovalov

This report is a Russion translation concerning the thermal conductivity of several refractory materials. The report deals with:

- (1) Study of the laws governing the variations in thermal conductivity of heat insulators;
- (2) Investigation of parameters which influence the effective thermal conductivity of refractory ceramics;
- (3) Description of the variety of equipment and experimental methods used.

Table I, Page 15: Variation of thermal conductivity with temperature differential at different average temperatures, (magnesite, forsterite, dianas, firebrick or chamotte).

Figure 7, Page 21: Comparison of existing data and experimental data for quartz glass (temperature vs. λ).

Figure 9, Page 25: Absolute thermal conductivity of ZrO₂ (temperature vs. thermal conductivity).

Figure 16, Page 44: Variation of thermal resistance of polycrystalline ${\rm Al}_2{\rm O}_3$ with temperature (experimental data vs. Kingery data).

Figure 17, Page 44: Variation of thermal resistance of polycrystalline MgO with temperature (experimental data vs. Kingery data).

Figure 19, Page 46: Temperature vs. thermal conductivity for polycrystalline ${\rm ZrO}_2$.

Table 9, Page 49: Thermal conductivity of dense refractories of the Al_2O_3 -SiO₂ system for various temperatures (calculated for zero porosity).

Table 10, Page 50: Same type of data as above for lightweight (porous) Al_2O_3 -SiO₂ system.

Figures 21 & 22: Graphical presentation of Tables 9 and 10.

Tables 12, Page 57: Thermal conductivity of the system $Si0_2$ -quartz glass.

Figure 28, Page 63: Variation of thermal conductivity with temperature in the case of high-silica content refractories (5 curves).

N71-15034 (cont.)

Figure 31, Page 71: Variation of thermal conductivity at 200°C at varying pressure for magnesite and dianas.

Table 15, Page 72: Variations in thermal conductivity of alumina silicate refractories at pressure of 1 \times 10⁻⁴mm. HqCol.

Figure 33, Page 73: Thermal conductivity vs. temperature for high alumina content ceramics.

Figure 41, Page 87: Thermal conductivity vs. temperature for ${\rm Al}_2{}^0{}_3$ with different porosity.

Figure 42, Page 89: Relationship of thermal conductivity with porosity at 200°C for Al $_2\text{O}_3$ and firebrick.

AD-726-401

STRUCTURE-PROPERTY RELATIONSHIPS IN LIQUID CERAMICS by J. J. Rasmussen, et al

The purpose of this study was to determine the surface tension, viscosity, volume change on melting, density, and compressibility of molten oxide ceramics and to study the interrelationship between these properties and the liquid structure.

From a practical standpoint, an understanding and control of the properties of liquid ceramics should result in improved ceramic processes and products and in more realistic predictions of behavior where the temperature exceeds the melting point of ceramics.

Fundamentally, precise measurement of liquid properties are the basis for understanding the structure of high temperature liquids. Thermal expansion, density, surface tension, viscosity and compressibility relate to thermodynamic properties and structural parameters of liquid ceramic materials, such as bond strength, bond length and free volume.

Summary. Techniques have been developed for measuring the volume change on melting, density, expansivity, surface tension, viscosity, and adiabatic compressibility of molten ceramics to temperatures as high as 3000° C. In working with materials which have melting points greater

AD-726-401 (cont.)

than 2000°C as in this program, vapor loss and sample decomposition must be considered, as these can change the properties of the liquid. The use of sealed capsules restricts changes in the samples, but released gases can build up pressure to cause excessive capsule swelling as was observed with MgO.

Figure 2, Page 5: Adiabatic compressibility and ultrasonic velocity for molten ${\rm Al}_2{\rm O}_3$.

tble I, Page 14: Surface tension, density and volume change on alting.

igure 6, Page 18: Change in density as a function of temperature ${\rm FMgAI}_2{\rm O}_a$.

ige 23, Table II: The viscosity of ${\rm Al}_2{\rm O}_3$ crystal, Lucalox, and ${\rm IAl}_2{\rm O}_4$ were measured.

igure 8, Page 24: Viscosity versus 1/T for ${\rm Al}_2{\rm O}_3$, ${\rm MgAl}_2{\rm O}_3$ and icalox.

AD-852-947

EXPLORATORY TESTS OF ALUMINA SPHERES UNDER EXTERNAL PRESSURE by E. F. Reardon

Twenty-nine, 10-inch diameter monolithic alumina spherical shell models were collapsed under hydrostatic pressure to explore the potential of alumina as a material for deep submergence structural floats. The results were encouraging in that stress levels in excess of 500,000 psi were achieved in a number of tests. Exploratory tests indicated that fused alumina models were relatively poor in comparison to monolithic models due to a notch effect at the inner surface of the joints. The results indicate that further development is required before large spheres of alumina can be considered practical.

Figure 1: Effect of stress rate on the ultimate strength of alumina; ultimate tensile stress vs. stress rate.

Table 2: Static tests of monolithic alumina models.

AD-852-947 (cont.)

Table 3: Summary of cyclic and sustained load static tests.

Table 4: Calculated and measured stress sensitivities for Model AL-9.

Figure 6: Summary of tests on monolithic alumina models.

AD-740-828

MICROSTRUCTURE STUDIES OF REFRACTORY POLYCRYSTALLINE OXIDES by W. H. Rhodes, et al

This program was divided into three tasks within the general topic of microstructure effects on properties of polycrystalline oxides. The first task was concerned with the identification, origin and elimination of strength limiting flaws in fine grained, high density, hot-pressed alumina. Careful examination of transverse bend bars fracture surfaces from four billets made with two different powders and two basically different process cycles revealed material flaw fracture origins in 60% of the bars. Three defects were studied in detail and in a number of cases the source of the defect was identified. The discussion also dealt with the three implications of these findings on the various brittle fracture theories.

The fabrication of complex alumina shapes by the press forging process was studied with a goal of achieving not only the prescribed shaped, but the unique optical and mechanical properties of press forged alumina. Presintered right circular preforms were forged into thin shell hemispheres with 60% in-line transmission at 2mm. thickness and 5 μm wavelength. Strain rate control was shown to be very critical and an effective deformation schedule was defined.

The consolidation of high purity fine particulate organo-metallic derived ${\rm Al}_2{\rm O}_3$ was studied on a cooperative program with the Air Force Materials Laboratory. Specimens in excess of 99% density with a 4 $\mu{\rm m}$ grain size were fabricated. Intra-agglomerate densification was identified as a possible rate and microstructure limiting process. Various powder preparation processes were identified and judged worthy of continued research.

Table III, Page 13: Fracture strength and flaw strength.

Table IV, Page 15: Summary of flaw analysis.

Figure 17, Page 26: Room temperature bend strength for flawed

and unflawed specimens compared with literature data.

Table V: Conditions and results for hemispherical forgings.

Figures 19 & 20: Deformation pressure-time plot for forgings.

Table VI, Page 49: 10 MW arc test summary.

Table VII, Page 50: Rain erosion test summary.

Conclusions:

- 1. Complete alumina hemispheres with high in-line transmission have been press forged from one pre-sintered preforms. Further improvements are possible, but properties near those of the best disc forgings were achieved.
- 2. A preferred basal crystallographic texture was developed parallel to the hemisphere surface which was attributed to basal slip playing a strong role in the deformation process. Improved orientation for a hemisphere was achieved in this program, but the results do not yet match the strongest orientation in disc forgings.
- 3. Deformation rate control is very critical as high rates crack the forging and low rates result in incomplete forgings. A deformation rate schedule was mapped out and resulted in four successful hemispheres. Two of these hemispheres subsequently developed cracks due to punch sticking problems during cool-down.
- 4. Lubrication in the form of BN cover coat over graphite paint is beneficial to the forging process.

N66-27434 or AD-630-776

MICROSTRUCTURE STUDIES OF POLYCRYSTALLINE REFRACTORY OXIDESby W. H. Rhodes, et al

This report studies the effects of surface structure on the transverse bend strength of polycrystalline ${\rm Al}_2{\rm O}_3$ and MgO. A consistent relationship between strength and improved surface structure was noted for MgO at lower temperatures, but not for ${\rm Al}_2{\rm O}_3$ (at high or low temperature) although there was some strengthening noted after several thermal cycles.

There is also some testing of hot forged MgO and ${\rm Al}_2{\rm O}_3$ and experimentation with ${\rm SiO}_2$ additives.

Many photomicrographs are presented.

Figure 10, Page 15: Effect of surface treatment on MgO fracture stress at 77° K and 296° K.

Figure 11, Page 17: Same as above for 770K only.

Tables III & IV, Page 25: Effect of surface treatment on fracture stress of ${\rm Al}_2{\rm O}_3$ and effect of annealing on fracture stress of ${\rm Al}_2{\rm O}_3$. Table V, Page 26: Effect of mechanical polishing on fracture stress of ${\rm Al}_2{\rm O}_3$.

Table VII, Page 29: Strength of flame-polished sapphire and polycrystalline alumina.

Table X, Page 53: Transverse rupture strength for forged ${\rm Al}_2{}^0{}_3$ and ${\rm Mg0}$.

Table XII, Page 63: Mechanical properties of MgO doped $A1_20_3$ (bend strength).

Table XIII, Page 64: Transverse rupture strength of ${\rm Al}_2{\rm O}_3$ with minor additions of ${\rm SiO}_2$ at room temperature.

Table XIV, Page 65: Transverse rupture strength of vacuum heated MgO.

REPRODUCIBILITY OF THE ORIGINAL PAGE IS POOR

RELATION BETWEEN PARTICULATE CHEMISTRY AND CERAMICS PROPERTIES

by W. H. Rhodes, et al

Many technologically important properties of ceramics are determined by their microstructure. Mechanical properties are but one notable example. The microstructure obtained in a body is, in turn, dependent upon a number of kinetic processes which occur during fabrication grain growth and change in pore size, distribution and morphology.

Table 1, Page 17: Experiments to form uniformly Ca-doped MgO.

AD-727-618

MICROSTRUCTURE STUDIES OF REFRACTORY POLYCRYSTALLINE OXIDES
by W. H. Rhodes
R. M. Cannon

This study was concerned with the interaction between microstructure and chemistry in polycrystalline MgO and ${\rm Al}_2{\rm O}_3$ and several facets of mechanical properties. Further, the press forging of ${\rm Al}_2{\rm O}_3$ hemispheres was undertaken as earlier work had shown that pressed forging developed unique optical and mechanical properties.

A direct comparison of deformation in the high purity ${\rm Al_2O_3}$ and less pure ${\rm Al_2O_3}$ + ${\rm 1/2}{\rm MgO}$ with nearly identical grain size and porosity demonstrated that the deformation rates were very close within a limited temperature regime. Several pieces of evidence to include a higher strain rate sensitivity which decreased with increasing temperature led to the conclusion that deformation in high purity fine-grained ${\rm Al_2O_3}$ shifts from grain boundary diffusion to a strong component of grain boundary sliding at higher temperatures. The differences between the grades of ${\rm Al_2O_3}$ were attributed to the influence of impurities and dopants on grain-to-grain bond strength.

Stress corrosion studies on two grades of hot pressed MgO and one grade of sintered MgO demonstrated marked differences among the grades and further

differences in test environments known to react chemically and/or to influence dislocation mobilities in MgO. The erosion curves as well as fractographic studies support the view that stress corrosion in $\rm H_2O$ is dominated by stress enhanced chemical corrosion which is strongly dependent on grain boundary impurity phases. Further, in the absence of $\rm H_2O$, a mechanical stress corrosion model may dominate as the static fatigue limit was influenced by organic media known to affect dislocation mobility.

The hemisphere press forging studied was preliminary and mainly concerned with preform preparations, die design, lubrication and establishing process limits. The central zone of several hemispheres were crack-free and translucent with limited edge tearing. Also, a basal crystallographic texture parallel to the surface was developed which together with the high density demonstrated the feasibility of achieving transparent ${\rm Al}_2{\rm O}_3$ hemispheres by press forging.

Figure 2, Page 7: Stress-strain rate curve for high purity Al₂0₃. Figure 4, Page 9: Stress-strain rate curve for fine-grained hot-pressed material.

Figure 5, Page 10: Strain rate versus 1/T showing the activation energy for deformation at two stress levels for high purity ${\rm Al}_2{\rm O}_3$ plus 1/4 w/o MgO.

Figure 6, Page 12: Dependence of the activation energy for deformation on grain size (${\rm Al}_2{\rm O}_3$).

Figure 7, Page 13: Bend strength as a function of temperature for several grades of alumina.

Figure 8, Page 15: Product of boundary width and diffusion coefficient versus reciprocal temperature for deformation in various aluminas and other measurements.

Table II, Page 21: Dynamic room temperature strength of sintered MgO.

Table III, Page 22: Delayed fracture tests on sintered MgO. Figure 12, Page 24: Delayed failure curve for Honeywell sintered MgO tested in distilled H₂O.

AD-727-618 (cont.)

Figure 13, Page 25: Delayed failure curve for Honeywell sintered MgO tested in DMF.

Figure 14, Page 26: Delayed failure curve for Honeywell sintered MgO tested in DMSO-10 v/o DMF.

Figure 19, Page 22: Delayed failure curve for the hot pressed and one sintered grade MgO in four test environments.

Figure 21, Page 38: Record of deflection and pressure versus time in a typical hemisphere forging run (Al $_2$ 0 $_3$).

Table IV, Page 40: Hemisphere forging experiments.

Table V, Page 42: Preform preparation and results after short sinter. Figure 31, Page 53: Thickness profiles for press forged ${\rm Al}_2{\rm O}_3$.

AD-717-984

RELATION BETWEEN PARTICULATE CHEMISTRY AND CERAMIC PROPERTIES by W. H. Rhodes, et al

Progress report describing efforts of first year of program designed to examine the relation of mechanical properties, grain growth kinetics. and impurity precipitate distributions to the characteristics and chemistry of MgO at progressive stages during microstructure evolution.

It was learned that abnormal grain growth begins at the 70% density level in ${\rm Mg(OH)}_2$ derived material. Fully dense $1150^{\rm O}{\rm C}$ hot pressed specimens had a marked duplex structure but pressing at $1450^{\rm O}{\rm C}$ resulted in material with a normal grain distribution. This unusual reversal from abnormal back to normal was probably due to competition between boundary and pore control on grain growth.

A discussion and explanation of the various grain growth studies in $\ensuremath{\text{MgO}}$ is included.

Figure 6, Page 11: Crystallite size distribution for high purity MgO powder ${\rm Mg(OH)}_2$ calcined ${\rm 1200}^{\rm O}{\rm C}$ for 1 hour.

AD-717-984 (cont.)

Figure 11, Page 21: [Grain growth in high purity MgO and comparison with literature values.

AD-661-487

DEVELOPMENT AND EVALUATION OF TRANSPARENT ALUMINUM OXIDE by W. H. Rhodes, et al

This paper is about a study to develop a transparent alumina by using hot working techniques on polycrystalline ${\rm Al}_2{\rm O}_3$ at temperatures above $1400^{\rm O}{\rm C}$. Optical and mechanical properties of alumina are given at room and elevated temperatures.

Figure 1, Page 2: Variation of recrystallized grain size with deformation.

Table 1: Processes conditions for forging of transparent Al₂0₃.

Figure 23: Total and in line transmission of forged Al_20_3 .

Figure 24: Total and in line transmission of forged Al_2O_3 .

Figure 26: Total transmission of Al_2O_3 .

Table 3: Forging of small specimens for annealing experiments.

Figure 33: Transverse bend strength of transparent ${\rm Al}_2{\rm O}_3$ versus temperature.

Table 5, Page 57: Bend strengths of transparent polycrystalline alumina.

AD-638-450

RESEARCH ON ANISOTROPY IN POLYCRYSTALLINE DIELECTRIC MATERIAL by Donald H. Rice & Richard W. Stowe

This report covers the continuation of studies of dielectric anisotropy found in polycrystalline ceramic bodies. During this program some of the mechanisms contributing to dielectric anisotropy were investigated. Specially,

these were: (1) preferred orientation of component crystals, (2) residual stresses in the crystal lattice, and (3) density gradient in the materials.

Figure 4: Dielectric constant (8.0-13.5) vs. temperature $(200^{\circ}-2800^{\circ}F)$ of alumina (99.9%). General trend distribution.

Figure 5: Dielectric constant (8.5-13.5) vs. temperature (200-2800°F) of alumina (99.5%). General trend distribution.

Figure 6: As above, alumina (99.0%).

Figure 7: As above, alumina (98%).

Figure 8: As above, alumina (97.6%).

Figure 9: As above, alumina (96.0%).

Figure 10: As above, alumina (94.0%).

Figure 11: Dielectric constant (5.8-9.4) vs. temperature (200-2800°F) of alumina and beryllium. General trend distribution.

Figure 12: Dielectric constant (7.5-10.0) vs. percent main constituent (80-100). Room temperature variation in dielectric constant of polycrystalline alumina vs. purity.

Figure 13: Dielectric constant (5.0-8.0) vs. percent main consituent (95-100%). Room temperature variation dielectric constant of polycrystalline beryllium vs. purity.

Table 2: Dielectric constant of test samples measured at room temperature at a frequency of 10 G.C. and 40 G.C.

Table 3: Density measurement.

Table 4: Dielectric constant of mixture of 2 phases as predicted by Equation 2 for samples of ${\rm Al}_2^{\,\,0}_3$ and spinel.

Table 5: Microscopic analysis of ceramic samples.

Table 6: Calculated dielectric constant, from Equation 2 vs. porosity of ceramic samples.

Table 8: Stress field measured for dry pressed and slip cast ${\rm Al}_2{\rm O}_3$ by diffractometer method.

IDENTIFYING OPTIMUM PARAMETERS OF HOT EXTRUSIONS by R. W. Rice & J. G. Hunt

This report is about a program to develop a technique for hot extruding MgO and determining the effects of such extrusion. The feasibility of extruding crack-free MgO bodies was confirmed repeatedly in extrusions of limited size. Cracking in larger bodies was also reduced by certain innovations (heated catch tube and insulated extrusion can).

Extruded MgO was shown to be 50 to 100% stronger than comparable (grain size, etc.) hot pressed MgO at room temperature. Also, extruded MgO is stronger at 2400° F than at room temperature.

Table VIII, Page 53: Surface finish effect on strength of extruded MgO (room temperature strength modulus of rupture).

Table X, Page 55: $A1_20_3$ strength (room temperature modulus of rupture). Figure 13, Page 71: Room temperature strength vs. grain size for MgO (extruded and hot-pressed).

Figure 14, Page 72: Petch plot of hot pressed and extruded MgO (room temperature).

Figure 51, Page 112: Strength vs. grain size of extruded MgO (room temperature).

Figure 56, Page 118: Strength vs. grain size of extruded MgO annealed to 2600° F.

Figure 57, Page 119: Strength vs. grain size of extruded MgO annealed above 2600° F.

Figure 59, Page 121: Strength vs. grain size of extruded MgO at 2400°F.

Figure 65, Page 127: Room temperature strength vs. grain size for Al_2O_3 .

Figure 14, Page 176: (Appendix) MgO strength and grain size vs. firing temperature.

Figure 16, Page 178: Room temperature strength vs. grain size of dense MgO (hot-pressed).

Figure 18, Page 180: Room temperature strength vs. grain size of MgO (with some porosity).

N67-27371 (cont.)

Figure 19A, Page 181: Room temperature fracture of MgO. Cleavage fracture vs. grain size and firing temperature. Figure 26: MgO strength at 2400° F.

Ceramics in Severe Environment; Proceedings of the Sixth University Conference on Ceramic Science, 1970.

THE COMPRESSIVE STRENGTH OF CERAMICS by R. W. Rice

A failure theory is developed for crystalline ceramics that is in accord with observed variations in microhardness and compressive strength, twin-induced fracture, and stress concentrations due to impurities and thermal and mechanical anisotropies. Numerous tables and graphs are presented.

Table 2: Compressive strength and hardness-derived yield stresses for carbides, nitrides, borides and oxides.

Figure 1: Grain size vs. compressive strength for $A1_20_3$, $Th0_2$, and $U0_2$.

Table 3: Room temperature compressive and tensile strength ratios for various ceramics.

Table 5: Effect of temperature on compressive strength and hardnes derived yield stress.

Figure 5: Short-term tensile and compressive strength of ${\rm Al}_2{\rm O}_3$ at $1600^{\rm O}{\rm C}$.

Table 7: Compressive strength and hardness-derived yield stress of commercial ceramics.

THERMAL RADIATION PROPERTIES OF CERAMIC MATERIALS by J. C. Richmond

The thermal radiation properties of materials are defined and basic physical laws governing the amount of thermal radiation emitted by a black body radiator and its geometric and spectral distribution reviewed. Equations relating thermal radiation properties such as emittance, reflectance, transmittance, and absorptance to optical properties such as index of refraction, absorption coefficient, etc., are given. The effect of porosity, grain size, and impurities on the optical properties are discusse

Representative normal spectral emittance data for alumina, thoria, magnesia and zirconia is given in graphical form.

Figure 3, Page 128: Temperature dependence of normal spectral emittance for Al_2O_3 , MgO, ThO_2 , ZrO_2 .

Figure 29: Thermal conductivity of solid solutions of MgO and nickel oxide.

Figure 31: Thermal conductivity of ${\rm Al}_2{\rm O}_3$, before and after indicated reactor irradiations.

Figure 40: Effect of porosity on thermal conductivity of MgO at 90°C. Figure 41, Page 93: Thermal conductivity of zirconia sample with 20% porosity, assuming various emittances.

Figure 42, Page 94: Calculated effect of grain size on effective thermal conductivity of polycrystalline materials.

MEASUREMENT OF THE DIELECTRIC CONSTANT OF ALUMINUM OXIDE by R. M. Riley

This paper gives frequency response curves and dielectric constants for ${\rm Al}_2{\rm O}_3$ that are derived by finding the cutoff frequency of air-filled waveguide by filling the waveguide with aluminum oxide.

The author notes that results have proven to have a high degree of accuracy.

Figure 4: Attenuation in DB vs. frequency response curves.

Figure 8: Attenuation in DB vs. frequency response curves.

Figure 9: Attenuation in DB vs. frequency response curves.

Figure 10: Attenuation in DB vs. frequency response curves.

Figure 11: Attenuation in DB vs. comparison of response for two different waveguides.

Figure 16: Attenuation in DB vs. frequency response curves.

Figure 17: Attenuation in DB vs. frequency response curves.

Table 1: Specimen sizes and corresponding cutoff frequencies.

Figure 18: Attenuation in DB vs. frequency response curves.

Figure 19: Attenuation in DB vs. frequency response curves.

Figure 20: Attenuation in DB vs. frequency response curves.

Figure 21: Attenuation in DB vs. frequency response curves.

Figure 22: Attenuation in DB vs. corrected response of specimen No. 4.

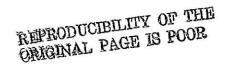
Figure 23: Attenuation vs. temperature frequency for 29 ± 4 DB.

.Figure 24: Determination of fc by attenuation below cutoff.

Figure 25: Total attenuation cutoff vs. E double prime.

Figure 26: Determination of fc by attenuation below cutoff.

Table II: Dielectric constants.



SPACE MATERIALS HANDBOOK - THIRD EDITION by John B. Rittenhouse & John B. Singletary

All the most important materials, phenomena, properties and principles covered in the original handbook are presentd and expanded in this revised and updated version. However, treatment of theoretical aspects have been condensed in order that more emphasis from design and successful launching of a wide variety of space systems could be incorporated.

Figure 12-8, Page 365: Flexural strength 0-60 (psi) vs. hours of glass-reinforced laminates at 600° F.

Table 12-4: Strength properties of polymide-E glass (A-1100) fabric laminates at $500^{\circ}\mathrm{F}$.

Table 12-5: Strength properties of polymide-E glass (A-1100) fabric laminates at 400° F.

Table 18-18: Recommended dielectric materials for spacecraft antennas.

Table 18-23: Electrical insulation and dielectric materials.

AD-803-384

STRUCTURE SENSITIVE PROPERTIES OF ARC-MELTED CARBIDES by R. C. Rossi & R. D. Carnahan

Investigation of composites of Group IVA carbides and graphite and their properties reveals a strong dependence on both microstructure and total carbon content. Of particular importance is the fact that hypereutectic carbide-graphite alloys, although weaker than hypoeutectic alloys, have a higher resistance to thermal stress environments—attributed to an inherent capacity for absorption of elastic energy released by a propagating crack and to the ability of graphite flakes within the structure to blunt a crack tip.

Figure 4, Page 6: Compressive strength as a function of carbon content of ZrC-C alloys.

AD-803-384 (cont.)

Figure 5, Page 7: Transverse bend strength vs. carbon content for ZrC-C alloys.

Figure 6, Page 8: Thermal shock performance for carbide-graphite alloys as a function of relative carbon content.

Figure 7, Page 10: Thermal shock criterion variation with carbon content for two approaches to thermal shock, normalized at the eutectic Figure 11, Page 14: Schematic representation of the crack blunting mechanism proposed by Cook and Gordon.

· AD-710-608

INTERMEDIATE STAGE DENSIFICATION IN VACUUM HOT PRESSING OF ALUMINA by R. C. Rossi & J. D. Bach

An analysis was made of the densification kinetics preceding the final stage densification of alumina, hot pressed in a vacuum. Tests were run at temperatures between 1150 and 1350°C and 2000 and 6000 psi. The analysis suggests a diffusional creep mechanism, possibly consistent with a Narbarro-Herring vacancy model. The measured activation energy (116 Kcal/mole) agrees with the activation energy for the final stage of densification and for the self-diffusion of aluminum ions in alumina. It is conjectured that the pore structure determines the stage of densification and further that pore structure has a profound effect on the apparent diffusion constant.

Figure 1, Page 6: Typical density-time relationships at various pressures.

Figure 2, Page 7: The observed densification rate with time showing an abrupt transition between stages.

Figure 5, Page 14: Grain size as a function of time.

Figure 6, Page 17: An Arrhenius plot of calculated diffusion coefficients.

Figure 7, Page 18: The dependence of porosity at the transition between phases on temperature and applied stress.

THE EVALUATION AND INTERPRETATION OF MECHANICAL PROPERTIES OF BRITTLE MATERIALS

by A. Rudnick, C. W. Marschall & W. H. Duckworth

Factors affecting the quality of mechanical-property data for brittle materials and the significance of such data were critically examined. It was found that major difficulties in property evaluation arise from insufficient attention to: (1) the influence of the nature of the material and its interplay with the testing environment, and (2) source of error in the tests used to obtain the data. This report brings together discussions of these factors and of ways in which their interrelationships should affect the design of testing programs.

Figure 23: $\sigma_{\rm f}$ 1000 psi (0-60) vs. $(\overline{\sigma})^{-\frac{1}{2}}$ Cn^{- $\frac{1}{2}$} 0-70. Fracture strength of MgO as a function of grain diameter.

Figure 25: Modulus of elasticity 10^6 psi 0-60 vs. temperature 0 C (0-1200). Temperature dependence of Young's modulus for various materials (MgO, Al₂O₃, SiC, ZrO₂, etc.).

Figure 26: Yield shear, Kg/mm² 0-4 vs. absolute temperature K 0-600, temperature dependence of yield strength of a lithium fluoride crystal.

Figure 27: Viscosity, poises $1-10^5$ vs. temperature 200-1600°C change in viscosity with temperature of a typical soda-lime-silica glass.

Figure 32: Maximum tensile stress and Weibull's criteria for fracture.

Figure 33: Modified distortion-energy criterion of fracture (compression strength set at 8 times tensile strength).

Figure 35: Griffith fracture criterion.

Figure 37: Compressive stress 10^{-3} psi vs. true strain, in/in 0-0.10 Stress-rate sensitivity of MgO single crystal.

Figure 38: Ultimate tensile strength 10^3 psi 23-37, stress rate psi/sec 10^2 - 10^8 . Effect of stress rate on tensile strength of an alumina ceramic.

CANDIDATE MATERIALS FOR WHISKERS COMPOSITES by M. J. Salkind

An analysis was made of candidate materials for whisker composites. The expected strength-to-weight ratio of composites of nineteen matrix materials with fourteen different fiber materials as a function of fiber content was calculated. The availability, bondability, and thermal expansion properties of candidate materials are discussed.

Table I: Fiber materials, melting point, density, modulus of elasticity, linear coefficient of thermal expansion, modulus to density ratio, of boron carbide, beryllium, silicon carbide, beryllium oxide, alumina, zirconium oxide, silicon oxide.

Table II: Matrix materials similar to Table I.

Table III: Matrix materials -- strong alloy.

Figure 1: Aluminum matrix strength/density (inches \times 10⁻⁷) 0-0.8 vs. volume % fiber 0-100.

Figure 2: Beryllium matrix strength/density (inches $\times 10^{-7}$) 0-0.8 volume % fiber 0-100.

Figure 10: Magnesium matrix, strength/density (inches \times 10⁻⁷) 0-0.8 vs. volume % fiber 0-100.

Figure 19: Zirconium matrix, strength/density (inches X 10⁻⁷) 0-0.8 vs. volume % fiber 0-100.

AD-696-303

THERMOPHYSICAL PROPERTIES OF ALLOYS IN THE SYSTEMS BORON-NITROGEN, BORON-CARBON, SILICON-NITROGEN, AND BORON-SILICON-CARBON

By G. V. Samsonov

This paper deals with an investigation of the properties of a number. of high-temperature semiconducting alloys manufactured by powder metal methods. It is shown that the compound BN in the boron-nitrogen system possesses an extensive region of homogeneity; the rearrangement of the boron lattice during nitregenization leads to the formation of alloys in the nitride homogeneity region with predominance of electronic conductivity. With an increase in the nitrogen content in the nitride, the electrical resistance of the latter sharply rises up to 35-38 percent of nitrogen, after which the rise in resistance is decelerated, which is accounted for by the participation in the conductivity of electrons effecting the bonds between the plane layers of atoms in the nitride structure.

It is established that $\mathrm{Si_3N_4}$ is a semiconductor with a resistance at room temperature of 10^{13} - 10^{14} ohm and a width of the forbidden zone of 3.9-4.0 ev. The nature of the effect of additions of carbon and titanium on silicon nitride conductivity is shown. The author shows the existence of two carbides--B₄C and B₁₂C--in the boron-carbon system, the latter being established for the first time. Both of them are semiconductors; the width of the forbidden zone for B₄C is established as 1.64 eV.

The solution of problems of automation of many thermal processes in modern technology requires the creation of semiconductor materials which can be utilized at high temperatures and during the simultaneous action of gaseous or other aggressive media.

Figures 5 & 6, Page 8: Concentration dependence of electrical resistance and thermal emf of nonannealed (annealed) alloys of boron with carbon.

Figure 8, Page 10: Volt-ampere characteristic of the carbide $\rm B_{12}C$. Figure 9, Page 10: Temperature dependence of electrical resistance of the carbide $\rm B_{4}C$.

Figure 10: Temperature dependence of electrical resistance of the carbide ${\rm B_4C}$, strongly contaminated by impurities.

RE-EVALUATION OF THE CRYSTAL STRUCTURE OF SELECTED OXIDE COMPOUNDS by Otto Sardi

The literature was studied for a total of 18 oxide compounds having the general formula types AX, A_2X , A_2X_3 and ABX_3 . From the data compiled, it was concluded that the most consistent 0^{2-} radius values for the compounds studied was 1.46Å at six-fold coordination. In all the compounds studied, the nature of the bond was never purely ionic. However, the higher the degree of ionic bonding, the closer the computed value of the 0^{2-} radius came to 1.46Å.

In the second phase of the study, the spinel and the inverse spinel crystal structures were evaluated. In addition, three oxide compounds having this specific type of crystal lattice were studied. The most recent crystal chemical data available for ${\rm MgAl}_2{\rm O}_4$, ${\rm MgCr}_2{\rm O}_4$, and ${\rm NiAl}_2{\rm O}_4$ were compiled and reviewed to determine the relationship between the crystal structure, lattice parameters, ionic radii, intersonic distances, coordination number, and bond angles. The relationship between the crystal structure and the thermal and electrical properties of the compounds were also studied. In this report emphasis is given to the stability field-of-the different phases both in the pure state and the presence of additives.

Section III: Oxide compounds having the wurtzite type structure. Figures 2 & 3, Page 10.

Section IV, Page 20: Oxide crystal having the rock salt type structure. Table II, Page 25: The percent ionic character versus the values.

Figures 12 & 13, Page 30: Effect of annealing on conductivity of TiO and thermoelectric e.m.f. of polycrystalline TiO.

Figure 14, Page 31: Conductivity versus composition for sintering TiO. Section V, Page 33: The corundum structure of α -Al₂O₃. Figures 15a,b. Pages 36-37: The last two paragraphs.

Section VI, Page 38: Oxide compounds having the fluorite and antifluorite type structures.

Section VII, Pages 38, 41, 42: Oxide compounds having the rutile type structure.

AD-817-638(cont.)

Section II, Page 97: Oxide compounds having the spinel type structure. Table IV, Page 102: Ultimate strength in compression of sintered spinel. Figure 4, Page 103: Thermal conductivity of spinel as a function of temperature.

Table V, Page 103: Electrical conductivity of sintered spinel. Figure 5, Page 104: Thermal expansion of magnesia (MgO), alumina (Al_2O_3) , Mg-aluminate (MgAl_2O_4), and Mg-chromate (MgCr_2O_4).

Pages 105. & 106: All are describing the electrical properties of spinels. Section 1. Introduction

Silicon dioxide, SiO₂, (silica) is a term applied to a family of materials, rather than a designation. Silica is widely used, primarily it is easily obtainable, inexpensive and chemically stable. A variety of silica is manufactured as glasses, whiteware, refractories, and as fluxes in metallurgical processes; it is also important as an abrasive and a filler. Highly pure quartz crystals are used in optical instruments. Another interesting application of quartz crystals utilizes their piezoelectric properties to measure pressure and to control the frequency of electrical impulses. Very high quality crystals are required for piezoelectric applications, and since the natural crystals always contain impurities, laboratory methods of growing suitable crystals have been developed.

Silica, SiO_2 , an oxide made by composition, is usually classified with the tekto-silicates because its structure consists of framework of SiO_4 tetrahedron with each oxygon linked to a silicon atom and each silicon linked to two oxygen atoms giving a coordination number of 4:2. The general formula for silica is AXO_2 , where A represents silicon and X stands for oxygen atoms: Without replacement of silicon by aluminum this framework is natural, and the structure is that of one of the silica polymorphs. Thus, silica and its crystalline and amorphous phases, except stishovite, are derived from tetrahedra of four oxygen atoms surrounding a central silicon atom. The silicon-oxygen tetrahedra are linked together to form a three-dimensional infinite network. However, the pattern of linkage is different for each of the polymorphs, resulting in differences in their crystal structures and properties.

AD-817 638 (cont.)

Section III, Page 142: Types of inversion in the crystalline phases of silica. (Most of the section is about the microstructure). Section IV, Page 146: Derivative and stuffed silica structures. Derivative structures are a group of crystal structures derived for a simpler structure either by distortion of the basic structure or by substitution of equivalent atoms.

Section V, Page 154: Properties of silica polymorphs.

Table V, Page 154: Thermal conductivity of quartz.

Figure 14, Page 157: Thermal expansion of quartz parallel and normal to the C-axis. Note the effect of the X-B transition at 573° C.

Figure 15, Page 158: Mean linear thermal expansion from 25°C to 500°C of keatite.

Figure 16, Page 162: Thermal expansion of some silica phases.

Table VI: Properties summary of silica compounds.

Trans. Brit. Ceramic Society, Vol. 69, No. 5, Sept. 1970, pp. 199-203.

FATIGUE BEHAVIOR OF HIGH A1₂0₃ CERAMICS by B. K. Sarkar & T. G. J. Glinn

Under single and repeated cycles of thermal and mechanical stressing, two high ${\rm Al}_2{\rm O}_3$ ceramics (Sintox and Lucalox) exhibit well-defined fatigue behavior. The fatigue curves have a characteristic high-stress plateau, followed by progressively increasing endurance with decreasing applied stress. The influence of cyclic frequency and environment is demonstrated and the significance of static effects is emphasized.

Figure 4: Probability of failure vs. quenching temperature.

Figures 5-7: Thermal fatigue of Sintox and Lucalox.

Figures 8-10: Mechanical fatigue of specimen.

Figure 11: Mechanical behavior of Sintox in various environments. Figure 12: Comparison between dynamic and static fatigue of sintex

AD-699-579

STUDY OF THERMAL AND MECHANICAL PROPERTIES OF SELECTED SOLIDS FROM 4 DEGREES TO THE MELTING POINT by H. F. Schaake

The theory of thermal expansion is briefly reviewed with special emphasis on the negative low temperature expansion frequently found in the diamond and sphalerite crystal structures. Lattice parameters of the rock salt compounds AgCl, AgBr and MgO and the sphalerite compounds CuCl, CuBr, CuI, AgI, BN, BP, SiC and CdTe measured from 4.2° K to 300° K are presented. The rock salt compounds are found to behave normally, i.e. positive through the temperature range. CuCl, CuBr, AgI, CdTe and probably BN and BP possess a region of low temperature negative expansion. The thermal expansion of AgI is found to be dependent on its preparation.

Table I, Page 2: Sphalerite and diamond crystal structure materials having low temperature negative thermal expansion.

Figure 3, Page 13: Thermal expansion of Indium. There are several tables listing the lattice parameter of different rock salt compounds.

Figure 4, Page 29: Thermal expansion of CuCl, CuBr, and CuI.

Figure 5, Page 30: Thermal expansion of BP, SiC and BN.

Figure 6, Page 31: Thermal expansion of AgI.

Figure 7, Page 33: Thermal expansion of AgCl, AgBr, and MgO.

Figure 8, Page 35: Thermal expansion of CdTe.

Figure 9, Page 36: Variation in thermal expansion of MgO with temperature. Conclusion:

- 1. The thermal expansion behavior of AgCl, AgBr and MgO, all with the rock salt crystal structure, is normal, i.e. positive everywhere.
- 2. Of the materials examined with the sphalerite crystal structure, CuCl, CuBr, CuI and CdTe possess a region of negative thermal expansion at

AD-699-579

low temperatures. BN and BP also appear to possess such a region.

3. The thermal expansion behavior of AgI is dependent on its method of preparation.

AD-642-550

THERMODYNAMIC OF CERTAIN REFRACTORY COMPOUNDS (Vol. 1) by H. L. Schick

Table 6, Page 1-79: Thermodynamic data for titanium monoxide (gas) for various input cases.

Table 7: Thermodynamic function differences (ΔC_p° , ΔS_T° , $\Delta \left[\frac{Ft-H298}{T}\right]$, $\Delta (H_T - H_{298.15})$ for Titanium monoxide (gas) at HS60 as Basic State, e.g., $\Delta CP = Cp$ (case i) - Cp (case Hs60)

Table 54: Heats of formation of SiC at 298.15K.

AD-647-955

THERMODYNAMICS OF CERTAIN REFRACTORY COMPOUNDS by Harold L. Schick

In the Volume 1 of this book, it presents a summary of the techniques to analyze thermodynamic data and gives the data analysis for refractories considered. While Volume 2 is a compilation of thermodynamic tables generated on this project, it also contains a bibliography and property file.

Table 96: Beryllium. Reference state (reference state for calcinating Hp, Ff and Log Kp solid Be from 0^{0} to 1556^{0} K liquid Be/from 1556 to 2786^{0} K gaseous Be from 2768^{0} to 6000^{0} K.

Beryllium Reference State. <u>Summary of Uncertainty Estimates</u>.

Table 97: Beryllium ideal monotomic gas.

Table 98: Beryllium oxide condensed phase. Be0.

Table 99: 'Beryllium oxide ideal molecular gas BeO. .

AD-647-955

Beryllium carbide condensed phase $\mathrm{Be}_2\mathrm{C}$. Table 100: Dimeric Beryllium oxide ideal molecular gas. Table 101: Beryllium nitride condensed phase Be_3N_2 . Table 102: Table 107: Carbon reference state. Table 113: Silicon carbide condensed phase CSi. Table 114: Tantalium carbide condensed phase CTa. Table 117: Titanium carbide condensed phase CTi. Table 118: Tungsten carbide condensed phase CW. Table 130: Ziconium carbide, condensed phase CZr. Table 151: Magnesium oxide condensed phase MgO. Table 153: Magnesium nitride condensed phase Mg3N2. Table 169: Titanium nitride condensed phase NTi. Zirconium nitride condensed phase NZr. Table 170: Silicon nitride condensed phase N₄Si₃. Table 172:

N69-28428

MELTING POINTS OF CERAMICS by S. J. Schneider

This paper discusses the melting behavior of ceramic materials. The melting point is discussed in terms of a one-component system and extended to more complex systems utilizing unary principles as basic building blocks. Phase diagrams are presented for real and hypothetical materials to illustrate the relationship between melting point and pertinent variables (such as pressure, composition, etc.). The effect of metastable equilibrium upon the melting point is emphasized.

Figure 2, Page 21: Phase diagram for SiO₂.

Figure 3, Page 22: Phase diagram for Carbon.

Figure 4, Page 23: Phase diagram for Li₂CrO₄.

Figure 7, Page 24: Phase diagram for GeO_2 .

Figure 8, Page 24: Phase relations of the silica minerals.

N69-28428

Figure 14, Page 26: Phase diagram for SiO_2 - Al_2O_3 system.

Figure 16, Page 27: Phase diagram for $Ti-Ti0_2$ system.

Figure 17, Page 28: Phase diagram for iron-iron oxide system as a

function of oxygen partical pressure in atmosphere.

Figure 18, Page 29: Phase diagram for Fe-Fe $_2$ 0 $_3$ system.

Figure 26, Page 34: Cooling curves for several ceramics.

Figure 27, Page 34: Heating and cooling curves for $H1_20_3$.

AD-671-472

REVISED DATA ON POLYCRYSTALLINE MAGNESIUM OXIDE by E. Schreiber & O. L. Anderson

This report gives revisions of data from an earlier publication by the authors on the pressure derivatives of the elastic moduli of polycrystalline MgO specimens. The below listed table details the comparison of the data.

Table I: Comparison between data obtained on single crystal & hot-pressed polycrystalline specimens of MgO. (Includes bulk modulus & pressure derivatives).

AD-638-279

ELASTIC CONSTANTS OF SILICON CARBIDE by Edward Schreiber & Naohiro Soga

Graphical and tabular data given on the elastic constants of a relatively porous sintered polycrystalline SiC is given.

Table I: Elastic modulûs of hot-pressed polycrystalline SiC (3.181 gm/cm^3).

Figure I: Young's modulus & Shear modulus vs. porosity.

AD-854-140

PROCESSING OF CERAMICS-SURFACE FINISHING STUDIES by R. Sedlacek

The influence of post-grinding treatments, such as vacuum_bakeout_and exposure to various environments before or during testing on the tensile strength of alumina has been studied. The independence of strength on attainable surface finish, post-grinding treatments, and microstructure is shown for four alumina bodies. Results of profilometric and microscopic evaluations of the ground surfaces are presented.

The tensile strength of four different alumina has been evaluated as a function of their microstructure, surface finish, and various post-grinding treatments.

The test materials varied in average grain size from 10 to $32\,\mu$ and in normal chemical composition from 96% to 99.5% Al_2O_3 . In grinding the test specimens, three sizes of diamond grit were employed, i.e. 12 grit for coarse finishes and 1200(or 600) grit for fine finishes.

It was found that the strength of alumina is primarily controlled by microstructure (grain size); and/or composition. The average tensile strength values of four test materials, determined on specimens ground with the same wheel, increase with decreasing grain size.

27,800 psi (32μ)

31,400 psi (18µ)

35,300 psi (13_µ)

39,600 psi (10μ)

The surface finish per se does not have a pronounced effect on strength, and it depends largely on micro-structure. For example, the surface finish obtained on the 10μ grain size body with the 120 grit. Wheel is the same or better than the finish produced with the 1200 grit wheel on the material having an average grain size of 18μ . An extensive study of the ground surface was made using the profilometer.

Table II, Page 6: Physical properties of the test material.

Page 33: Test data on tensile strength of alumina groups A1, A2.

AD-854-140

Page 34: Groups A3, A4, A5, A6.
Page 35: Groups A7, A8, A9, A10.
Page 36: Groups B1, B2, C1, C2.
Page 37: Groups C3, C4, C5, C6.
Page 38: Groups C7, C8, C9, C10, C11.
Page 39: Groups D1, D2, D3, D4.
Page 40: Groups D5, D6, D7, D8.
Page 41: Groups D9, D10, D11.

N67-37262 or AD-654-209

PROCESSING OF CERAMICS - SURFACE FINISHING STUDIES by R. Sedlacek & E. P. Farley

An experimental grinding facility was established for a systematic study of the effects of grinding variables on the strength of ceramics. (Alumina).

The specimens were hollow cylinders that were ground internally, externally, and on the ends. They were tested using the expanded ring test method. All maching in this experiment was done with diamond wheels. The variables studied were related to the rate of material removed and the quality of the finished surface.

Table I, Page 39: Tensile strength of alumina specimens with different surface finishes of the inside wall.

N64-25341 or AD-601-127

TENSILE STRENGTH OF BRITTLE MATERIALS by R. Sedlacek

The tensile strength of commercial high alumina bodies (99.5%) was investigated using a new test method - a hydraulically expanded rubber bulb inside of cylindrical test specimens. Results were evaluated with respect to loading rate, surface finish, and microstructure.

Formulas for calculations of stress, and standard deviations are included.

Table 2-6, Pages 11-16: Tensile strength of WESGO Al-995 (at various loading rates) includes sample, weight, ultimate tensile strength, and standard deviation.

Table 7, Page 17: Young's modulus (at various loading rates).

Table 8, Page 19: Average values of tensile strengths of WESGO

Al-995 specimens of comparable surface finish.

AD-870-158

PROCESSING OF CERAMICS - SURFACE FINISHING STUDIES by R. Sedlacek

Report deals with the comparison of tensile strength between specimens having as-fired surfaces and those ground by conventional means. Also the effect of atmosphere on tensile strength of ceramics is demonstrated and the concept of delayed fracture is discussed.

Note: All tensile strength measurements were made by the SRI expanded ring test method.

Table II, Page 14: Tensile strength of Al-995 alumina having as-fired or ground surfaces (This table is a summary of the results of many tests - the individual data is also given in Appendix or Tables A-1, 2, 3, 4) Stress rate for this table is 3000 psi/sec.

AD-870-158

Table III, Page 17: Vacuum tensile strength of Al-995 alumina (individual data given in table A-6, 7, 8) Stress rate 300 psi/sec and 30 psi/sec.

Figure 3, Page 19: Effect of stress rate on ultimate strength of alumina (chart plots stress rate and strain rate vs. ultimate tensile strength).

Results: "Strengths of ceramics are rather insensitive to grinding variables and the resulting surface finish, as we can now measure and interpret that finish. There is strong evidence that microstructure is the chief factor controlling strength as well as surface finish obtainable by grinding. Furthermore, the effect of atmosphere greatly outweighs the changes in strength produced by manipulating grinding variables."

AD-730-768

PROCESSING OF CERAMICS SURFACE FINISHING STUDIES by R. Sedlacek & P. J. Jorgensen

The SRI expanded ring test was used to determine the tensile strength of high purity, dense alumina. The test materials were prepared in five different nominal grain sizes ranging from 10 to $50\,\mu$ m. The blanks were diamond ground to final dimensions by a technique developed earlier in the program. It was found that in grinding this material extensive damage occurred which had not been observed in any other alumina body ground under identical conditions. The only difference in strength was found between groups of specimens having grain sizes equal to or smaller than $30\,\mu$ m, and those whose grain size was equal to or larger than $40\,\mu$ m. The vacuum strength of this material was the same as the strength in air regardless of grain size. In all other aluminas investigated previously in this program, the vacuum strengths were considerably higher than the strength measured in air.

AD-730-768 (cont.)

Griffith's theory was applied to test the data, assuming that the grain size determined the flaw length and a good correlation between observed and calculated strength values was obtained for all alumina tested with the exception of the high-purity alumina. In this material, the mechanical damage occurring during grinding extended beyond the first grain boundary in the smaller grain size samples, and thus the mechanical damage controls the strength. When the grain size is equal to or larger than the mechanically damaged region, the microstructure controls the strength.

Summary: The tensile strength of a high-purity dense alumina was determine in air and vacuum using the SRI expanded ring test. The test materials wer supplied by the manufacturer in the five groups of rings having different nominal grain sizes, i.e., 10, 20, 30, 40 and 50 µm. The actual measured grain sizes varied considerably from the nominal values. The rings were ground to size by the technique developed earlier in this program. The ty types of abrasives were used, i.e., 120-grit natural metal-bonded diamond and 100-grit synthetic resineid bonded diamond. After grinding, the specimens were dye checked and, although no individual flaws were detected, all rings showed a considerable dye retention which has not been observed previously on any other test material used on this program. It was determined that the coloration is the result of extensive damage incurred in grinding.

The following tensile strength values were obtained on the highpurity alumina specimens:

AVERAGE STRENGTH
(psi)
35,700
34,300
33,500
. 29,800
28,100

The above values comprise all strength measurements regardless of test conditions and diamond used in grinding, because statistical analyses

show that there is no statistical significant difference between the air and vacuum strengths, nor between the strengths of rings ground with different types of diamond. The only difference found on the 0.01 significance level is between groups of specimens having grain sizes equal to or smaller than 30 μm and those having grain sizes equal to or greater than 40 μm .

Table I, Page 13 Relationship between grain size, diamond grit, and surface roughness (AA).

Table II, Page 23: Tensile strength of a high-purity alumina as a function of grain size.

Table III, Page 24: Tensile strength of high-purity alumina as a function of grain size, grinding, technique, and test conditions.

Table IV, Page 26: Comparison of air and vacuum strengths of various aluminas.

Table V, Page 29: Tensile strength of various aluminas.

Figure 9, Page 30: Plot of relationship between strength and grain size for different aluminas.

Table 6, Page 32: Calculated and experimental strength of high-purity alumina.

Figure 10, Page 33: Plot of relationship between strength and grain size for high-purity alumina.

Table A-1, Page 38: Tensile strength of high-purity alumina (tested in air, ground with 120-grit natural diamond).

Table A-2, Page 39: Tensile strength of high-purity alumina.

Table A-3, Page 40: Tensile strength of high-purity alumina.

Table A-4, Page 41: Comparison of air and vacuum strength of A1-300 alumina.

Table A-5, Page 42: Comparison of air and vacuum strength of A1-995 alumina.

Table A-6, Page 63: Comparison of air and vacuum strength of A1-600 alumina.

Table B-1, Page 46: Difference in strength of high-purity alumina as a function of grain size.

Table B-2, Page 47: Difference in strength of high-purity alumina as a function of grain size.

AD-730-768 (cont.)

Table B-3, Page 68: Difference in strength of Al-600 alumina as a function of grinding and environment.

Table B-4, Page 68: Difference between vacuum and air strengths of Al-600 alumina regardless of grinding condition.

Table B-5, Page 49: Difference between vacuum and air strengths of A1-300 alumina.

Table B-6, Page 69: Difference between vacuum and air strengths of Al-995 alumina.

AD-850-929

INVESTIGATION OF ELASTICITY AND STRENGTH OF CERAMICS SUBJECTED TO TENSILE AND COMPRESSIVE LOADS by R. Sedlace

A new method of compressive testing of ceramics was perfected, and the average ultimate compressive strength of Al-995 alumina was determined to be $448,000\pm36,000$ psi at a loading rate of 10,000 psi/sec. Compressive prestressing was found to have no significant effect on the ultimate tensile strength of alumina, but extensive cyclic testing did lower the ultimate tensile strength.

N72-29527

THE EFFECT OF GRINDING VARIABLES ON THE STRENGTH AND SURFACE FINISH OF ALUMINA by R. Sedlacek, et al

This report studies the variables of grinding (grit size of diamond, rate of material removal, and spark-out time) and their effect on the tensile strength of alumina. The specimens tested were 99.5% pure alumina with \sim 97% density. The specimens were hollow tubes. The internal surface

N72-29527

was ground with different grit wheels at varying rates of feed, using both dry and wet grinding. The external surface was not considered a variable, since it was kept constant throughout the study. Profile traces were also made.

Table I, Page 393: Tensile strength as a function of grit size of natural diamond in metal-bonded grinding wheels.

Table II, Page 394: Tensile strength of alumina ground with and without coolant.

Table III: Tensile strength of alumina having as-fired or ground surfaces.

AD-714-741

STUDY OF THE THERMAL EXPANSION OF REFRACTORY OXIDES AT HIGH TEMPERATURES by D. M. Shakhtin, et al

The coefficient of thermal expansion from $1997-2297^{\rm O}$ C was determined experimentally for aluminum and magnesium oxides and ${\rm Al}_2{\rm O}_3$ solid solution in MgAl $_2{\rm O}_4$. The nature and characteristics of thermal expansion (many graphs) were established for a series of ${\rm ZrO}_2$ samples that were stabilized with varying amounts of MgO, CaO, or ${\rm Y}_2{\rm O}_3$.

AD-733-698

AN EXPERIMENTAL STUDY ON THE COMPRESSIVE BIAXIAL STRENGTH OF CERAMICS by G. Sines & M. Adams

Discussion of the Griffith flaw theory is the main topic of this paper.

Appendix B discusses buckling tendencies of hollow cylindrical test specimens. Equations are also presented.

Figure B-3, Page 26: Specimen length vs. critical buckling pressure. Appendix C - Analysis of prestressing fixture for 1:1 stress state.

Ohio State University, Columbus, Ohio

AD-605-393

PROCEEDINGS OF THE OSU-RTD SYMPOSIUM ON ELECTROMAGNETIC WINDOWS Editor: A. I. Slonim

Based upon the needs of advance weapon systems having multimode missions to perform, complex requirements are placed on the radar system. These multimode missions demand optimum radar performance for each mode of operation. Since the optimum radar performance requires different radar parameters for each mode, complex design requirements are placed upon the radar. Consideration must be given in the design of the radar to optimize the radar performance for each mode without too many compromises. One way in which the radar performance can be enhanced for the various mode requirements is to utilize a dual frequency radar concept.

Figure 1: Density vs. firing temperature of several fabricating procedures.

Figure 2: Data and particles size distribution of base body.

Figure 4: Percent total porosity vs. time in hydrogen, helium and vacuum at several temperatures.

Figure 5: Grain size vs. firing time at several temperatures and atmospheres (C, Cr, R).

* (Here all the graphs, tables and other forms of data are concerning the design of antennas).

AD-605-391

PROCEEDINGS OF THE OSU-RTD SYMPOSIUM ON ELECTROMAGNETIC WINDOWS

Editor: A. J. Slonim

The paper is Volume III of the proceedings and concerns the fabrication and testing of airborne radomes and hypersonic environment. Data on electrical and mechanical properties as well as fabrication data is presented. There is also data on thermal shock and thermodynamic properties.

Table 1: Rain erosion test results for two ceramic materials (pyroceram 9606 and alumina).

Figure 2: Skin thickness vs. optimum core thickness for alumina sandwich radome with an air core fins at various angles of incidence and perpendicular polarization.

Table I, Page 25: Schedule for firing large ogival radomes.

Figure 9: Segment bodies--dielectric constant vs. temperature at 9.375 Gc (Al $_2$ 0 $_3$, Zr0 $_2$ and BeO).

Figure 10: Segment bodies--loss tangent vs. temperature at 9.375 Gc (Al $_2$ 0 $_3$, Zr) $_2$ and BeO).

Figure 11: Mean coefficient of thermal expansion vs. temperature (BeO, $A1_20_3$) $100-1600^{O}F$.

Table 2: Flexural strength of segment bodies (97.5%-99.5% of $A1_20_3$).

Table 3: Compressive strength of segment bodies (97.5%-98.5% of ${\rm Al}_2{\rm O}_3$).

Table 4: Tensile strength of segment bodies. (97.6% ${\rm Al}_2{\rm O}_3$).

Table 5: Typical properties of candidate inorganic adhesives (property, devitrified sealing glass, ceramic eutectic and aluminosilicate glass of Al_2O_3 , etc.).

Table 6: Typical properties of modified magnesium-aluminosilicate adhesive.

Table I, Page 5: Mechanical and thermal properties of ceramic radome materials (Al_2O_3 , MgO, BeO, slip-cast fused silica, spinel, and zirconia).

Figure 1: Relative thermal shock resistance of ${\rm Al}_2{\rm O}_3$ and BeO as a function of thermal shock environment.

AD-605-391 (continued)

Figure 2: Relative thermal shock resistance of candidate reentry radome materials as a function of thermal shock environment.

Figure 5: Surface temperature weight change and length change of slip-cast fused silica as a function of time exposed to oxy-acetylene test Figure 8: Surface temperature and length change of slip-cast fused silicate with flame shield as a function of time exposed to oxy-acetylene test facility.

Figure 10: Effect emittance vs. corrected surface temperature for slip-cast fused silica.

Figure 13: Surface and backside temperature vs. time for slip-cast fused silica.

Figure 15: Loss tangent vs. temperature for unmodified and ${\rm Cr_2}{}^0{}_3$ modified slip-cast silica.

Figure 16: Dielectric constant vs. temperature for unmodified and ${\rm Cr_20_3}$ modified slip-cast fused silica.

AD-720-383

STUDIES OF CERAMIC PROCESSING by E. J. Smoke, W. C. Jacobs, D. R. Mangino

Spinel (MgAl $_2$ 0 $_4$) is the elementary member and often considered the parent compound of a family of materials referred to as spinels. This family has the general formula AB_20_4 and is a face-centered cubic crystal. A unit cell contains thirty-two oxygen ions with a space lattice of cubic closest packing. Within this array of oxygen ions there are sixty-four tetrahedral interstices or A sites, of which eight are filled, and thirty-two octahedral interstices or B sites with sixteen of these occupied. Consequently, a unit cell is composed of eight stoichiometric molecules. There are three general stuctures for spinel: the normal, the reverse, and the random. In the normal, A or tetrahedral sites are filled with

trivalent metal ions and the B octahedral sites are filled with trivalent metal ions. The reverse occurs when the A sites are filled with trivalent metal ions, and eight divalent metal ions and the remaining eight trivalent metal ions reside in the B or octahedral sites. A mixture of these two extreme cases defines the random structure.

In the case of MgAl $_20_4$, the tetrahedral sites are occupied mainly by Mg $^{+2}$ and are smaller than the octahedral sites but larger metal ions are readily accomodated in other spinels by an enlargement of these sites resulting in an enlargement of the unit cell along unit cell diagonals. Although the term spinel finds general usage, it is here defined in its exact technical sense to indicate the compound MgAl $_20_4$.

Figure 3, Page 20: Thermal analysis of $MgSO_4 \cdot (NH_4)_2 SO_4 \cdot 6H_2 O$.

Figure 4, Page 20: Thermal analysis of Al(SO_4)₂·NH₄·12H₂O.

Figure 7, Page 22: Firing schedule for the calcination of stoichiometric spinel used in evaluating particle size-temperature relationship.

Figure 8, Page 23: Plots of the average particle size of spinel dependent on calcination temperature.

Figure 11, Page 29: Firing schedule for the sintering of samples of compositions A, S, and M under controlled atmosphere conditions.

Table 1, Page 38: Analysis of variance for the physical properties of sintered spinel.

Table 2, Page 39: Bulk density data.

Table 3, Page 40: Modulus of rupture data for compositions A, S, and M.

Table 4, Page 41: Water absorption data for compositions A, S and M.

Table 5, Page 42: Apparent specific gravity data for composition A, S, and M.

Sec. #4, Page 51: Analysis of bulk density and water absorption.

Table 6, Page 57: Physical properties of spinel sintered in atmospheres with controlled dew point for the evaluation of the effect of water vapor.

Table 7, Page 59: Physical properties for spinel compositions A, S and M sintered under a number of optimized conditions.

Figure 36, Page 77: Thermal expansion characteristics of compositions 20 GlCo and 10 GlCo.

AD-720-383

Figure 37, Page 79: Thermal expansion characteristics of composition 10 G1Co as a glass and as a body.

Figure 46: Log viscosity vs. temperature ($^{\circ}$ C) for glasses 10 GlCo and Co.

Figure 47: Log viscosity vs. reciprocal absolute temperature ${}^{\rm O}{\rm K}$ for glasses 10 GlCo and Co.

Table 15, Page 110: Properties of improved cordierite compositions.

AD-612-959

DEVELOPMENT OF REFRACTORY CERAMICS THAT CAN BE PROCESSED AT TEMPERATURES CONSIDERABLY LOWER THAN THEIR MAXIMUM-USE TEMPERATURES by E. J. Smoke, et al

The objective of this study is to determine the compositions, mechanisms and procedures necessary to lower the firing temperature of high quality ceramics which approach true density, yet retain all engineering properties including refractoriness. The effort was divided into three temperature ranges: higher than $3000^{\circ}F$, $2600^{\circ}F$ - $3000^{\circ}F$ and below $2600^{\circ}F$.

Table III: Verification of atmospheric firing, 2% MgO/98% Al $_2$ 0 $_3$; .25% MgO/99.75% Al $_2$ 0 $_3$.

Table V: Bulk density and moisture absorption for spinel composition.

Figure 18: bulk density, moisture absorption vs. temperature; spinely prereacted from alumina and magnesia bulk density and moisture absorption vs. temperature.

Table VII: Density and moisture absorption vs. firing temperature conventional fabrication.

Table VIII: Density and moisture absorption vs. firing temperature prereacted compositions.

Figure 1: Density vs. firing temperature 2.9-3.5 vs. 2400-2800 (both prereacted bodies and conventional fabrication).

Table IX: Dielectric properties.

Table X: Transverse strength measurements of prereacted composites and conventional fabrication.

Table XI: Weight loss in water prereacted and conventional.

Table XII: SiO_2 , MgO, AI_2O_3 firing temperature 0F , bulk density g/cc. moisture absorption (%), coefficient of expansion X: 10^{-6} in/in/ 0C , crystalline phase.

Table XIII: Frit Co, SiO_2 , AI_2O_3 , MgO; Frit Cb-9; max. density, moisture absorption (%), coefficient of linear expansion X 10^6 and loss of weight in water.

Table XIV: Similar to Table XIII.

Table I: Bulk density of several firing temperatures and soaking periods in hydrogen (helium).

Figure 1: Density vs. time in hydrogen and helium at 1550° C; 3.70-4.00-hours 1-7.

Figure 2: Density vs. time in hydrogen and helium at 1750°C.

Figure 3: Density vs. temperature ${}^{\rm O}{\rm C}$ samples fired in hydrogen and helium for 7 hours.

Figure 4: Bulk density vs. firing temperature in dry hydrogen.

Figure 5: Bulk density vs. firing temperature in dry helium.

Figure 6: The plot of bulk density in vacuum.

Figure 7: Percent total porosity vs. time in hydrogen and helium at 1550° C.

Figure 8: Percent total porosity vs. time in hydrogen and helium at 1750°C .

Figure 9: Percent total porosity vs. time at 1550° C in vacuum,

Figure 11: Percent total porosity vs. temp. in helium and hydrogen for 7 hours.

Table IV: Microstructure of the sintered composites in hydrogen and helium. (composition--100% Al_20_3)

Figure 13: Grain size vs. time at 1550°C in hydrogen and helium.

Figure 14: Grain size vs. time at 1750°C in hydrogen and helium.

Figure 15: Grain size vs. temperature for a seven hours soaking time

DIELECTRIC LOSS IN MgO AND SAPPHIRE by G. S. Snow

Dielectric loss measurements were made on single crystal MgO and sapphire and pure and doped polycrystalline MgO. The measurements were made in air and in dry argon gas at audio frequencies from room temperature to approximately 800° C. Both two and three terminal measuring apparatus were used in the investigation.

Figure 1, Page 9: Dielectric constant and loss factor vs. frequency as given by Debye equations.

Tables I & II, Pages 37-42: List of samples, chemical compositions, firing conditions, types of electrodes used, etc.

Figure 11, Page 54: Loss tangent vs. frequency for single crystal MgO in air.

Figures 12 & 13, Pages 55 & 57: Peak frequency vs. temperature for MgO and sapphire .

Figure 14, Page 59: Loss tangent vs. frequency for single crystal MgO in air.

Figure 15: Loss tangent vs. frequency--effect of quench and anneal treatment on loss in single crystal MgO.

Figure 16, Page 62: Loss tangent vs. time--variation of loss with time after quenching (MgO).

Figure 17, Page 64: Loss tangent vs. frequency--MgO.

Figure 18, Page 66: Loss tangent vs. temperature for sapphire single crystals at 10Kc.

Figure 19, Page 67: Loss tangent vs. frequency--single crystal sapphire.

Figure 21: Loss tangent vs. time--time dependence of room temperature dissipation factor of single crystal sapphire.

Figure 22, Page 72: Temperature dependence of loss factor for single crystal sapphire at 10Kc.

Figure 23, Page 73: Conductivity vs. temperature for $A1_20_3$.

Figure 24, Page 7.9: Loss factor "E" vs. 1/T for polycrystalline MgO.

Figure 25, Page 80: Loss factor "E" vs. frequency for polycrystalline MgO.

Figure 26, Page 81: Peak frequency vs. temperature—temperature dependence of peak frequency for the low temperature loss peaks in polycrystalline MgO.

Figure 27: E vs. temperature for doped MgO (polycrystalline).

Figure 28, Page 86: E vs. temperature Al₂O₃.

Figure 29, Page 91: Loss factor vs. frequency

Figure 30, Page 92: " " " "

Figure 31, Page 93: " " " "

Figure 32; Page 94: Dielectric constant vs. frequency.

Figure 33, Page 95: Thickness dependence of peak height ("E")

for samples #9 & #10.

Figure 34, Page 96: Thickness dependence of relaxation time for sample number 10 at two temperatures.

Figure 35, Page 100: Loss factor vs. frequency for sample #10.

Figure 36, Page 103: Electrical conductivity vs. temperature for sample #9.

Figure 37, Page 104: Electrical conductivity vs. temperature for sample #11.

Figure 38, Page 105: Electrical conductivity vs. temperature for sample #13 & #16.

N63-12406

INVESTIGATION OF SIMTERABLE MgO POWDERS AND CERAMICS MADE FROM THEM by M. J. Snyder

This report describes attempts made to fabricate dense reproducible specimens suitable for strength measurements and having controlled microstructural differences. A sinterable, high density MgO powder was used.

Also in this report a new test is developed and results given. The test is the diametral-compression test, where short cylinders are broken by applying a load across the diameter. Procedures were established for measuring a tensile strength by this method.

Table 3, Page 12: Effects of type of calcining furnace on sintered bulk density.

Figure 2, Page 13: Graphical presentation

Table 7, Figure 4, Pages 22-23: Effects of rate of heating during sintering on sintered bulk density.

Figure 11, Page 42: Moduli of rupture vs diametral compression strengths.

Table 10: Summary of diametral-compression tests on MgO specimens. Table 9, Page 26: Variability in strength values (for different manufacturing processes.)

AD-638-280

SIMPLIFIED METHOD FOR CALCULATING ELASTIC MODULI
OF CERAMIC POWDER FROM COMPRESSIBILITY AND DEBYE TEMPERATURE DATA
by N. Soga & O. L. Anderson

This paper presents a new method of calculating the elastic modulus of ceramic powder from the compressibility and Debye temperature. Values derived for Mg0, ${\rm Al}_2{\rm O}_3$, BeO, and ${\rm TiO}_2$ by the new method are compared with values determined by the standard resonance method.

AD-638-280

Figure 4: Shear modulus and Young's modulus vs. porosity for MgO.

Figure 5: Shear & Young's modulus vs. porosity for $A1_20_3$.

Table III: Comparisons of experimental and computed moduli for Al_2O_3 , BeO, MgO, TiO_2 .

AD-601-447

ANISOTROPIC MECHANICAL BEHAVIOR IN SAPPHIRE WHISKERS by P. J. Soltis, et.al

This paper describes a static tension test for testing ${\rm Al}_2{\rm O}_3$ whiskerat room temperature. Whiskers having different grain orientation (<0001>, <1120>, <1100>) were examined and differing behaviors noted. (i.e. ductile to brittle).

Table 1: Tensile data on sapphire (Al_20_3) whiskers.

Table 2: 'Anisotropic tensile properties of ${\rm Al}_2{\rm O}_3$ whiskers.

Figure 2: Discontinuous yielding in Al_2O_3 (c-axis) whiskers.

Figure 3: Log-log plots of σ_f versus t for Al $_2$ 0 $_3$ whiskers -(a) c-axis whiskers.

Figure 4: Log-log plots of σ_f vs. t for Al $_2$ 0 $_3$ whiskers - (b) A $_z$ -axis whiskers.

Figure 5: Log-log plot of $\sigma_{\rm f}$ vs. A for Al $_2$ 0 $_3$ whisker - (a) c-axis whiskers.

Figure 6: Log-log plots of $\sigma_{\rm f}$ vs. A for Al $_2$ 0 $_3$ whiskers.

Figure 7: Log-log plot of $E_{\rm m}$ vs t for ${\rm Al}_2{\rm O}_3$ whiskers - (a) c-axis whiskers.

Figure 8: Log-log plot of $E_{\rm m}$ vs. t for Al_20_3 whiskers - (b) a-axis whiskers.

Figure 9: Log-log plot of $\rm E_m$ vs. A for $\rm Al_20_3$ whisker - q) c-axis whiskers.

Figure 10: Log-log plot of $\rm E_m$ vs. $\rm Al_2 0_3$ whiskers - (b) a-axis whiskers.

AD-601-447

Figure 11: Semi-log plot of y vs. $E_{\rm m}$ for ${\rm Al}_2{\rm O}_3$ whiskers. Figure 12: Semi-log plot of size vs. $E_{\rm m}$ for ${\rm Al}_2{\rm O}_3$ (c-axis) whiskers.

N69-28434

INELASTIC DEFORMATION OF OXIDE CERAMICS by R. M. Spriggs

The state-of-the-art of understanding the inelastic deformation of oxide ceramics is briefly reviewed. Special emphasis was given to the permanent deformation caused by phenomena such as stress-enhanced diffusional creep, dislocation motion, and grain-boundary sliding.

The primary mechanism by which most polycrystalline oxide ceramics deform at high temperatures, low stress, and fine grain size was cited as Nabarro-Herring diffusional creep. It was recognized however that under most experimental conditions that deformation is the result of more than one process.

A brief summary of the major findings for ${\rm Al}_2{\rm O}_3$, BeO, MgO, and SiC is presented in tabular and graphical form.

Table 11, Page 153: Slope of elastic modulus vs. porosity curve at zero porosity.

Figure 7, Page 158: Young's modulus of single-crystal ${\rm Al}_2{\rm O}_3$ as a a function of temperature.

Table 13: Temperature coefficients for some single crystal elastic constants.

Table 14: Temperature coefficients for elastic moduli of some polycrystalline ceramics.



N72-29526

THE INFLUENCES OF MATERIAL REMOVAL ON THE STRENGTH AND SURFACE OF AN ALUMINA by H. S. Starrett

This paper is a discussion of why a series of tests did not produce the generally accepted results. The tests indicated that surface finish had no effect on tensile or flexural strength. It was postulated that the test results may have been due to subsurface damage that occurred during machining (grinding) operations.

Equations for the Weibull distribution are presented and numerous graphs and tables of data are also included.

Figure 13, Page 384: Average flexural strength vs. minimum fired thickness.

Figure 14: Dimensionless stress vs. porosity.

Figure 15: Dimensionless stress vs. grain size.

Figure 16 & 17, Page 387: Probability of failure vs. normalized stress for marco tensile and macro flexural specimens.

Figure 19, Page 388: Strength ratio versus tensile volume for tensil and flexural (4-point) specimens.

AD-619-87

ANALYTICAL STUDIES OF HOLLOW SPHERES FOR LOWER DENSITY
HIGHER STRENGTH BUOYANCY MATERIALS
by Bernard G. Stechler, Israel Resnick

The object of this program is to develop a low density, high strength buoyancy system of materials with a target density of 0.3 to 0.4 gm/cm³ which will be able to withstand 13,500 psi hydrostatic pressure. It is the intent of this phase of the program to perform analytical studies of significant variables for glass, ceramics, and metal hollow spheres in order to determine promising optimum materials and sphere sizes.

AD-619-872

Figure 2: Outer diameter to thickness ratios of hollow sphere.

Figure 3: Volume of sphere (0.01-100)in. 3 vs. outer diameter

(1-4) in. of sphere.

Figure 4: Net buoyancy lbs. (0.1-4) vs. outer diameter of sphere

(1-4) in.

- AD-722-239

CHARACTERIZATION OF HOT-PRESSED A1203 WITH A Mo-DISPERSED PHASE by J. J. Stiglich, et. al.

"Cermet" materials are a mixture of metal and ceramic phases which are devised for applications in which neither ceramics nor metals provide the necessary properties. Cermet materials containing a ceramic matrix with dispersed metallic particles or metallic fibers have generally provided increases in mechanical strength properties over the pure ceramic. Such properties as ductility, fracture strength, impact strength, and flexural strengths are often enhanced in ceramics.

Table II, Page 5: Tensile strength data and grain size of ${\rm A_2O_3\text{-Mo}}$ composites.

Table III, Page 8: Phase present in ${\rm Al}_2{\rm O}_3$ -Mo composites and lattice parameters and unit cell volumes of the alpha- ${\rm Al}_2{\rm O}_3$ phase.

Table Iv, Page 9: Density, elastic moduli, and microhardness of ${\rm Al}_2{\rm O}_3{\rm -Mo}$ composites.

N64-17614 or AD-433-207

BRITTLE FRACTURE OF CERAMICS by E. Stofel, H. Conrad

This paper reviews various topics relevant to the brittle fracture of ceramics, including theoretical strength of solids, the Griffith theory, the Weibull theory, the role of dislocations, microstructure, stress distribution, environment, crack propogation, etc. It is concluded that the behavior of ceramics can not yet be predicted quantitatively, but the available theoretical and experimental information is useful as a qualitative guide for the design of components.

Figure 3, Page 27: Strength of hot pressed BeO as a function of temperature and manufacturer.

Figure 5, Page 28: Fracture strength of glass vs. crack size.

Figure 17, Page 36: Static fatigue. Fracture strength as a function of load duration (fused silica glass, soda-lime glass, porcelain).

Figure 29, Page 45: Dependence of strength on porosity in Lucalox.

Figure 30, Page 45: Weibull fracture probability as a function of stress for polycrystalline Al_2O_3 .

Figure 33, Page 47: Variation of strength with temperature for ${\rm Al}_2{\rm O}_3$. There are also a number of other figures and graphs that are relevant to the theoretical discussions of the topics listed earlier.

N64-17441 or AD-407-614

MICROSTRUCTURE AND MECHANICAL PROPERTIES OF CERAMICS by R. J. Stokes

This paper attempts to correlate the following mechanical properties with the fundamental microstructural properties of grain size, porosity, crystal structure, impurities, vacancies and dislocations, etc.:

1) elastic deformation

N64-17441 or AD-407-614

- 2) anelastic behavior
- 3) plastic deformation
- 4) brittle fracture
- 5) high temperature deformation and creep

Figure 2, Page 6: Effect of porosity on elastic and shear moduli of polycrystalline MgO at room temperature.

Figure 3, Page 9: Change in damping capacity (internal friction) and dynamic elastic modulus with frequency.

Figure 4, Page 11: Internal friction spectrum of single crystal and polycrystalline Al_2O_3 .

Figure 6, Page 14: Effect of plastic deformation on the internal friction spectrum of MgO single crystals.

Figure 9, Page 24: Effect of heat treatment on the room temperature yield strength of commercial purity MgO single cyrstals.

Table I, Page 26: The number of independent slip systems for some common ceramic crystal structures.

Table II, Page 37: Tensile strength of MgO in the absence and presence of "fresh" surface dislocations.

Table III, Page 45: Comparison of torsional creep rate for different polycrystalline materials (Al_2O_3 , ZiO_2 , MgO (slip cast & hot pressed), BeO, ThO).

Table IV, Page 46: High temperature deformation and creep of single and polycrystalline ${\rm Al}_2{\rm O}_2$.

Figure 13, Page 48: Effect of purity on the steady state creep rate of ${\rm Al}_2{\rm O}_3$.

Figure 16, Page 53: Effect of porosity on the torsional creep of sintered alumina at 1275° C.

N71-21221 or (AD-716-886)

AND OTHER PHYSICAL PROPERTIES OF CERAMICS by R. J. Stokes

This report reviews the effects of mechanical finishing operations on the mechanical, electrical, magnetic, and optical properties of ceramics. It is known that machining results in a defective surface containing cracks, dislocations, point defects and residual stresses. The relative significance of these defects depends on the physical property of interest. The mechanical properties of single crystals are sensitive to dislocations (for semi-brittle materials) and surface cracks (for brittle materials). The mechanical properties of polycrystals are sensitive to surface cracks. The electrical properties of semiconductors are sensitive to surface trapping sites; magnetic, piezo-electric and optical properties are particularly sensitive to residual stresses. To optimize physical properties these defects must be eliminated by mechanical lapping, chemical etching or thermal annealing.

Table III, Page 11: Effect of surface condition on the tensile strength of alumina single crystals.

Figure 3, Page 14: Fracture strength of polycrystalline magnesium oxide as a function of grain size and surface condition.

Table IV, Page 16: Effect of surface treatment on the bend strength of polycrystalline alumina.

Figure 4, Page 19: Effect of machinery and annealing on the shape of B-H loop for torriod cut from $Ni_{36}Zn_{64}$ ferrite.

Figure 5: Variation of remanence (B_r) and magnetic saturation (B_s) with specimen size in as-machined and annealed conditions.

Figure 6, Page 24: Effect of surface condition on PEM (photoelectro-magnetic) voltage of germanium.

AD-601-863

OF YIELDING IN MgO by R. J. Stokes & C. H. Li

This paper looks at 'fresh', 'aged', 'grown in' and high temperature dislocations in the initiation of plastic flow in single crystal MgO.

Figure 1, Page 5: Effect of heat treatment time and temperature on the stress to initiate slip from aged dislocations.

Figure 2: Resolved shear stress vs. strain curves for aged MgO single crystals. (curve 1 - room temperature prestrain relation curves 3, 2, 4, 5, - after 2 hours aging at 1050° C, 1200° C, 1350° C, and 1900° C respectively).

N64-15533

RESEARCH ON LOW DENSITY THERMAL INSULATION MATERIALS

FOR USE ABOVE 3000°F

by K. H. Styhr

This paper (a quarterly report) investigates the concept of reducti of radiation transfer of heat thru the pores of a low density ceramic structure at high temperature by the incorporation of various radiation barrier phases in these voids. Thermal conductivity data up to specimen hot face temperatures of 4235°F are reported for zirconia foam samples.

Figure 3 & 4, Page 17 & 19: Thermal conductivity vs. temperature (for various zirconia foam samples).

NOTE: Calculations and equations also presented.

AD-630-345

INTERFACIAL POLARIZATION AND ELECTRICAL CONDUCTIVITY IN SAPPHIRE by N. M. Tallan & H. C. Graham

Several electrical properties (dielectric constant, unsample of factor, conductivity, and capacitance) are presented in graphical form as a function of frequency and at varying temperatures. All data is for Al_2O_3 .

AD-679-846

by Lawrence H. Van Vlack

Materials contain an internal structure rather than having a homogeneous continuium. A significant features of these internal structures is the arrangement of the grains and phases and their associated boundaries. We use the term microstructure for internal structures of this type.

Figure 13: Conduction through two phase microstructures. Data points are for periclase (MgO) for strite (Mg $_2$ SiO $_4$) ceramics.

N63-16176

MICROSTRUCTURE STUDIES OF POLYCRYSTALLINE REFRACTORY OXIDES by T. Vasilos, et. al.

Log-log plots of room-temperature strength (extrapolated to zero porosity) versus grain size for alumina and MgO revealed these relationships. ${\rm S=86.000G^{-1/3}for~Al_2O_3} \\ {\rm S=50.000G^{-1/6}~for~MgO}$

Where

G=grain size in microns:

N63-16176

Figure 3, Page 9: Transverse bend strength vs. grain-size for ${\rm Al}_2{\rm O}_3$.

Figure 4, Page 10: Transverse bend strength vs. grain-size for MgO.

Figure 5, Page 11: Density vs. time plot for hot-pressed MgO.

AD-606-883

THE ELECTRICAL BEHAVIOR OF REFRACTORY OXIDES II by R. W. Vest, J. A. Crawford & W. C. Tripp

The research was directed toward achieving a more fundamental understanding of change and mass transport mechanisms in refractory metal oxide. Special research apparatus and instrumentation was developed in order to comfort the experimental program.

Figure 4: Zirconia heating and cooling - 200 Mg samples $\Delta w \mu g$ -100+100 vs ^{0}C 200-1000.

Figure 10: Conductivity of pure zirconia; $\log \sigma(mho/cm)$ -6.0- -4.0 vs $\log Po_2$ (atm.) -28 - 0.

Figure 11: Wt. change of pure zirconia. Log. Po_2 -6-0 vs log dw/ Po_2 2.0-5.0.

Figure 12: Deviation from Stoichiometry for pure zirconia $\Delta w(\mu g)$ · 0-160 vs 0-1.0.

Glastech Ber, Volume 45, No. 11 (Nov. 1972), PP. 494-498.

MASS TRANSPORT AND CHEMICAL REACTION IN POLYCRYSTALLINE OXIDES by Werner Richarz & Alfred Schindler

The decomposition of magnesium aluminum spinel in polycrystalline alumina by vanadium pentoxide in the temperature range 700 to 960° C can be described by models for non-catalyzed solid-liquid reactions. It was

Glastech Ber, Volume 45, No. 11 (Nov. 1972), PP. 494-498.

shown that the growth of the reaction zone was determined by the influence of V_2O_5 on the rate of decomposition MgO $^{\circ}$ Al $_2O_3$. The activation energy was found to be 40,3 $^+$ 0, 1 Kcal/mol. An electron microprobe was used to determine the distribution of vanadium in sinters and thus to evaluate the diffusivity of the product in the central zone.

N69-28432

ELASTIC DEFORMATION OF CERAMICS AND OTHER REFRACTORY MATERIALS by J. B. Wachtman

Elastic deformation of ceramics is reviewed from a continuum, thermodynamic point of view; non-linear effects and pressure dependence of elastic moduli are included. The results of wave propagation, resonance, and micro-structure on elastic moduli are discussed in terms of continuum elasticity. Correlations of other physical properties with elastic moduli is also discussed. The measurement of elastic moduli and the characterization of ceramics with respect to elastic moduli are considered.

Figure 1, Page 143: Compressibility of ${\rm Al}_2{\rm O}_3$.

Table 3, Page 146: Single crystal elastic constants of some non-piezoelectric ceramics and some refractory (metallic) crystals.

Table 5: Elastic moduli of isotropic polycrystalline ceramics at or near zero porosity.

Table 7: Third order elastic constants of some ceramic crystals.

Table 6: Dependence of effective second order elastic constants upon pressure.

Table 11: Slope of elastic modulus vs. porosity curve at zero porosity.

Figure 7, Page 158: Youngs modulus of single-crystal ${\rm Al}_2{\rm O}_3$ as a function of temperature.

N69-28432 ·

Table 13: Temperature coefficients for some single crystal elastic constants.

Tabl3 14: Temperature coefficients for elastic moduli of some polycrystalline ceramics.

Proceedings of the British Ceramic Society, No. 15, Jan. 1970, pp. 157-172.

THE CREEP OF CERAMIC MATERIALS COMPARED TO THAT OF METALS by K. F. A. Walles

The paper presents a great deal of test data on alumina and SiC. The author suggests that a correlation between stress, time, and temperature by observing similarities between the creep of ceramics and metals.

Figure 3: Creep-rupture data for SiC.

Figure 4: Time/temperature graph for SiC.

Figure 5: Creep-rupture data for Al_2O_3 .

Figure 6: Time/temperature graph for Al_20_3 .

Figure 7: Log log strain/time graphs for Al_20_3 and SiC.

Figure 9: Log creep rate vs. temperature for $A1_20_3$.

Figure 10 & 11: Scatter of alumina creep-rupture and strength (from 3-point bend test).

AD-609-667

SLIP-CAST FUSED SILICA by J. D. Walton, et. al.

This workbook provides a collection of technical data and information on the slip-cast fused silica work of the Georgia Institute of Technology. It is intended to provide scientists and engineers with thermo-physical,

mechanical, electrical and nuclear properties of slip-cast fused silica. Fabrication techniques and engineering data related to the use of this material for thermal protection systems and radomes are presented.

Figure 1: Volume (c.c.) occupied by 1 Kg. of material, temperature $0-2400^{\circ}F$. Specific volume of different forms of silica.

Figure 2: Specific heat vs. temperature for fused silica, graphite, and copper.

Table 1: Properties of fused silica slip.

Figure 3: Particle size distribution of fused silica slip.

Figure 4: Last wall thickness vs. casting time for fused silica slip.

Figure 6: Cristobalite content of slip cast fused silica fired under one atmosphere of pressure.

Figure 10: Thermal conductivity vs. mean specimen temperature (clear fused silica).

Figure 11: Thermal diffusivity of slip cast fused silica and foamed fused silica.

Figure 13: Effect of temperature and time at temperature on thermal conductivity of slip cast silica studied by Midwest Research Institution.

Figure 14: Bulk density of slip-cast fused silica fired under one atmosphere of air.

Figure 15: Porosity of slip-cast silica under one atmosphere of air.

Figure 16: Modulus of rupture as a function of firing conditions.

Figure 17: Modulus of rupture vs. firing temperature.

Figure 18: Time to reach maximum strength in slip cast fused silica during firing at one atmosphere pressure.

Figure 19: Tensile strength 0 - 8000 vs. firing time hr. 0 - 13 at different temperature. Room temperature $- 2000^{0}$ F.

Table II: Effect of temperature on dielectric constant and loss tangent of slip-cast fused silica.

Figure 20: Compressive strength (10^3 psi) 0 - 30 vs. firing time (hr.) 1 - 100.

AD-609-667

Figure 21: Resistivity of clear fused silica and slip-cast fused silica as a function of temperature.

Figure 22: Dielectric strength of fused silica glass as a function of temperature.

Figure 23: Transverse strength (psi X 10^{-3}) 0 - 10 vs. fast dose (wt. X 10^{-20}) 2 - 7. Effect of irradiation on the modulus of rupture of slip-cast fused silica.

Table III: Cristobalite content of slip cast fused silica sample after irradiation.

Table IV: Nuclear properties of fused silica.

Figure 52: Effective emittance vs. corrected surface temperature for slip cast fused silica.

Table I, Page 95: Mechanical and thermal properties of ceramic radome materials. Thermal conductivity, transverse strength, Youngs modulus, thermal expansion, specific heat, melting temperature of Al_2O_3 , beryllium oxide, boron mitride, magnesium oxide, pyroceram 9606, slip cast fused silica, spinel, steatite, and zirconia. Figure 2, Page 96: Relative thermal shock resistance of candidate re-entry radome materials as a function of thermal shock environment.

AD-853-733

NEW AND IMPROVED CUTTING TOOL MATERIALS by E. D. Whitney & Y. Murata

This is a final report covering work done over a three year period. The entire works (approximately 800 pages) covers fabrication techniques of new cutting tool inserts from carbide, nitride, boride, and aluminabase materials, as well as the results from cutting tests using these new inserts. There are also many, many, tables of material properties. However, most of the materials studied are not pure materials but alloys, and there

AD-853-733 (cont)

is only limited information on the preliminary candidates for this research project.

Tables on Boron Carbide - page 75-87 (mechanical properties, microstructure, densification studies, phase relations, etc.)
Alumina-base tools - (alumina + carbides, nitrides, borides) page 114-128.

Also there are many graphs on rate of densification of the subject materials at different compositions, temperatures, pressures, etc.

N69-28436

FRACTURE OF CERAMICS by S. M. Wiederhorn

In this paper the fracture of ceramics is considered primarily from a fracture mechanics point of view. The maximum theoretical strength of ceramics is discussed. The ideas of a stress intensity factor and a fracture surface energy are developed. Examples are presented of the use of these parameters to describe strength, thermal shock resistance and stress corrosion of ceramic materials.

Table 1 & 2: 219 - Theoretical and measured strength of silica glass and sapphire.

Table 3: 225 - Surface energies of glass.

Table 4: 226 - Surface energies of single crystals.

Table 5: 227 - Surface energies of polycrystalline ceramics.

Figure 17, Page 232: Petch plot of MgO bending data.

Table 9, Page 238: Effect of water vapor on the strength of cerami materials (${\rm Al}_2{\rm O}_3$, MgO, fused silica and others)

Journal of the American Ceramic Society, Vol. 52, No. 9, pp. 485-491.

FRACTURE OF SAPPHIRE by S. M. Wiederhorn

This paper studies the fracture of sapphire using a double-cantilever-cleavage technique. Fracture surface energies were successfully measured in the (1010) and (1012) planes, but unsuccessfully in the (0001) plane.

Table I: Fracture surface energy of sapphire.

Table II: Strength of sapphire (various forms, i.e. whiskers and flame polished rods).

AD-672-428

MEASUREMENT OF TENSILE STRENGTH OF CERAMICS by T. R. Wilshaw

This brief article discusses an alternative method (an inexpensive one) of measuring the tensile fracture strength of very brittle materials. A schematic of the testing assembly is given and test results are compared with other researcher's data.

Table I, Page 1: Fracture stresses of polycrystalline alumina.

AD-601-638

THE EVALUATION OF HIGH TEMPERATURE MATERIALS

Part I: Evaluation of coatings for refractory alloys

Part II: Materials evaluation with an arc-plasma-jet

by John C. Wurst

This report concerns work done at the University of Dayton on the development of tests to evaluate refractory alloy coatings and also the

results of tests on various ceramic compounds. Mechanical and thermal data is reported. Also, in the appendix to this report is data on the application of the Weibull function.

Figure 4: Stress-rupture curve for 20 mil Mo-0.5 Ti sheet coated with PFR-6.

Figure 5: Stress-rupture curve for 20 mil. FS 82 sheet coated with Ti-Cr-Si.

Figure 8: Stress-rupture curves for 10 mil Mo-0.5 Ti sheet.

Figure 9: Stress-rupture curves for 50 mil Mo-0.5 Ti sheet.

Figure 10: Typical stress-strain diagram of coated Mo-0.5 Ti sheet.

Figure 11: Typical stress-strain diagrams of coated Mo-0.5 Ti sheet.

Figure 19: Typical Temperature-Time History of phenolic-zirconia exposed to a $100~\text{Btu/ft}^2$ sec environment.

Figure 20: Typical Temperature-Time History of phenolic-zirconia exposed to a 500 Btu/ft 2 sec environment.

Figure 21: Temp-Time History of phenolic-zirconia with Type A Fiber exposed to a 500 Btu/ft^2 sec environment.

Figure 22: Temp-Time History of phenolic-zirconia with Type D fiber exposed to a 500 Btu/ft^2 sec environment.

Figure 24: Temperature-Time History of epoxy- $Ti0_2$, $Zr0_2$ - $Ri0_2$ exposed to heat flux levels of 275, 500 and 1000 Btu/ft² sec.

Figure 25: Temperature-Time History of epoxy- $Ti0_2$, $Zr0_2$ - $Na0_2$ exposed to heat flux levels of 275, 500 and 1000 Btu/ft² sec.

Figure 26: Temperature-Time History of Phenolic-Ti0 $_2$, Zr0 $_2$, C exposed to heat flux levels of 275, 500, and 1000 Btu/sec 2 sec.

Figure 53: Temperature-Time History of Phenolic Resin filled zirconia and alumina exposed to a 430 Btu/ft^2 -sec heat flux environment.

Figure 54: Temperature-Time History of Phenolic Resin filled Magnesia exposed to a 430 Btu/ft^2 -sec heat flux environment.

Figure 55: Temperature-Time History of siliconized RVC graphite exposed to 500, 750 and 1000 Btu/ft 2 sec heat flux environments.

- Figure 56: Temperature-Time History of graphite composite exposed to 750 and 1000 Btu/ft^2 sec heat flux environments.
- Table 2: Static oxidation test results for coated Mo-1/2 Ti sheet.
- Table 4: Results of strain sensitivity tests of coated Mo-0.5 Ti sheet.
- Table 5: Results of low pressure oxidation tests at 2800°F of several coatings on 12 mil Mo-0.5 Ti.
- Table 6: Dynamic oxidation test results.
- Table 7: Stress-rupture test results for 20 mil Mo-0.5 Ti coated with PFR-6 (Pfaudler) and tested in air at 2500° F.
- Table 8: Stress rupture test results for 20 mil FS-82 coated with Ti-Ar-Si (TAPCO) and tested in air at 2500° F.
- Table 9: Stress-rupture test results for uncoated Mo-0.5 Ti tested in vacuo at 2600° F.
- Table 10: Stress-rupture test results for Mo-0.5 Ti coated with PFR-6 (Pfaudler).
- Table 11: Tensile fatigue test result for 50 mil. Mo-0.5 Ti sheet coated with PFR-6 (Pfaudler) and tested in air at 2600° F.
- Table 12: Mechanical properties data for coated Mo-0.5 Ti sheet.
- Table 15: Summary of ablative material tests.
- Table 55: Results of tests of several phenolic resin composites evaluated at 500 and 1000 Btu/ft 2 sec for 24 second exposures.
- Table 56: Percentage increase of erosion parameters for an increase of heat flux from 500 to 1000 Btu/ft^2 sec.
- Table 57: Relative erosion resistance of several phenolic resin composites tested at two heat flux levels.
- Table 59: Performance rank of ablative materials considering erosion and density.
- Table 60: Description of foamed ceramic systems evaluated at a heat flux level of 275 Btu/ft^2 sec.
- Table 75: Summary of manufacturer NC oxidation studies.

AD-601-638 (cont.)

Table 76: Summary of thermal shock test of various sprayed coatings.

Table 77: Summary of bond strength measurements of various plasma sprayed coatings.

Table 82: Experimental layout and analysis of variance for the stress rupture test of PFR-6 coated 10 mil Mo-0.5 Ti.

Figure 70: Weibull plot of PFR-6 static oxidation test results.

Figure 71: Weibull plot of W-2 static oxidation test results.

N67-18053

IDENTIFYING OPTIMUM PARAMETERS OF HEAT EXTRUSIONS

Several sets of canned ceramic billets were successfully extruded. Variations in the shape or placement of these billets relative to the extension axis, as well as the use of MgO in the components of the can, all indicate considerable versatility in the shape that can be extraded. Analysis of billets is consistent with previous observations and supports the hypothesis that thermal stress is more important than surface shear in causing cracks. Further success in reducing cracking was achieved by again slowing cooling and by use of smaller billets.

Initial comparison shows that starting orientation has little or no effect on extended orientation.

Successful extension of an insulating can consisting of alternate tungsten and MgO layers indicates that extrusion heating temperature may lowered to reduce grain size, and thus increase strength.

Table I, Page 14: Billet fabrication (time, temperature, etc.). Table II, Page 17: Extrusion parameters (size, temperature, area reduction ratio, speed, force).

Table III: Extruded billet data (grain size, composition, densities, area reduction, etc.).

Material Property Questionnaire Survey Results

26/

The following is an itemized listing of the questionnaire sent to ceramics users, manufacturers, and researchers as described in the introduction of this report. Regarding all replies, answers which were unclear, not applicable, or illegible, were for obvious reasons, deleted from the record or replies. In each case, the original question will be listed, as it appeared in the mailing, a set of answers will be given, and a discussion where appropriate will follow.

Q1) WHAT ADDITIONAL CERAMIC MATERIALS WOULD YOU LIKE TO HAVE CHARACTERIZED IN HANDBOOK FORM? LIST IN DECREASING ORDER OF INTEREST TO YOU.

OF INTEREST TO TOU.		
Candidates listed in replies	Mumber of	times listed
Mullite (3A1 ₃ .2Si0 ₂)		7
Beryllium Oxide (BeO)		6
Sialons .		5
Boron Nitride (BN)		4
Cordierite (2MgO.2A1 ₂ O3.5SiO ₂)		4
Zirconia (ZrO ₂)		4
Generalized Silica (SiO ₂)		8
(categories include:		
foams fused quartz synthetic silica various silica fiber/matrix co	mposites)	
Boron Carbide (B _A C)		3
Spinel		2
Pyroceram(s)		2
Titanium oxides (TiO, TiO ₂)		2 .
This group appeared with a frequency of	1:	
Aluminum Nitride (AIN) Barium Titanate (BaTiO ₃) Chromium Oxide (Cr ₂ O ₃) Hafnium Bromide (HfB) Hafnium Carbide (HfC) Hafnium Oxide (HfO ₂) Thorium Oxide (ThO ₂) Titanium Carbide (TiC) Zirconium Carbide (ZrC) Zinc Sulphide (ZnS)		

As the replies were received, it was found that many suggestions were made concerning interest in new materials, not specifically limited to ceramics. Each of these as received carries a frequency of 1, as follows:

> Various grades of Alumina (A-2,...,A-20) also beta phase Alumina Mixed Oxides of Aluminum, Magnesium and Chromium Pyrolytic Graphite and Graphite Composites Glassy Carbon Graphitized Alumina Glasses

Further replies were also received but were very sketchy in nature and hence were not included. For most candidate materials, it appears that more intensive property data is what is desired. Total response was 96 replies to 01.

WOULD YOU OR YOUR ORGANIZATION, DEPARTMENT, ETC., BE WILLING TO CONSIDER SHARING FINDINGS FOR PUBLIC RELEASE PERTAINING TO PRESENT OR FUTURE CANDIDATE MATERIALS? ACKNOWLEDGEMENTS WILL BE GIVEN FOR ALL SUCH INFORMATION.

REPLIES

Yes	86%
No	8%
No Opinio	on 6%

(Total responses to this question was 50)

PLEASE LIST BRIEFLY THE TYPES OF PROPERTIES YOU FEEL HAVE Q3) BEEN OVERLOOKED IN PAST SURVEYS WHICH ARE IMPORTANT TO YOUR WORK.

Replies in order of decreasing frequency number of times listed

11

Thermal shock characteristics (Since thermal shock characteristics can be predicted analytically on information concerning more basic properties such as Modulus, coefficient of expansion, etc., it remains unclear as to whether the bulk of replies directed to basic property clarification or to some thermal shock experimental procedure, standardization or neither)

11

4

Abrasion, erosion, impact, and wear resistance 11 (as a function of density, temperature, manufacturing technique - alumina mentioned once)

Physical/Chemical properties - miscellaneous (these include inquiries about reactivity of nitrides and carbides at elevated temperature with other ceramics, permeability to common gasses, as H, He, N, O, (precise chemical composition), latent heats, specific heat, EM wave absorption and emission spectra, particularly IR, electrical resistance and dielectric strength)

General strength data
(statistical mechanics parameters, dislocation modes, miscostructure, fracture strength, all of these vs. density, temperature, and second phase percentage)

Machining and fabrication properties (versus impurity content, fabrication method and surface finish)

Other properties (one response each)

% of vitrious phase
Coefficient of friction
Grain size distribution
Fatigue properties
Computer software codes
(suitable for various ceramics)
Metalizing of alumina
General creep parameters
Elastic/plastic transition temperature
Brittle/ductile transition temperature

Replies totaled 66 including several unused replies due to vagueness.

There is occasion for comment here on the types of replies to question three in that a certain liberty has been taken in the grouping of responses. In many replies multiple comments were made, and in a few cases, respondees indicated an interest in a property as applied only to a particular material. In these cases, the material was mentioned, otherwise it is assumed that the property is a general interest one.

Q4) DO YOU FEEL THAT AN UPDATING SERVICE FOR CERAMIC CANDIDATES SHOULD BE MAINTAINED ON A PERMANENT BASIS?

	THE TO VELLE
REPRODUC	BILITY OF THE
ORIGINAL	PAGE IS POOR

туре от Керју	Frequency of	Reply
Yes	36	
No	2	
No Reply (at least some of questions answer	6 cher red)	
Other	. 6	

The other category includes comments which indicate that an updating service which is intermittent or periodic in nature would be more suitable than either no such service or a permanent data collection facility. In several cases a comment followed the formal reply; in these cases, it was suggested that an organization or researcher would need to "prove" himself before attempting to obtain such funding as necessary to provide this service. Even when several institutions providing a partial service of this nature exist, e.g., The Metals and Ceramics Information Center, Battelle-Columbus Laboratories, Pennsylvania State University, and NBS, it was felt that no such service or organization significantly qualified as a candidate for Question Four.

Q5) DO YOU FEEL SUCH A SERVICE SHOULD ALSO ACT IN AN ADVISORY CAPACITY ON THE USE OF CANDIDATES, MODELS, AND STRUCTURAL ANALYSIS TECHNIQUES FOR DESIGNERS AND INDUSTRY? SUCH A SERVICE WOULD PROVIDE CURRENT INFORMATION ON RESEARCHERS, MATERIALS, AND METHODS.

Type of Reply	Frequency of Reply
Yes	25 (50%)
No .	6 (12%)
Other	19 (38%)

The other category included information content which included the following response types and frequencies: No reply, 7; Don't know, 2; Possible (no other qualification), 4; No opinion, 1; General verbal, 5. The general verbal category contained the following responses:

"This I suspect would be too expensive."

"Would this function compete with the Metals and Ceramics Information Center, Battelle's Columbus Center?"

"A monumental task but certainly the most significant contribution any such service could offer."

"...doubtful that acting in an advisory capacity would be practicable, considering need for specialized expertise."

"The people who do the research could do this better."

Q6) IF FUTURE CORRESPONDENCE SHOULD BE CONDUCTED TO ANOTHER RECIPIENT, PLEASE LIST THE NAME AND ADDRESS AND TRANSFER THIS CORRESPONDENCE. THANK YOU.

NAME TITLE ADDRESS

The response to this question was used to modify the original list of recipients of this questionnaire. In the industrial sector, many recipients were eliminated through redirected dead letters where the organizations had to be assumed defunct. Original industry lists were devised from information in the Thomas Register Publications; University listings are more numerous and several were consulted to site those having Ceramics and Ceramics Engineering Studies. Foreign Universities are also given, but a decision was made not to try to include them in the mailing lists. A total of thirty-eight corrections were received and were incorporated into the original list. What follows is a general "ceramics interest" list which represents an undated source of ceramics industry and research information users. A total of 390 entries follow:

SURVEY MAILING LIST

Ceramics Manager Adolf Meller Co. P.O. Box 6001 Providence, RI 02904

Ceramics Manager Airco Speer Carton Products 800 Theresia St. St. Marys, PA 15857

Ceramics Manager Alberox Corp. Industrial Park New Bedford, MA 02745

Ceramics Manager America Lava Corp. Manufacturers Rd. Chattanooga, TN 37405

Ceramics Manager American Optical Corp. Mechanic St. Southbridge, MA 01550

Ceramics Manager American Saint Gobain Corp. Box 929 Kingsport, TN 37660

Ceramics Manager America Viscose 1617 J.F. Kennedy Blvd. Philadelphia PA 19103

Ceramics Manager Aremco Products, Inc. Dept. TS · P.O. Box 145 Briarcliff Manor, NY 10510

Ceramics Manager Amersil Inc. 685 Ramsey Ave. Hillside, NJ 07205 Ceramics Manager Argus Engineering Company P.O. Box 246-T Hopewell, NJ 08525

Ceramics Manager Associated Ceramics and Technology Inc. 4000 N. Pike Rd. Sarver, PA 16055

Ceramics Manager Astro Met Associates 95 Barron Dr. Cincinnati, OH 45215

Ceramics Manager Athboro Precision Engineering Corp. Hall Rd. Sturbridge, MA 01566

Ceramics Manager Atlantic Equipment Engineers 181 Reid Ave. Bergenfield, NJ 07621

Ceramics Manager Atomergic Chemicals Co. 584 Mineola Ave. Carle Place, NY 11514

Ceramics Manager Avco Corp. Lowell Industrial Park Lowell, MA 01851

Ceramics Manager Babcock and Wilcox Co. Old Savannah Rd. Augusta, GA 30903

Ceramics Panager Basic Ceramics Inc. 221 Seventh Ave. Hawthorne, NJ 07507 Ceramics Manager Basic Inc. Hanna Bldg. Cleveland, OH 44115

Ceramics Manager Bausch and Lomb Inc. 98469 Bausch St. Rochester, NY 14602

Ceramics Manager Berylares Co. 10000 Alkire St. Arvaca, CO 80002

Ceramics Manager Beckwith Carton Corp. 16140 Raymer St. Van Nuys, CA 91406

Ceramics Manage Bjorksten Research Labs, Inc. P.O. Box 265 Madison, WI 53701

Ceramics Manager Carborundum Co. P.O. Box 337 Niagara Falls, NY 14302

Ceramics Manager Carmet CC. 8322 Standustrial St. Stanton, CA 80680

Ceramics Manager Cerac Inc. P.O. Box 597 Butler, WI 53007

Ceramics Manager Centralae Inc. 5757 N. Green Bay Ave. Milwarkee, WI 53201

Ceramics Manager Ceram Corp. 5345-G Timken Sq. La Mesa, CA 92041 Ceramics Manager Ceramic Fabricators, Inc. 14-18 Sindle Ave. Little Falls, NJ 07424

Ceramics Manager Ceramics International Div. of Fansteel Inc. 39 Siding Pl. Mahwah, NJ 07430

Ceramics Manager Ceramco Inc. Chemists 171 Ridge St. Newark, NJ 07104

Ceramics Manager Ceramic Coatings Inc. 1719 Roy St. Houston, TX 77007

Ceramics Manager Ceramic Finishing Co. P.O. Box 498 State College, PA 16801

Ceramics Manager Ceramic Magnetics Inc. 87-T Fairfield Rd. Fairfield, NJ 07006

Ceramics Manager Chas. Pfizer 235 E. 42nd St. New York, NY 10017

Ceramics Manager Champion Spark Plug Co. Ceramic Div. 20000 Conner Ave. Detroit, MI 48234

Ceramics Manager Chemtree Corp. Chemtree Park Central Valley, NY 10917

Ceramics Manager Cleveland Hard Facing Inc. 3049 Stilson Ave. Cleveland, OH 44105 Ceramics Manager O M Mfg. and Machine Co., Inc. 101 Dewey St. Bloomfield, NJ 07003

Ceramics Manager Coatings for Industry Inc. P.O.Box 4316-T Philadelphia, PA 19118

Ceramics Manager Commonwealth Scientific Corp. 500 Pendleton St. Alexandria, VA 22314

Ceramics Manager
Consolidated Ceramics and
Metalizing Corp.
Molasses Hill Rd. Rt. 1
Lebanon, NJ 08833

Ceramics Manager
Consolidated Ceramics and Metalizing
Corp.
P.O. Box 352
Flemington. NJ 08822

Ceramics Manager Coors Porcelain Co. 600 Ninth St. Golden, CO 80401

Ceramics Manager Corning Glass Works Corning, NY 14830

Ceramics Manager Davison Chemical 4000 N. Hawthorne St. Chattanooga, TN 37406

Ceramics Manager Degussa Inc. 2 Penn Plaza New York, NY 10001

Ceramics Manager Diamonite Products Mfg. | Shreve OH 44676 Ceramics Manager D.M. Steward Mfg. Co. Box 510 Chattanooga, TN 37401

Ceramics Manager Dow Corning Corp. So. Saginaw Rd. Midland, MI 48640

Ceramics Manager DL-CC Ceramics Co. Saxonburg, PA 16056

Ceramics Manager Ducommon Inc. 11120 S. Norwalk Blvd. Santa Fe Springs, CA 90670

Ceramics Manager Douglas Corporation P.O. Box K-T Iekonsha, MI 49092

Ceramics Manager Duramic Products Inc. 426 Commercial Ave. Palisades Park, NJ 07650

Ceramics Manager Electrical Pefractories Co. East Clark St. East Palestine, OH 44413

Ceramics Manager Electrical Specialty Co. 213 E. Harris Ave. S. San Francisco, CA 94080

Ceramics Manager Electro-Ceramics Inc. 2645 S. 2nd St. M. Salt Lake City, UT 84404

Ceramics Manager Electro Ceramic Industries 77 Kennedy St. Hackensack, NJ 07601 Ceramics Manager Electronic Space Products Inc. 854 S. Robertson Blvd. Los Angeles, CA 90035

Ceramics Manager Electro Materials Corp. of America 605 Center Ave. Mamaroneck, NY 10543

Ceramics Manager
Electro Refractories and Abrasives
Division of Ferro Corporation
213 Vars Bldg.
Buffalo, NY 14202

Ceramics Manager Electro-Thermo Ceramics Inc. Rt. 1, Box 198 Enumolaw, WA 98022

Ceramics Manager Engelhard Min. and Chem. Corp. Essex Tpke. Menlo Park Edison, NJ 08817

Ceramics Manager Engineered Ceramics P O. Box 1 Gilberts, IL 60136

Ceramics Manager Ferro Corp. 344 Delaware Ave. Buffalo, NY 14202

-Ceramics Manager Ferronics Incorporated 70 N. Main St. Fairport, NY 14450

Ceramics Manager Ownens-Corning Fiberglas Corp. P.O. Box 901 Toledo, OH #3601

Ceramics Manager Owens-Illi ois Inc. P.O. Box 1035 Toledo, OH 43601 Ceramics Manager Page Madden Co. 193 Belleville Ave. Belleville, NJ 07109

Ceramics Manager Pars Mfg. Co. 101 S. Main St. Ambler, PA 19002

Ceramics Manager Pekay Industries Inc. 76-T Woolsev St. Irvinoton, NJ 07111

Ceramics Manager Pfaudler Co. P.O. Box 1600 Rochester, NY 14603

Ceramics Manager Plessey Ceramic Div. 8th and Harrison Sts. Frenchtown, NJ 08825

Ceramics Manager Polysciences Inc. Paul Valley Industrial Park Warrington, PA 18976

Ceramics Manager PPG Industries Inc. One Gateway Center Pittsburgh, PA 15222

Ceramics Manager Pure Carbon Co. Hall Ave. St. Marys, PA 15857

Ceramics Manager GCI Corporation P.O. Box 606-T Farmingdale, NJ 07727

Ceramics Manager General Electric Co. TCEE Dept. Schenectady, NY 12305 Ceramics Manager Glass Beads Co. Glass Beads Bldg. Latrobe, PA 15650

Ceramics Manager Great Lakes Carbon Corp. 229 Park Ave. New York, NY 10017

Ceramics Manager Griffith Polymers Inc. 2311 N.W. 21st Pl. Portland, OR 97210

Ceramics Manager Hawley Products Co. 333 N. 6th St. St. Charles, IL 60174

Ceramics Manager Hayden Mica Co. P.O. Box C Wilmington, MA 01887

Ceramics Manager Heany Ind. Inc. P.O. Box 38 Scottsville, NY 14546

Ceramics Manager Hitco 1600 W. 135th St. Gardena, CA 90249

Ceramics Manager Honeywell Inc. Ceramics Dept 1885 Douglas Dr. Minneapolis, MN 55422

Ceramics Manager Howell Manufacturing Inc. 263-C Myrtle Ave. Boonton, NJ 07005

Ceramics Manager Industrial Mica 223 S. Van Brunt St. Englewood, NJ 07631 Ceramics Manager
Insacc Incorporated
Box 422-T
Quakertown, PA 18951

Ceramics Manager Isolantite Mfg. Corp. 335-341 Warren Ave. Stirling, NJ 07980

Ceramics Manager
Insen Ceramics an Alco Standard
Corporate Partner
330 John St.
Pecatonica, IL 61063

Ceramics Manager Ipsen Industries 17 100 Ipsen Rd. Cherry Valley, IL 61016

Ceramics Manager U.S. Stoneware Inc. P.O. Box 350 Akron, OH 44309

Ceramics Manager Kaiser Refractories 1083 Kaiser Center Oakland, CA 94612

Ceramics Manager Kaufman Glass Co. P.O. Box 1729 Wilmington, DE 19899

Ceramics Manager Kawecki Berylco Industries Inc. 220 E. 42nd St. New York, NY 19017

Ceramics Manager Kopp Glass Inc. P.O. Box 8255 Pittsburgh, PA 15218

Ceramics Manager Krera Corp. of America 116 E. Alondra Blvd. Gardena, CA 90148 Ceramics Manager Lava Crucible-Ref. Co. 1045 Oliver Bldg. Pittsburgh, PA 15222

Ceramics Manager Leoo Corporation 3000 Lakeview Ave. St. Joseph, MI 49085

Ceramics Manager Libbey-Owens-Ford Co. 811 Madison Ave. Toledo, OH 43624

Ceramics Manager Liberty Mirror 851 Third Ave. Brackenridge, PA 15014

Ceramics Manager Magnetic Specialties Inc 1834 S.E. 50th Ave. Portland, OR 97222

Ceramics Manager Magno Ceram Co. 2612 S. Clinton Ave. South Plainfield, NJ 07080

Ceramics Manager Mansol Ceramics Co. 140 Little St. Belleville, NJ 07109

Ceramics Manager Marguardt Corp. 16555 Satiooy St. Van Nuys, CA 91406

Ceramics Manager Martin Marietta Corp. Orlando Division P.O. Box 5837 Orlando, FL 32805

Ceramics Manager Materials for Electronics Corp. 149-32 132nd St. Jamaica, NY 11420 Ceramics Manager Maryland Ceramic and Steatite Co. Mill Green Rd. Bel Air, MD 21014

Ceramics Manager Maryland Lava Company Darlington and Dening Rds. Bel Air, MD 21014

Ceramics Manager Materials for Industry Inc. P.O. Box 204 Ambler, PA 19002

Ceramics Manager McDaniel Refractory Porcelain Co 510 9th Ave. Beaver Falls, PA 15010

Ceramics Manager Metallized Carbon Co. 19 S. Water St. Ossining, NY 10562

Ceramics Manager
Materials Research Corp.
Route 303
Orangeburg, NY 10962

Ceramics Manager M and T Chemicals Inc. Subsidiary of American Can Co. Rahway, NJ 07065

Ceramics Manager M and T Mfg. Co. P.O. Rox 9099 Grand Rapids, MI 48509

Ceramics Manager Metal Construction Services Corp. P.O. Box 309 Kensington, MD 20795

Ceramics Manager Met-Bay Inc. P.O. Box 610 Bay City, MI 48706 Ceramics Manager Mica Fabricating Co. 53 Central Ave. Rochelle Park, NJ 07662

Ceramics Manager Micacraft Prod. Inc. 49 Liberty St. Newark, NJ 07102

Ceramics Manager Mitronics Products P.O. Box 196-T Gillette, NJ 07933

Ceramics Manager 3M Co. 3M Center St. Paul, MN 55101

Ceramics Manager Monsanto 800 North Lindbergh Blvd. St. Louis, MO 63166

Ceramics Manager Mycalex Corp. of America 125 Clifton Blvd. Clifton, NJ 07015

Ceramics Manager NARMCO 600 Victoria St. Costa Mesa, CA 92627

Ceramics Manager National Beryllia Corp. Greenwood Ave. Haskell, NJ 07420

Ceramics Manager National Lead Co. 111 Boardway New York, NY 10006

Ceramics Manager New Jersey Porcelain Co. Inc. 100 Plum St. Trenton, NJ 08638 Ceramics Manager Niemand Bros. Inc. 45-10 94th St. Elmhurst, NY 11373

Ceramics Manager Norton Co. 1 New Bond St. Worcester, MA 01606

Ceramics Manager Nuclear Materials Equipment Corp. 609 Marren Ave. Apollo, PA 15613

Ceramics Manager Chic Carbon Co. 12508 Berea Pd. Cleveland, OH 44111

Ceramics Manager Fiberglas Canada Ltd. 48 St. Clair Ave. W. Toronto, ONT

Ceramics Manager Fiber Glass Industries Inc. Homestead Pl. Amsterdam, NY 12010

Ceramics Manager
Fiber Materials Inc.
Broadway and Main St.
Graniteville, MA 01829

Ceramics Manager
Filtros Plant Electro Pefractories
and Abrasives Div. of Ferro Corp.
9 McDonald Park
East Pochester, NV 14445

Ceramics Manager Fluid Process Systems Owens-Illinois In P.O. Box 187 Vineland, NJ 08360

Ceramics Hanager Frenchtown/CFI Inc. 8th and Harrison Sts. Frenchtown, NJ 08825 Ceramics Manager Franklin Mineral Products Co. P.O. Box O Wilmington, MA 01887

Ceramics Manager General Electric Co. Insulating Materials Dept. 1 Campbell Rd. Schenectady, NY 12306

Ceramics Manager P.O. Box 237 Detroit, MI 48232

Ceramics Manager Glassrock Products Inc. Findlay Refractories Div. P.O. Box 93407-T Martech Station Atlanta, GA 30318

Ceramics Manager General Electric Co. 24400 Highland Rd. Richmond Heights, OH 44147

Ceramics Manager Raytheon Co. 28 Seyon St. Waltham, MA 02154

Ceramics Manager REA Magnet Wire Co. Inc. Dept. KT66 Fort Wayne, IN 46801

Ceramics Manager R and W Products Inc. 515-77 Price Ave Redwood City, CA 94063

Ceramics Manager St. Marys Carbon Co. State St. St. Marys, PA 15857

Ceramics Manager Serme Tel Div. Teleflex Inc. P.O. Box 187 N Wales, PA 19454 Ceramics Manager Shenango Pefractories Div. of Interpace Corp. Glass and Grant Sts. New Castle, PA 16101

Ceramics Manager Space Age Materials 235 E. A2nd St. New York, NY 10017

Ceramics Manager Semimetals Inc. 172 Spruce St. Westbury, NY 11591

Ceramics Manager Sintercast 169 West Highway West Nyack, NY 10994

Ceramics Manager Southern Porcelain Inc. 506 Clay St. Marietta, GA 30060

Ceramics Manager Specialty Glass Products Inc. 143 Terwood Rd. Willow Grove, PA 19090

Ceramics Manager Star Porcelain Co. 23 Muirhead Ave. Trenton. NJ 08638

Ceramics Manager Stackpole Carbon Co. Stackpole St. St. Marys, PA 15857

Ceramics Manager Superior Graphite Co. 20 N. Wacker Dr. Chicago, IL 60606

Ceramics Manager Superich Steatite and Ceramics Corp. 83-91 W. Forest Ave. Englewood, NJ 07631 Ceramics Manager Technical Ceramics and Lava Corr P.O. Box 676-T Ray Place Fairfield, NJ 07006

Ceramics Manager Thermal Amer. Fused Quartz Co. Rt. 202 and Change Bridge Rd. Montville, NJ 07045

Ceramics Manager Thermal Corporation Indian Creek and Blake Bottom Rd P.O. Box 5327 Huntsville, AL 35804

Ceramics Manager
Thermetrics A Division of Exotic
Materials Inc.
2968 Randolph Ave.
Costa Mesa, CA 92626

Ceramics Manager
Ultraform Pyrocircuits Div.
Microtron Inc.
Toms Point Rd.
Port Washington, NY 11050

Ceramics Manager Tyco Lab. Inc. Bear Hill Waltham, MA 02154

Ceramics Manager Ultra Carbon Corp. P.O. Box 747 Bay City, MI 48706

Ceramics Manager Unicast Development Corp. 345 Tompkin Ave. Pleasantville, NY 10570

Ceramics Manager Union Carbide Corp. 1020 W. Park Ave. Kokomo, IN 46901

Ceramics Manager Union Carbide Corp. 270 Park Ave. New York, NY 10017 Ceramics Manager United Products Company 55 S. Denton Ave. New Hyde Park, NY 11040

Ceramics Manager United States Graphite 1621 Holland Ave. Saginaw, MI 48607

Ceramics Manager Wisconsin Porcelain Co. Main and Lincoln Sts: Sun Prairie, WI 53590

Ceramics manager Zirconium Corp. of America P.O. Box 39217 Solon, OH 44139

Ceramics Manager Zircoa Div. of Corhart Refractories Co. P.O. Box 39217 Solon, OH 44139

Mr. Samuel J. Acouaviva Army Materials and Mechanics Research Center Watertown, MA 02172

Mr. Jon J. Aho Bausch and Lomb 635 St. Paul St. Rochester, NY 14602

Mr. Guy H. Allgever -Owens-Illinois 1700 North Westwood Toledo, OH 43607

Mr. Jan Appelo D.M. Stewart Manufacturing Co. P.O. Box 510 Chattanooga, TN 37701

Mr. F. Gray Augeri MIT/Draper Lab 275 Massachusetts Ave. Cambridge, MA 02139 Mr. Frank P. Bailey Chemical Research Laboratories C.S.I.P.C. P.O. Box 4331 Melbourne, Victoria, Australia

Mr. Jimmy D. Bailey American Lava Corporation Laurens, SC 29360

Mr. Spencer P. Baker Norton Company New Bond St. Worcester, MA 01606

Can-Tex Industries Division of Harsco Corporation P.O. Box 254 Weatherford, TX 76086

Mr. Y. Baskin Ferro Corporation Technical Center 4150 East 56th St. Cleveland, OH 44105

Mr. C. H. Bates Bell Aerospace Company P.O. Box 1 Buffalo, NY 14240

Mr. F. F. Becher Naval Research Laboratory Code 6136 Mr. Richard Behrens Washington, DC 20390

Dr. J. L. Bentecost School of Ceramic Engineering Georgia Institute of Technolog Atlanta, GA 30332

Mr. L. Berrin Bell Telephone Laboratories 555 Union Boulevard Allentown, PA 18103

Mr. C. Bersch Naval Air Systems Command Jefferson Plaza Room 1000 Arlington, VA 22901 Mr. R. E. Bickelhaupt Southern Research Institute 2000 Ninth Avenue South Birmingham, AL 35205

Mr. Joe Blaze McDaniel Refractorv Porcelain Co. 510 Ninth Ave. P.O. Box 560 Beaver Falls, PA 15010

Mr. Sherman D. Brown University of Illinois Dept. of Ceramic Engineering Oreana, IL 61801

Mr. James P. Brazel GE/RESD PMU7032 VF/STC Pox 7722 Philadelphia, PA 19101

Mr. W. R. Brown Corning Glass Works Fluidic Products Department Corning, NY 14830

Mr. O. J. Cameron Atomic Energy of Canada Ltd. Whiteshell Nuclear Research Pinawa, Manitoba, Canada

Mr. William B. Campbell The Ohio State University 2041 North College Road Columbus, OH 43210

Mr. John J. Capellman PPG Industries Creighton, PA 15030

Mr. David W. Chalkley Trans Tech Inc. 12 Meem Avenue Gaithersburg, MD 20760

Mr. Donald G. Cooper Avco Bay State Abrasives Division Union St. Westboro, MA ∩1581 Mr. L. V. Colwell University of Michigan 2046 East Engineering Bldg. Ann Arbor, MI 48104

Mr. Wade Cooper McDaniel Refractory Porcelain Co. 510 Ninth Ave. P.O. Box 560 Beaver Falls, PA 15010

Mr. Kristofer T. Dahl 2nd Lt. USAF SMANA (MAGGLC) McClellan Air Force Base CA 95650

Mr. Gleason Danford ASD/ENADE AREA B Bldg. 125 Wright-Patterson AFB, OH 45433

Mr. A. C. Daniels Air Force Machineability Data Center 3980 Rosslyn Dr. Cincinnati, OH 45209

Mr. William H. Daniels Westinghouse Research Lab Beulah Road Pittsburgh, PA 15235

Mr. N. S. Demster Embassy of Australia 1601 Massachusetts Ave. N.W. Washington, DC 20036

Mr. James A. Dickinson PITCO 1600 West 135th St. Gardena, CA 90249

Mr. Frank V. Dimarcello Bell Laboratories Inc. Mountain Ave. Murray Hill NJ 07974

Mr. A. M. Diness Office of Naval Research Martin Marrietta Aerospace P.O. Box 5837 Orlando, FL 32805 Mr. Sam Divita U.S. Army Electronics Command AMSEL-KL-EC Port Monmouth, NJ · 07703

Mr. Louis P. Domingues Trans-Tech Inc. 12 Meem Avenue Gaithersburg, MD 20760

Mr. David J. Donovan Data Magnetics 355 Maple Avenue Torrance, CA 90503

Mr. S. Doroff Office of Naval Pesearch Washington, DC 20207

Mr, James W. Douglass Perkin Elmer Norwalk, CT 06553

Mr. Bruce W. Dunnington The Glennel Corporation 908 Chickadee Lane West Chester, PA 19380

Mr. Richard A. Edsall Tran-Tech. Inc. 12 Meem Avenue Gaithersburg, ND 20760

Mr. Shane A. Ellis Ferroxcuee Corporation Saugerties, NY 12477

Mr. J. K. Emery Accumet Engineering Corp. 25 Braod St. Hudson, MA 01749

Mr. Fred Ernsberger PPG Industries Box 11472 Pittsburgh, PA 15238

Mr. James W. Evans Corning Glass Works Process Pesearch-Sullivan Park Corning, NY 14830 Dr. J. C. Everhart Dept. of Ceramic Engineering The Ohio State University Columbus, OH 43210

Mr. George F. Everitt 3M Co. 3M Center St. Paul, MN 55101

Mr. George Eyerly D.N. Stewart Manufacturing Co. P.O. Box 510 Chattanooga, TN 37401

Mr. Iain Finnie University of California Berkeley, CA 94720

Mr. Ross Firestone Case Western Reserve University White Building University Circle Cleveland, OH 44118

Mr. P. L. Fleischner National Beryllia Haskell, NJ 07420

Mr. Kenneth Foulke Naval Air Development Center Warminster, PA 13974

Mr. R. K. Frazer Applied Physics Lab John Hopkins University Scaggsville, MD 20910

Dr. W. G. D. Frederick
AF Materials Laboratory
Attn: AFML/LPH
Wright Patterson AFB, OH 4543:

Mr. Nicholas Friedman Duramic Products Inc. 426 Commercial Avenue Palisades Park, NJ 07650

Mr. Frank S. Gardner Office of Naval Research 495 Summer Street Boston, MA 02210 Dr. A. L. Friedberg Dept. of Ceramic Engineering University of Illinois Urbana, IL 61801

Mr. Peter J. Geilisse University of Rhode Island Kingston, RI 02881

Mr. Bernard A. Greene Griffin Pipe Products Co. Milledgeville, GA 31061

Mr. J. A. Graves Martin Marietta Aerospace P.O. Box 5837 M.P. 150 Orlando, FL 32805

Mr. Victor A. Greene Automated Business Systems 550 Central Ave. Orange, NJ 07051

Mr. Irwin G. Greenfield Mechanical and Aerospace Engr. Dept. Newark, DE 19711

Mr. William Greenfield Corning Glass Works Fluidic Products Department Corning, NY 14830

Mr. A. J. Gitter Engineered Naterials Division Hi-Purity Materials Inc. Box 363 Church St. Station New York, NY 10008

Mr. Willaim F. Gilbert, Jr. Bell Telephone Laboratories Inc 555 Union Boulevard Allentown, PA 18103

Mr. William R. Griffin Raytheon Company 130 Second Ave. Waltham, MA 02154

Mr. Nelson Grimm General Electric Company 24400 Highland Rd. Richmond Heights, OH 44143 Mr. William E. Gurwell Easton Yale and Towne Inc. 26201 Northwestern Highway Southfield, MI 48075

Dr. W. C. Hackler Dept. of Metals and Cer. Eng. Virginia Polytechnic Institute Blacksburg, VA 24061

Mr. Robert S. Hahn Heald Division-Cincinnati Milacron New Bond Street Worcester, MA 01606

Mr. David M. Haines INSACC Inc. P.O. Box 422 Quakertown, PA 18951

Mr. Joe N. Harris Georgia Institute of Technology High Temperature Materials Div. Atlanta, GA 30332

Mr. Pat Hart Battelle Northwest P.O. Box 999 Richmond, WA 99352

Mr. D. P. H. Hasselman Lehigh University Bethlehem, PA 18015

Mr. M. Henika Carbon Products Div./Union Carbide 270 Park Ave. New York, NY 10017

Mr. Howard Herzig NASA Goduard Space Flight Center Codes 284.1 Greenbelt, MD 20771

Mr. A. H. Heler Case Western Reserve University Cleveland, OH 44106 Mr. Terrence P. Hobin British Embassy 3100 Massachusetts Ave. Washington, DC 20008

Mr. B. J. Hookev National Bureau of Standards Room A359 Ruilding 223 Washington, DC 20234

Mr. M. W. Hoelscher RCA Incorporated New Holland Pike Lancaster, PA 17604

Mr. E. Horowitz Institute of Materials Research National Bureau of Standards Washington, DC 20234

Mr. J. W. Hunt Dunlate Canada Limited Ceramics Division First Avenue Cshawa, Ontario, Canada

Mr. Robert O. Howe Raytheon CC. Missile System Div. Mail STCF H-78 Burlington, MA

Mr. Robert H. Insley Champion Spark Plug Company 20000 Conner Avenue . Detroit, MI 48234

Mr. Virgil Irick, Jr. American Lava Corporation Cherokee Boulevard Chattanooga, TN 37405

Mr. Lonnie F. Ivey American Standard P.O. Box A Paintsville, KY 41240

Mr. R. Jackel Office of Naval Research Shington, DC 20207 Mr. Paul J. Jorgensen Stanford Research Institute 333 Ravenswood Ave. Menlo Park, CA 94025

Mr. Paul G. Juenemann Trans-Tech Inc. 12 Meem Ave. Gaithersburg, MD 20760

Mr. Edward Keng Georgia Tech. E.E.S. Atlanta, GA 30332

Mr. Erwin E. Kipfer Pfaudler Company 1000 West Avenue Rochester, NY 14603

Dr. W. D. Kingery Dept. of Met. and Mat. Sci. Mass. Institute of Technology Cambridge, MA 02139

Mr. Henry P. Kirchner Ceramic Finishing Company Post Office Box 498 State College, PA 16801

Dr. W. J. Knapp Dept. of Engineering University of Cal. at Los Angeles Los Angeles, CA 90024

Mr. B. G. Loefke Honeywell Corporate Research 500 Washington Ave. S. Hopkin, MN 55343

Mr. J. Koorneef Philips Research Labs Bindhoven, Netherlands

Mr. Paul L. Kuzmick, Jr. Paul L. Kuzmick Company 271 Grove Avenue Verona, NJ 07044

Mr. William Kovacs Atomic Energy of Canada Ltd. Whiteshell Nuclear Research Pinawa, Manitoba, Canada Mr. Don A. Kubose Naval Ordnance Laboratory White Oak, MD

Mr. E. A. Kuhlman McDonnell Douglas Astronautics Cc Box 516 St. Louis, MO 63166

Mr. Richard Lane Hamco 1000 Millstead Way Rochester, NY 14624

Mr. Fred F. Lange Westinghouse R and O Churchill Boro Pittsburgh, PA 15235

Mr. D. W. Lee Arther D. Little, INC. Acorn Park Cambridge, MA 02140

Mr. Henry C. Leistner National Bureau of Standards 325 South Broadway Boulder, CO 80302

Mr. James D. Lester U.S. Army Frankford Arsenal Philadelphia, PA 19137

Mr. Kenneth N. Letson Commanding General U.S. Army Missle Command AMSMI-RLP Attn. K. N. Letson Redstone Arsenal, AL 35809

Mr. F. W. Levv Physics Department Brookhaven National Laboratory Upton, NY 11973

Mr. Jack Liker Basic Ceramics Inc. 211 7th Avenue Hawthorne, NJ 07507 Dr. Ruey Y. Lin The Carborundum Company Buffalo Avenue Niagara Falls, NY 14302

Mr. Alan Little Duplate Canada, Ltd. 50 St. Clair Avenue West Totonto, Ontario, Canada

Mr. W. C. Lo Bell Telephone Laboratories Inc 555 Union Boulevard Allentown, PA 18103

Mr. William D. Long Kaman Sciences 1700 Garden of the Gods Road Colorado Springs, CO 80907

Mr. Evan C. Luce Norton Company 1 New Bond Street Worcester, MA 01606

Dr. C. R. Manning
Dept. of Materials Engineering
North Carolina State University
Raleigh, NC 27807

Mr. B. A. MacDonald Office of Naval Research Washington, DC. 20207

Mr. I. Machlin Office of Naval Research Washington, DC 20207

Mr. Donald J. MacIntyre Basic Ceramics Inc. Box 2090 Hendersonville, NC 28739

Mr. Frank Magnanelli Trans-Tech Inc. 12 Meem Avenue Gaithersburg, MD 20760

Mr. Alan Maietta Paul L. Kuzmick Co. 271 Grove Avenue Verona, NJ 07044 Mr. Joseph Martis Metallurgy Product Department General Electric Co. 11177 E. Eight Mile Rd. Detroit, MI 48232

Mr. John Matsko Division 5332 Sandia Laboratories Alburquerque, NM 87115

Mr. George Maver U.S. Army Research Office Box CM Duke Station Durham, NC 27706

Mr. Howard L. McCollister Owens-Illinois Inc. 1700 North Westwood Toledo, OH 43607

Mr. J. F. McMahon 13 Sayles Street Alfred, NY 14802

Mr. William McDonough Naval Research Laboratory Washington, DC 20390

Mr. Karl R. McKinney Naval Research Laboratory Washington, DC 20390

Mr. H. A. McKinstry Pennsylvania State Univers 161 Engineering Science Bl University Park, PA 16802

Mr. M. G. McLaren Dept. of Ceramics Rutgers State University New Brunswick, NJ 08902

Mr. Keith E. Meade Sandia Laboratories DW. 5844 Box 5800 Alburquerque, Nº

Mr. George L. Metzger James H. Rhodes and Co. 1026 West Jackson Boulevar Chicago, IL 60607 Mr. H. C. Miller Super-Cut Inc. 3418 North Knox Chicago, IL 60641

Dr. John J. Miller Sherwood Refractories 16601 Euclid Ave. Cleveland, OH 44121

Mr. Herbert R. Moeller Union Carbide Corporation P.O. Box 985 Union, NJ 07083

Mr. J. A. Mueller The Carborundum Company P.O. Box 403 Niagara Falls, NY 14302

Dr. J. L. Mueller
Ceramic Engineering Division
Dept. of Mining Metallurgical and
Ceramics Engineering
University of Washington
Seattle, WA 98105

Mr. M. K. Murthy
Ontario Research Foundation
Sheridan Park
Ontario, Canada

Mr. Donald R. Ness Western Gold and Platinum Co 555 Harbor Boulevard Belmont, CA 94002

Mr. M. J. Noone General Electric Company Space Sciences Laboratory Room M-9126 P.O. Box 8555 Philadelphia, PA 19101

Mr. Dean E. Norris Motorola Inc. 8201 E. McDowell Rd. Scottscale, AZ 85257 Mr. Theodore Nussbaum Burroughs Bos 472 Piscataway, NJ 09854

Mr. Martin J. Chara Rattelle Memorial Institute 505 King Avenue Columbus, OH 43201

Mr. William J. Otto Ferroxcuee Corporation Mr. Ray Van Pamel Arnold Engineering P.O. Box G Marengo, IL 60152

Mr. Hayne Palmour, III N.C. State University Dept. of Engineering Research Raleigh, NC 27607

Mr. W. H. Parker Kaiser Refractories Post Office Box 879 Pleasanton, CA 94566

Mr. Edwin A. Pascoe General Electric Company 6325 Huntley Worthington, OH 43085

Mr. Damon S. Paulley Coors Porcelain Company 600 9th Street Golden, CO 80401

Mr. Robert A. Penty Fiber Materials Inc. Biddeford, ME 04005

Mr. D. J. Perolyn N.V. Philips Bindhoven, Netherlands

Mr. H. A. Perry Naval Ordnance Laboratory Code 2301 Silver Spring, MD 20910 Mr. Raymond Fietras Howmet Corporation Roy Street Dover, New Jersey 07801

Mr. J. T. A. Pollock TYCC Laboratories, Inc. 16 Hickory Drive Waltham, MA 02154

Mr. Kenneth Prince Norton Company 1 New Bond Street Worcester, MA 01606

Mr. W. G. Rauch Office of Naval Research Washington, DC 20207

Mr. Robert F. Rea Champion Spark Plug Company 20000 Conner Avenue Detroit, MI 48234

Mr. John P. Reed Lamp Glass Dept. General Electric Co. 24400 Highland Road Cleveland, OH 44143

Mr. William H. Rhodes AVCO Corporation Lowell Industrial Park Lowell, MA 01851

Mr. R. Rice
 Naval Research Laboratory
 Code 6136
 Washington, DC 20390

Dr. S. E. Rinocne Material Sciences Department Ceramic Science Section The Pennsylvania State University University Park, PA 16802

Dr. G. C. Robinson Dept. of Ceramics Engineering Clemson University Clemson, SC 29631 Mr. Kenneth S. Rolley Hamco Division Dayex Corp. 1000 Millstead Way Rochester, NY 14624

Mr. George W. Roust Lawrence Radiation Laboratory P. O. Box 808 Livermore, CA 94551

Mr. Arthur T. Sales GA. Tech. EES/HTMD GA. Institute of Tech. Atlanta, GA 30332

Mr. George F. Schmitt Air Force Materials Laboratory/MBE AFML/MBE Wright Patterson AFB, OH 45433

Mr. A. W. Searcy Dept. of Materials Science and Engineering University of Calif. at Berkeley Berkeley, CA 94720

Mr. W. A. Schmidt Naval Research Laboratory Code 5210 4555 Overlook Avenue S.W. Washington, DC 20390

Mr. George F. Schmitt, Jr. Air Force Materials Lab/MBE AFML/MBE Wright Patterson AFB, OH 45433

Mr. Arthur H. Schaufelberger Sperry Microwave Electronics P. O. Box 4648 Clearwater, FL 33518

IIr. S. J. Schneider B214 Materials Building National Bureau of Standards Washington, DC 20234

Mr. Rudolf Seclacek Stanford Research Institute 333 Ravenswood Avenue Menlo Park, CA 94025 _Mr. D. J. Shanefield Western Electric Company Post Office Box 900 Princeton, NJ 08540

Mr. Earl P. Shapland FLO-CON Systems, Inc. P. O. Box 355 Fisher, IL 61843

Mr. Lawrence Sharper Frankford Arsenal Philadelphia, PA 19137

Mr. H. Shapiro Duramic Products Inc. 426 Commercial Avenue Palisades Park, NJ 07650

Mr. William A. Shelton National Lead Co. 4511 Hide Park Blvd. Niagar Falls, NY 14305

Mr. Charles R. Sherman The Babcock and Wilcox Comapny Lynchburg, VA 24505

Mr. J. D. Shipley MP-136 Martin Marietta Aerospace P. O. Box 5837 Orlando, FL 32805

Mr. C. R. Shuff
American Standard Inc.
P. O. Box A
Paintsville, KY 41240

Mr. Melvin W. Shupe Los Alamos Scientific Lab Los Almos, NM 87544

Mr. Carl J. Smith Dow Chemical Company Rocky Flats Division P. O. Box 888 Golden, CO 80401

Mr. K. M. Smith Applied Physics Laboratory John Hopkins University Scaggsville, MD 20910 Mr. Leonard I. Smith Norton Company 1 New Bond Street Worcester, MS 01606

Mr. George H. Spragle, Jr. MP434 Martin Marietta Orlando P. O. Box 5837 Orlando, FL 32806

Mr. Craig Sparling Rockwell International-B-1 Div. Los Angeles International Airport Los Angeles, CA 90009

Dr. Joseph Stanislac Department Chemical Engineering University of Rhode Island Kingston, RI 02881

Dr. A. Sosin
Division of Mat. Science and Eng.
College of Engineering
The University of Utah
Salt Lake City, UT 84112

Mr. John M. Stanley Griffin Pipe Products Co. Orchard Hill Road Milledgeville, GA 31601

Mr. H. Stuart Starrett Southern Research Institute 2000 Ninth Avenue South Birmingham, AL 35205

Mr. H. Nathan Stone AVCO Bay State Abrasives Div. Westboro, MA 01581

Mr. R. C. Sundahl Bell Telephone Laboratories 555 Union Boulevard Allentown, PA 18103

Mr. C. J. Swafford Georgia Tech Atlanta, GA 30332

Mr. Jeff Templeton James P. Rhodes and Company 1026 West Jackson Boulevard Chicago, IL 60607 Mr. George R. Thompson Commonwealth Scientific Corp. 500 Pendleton Street Alexandria, VA 22314

Dr. R. A. Tanzilli GE/RESD. Rm U7032 VF/SIC Box 7722 Philadelphia, PA 19101

Mr. Ronald J. Tillen American Optical Corporation Southbridge, MA 01550

Dr. M. A. Tuttle
Division of Engineering
and Science
Alfred University
New York State University
- Alfred, NY 14802

Mr. James J. Tuzżeo General Electric Company 6325 Huntley Road Worthington, OH 43085

Mr. John E. Tydings Naval Ordnance Laboratory White Oak, MD

Mr. Basil E. Walker, Jr. Naval Research Laboratory Code 6130 Washington, DC 20390

Mr. Thomas W. Wallace Westinghouse Cheswick, PA 15024

Mr. Addison Watkins American Lava Corproation Cherokee Boulevard Chattanooga, TN 37405

Mr. L. B. Weckesser Applied Physics Lab. John Hopkins University 8621 Georgia Avenue Silver Spring, MD 20910

Mr. J. B. Wachtman, Jr. 8308 Materials Building National Bureau of Standards Washington, DC 20234 Dr. A. G. Wehr Dept. of Materials Engineering Mississippi State University State College, MS 39762

Mr. Earle A. Welsh Martin Marietta Aerospace P. O. Box 5837 MP 275 Orlando, FL 32805

Mr. S. Wells International Business Machines Dept. 205 1701 North Street Endicott, NY 13760

Mr. Warren W. West E.I. Du Point De Nemours and Co. Eastern Laboratory P. O. Box 67 Gibbstown, NJ 08207

Mr. Rodgers Westlake Diamonite Products Mfg. Co. Shreve, OH 44676

Mr. A. R. C. Westwood R.I.A.S. Martin Marietta Corporation 1450 South Rolling Road Baltimore, MD 21227

Mr. E. W. White Pennsylvania State University 161 Engineering Science Bldg. University Park, PA 16802

Dr. D. R. Wilder Dept. of Ceramics Engineering Iowa State University of Science and Technology Ames, IO 50010

Mr. William A. Wilson National Bureau of Standards 325 South Broadway Boulder, CG 80302

Mr. Sheldon Wiederhorn Inorganic Materials Division National Bureau of Standards Washington, DC 20234 Mr. James C. Williams C-E Refractories Valley Forge; PA 19481

Mr. Vladimir E. Wolkodoff Coors Porcelain Company 600 9th Street Golden, CO 80401

Mr. David S. Yang C-E Refractories 2563 West 18th Street Chicago, IL 60608

Dr. John C. Wurst University of Dayton Res. Institute 300 College Park Dayton, OH 45469

NOTICE

THIS DOCUMENT HAS BEEN REPRODUCED FROM THE BEST COPY FURNISHED US BY THE SPONSORING AGENCY. ALTHOUGH IT IS RECOGNIZED THAT CERTAIN PORTIONS ARE ILLEGIBLE, IT IS BEING RELEASED IN THE INTEREST OF MAKING AVAILABLE AS MUCH INFORMATION AS POSSIBLE.